RADAR STUDIES OF THE AURORA.

GODFREY COE

being a dissertation submitted to the Faculty of Science, Leicester University, in candidature for the degree of Philosophiae Doctor.

Department of Physics,

University of Leicester,

August 1985.

UMI Number: U360110

UMI

Dissertation Publishing

ProQuest

ProQuest LLC
789 East Eisenhower Parkway
P.O. Box 1346
Ann Arbor, MI 48106-1346

ACKNOWLEDGEMENTS.

CONTENTS

List of abbreviations employed in this document.

Terminology employed within this document.

<u>List of abbreviations employed in this document.</u>

(Each formula in the text also has its symbols and abbreviations described.)

A	Azimuth angle
B	Magnetic field strength
B_N	Receiver bandwidth
c	Velocity of light
c_A	Particle backscattering cross section
C.R.P.L	Central Radio Propagation Laboratory
C_s	Ion-acoustic velocity
E	Electric field strength
F_D	Doppler frequency
F.F.T	Fast Fourier Transform
f_l	Layer plasma frequency
$G_r(\theta)$	Receiver array gain at elevation angle θ
$G_t(\theta)$	Transmitter array gain at elevation angle θ
H_A	Antenna height
I	Magnetic dip angle
I.G.R.F.	International Geomagnetic Reference Field
k	Boltzmann's constant
K_L	Lerwick magnetic index
L_{AS}	Aspect angle loss
L_{FIL}	System filter loss
L_N	Vertical gradient scale length
L_s	Beam pointing loss
L_{ST}	Local sidereal time

L_{SYST}	System losses
M_e	Electron mass
M_i	Ion mass
M.U.F.	Maximum Usable Frequency
N_e	Electron density
N_F	Receiver noise figure
N_r	Receiver noise power
π	3.14159
P_R	Receiver signal power
P_r	Peak received power
P.R.F	Pulse Repetition Frequency
P_t	Peak transmitted power
R	Radar slant range
R_C	Earth reflection coefficient
R_E	Mean earth radius, 6371.2 km
R_R	Rainfall rate
s	Antenna separation
SABRE	Swedish And British auroral Radar Experiment
STARE	Scandinavian Twin Auroral Radar Experiment
S/N	Signal to noise ratio
T_A	Antenna temperature
T_e	Electron temperature
T_i	Ion temperature
T_o	300 degrees Kelvin
V_D	Electron drift velocity
ν_e	Electron collision frequency
ν_i	Ion collision frequency
V_{DO}	Doppler velocity
$V_{D(WICK)}$	Doppler velocity measured at Wick
$V_{D(UPPSALA)}$	Doppler velocity measured at Uppsala

V_T	Resultant velocity
z	Zenith distance
Z_V	Volume reflectivity factor
ϵ_o	Permittivity of free space
ϕ	Electric potential
θ	Elevation angle
θ_{AO}	Zero azimuth angle from antenna
θ_{BW}	Azimuth beam width
$\theta(n)$	Phase angle
θ_G	Radar grazing angle
θ_R	Flow angle
τ	Pulse width
τ_B	Angular refraction of radar beam
α	Recombination coefficient
σ'	Reflectivity
β	Angle between the SABRE radar beams
λ	Wavelength
λ_D	Debye length
ω	Radial velocity
γ	Right Ascension
δ	Declination
Ω_e	Electron gyrofrequency
Ω_i	Ion gyrofrequency
η	Antenna efficiency

Terminology employed within this document.

Aspect angle: The angle between the radar beam and the magnetic field line, usually intended to be 90 degrees.

Off-aspect angle: The angle by which the radar beam is not perpendicular to the magnetic field line.

Flow angle: The angle between the radar beam and the electrojet direction.

Doppler velocity: The radial velocity of a target as determined by its relative Doppler shift.

Reflectivity: The radar cross-section of a target per unit area illuminated.

Angel echoes: Radar echoes from meteorological disturbances.

CHAPTER ONE

Introduction

The ionized region of the Earths atmosphere can be investigated by means of a variety of techniques varying from ground-based radio methods to rocket and satellite borne experiments. This Thesis describes investigations undertaken by means of an auroral backscatter radar system.This radar can detect the coherent backscatter returns from small fluctuations in electron density and can determine the current flow and hence the electric fields present at a height of about 110km,at high latitudes.

This chapter will provide a brief description of the characterictics of the Earth's atmosphere which are discernable by means of radar techniques, at low and high latitudes. A comparison is made of existing radars employed in such relevant atmospheric research,with an introduction to the basic radar techniques and scattering processes frequently encountered.A survey of radar echo signals obtainable at heights below the aurora has been included because of the reception of the Short-Range-Signals which are examined in detail in chapter 7. Chapter 1 will conclude with an outline of the investigations to be presented in this Thesis.

1.Exploration of the Ionosphere using radar techniques.

The Ionosphere is generally assumed to be that part of the Earth's upper atmosphere which is partly ionised and capable of electrical conduction extending from approximately 80km to 1000km altitude.The primary cause of the ionization is due to photoionization by incoming solar radiation (x-rays

and extreme ultra-violet rays),of the atoms and molecules in the upper atmosphere (mainly oxygen and nitrogen). The ionosphere normally consists of three major regions as indicated below:

(a) below 90km   D region

(b) from 90km to 160km   E region

(c) above 160km   F region. During the daytime the F

                                  region often subdivides into the F1 and

                                  F2 layers.

Initial radar experiments in the 1920's utilised the specular reflecting properties of the ionosphere in order to determine layer heights and the value of electron densities. However,modern radar techniques operating at much higher frequencies can utilise the back-scattering properties of the medium.The reflecting and back-scattering radar techniques will now be reviewed.

1.1 Radar reflection techniques.

In a typical radar reflection (or height-sounding) experiment,a pulsed signal of carrier frequency below 20 MHz is sent vertically upwards to the ionosphere and the time taken for its return is accurately measured. From this time-of-flight of the pulse the vertical height of the layer can be derived,after allowing for the retardation of the wave in passing through the lower altitudes.

The electron density,N_e,of the layer at this height can then be derived from the expression

$$f_1 = 9\left(\sqrt{N_e}\right) \text{Hertz.} \tag{1.1}$$

where f_1=carrier frequency,or layer plasma frequency.

Because of the presence of the Earth's magnetic field,the transmitted wave is separated into the ordinary wave and the extra-ordinary wave modes,and each will have its own critical frequency. However,for the purposes of this study, the region of most interest is the E-layer,for which

the ordinary wave predominates,because of the high absorption of the extra-ordinary wave in the lower ionosphere.

The critical frequency of the E-layer has a regular diurnal and seasonal variation. It is at a maximum at noon on a summer day,and can be approximated by the expression:

$$f_E = s\left(\sqrt[4]{\cos(u)}\right) \tag{1.2}$$

where (u) is the zenith angle of the sun and s is a factor proportional to the intensity of the sun's radiation.

The E-layer is well formed during the day-time. However the electron density is generally reduced during the night-time when the photo-ionization process ceases.

Local irregularities and disturbances in the electron density of the E-region (between 100km to 120km), can occur and are referred to as Sporadic-E. At the higher latitudes considered in the bulk of this Thesis, the auroral Sporadic-E irregularities are best considered in the context of magnetic substrata phenomena and will be considered in detail in chapter 2.

The critical frequencies of the F-layers do not follow such a simple expression as equation (2). The F2 critical frequency has a diurnal maximum which lags behind the altitude of the sun,and in the northern hemisphere the day-time critical frequencies are higher in winter than in summer.

The highest layer which can be measured by a ground-based radar reflection method is the peak of the F2 layer, but the electron density profiles at greater heights can be monitored by reflection radars (i.e. ionosondes) mounted in artificial satellites. This technique,sometimes referred to as "top-sounding",has enabled electron density profiles to be obtained at heights of up to 1000km.

Local irregularities in electron density can also occur in the F2 region,referred to as Spread-F and generally these cause a spreading in range and frequency of the F2 echo returns.

Generally,ionosondes monitor the critical frequencies of the ionospheric

layers with vertical radiation,either from ground level or from above the ionosphere. However,although the critical frequency for any layer refers to the highest frequency that will be reflected back for vertical incidence,the actual value of the highest frequency that could be reflected from that layer depends on the angle of incidence of the radiation. Hence,the maximum usable frequency (M.U.F.) for a given ionospheric layer height that can be reflected back for a given distance between transmitter and receiver is given by;

$$\text{M.U.F.}=(\text{critical frequency})(\sec(i)) \quad \text{Hertz} \qquad (1.3)$$

where (i)=angle of incidence.

One of the earliest methods of investigating the ionosphere was based upon the Vertical Incidence Ionosonde. This technique is basically that of an H.F. pulse radar with the transmitted frequency variable from 1 to 20 MHz and with the time of flight,(t), of the echo pulse measured.Assuming that the pulse travels with the speed of space velocity,(c),then the equivalent height profile,h" can be obtained from;

$$h"= c \ (t/2) \qquad (1.4)$$

When this information is displayed as a plot of h" against frequency f i.e. the so called ionogram,an excellent overview of the characteristics of the ionospheric layers can be obtained,as in fig (1.1).From this h"(f) information it is possible to derive the electron density variation with true height (h) and several analysis procedures for deriving h"(f) and $N_e(h)$ profiles have been developed,as described in refs (3),1970,by Eccles and King, and (4),1967,by Wipperman.

A typical $N_e(h)$ profile is reproduced in fig(1.2).

1.1.1 Partial reflection radar techniques.

The partial reflection process was originally employed to obtain radar echoes which were back-scattered from D-region structures for transmission frequencies greater than the critical values. These structures may consist

SCHEMATIC ILLUSTRATION OF IONOGRAM FOR SUMMER DAY TIME
AT MID LATITUDES
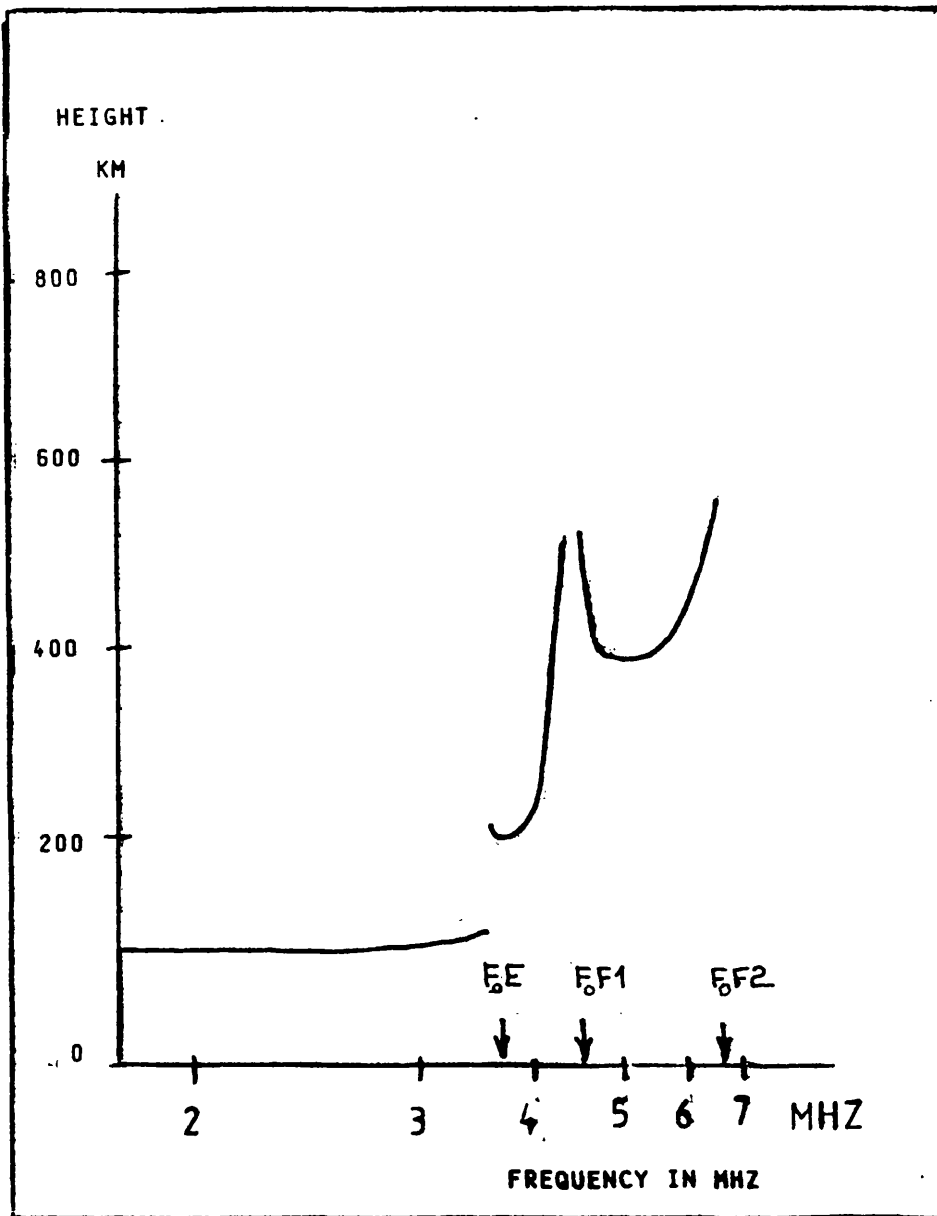
f_oE, f_oF1, f_oF2 ARE THE CRITICAL FREQUENCIES OF THE E,F1,F2 LAYERS

FIGURE 1.1

SCHEMATIC ILLUSTRATION OF ELECTRON DENSITY VERSUS HEIGHT IN
DAY TIME AT MID LATITUDES.

HEIGHT IN KILOMETRES

300

250

200
F2

150
F1

E

100

1   2   3   4   5   6

ELECTRON DENSITY $m^{-3}.10^{11}$
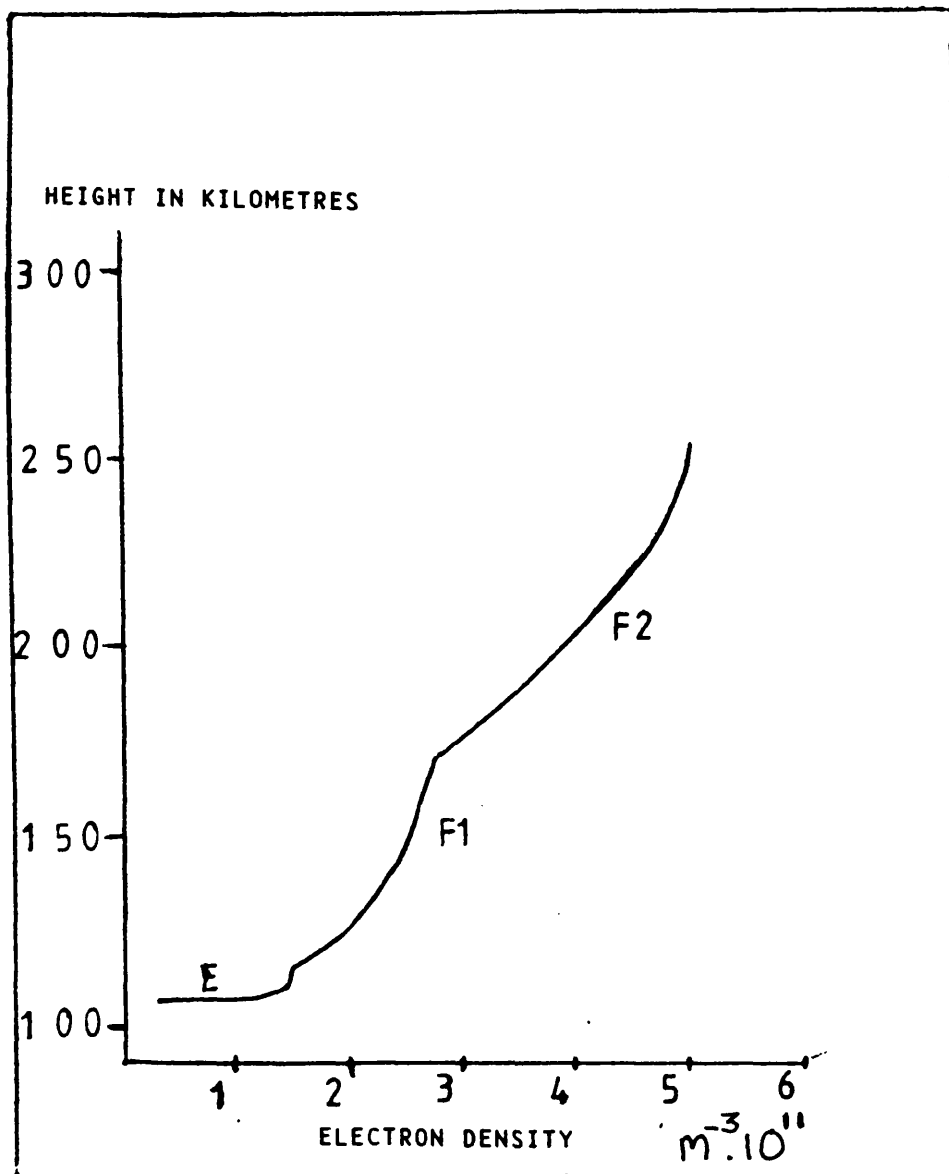
FIGURE 1.2

of irregularities in the electron density or refractive index which may be turbulent or contain horizontally stratified layers. This technique is examined in more detail in section 1.4 of this chapter and in ref (130),by Belrose and Burke,1964.

Generally,the results of ionospheric sounding utilising both topside and groundside reflection sounding,with partial reflection sounding in the D-region might typically be as follows;

Layer	Frequency (MHz)	Height in km	peak electron density
D	0.28	60 to 90	10^9 per cubic metre
E	2.8	90 to 160	10^{11}
F1	4.0	160 to 200	2×10^{11} " " "
F2	9.0	above 200	10^{12} " " "

Sounding techniques have thus been extensively employed in order to monitor the variation of electron density with height,utilising the radar reflection properties of the ionosphere. A review of modern height sounding techniques and systems,including pulse-compression systems,can be found in ref (4),1967,by Wlpperman and ref(3),1970,by Eccles and King.

1.1.2. Ionospheric refraction radar systems.

The refractive effects of the ionosphere have been utilised by a certain class of radar system in order to investigate target areas which are beyond the normal line-of-sight horizon--the so-called "Over-The-Horizon" (O.T.H.) radars.

Basically,high power radiation is directed towards the target area in a sky-wave mode,of frequency such that the F-region of the ionosphere causes the wave to be refracted back towards the Earth. Backscattered energy from the target can follow a reciprocal path and return as a radar signal to the transmitter site. Ranges of up to 3500 km. are possible using a "one-hop" refraction from the F-layer but by using a second reflection between earth and F-region (two-hop),the range can be extended even further.

Many experiments have been carried out with oblique incidence ionosondes but a description of a typical O.T.H. radar is outside the scope of this Thesis. Such radars have been employed to examine the sea-state from extreme ranges and system descriptions can be found in ref(16),1974,by Barrick and ref(17),1979,by Shearman et al.

1.2   Radar back-scattering techniques.

When the ionosphere is illuminated by radio waves of frequency greater than the maximum critical frequency weak backscatter signals are frequently observed. The "normal" reflection processes referred to in section (1.1) are not involved because of the high frequencies employed. The echo signals are caused by scattering of the radar energy at small irregularities in the structure of the plasma. If the carrier frequency is increased still further to values greatly in excess of the maximum critical frequencies,radar energy may be weakly backscattered from the elements of the plasma itself.

It is important to distinguish between coherent and incoherent scattering processes since they produce scattered echo signals differing in amplitude by an order of magnitude. Furthermore the ionospheric characteristics that can be measured differ appreciably for the two types of scatter radar. Generally,strong coherent radar echoes are returned from irregularities in electron density or refractive index which have a scale length equal to half the radar wavelength.

1.2.1 Incoherent scatter radars.

At extremely high frequencies very weak backscattered signals can occur as a result of the small but finite cross-section of the individual electrons in the ionosphere. Each electron in the E-region can be considered

as a back-scatterer of radiation with cross-section of about 10^{-28} square metres when the radiation wavelength is less than 6cm.. The effective target area of a volume of space of 100 cubic kilometres (as might be illuminated by a typical radar beam) and probably containing at most 10^{22} electrons, would be about 1 square millimetre.

The electrons within the plasma are not to be considered to be independent or "free electrons" because of the electrostatic forces of the positively charged ions which surround them. These ions form a layer around each electron of spacing given by the so-called Debye length, λ_D, where

$$\lambda_D = 69\sqrt{T_e/N_e} \qquad (1.5)$$

$$\text{where } T_e = \text{electron temperature}$$

$$N_e = \text{electron density}$$

In the E-region λ_D may be about 6 cm. whilst in the F-region peak at a height of about 250 km., λ_D may be about 0.3 cm..

As a result of the electrostatic coupling between the ions and electrons within the plasma, the random thermal motions of the electrons generate plasma waves. These waves are known as "ion-acoustic" or "electron-acoustic" waves and produce the fluctuations in electron density which give rise to the observed back-scattered radar signals.

By employing a radiation wavelength much greater than the Debye length, the incoherent back-scatter signal spectra can be obtained, as in fig(1.3), for the F-region. However, the radiation wavelengths must not be chosen so as to be so great that coherent signals from irregularities within the ionosphere are received, since these will swamp the much weaker incoherent back-scatter signals from the plasma waves.

The typical F-region incoherent scatter spectra as shown in fig(1.3) contains a double-humped ion spectrum, spread about the transmitted frequency and two sharp plasma lines corresponding to the electron spectrum. The frequency shift of the centre of the ion spectrum, away from the transmitted

SCHEMATIC ILLUSTRATION OF INCOHERENT-SCATTER SPECTRA
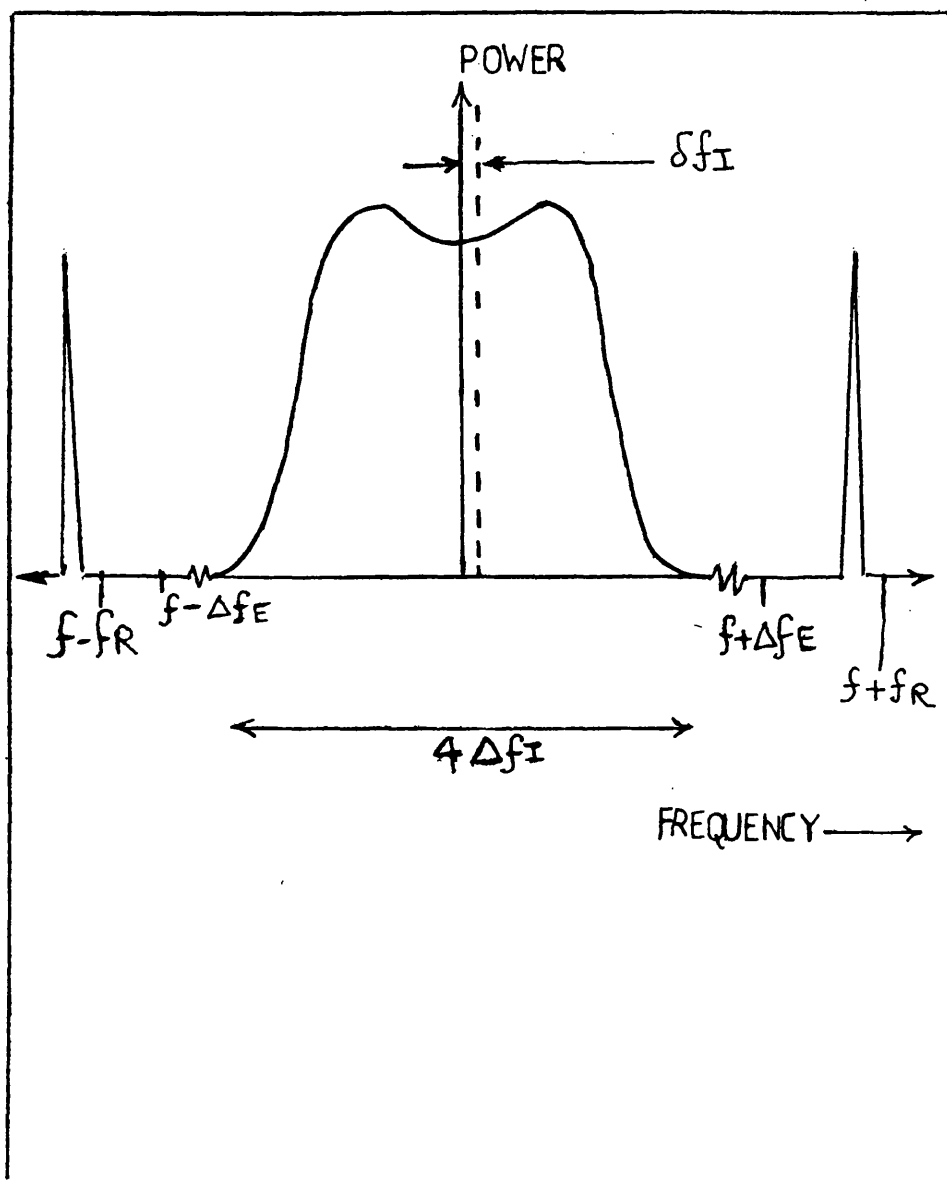
FIGURE 1.3

frequency,corresponds to the ion drift velocity and the frequency shift of the line spectrum away from the frequency value of (transmitted frequency+plasma frequency $9\sqrt{N_e}$) is related to the electron drift velocity.

The breadth of the ion spectrum,$4\Delta f_i$,is related to the ion temperature,T_i,and the ion mass,M_i,as follows:

$$f_i=((258/wavelength).(\sqrt{(T_i/M_i)}))\qquad \text{Hertz}\qquad (1.6)$$

The ratio of electron temperature,T_e,to ion temperature,T_i.can be derived from the shape of the hump of the ion spectrum and from an analysis of the complete spectrum it is possible to derive the parameters:

DIRECTLY DERIVED	SUBSEQUENTLY DERIVED
electron density,$N_e(h)$	static field strength,E
electron temperature,T_e	Hall and Pederson conductivities
ion temperature,T_i	wind speed and temperature of the neutral atmosphere, V_n and T_n
plasma drift velocity, V_p	
ion neutral collision frequency V_{in}	the downward flux of heat
electric currents	
part of the spectrum of suprathermal electrons	

A more complete analysis of the method of obtaining these parameters may be found in ref(5),1978,by Beynon and Williams.

An example of a modern incoherent scatter radar facility is the EISCAT system operating in northern Scandinavia,with the following characteristics;

	U.H.F.	V.H.F.
peak power in megawatts =	2	5
operating frequency in MHz =	933.5	224
maximum pulse repetition frequency =	1000 pps	1000 pps
duty cycle =	1/9	1/9
beamwidth in radians =	0.01	0.03 x 0.01
mean power in kilowatts =	250	600
pulse length in microseconds =	10 to 10,000	10 to 10,000

Such a system would be incorporated into a multistatic radar scheme, in order to measure the true drift velocity of a volume of plasma, rather than just the line-of-sight velocity as provided by a single beam radar.

The Eiscat 933.5 MHz system, for example, is tri-static with the transmitter and one receiver at Tromso in Norway, another receiver at Sodankyla in Finland and a third receiver at Kiruna in Sweden. All three parabolic antennae can be steered together such that they all observe the same volume of plasma.

1.2.2 Coherent-scatter radars.

Generally coherently scattered signals are far stronger than those of the incoherently scattered type and hence simpler transmitter systems can be employed. The coherent scatter process forms the basis of the auroral radar technique which is employed in the examination of the electron density fluctuations at E-region heights. Coherent echoes can also be obtained from Fresnel-type structures (i.e. thin stable layers) in the refractive index of the neutral atmosphere at tropospheric and stratospheric heights. Echoes from such structures form the basis of the class of radar known as S.T.

(stratospheric+tropospheric) radars,as described in ref (22),1974,by Woodman et al.

At D-region heights partial reflection of radio waves of frequency greater than the critical frequency can also occur. This type of backscatter can yield information regarding the electron density height profile,$N_e(h)$,in the D-region from 65 km to 95 km.,as detailed in ref (2),1953,by Gardner et al, and in ref (130),1964 by Belrose and Burke.

The studies described in this Thesis are mainly concerned with the investigation of the sub-auroral ionosphere by means of a V.H.F. coherent radar. A detailed description of this radar,(and other auroral radars) is presented in chapter 2. Radar signals which are returned from irregularities in electron density that have a scale length equal to half the radar wavelength will generally be of a strong,coherent nature. Such electron density irregularities exist throughout the ionosphere and have scale lengths ranging from about 1 metre to several kilometres.

Of particular interest in the examination of the Short-Range-Signals in chapter 7,however,is the method of coherent radar investigation of the D-region employing the Urbana,Illinois, radar system as described in ref(18),1983, by Gibbs and Bowhill. Using basic pulse-Doppler radar techniques,(as reviewed in chapter 2), these researchers found that

(a)for vertical heights above 75 km bulk scattering of the radar beam by electron density fluctuations caused by the atmospheric turbulence predominated. These signals changed in level in step with changes of solar flux.Generally they did not appear at night unless conditions of enhanced ionisation prevailed,such as unusual solar activity or meteor showers. The spectra for these signals was relatively wide.

(b) For heights below 75 km the spectra were relatively narrow and the signals were present day and night-time. These echo signals were due to Fresnel (or partial) reflection from irregularities in the dielectric layers,rather than in the electron density layers.

The nature of these echoes will be examined in more detail section 1.4.

Before concluding this survey of radar investigations of the ionosphere,there is one further radar technique which involves ionospheric effects---namely the examination of meteor trail echo signals.

1.3 Meteor trail radars.

Generally the majority of meteors which enter the Earth's atmosphere are too small to be detected directly by their radar echo.However they create a trail of ionosation during their passing which can be detected, usually in the height range of 80 km to 100 km by radars operating at below 200 MHz. These trails can scatter the V.H.F. radiation but rarely last for time periods of even a minute. The echoes are characterised by having a low Doppler shift and a noise-like spectrum.

The passage of these meteor trails have been utilised by some investigators to examine the winds in the upper atmosphere since the trail drifts with the neutral atmosphere below about 100 km. Relatively powerful radar transmitters are needed,however,and one example of such a radar is the Urbana facility in Illinois which uses a radiation frequency of 40.9 MHz at peak powers of megawatts in a pulse-Doppler mode,as described in ref(15), by Hess et al,1976.

1.4 Radar investigation of the atmosphere below 100 km.

Because of the suspected origin of the echoes received by the SABRE

auroral radar at ranges below 300 km, a brief review of the radar techniques used to investigate the atmosphere at heights below 100 km will now be given.

Such radars have generally been described as "M.S.T. radars" where MST stands for mesosphere,stratosphere,troposphere,respectively. Radars which can only observe up to stratospheric heights have similarly been described as "S.T. radars".

Radar echoes from meteorological targets were originally investigated in some detail in the early 1960's,as soon as radar systems became sensitive enough to detect the relatively weak signals which were returned from the clear atmosphere. Such signals,which originally were considered to be unexplainable,were termed "Angel Echoes". Initial investigations were undertaken at microwave frequencies and early reports included those by Planck,1960,ref(19),and Hardy et al,1966,ref(20).

With the development of the powerful VHF and UHF radars,which were intended for the investigation of the incoherent back-scatter signals from the ionosphere (as described in section 1.2),it became apparent that signals were obtainable from heights below 100 km. Such signals which were obtained from the Jicamarca 49.9 MHz radar,pointed vertically,were found to be stronger than expected from incoherent (or Thompson) back-scatter.

Bowles,1964,ref(21),suggested that such signals were due to scatter from the turbulence in the mesosphere. The first measurements of such turbulence and atmospheric winds were reported in 1974 by Woodman and Guillen,ref(22),using the Jicamarca radar. The radar was developed as a VHF pulsed Doppler system in order to measure wind velocities. Since then other similar radar systems have been developed primarily for study of the neutral atmosphere.

The main advantage of employing such radar systems to monitor the wind and turbulence lies in the availability of the systems,in comparison with the more conventional radiosondes. For example,Goss and

Bowhill,1983,ref(23),quote typical figures of availability of wind profile (against height) of 1 hour for the Urbana radar,whilst Green et al,1979,ref(24),quote a figure of 1 minute for the Sousy radar.

1.4.1   M.S.T. radars.

Generally MST radars operate in the VHF band of 30 MHz to 300 MHz,and the scattering mechanism by which the radar signals are returned from the clear air can be divided into two groups:

Group one: Turbulent scattering,either isotropic or anisotropic

Group two: Fresnel reflection or partial reflection.

In both groups the radar signals are scattered or reflected by structures,gradients or fluctuations in the radio refractive index,of scale length of the order of half the radar wavelength. Isotropic turbulent scattering occurs when the active turbulence of the clear air generates gradients in the refractive index,but when the turbulence is of very large scale,then the scattering can become anisotropic. Fresnel reflection usually occurs when the radar beam is pointed vertically,or near vertically, and radar echoes are obtained from stable layers,usually thin.When more than one layer is present in the scattering volume,Fresnel scattering occurs.

Detailed descriptions of these groups of scattering and details of the anisotropy of some signals have been presented by Green et al,1979,ref(24) Ecklund et al,1979,ref(25),and Gage and Balsely,1980,ref(26).

A graph of the variation of turbulent scale length (and hence required radar wavelength) against height is displayed in fig(1.4) from ref(26).From this same reference the variation in signal strength with height is illustrated in fig(1.5).

Because of the relatively low signals from the clear air turbulence and the requirement for relatively long wavelengths,MST radars generally require

SCHEMATIC ILLUSTRATION OF THE MINIMUM SCALE OF TURBULENCE
AGAINST ALTITUDE
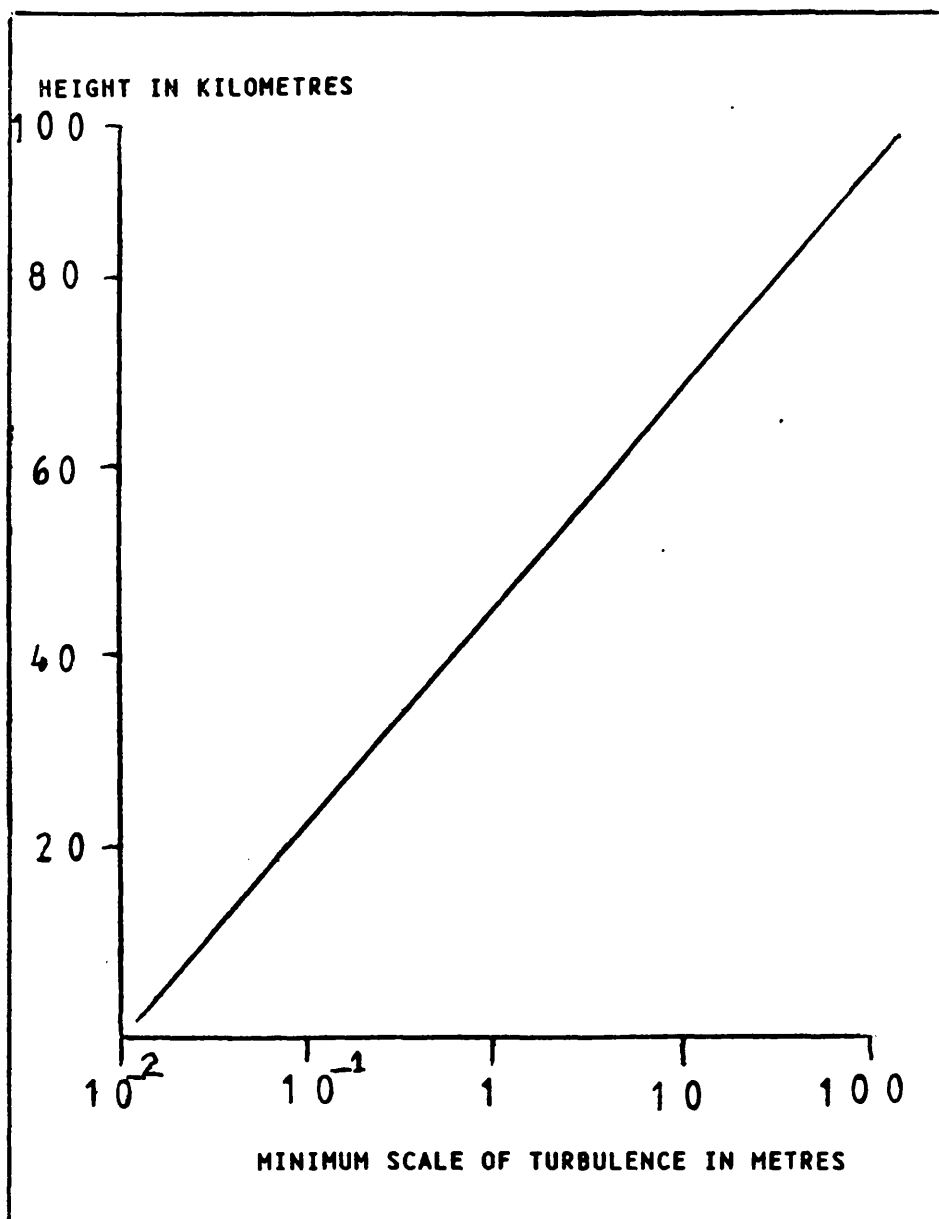
FIGURE 1.4

SCHEMATIC ILLUSTRATION OF THE HEIGHT VARIATION OF POWER

RETURNED FROM THE ATMOSPHERE FOR A 50 MHz RADAR

HEIGHT IN KILOMETRES

LOG OF RECEIVED POWER
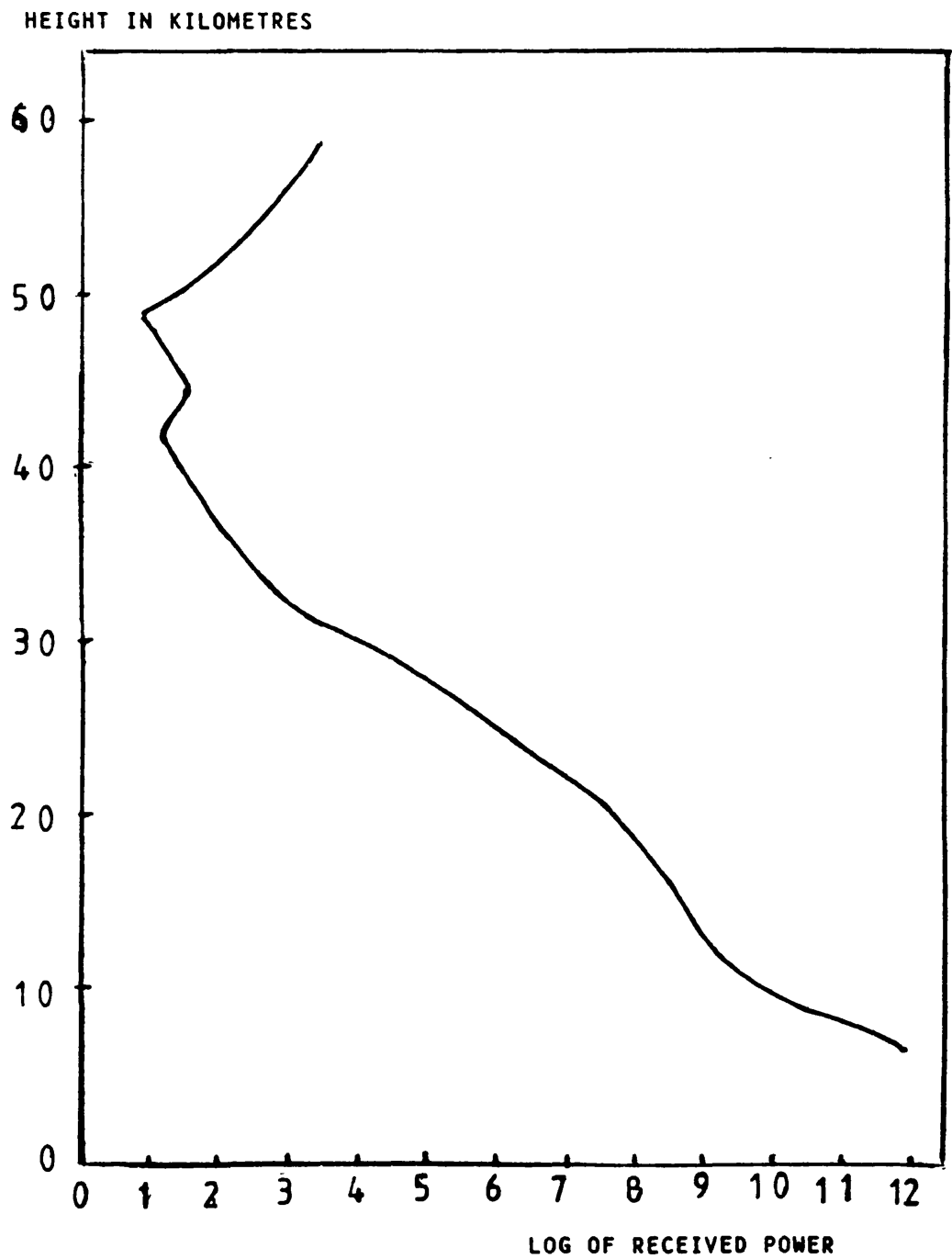
FIGURE 1.5

powerful transmitters,narrow beamwidths and operate at frequencies near 50
MHz. Frequencies below 50 MHz could be used but would suffer problems with
interference. At this frequency it is possible to construct,very
cheaply,large array antennae with the ability to scan about the zenith by
means of phase adjustment in the array pattern. A typical MST radar with
such phase adjustment is the Sunset radar at Colorado which uses a phased
dipole array and a radiation frequency of 40.5 MHz. Similarly,the Sousy MST
radar uses a phased Yagi array at 53.5 MHz. These two radars are fully
described in ref(24),1979,by Green et al,and ref(27),1979,by Rottger and
Schmidt,respectively.

As an example of the antenna size employed in MST radars,the Jicamarca
array,as described in ref(22),1974 by Woodman and Guillen,has an area of 290
metres by 290 metres and uses phased dipoles. The transmitter power is
quoted as 4 megawatts peak,0.4 megawatts mean and the beamwidth quoted as
one degree.

A parameter in common usage in describing MST radars is the "average
power aperture". This is the product of the transmitter mean power and the
antenna aperture,and typical quoted figures are:

	FREQUENCY	AVERAGE POWER APERTURE	BEAMWIDTH
Jicamarca	49.9 MHz	2.10^{10}	1 degree
Poker Flat,Alaska	49.9 MHz	5.10^{9}	1.5 degrees

The Poker Flat radar is described more fully in ref(28),1979 by Balsley
et al, and actually consists of two independent frequency-coherent
monostatic radars having antenna beams directed 15 degrees from the zenith
towards the north and the east. By using these two beams it is possible to
deduce the full horizontal component of the wind by vertically combining the
radar velocities from the north- and east- directed beam positions. The
assumption is made that the horizontal component of the wind is much greater
than the vertical component.

Typical vertical velocities reported by Rottger,et al,1979,ref(27),for

the height ranges below 80 km are of the order of ± 1 metre per second.Woodman and Guillen,1974,ref(22),reported short-period fluctuations in velocity measurements and attributed them to gravity-wave activity.

Typical horizontal wind-velocity profiles (against altitude) might contain a peak in velocity of the order of 65 m/sec at the height of the Tropopause (10 km) as in ref(29),1978, by Van Zandt et al,for a northward wind during a jetstream. Goss and Bowhill,1983,ref(23),have reported a horizontal velocity peak in the south-east direction,at approximately 11 km altitude,of about 35 m/sec. This same reference reports maximum velocities of the order of 80 m/sec occurring at heights of 25.5 km,and maximum echo strengths occurring at heights of between 13.5 km to 19.5 km.These figures were based upon hourly averaged readings.

Ecklund,et al,1979,ref(25),have investigated velocity profiles at altitudes between 50 km and 80 km at Colorado,and found that radar echoes were returned during day-time only,being strongest just before local noon-time.The strongest continuous echoes ocurred at about 74 km,with stronger but short-lived echoes ocurring at greater heights,thought to be due to meteoric ionization.The horizontal wind velocities,averaged over 3 minute periods,were generally below 60 m/sec.These day-time echoes from the mesosphere are thought to occur as a result of the effect of the free electrons in enhancing the scattering from the irregularities in the refractive index. These investigators also report a decrease in volume reflectivity of 1 db per kilometre altitude over the height range 2 km to 18 km.

When examining the spectra of the signals from MST radars the mean spectral shift is used to derive the mean radar velocity of the wind.

The characteristic shapes of the turbulence in the Mesosphere have been described in ref(31),1979,by Rottger et al,who identified three structures; blobs,sheets and layers.Blobs and sheets ocurred sporadically,predominantly at heights of 60 km to 70 km.Above 70 km layers thicker than 1 km were

dominant,which were advected with the background wind.Generally,velocity fluctuations were proportional to the structure thickness.

MST radars can thus be characterised as having large antennae apertures,high peak powers,of frequency near 50 MHz and have pulse-Doppler signal processing. Such radars can be used to provide useful commercial data as well as scientific--for example,studies of the jetstream may be used by commercial airlines to enable a reduction in aircraft fuel consumption on some flights.This topic has been studied by Carlson and Sundararaman,in ref(30),1982.

A radar system which has been employed to investigate the Troposphere at heights up to 2 km and which uses a range-measurement technique other than the usual pulsed radar system,is the high-resolution radar at the Naval Electronics Laboratory centre,San Diego.This system,as described in ref(32),by Richter,1980,has a vertically pointed narrow radar beam with very low sidelobes,at a radiation frequency of 2 gigahertz,in an FM-CW mode.Because of the requirement for very close-range (i.e. 1 km) investigation, a pulse-compression radar was considered to be inapplicable and a basic single-pulse radar system was eliminated because of the extremely high peak powere that such a radar would require.

1.4.2 <u>Weather radars.</u>

Finally it should be noted that microwave pulse-Doppler radar systems have been employed to explore the meteorological parameters of the lower atmosphere under the general description of weather radars. A weather radar system might have the following typical parameters;

WAVELENGTH	BEAMWIDTH	ANTENNA DIAMETER	PEAK POWER	PULSE-WIDTH
3.2 cm	1 degree	2.3 metres	200 kwatts	1 microsec
5.4 cm	1 "	3.9 "	200 "	1 "
10 cm	1 "	7.1 "	500 "	1 "

Doppler weather radar systems are described more fully in ref(34), 1974,by Smith et al.

The scattering mechanism wherebye echoes are obtained from precipitations generally occurs for wavelengths of less than 10 cm,for particles of radius A,of backscattering cross-section C_a,where:

$$C_a \propto A^6/(\text{wavelength})^4 \qquad (1.7)$$

Intense storm systems usually develop large condensation particles of such diameter that they are easily detected by radar systems using wavelengths of about 10 cm. Observations of such storms by weather radars can enable the prediction to be made of the further position and intensity of the storms. Furthermore,the rainfall rate can be estimated by the relationship between the radar reflectivity,Z,and the rainfall rate ,R_R,as:

$$Z =200 \cdot R_R^{1.6} \qquad \text{where } R_R \text{ is in millimetres per hour.} \qquad (1.8)$$

For a narrow-beam radar system the power received,P_R,from a volume of rain which entirely fills the beamwidth can be proportional to:

$$P_R \propto Z/(\text{range})^2 \qquad (1.9)$$

Hence power received is $\propto(\text{rainfall rate})^{1.6}$. Further details and derivation of the full radar equations for weather radars can be found in refs(34),1974,by Smith et al and (35),1973,by Battan.

The Doppler frequencies,F_D,derived from a weather radar pulsed Doppler system are related to the radial velocity,V,of the scattering volume by:

$$F_D=2 \cdot V/(\text{operating wavelength}). \qquad (1.10)$$

The maximum Doppler frequency which can be resolved unambiguously is given by $\qquad F_D(\text{max})=(\text{pulse repetition frequency})/2 \qquad (1.11)$

The maximum unambiguous range and velocity are related by:

$$V(\text{max})=(\text{operating wavelength} \times c)/(8 \times \text{maximum range}) \qquad (1.12)$$

Hence if the weather-radar wavelength were 5 cm and the maximum range were to be 100 km,then the maximum Doppler shift to be measured would be 19 m/sec.

Typically, weather radars can monitor up-drafts of the order of 18 m/sec, at the leading edges of showers, for vertical heights of up to 12 km.

It is apparent that the Earth's atmosphere has been investigated by a wide range of radar techniques, over a broad band of frequencies. The exploration of the atmosphere undertaken by the VHF radar employed for the analysis within this Thesis will now be described.

1.5   Outline of the present investigation.

The ionospherics group at Leicester University have recently constructed a bistatic phased-array VHF (150 MHz) radar, SABRE (Swedish And British auroral Radar Experiment). The system has two independent radars operating at Wick in Scotland and Uppsala in Sweden. It is evident from the previous work already described in this Thesis that the radar will be sensitive to the auroral back-scattering irregularities and may also respond to structures which yield coherent backscatter in the neutral atmosphere.

The strongest returns are obtained from auroral irregularities and an attempt has been made to quantify the electrojet parameters which give rise to these scatter centres. Particular attention has been given to the variation of echo strength and electrojet velocity with height, auroral activity and geomagnetic conditions. In order to implement the studies a careful examination of the radar performance was undertaken. The vertical polar diagram was established and attention given to the aspect and beam-pointing loss characteristics. From this information a detailed evaluation of the expected radar performance was established. These investigations revealed some weaknesses in the radar operation and a number of software and hardware developments were initiated to overcome these difficulties.

One of the unexpected features of the SABRE radar was the occurrence of weak echoes at relatively short ranges (less than 300 km). Several possible

causal mechanisms were examined which included equipment-generated erroneous signals together with various scattering processes in the neutral atmosphere. The investigation concluded that Aircraft flying in the antenna sidelobes of the SABRE radars are predominantly the cause of these echoes.

The remainder of this Thesis contains a review of radar aurora and auroral radar systems, a detailed derivation of the SABRE radar equation and an analysis of the SABRE echo signal data. From the measurements of the returned power and Doppler frequency shift, it was possible to determine the parameters of the scattering region and to relate these to the geophysical conditions. Methods of improving the SABRE radar in order to determine auroral height and velocity spectrum more accurately are then outlined, together with a description of the many computer programmes developed in this analysis.

2. Radar studies of the Aurora

Radar systems which have been employed to study the auroral regions of the ionosphere differ in two main features from the radar systems which were reviewed in the first chapter of this Thesis:

1. The strength of echo returned from the aurora is very dependent upon the aspect-angle between the radar beam and the magnetic line of force. Maximum signals are returned when the radar beam is orthogonal to the line.

2. The majority of echoes are from the diffuse aurora which is distributed over large areas of the E-region.Scattering areas viewed are quite large and hence relatively moderate transmitter peak powers (~45 kwatt) can be employed.

This chapter will review the basic features of the radar aurora,the production mechanisms of the electrojet and its radar backscattering processes. The radar auroral features will then be compared with those of the equatorial electrojet which has also been extensively investigated by radar techniques. In conclusion,this chapter will provide a description of the SABRE auroral radar which was employed in the investigations contained in the remaining chapters of this Thesis.

2.1 Radar aurora.

The term "radar aurora" has been widely employed to denote the type of scattering irregularities which occur in the auroral zone of the ionosphere at E-region heights.The range of ionospheric heights normally associated with such irregularities lies in the range 100 km to 120 km,and occur both

in the Northern and Southern auroral zones.

Irregularities of a similar nature also occur in the equatorial electrojet, which has been extensively studied particularly by the incoherent scatter radar facility at Jicamarca, in Peru. This radar is located near the geomagnetic equator and can therefore employ vertical beams which achieve orthogonality with the horizontal magnetic field lines at ranges of 100 km or so.

Because of the aspect-angle requirement of 90 degrees between radar beam and magnetic field-line, auroral radars in the Northern hemisphere operate at L-values of between 4 to 7 with slant ranges of the order of 1000 km. However, because of the effectiveness of the aurora as a backscatterer of VHF radiation, these radars can still achieve signal to noise ratios of the order of 30 dbs, even when at peak powers of only 45 kwatts.

The irregularities which back-scatter the radiated energy have been investigated over a frequency band of between 40 MHz to 3,000 MHz, and generally the radar returns are stronger at the longer wavelengths. Hodges and Leadabrand, ref(53), 1965, found a wavelength dependence of the fifth power for transmissions from 139 MHz to 398 MHz.

In order to describe the auroral scattering processes, it is necessary to review the background physics of the interaction between the magnetosphere and the high-latitude ionosphere. Precise details of the theoretical background can be found in refs(36), 1972, by Ratcliffe and (37), 1974, by Jones but for the purpose of this review, a general summary will suffice.

2.2 The solar wind and the auroral zone.

The solar wind consists of hot plasma escaping from the sun and striking the earth's atmosphere at flow velocities in the range 200 to >1000 km/second. This plasma carries with it a weak magnetic field from the sun, which will interact with the earth's magnetic field, particularly when the solar wind has a southward magnetic component.

The pressure of the solar wind plasma confines the earth's magnetic field to a cavity,known as the "magnetosphere". As illustrated schematically in fig(2.1),the earth's magnetic field on the day-side,i.e. nearest to the Sun, terminates at an altitude of about 60,000 km,but on the night-side the magnetic field is stretched out behind the earth to beyond the orbit of the moon into a long "magneto-tail". This distorted configuration is maintained throughout the earth's rotation by the continuous transfer of the high latitude magnetic field lines from dayside to nightside.This transfer is assisted whenever the solar magnetic field has a southward component,as in fig(2.1). The shape of the magnetosphere and its comet-like tail has been confirmed by satellite measurements but the role of the magneto-tail in producing visual auroral displays is probably best visualised as an accelerator of solar plasma particles which enter the tail. These particles are accelerated back along the tail into the earth's atmosphere at points along the hemisphere where the open lines of magnetic field join the earth.These points are over the polar caps,inside the so-called "Auroral Ovals".

The auroral zone is defined as a narrow band centred on a line of maximum average-annual-frequency of auroral visibility. The overall probability of seeing aurora reaches a maximum in an approximately circular zone of radius of about 22 degrees centred on the geomagnetic poles. If local time is taken into account the locus of maximum occurrence is an oval aligned along the sun to earth direction,with radii from the geomagnetic pole of about 12 degrees and 22 degrees respectively,in the solar and anti-solar directions. Typical positions of the auroral oval for different times of day in the northern hemisphere are displayed in fig(2.2).During intense solar storms or geomagnetic storms the auroral oval will shift further south toward the equator,and usually the most dynamic visual display will accompany such storms.

SCHEMATIC ILLUSTRATION OF THE DISTORTION OF THE EARTH'S MAGNETIC
FIELD, CAUSED BY THE SOLAR WIND.
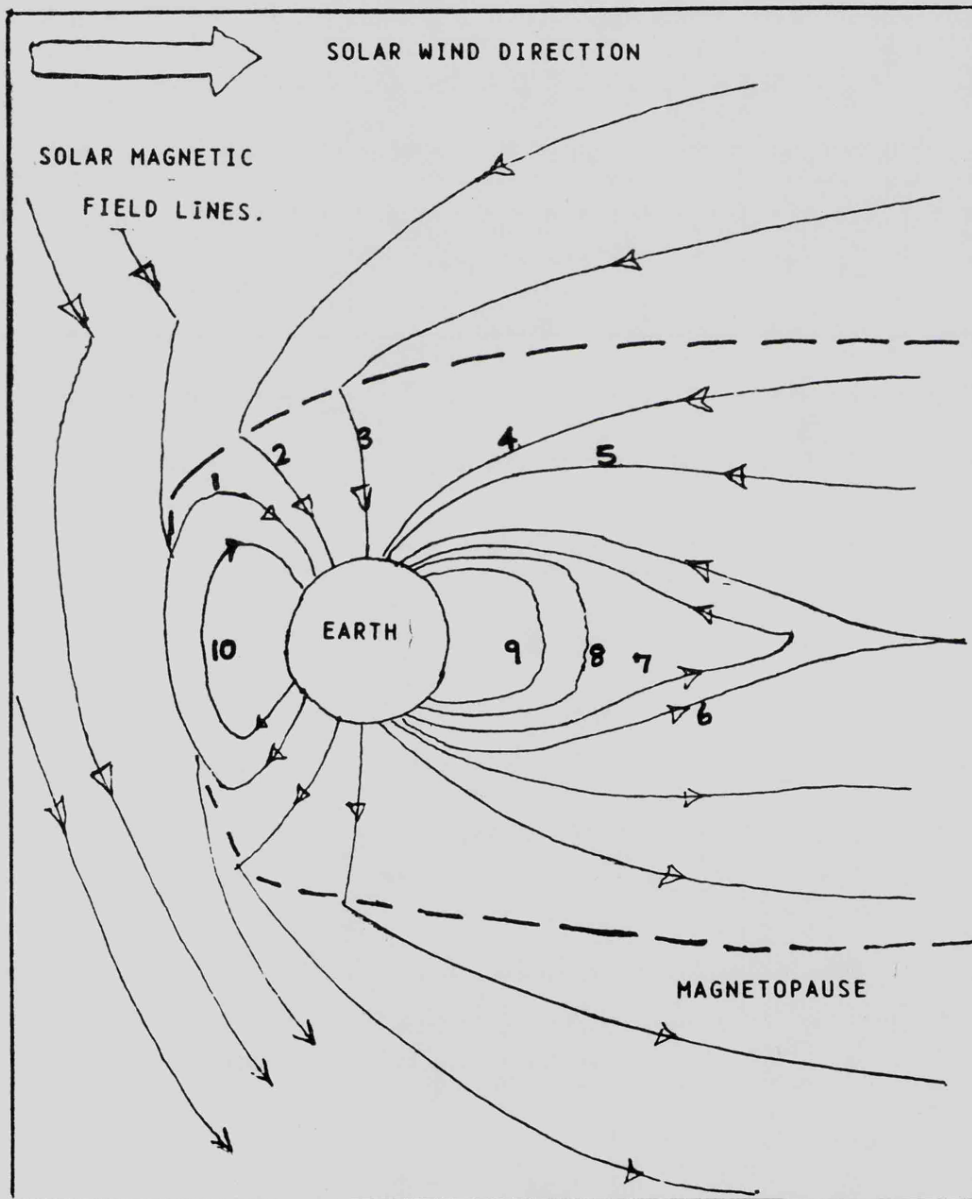
THE NUMBERS INDICATE THE SUBSEQUENT POSITION OF THE
MERGED FIELD LINES AT INTERVALS OF ONE HOUR.

FIGURE 2.1

SCHEMATIC ILLUSTRATION OF THE POSITION OF THE AURORAL OVAL
FOR A STRONG MAGNETIC DISTURBANCE.
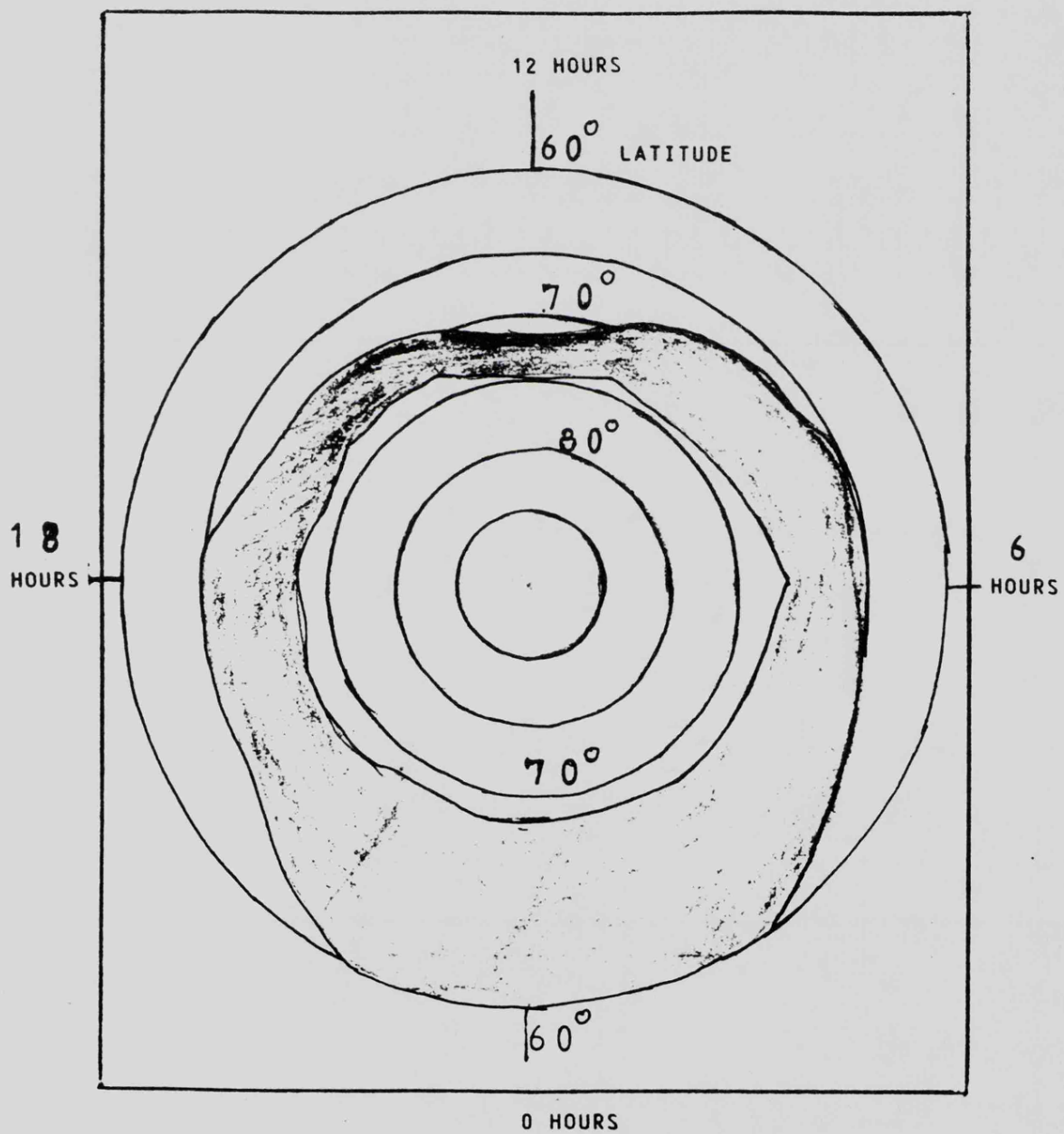
FIGURE 2.2

2.3 The auroral electrojets.

The storm-enhanced electrojets produce strong radar echoes and have been investigated by radar techniques for more than 30 years.

Generally auroral storms which produce bright visual displays and electrojet flow have been called "substorms" and are thought to occur whenever the interplanetary magnetic field within the solar wind develops a sustained southward component which interacts with the earth's magnetic field and transfers extra magnetic lines to the magneto-tail. In a situation whereby any unstable accumulation or transfer of field lines from dayside to nightside of the earth occurs, charged plasma particles can be accelerated at high speed down a spiralling path around a magnetic line of force, into the lower parts of the atmosphere.

The effect of this extra particle concentration in the E-region is to increase its conductivity even more. Normally the conductivity of the E-region is the highest for all layers of the atmosphere, because at these heights the positive ions tend to collide more frequently with other particles than do the electrons, resulting in an availability of electrons to constitute a current flow.

Now when the charged particles flow out from the tail of the magnetosphere towards the earth's auroral zone they develop an electric field, which at night points south in the northern hemisphere. This electric field, directed at right-angles to the magnetic field cause both electrons and positive ions to be deflected eastward. The ions, however, have a lower mobility than do the electrons and hence there is a net drift of electrons towards the east. Because of the circulatory nature of the plasma as it enters the earth's atmosphere from the magnetotail, the actual pattern of the electrojet currents is in the form of two complex loops, as presented schematically in figs(2.3),(2.4) and is referred to as a 2-cell convection model.

SCHEMATIC ILLUSTRATION OF THE PROBABLE CURRENT FLOW SYSTEMS
DURING A MAGNETIC SUBSTORM.
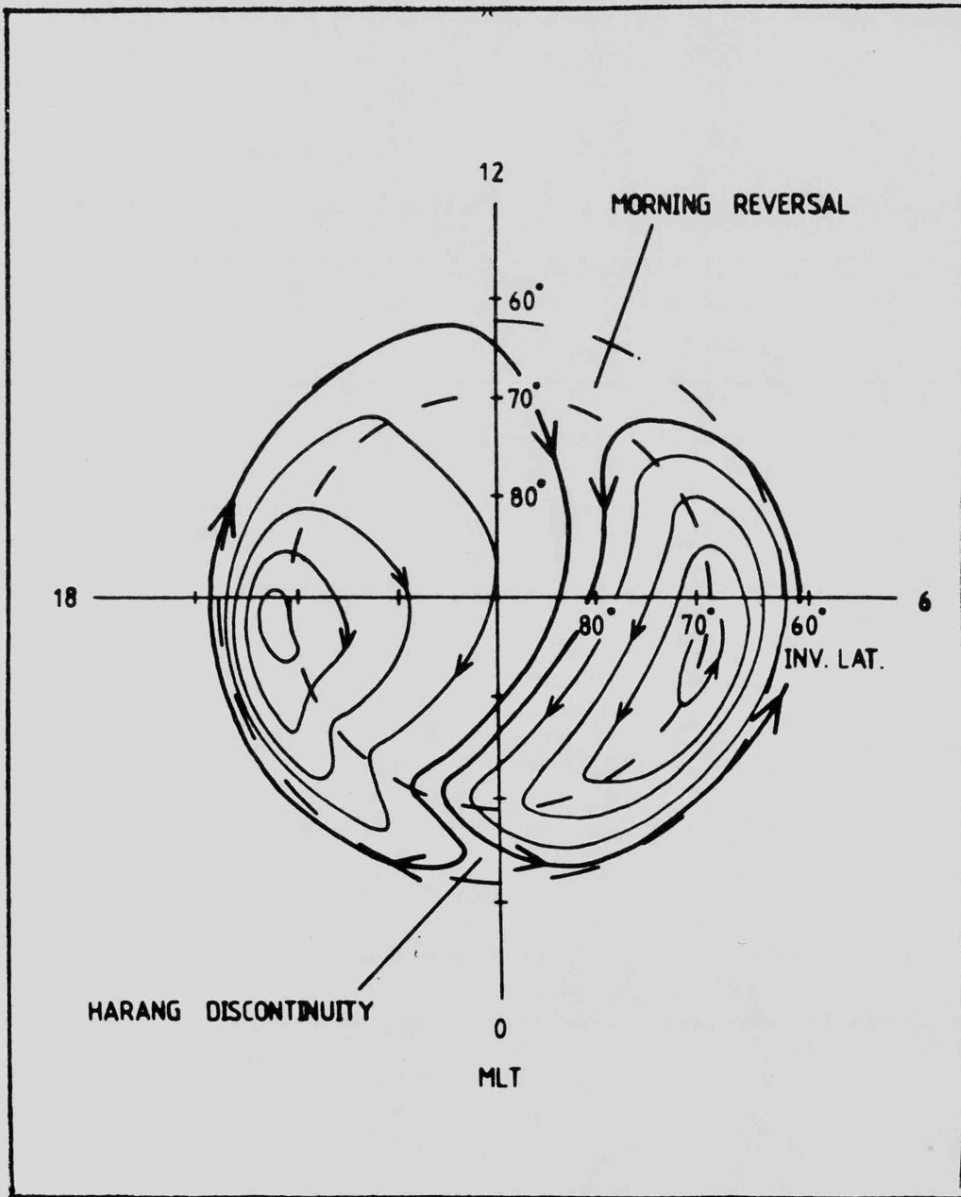
FIGURE 2.3

SCHEMATIC ILLUSTRATION OF THE FORMATION OF THE POLAR CURRENT
LOOP SYSTEM.
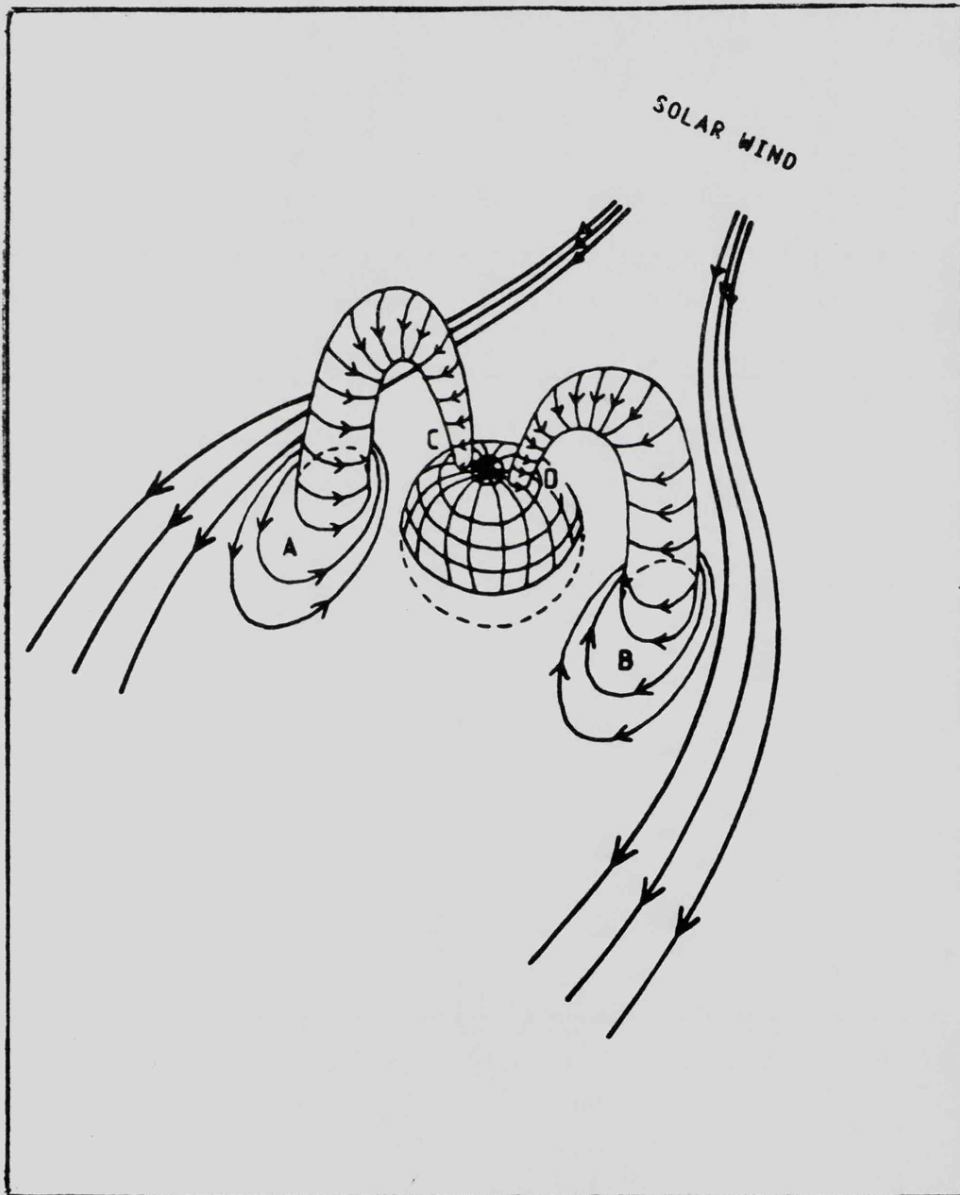
THE SOLAR WIND PRODUCES CIRCULATORY MOVEMENTS OF THE PLASMA
AT POINTS C AND D.

FIGURE 2.4

An important feature of the two-cell convection model is the reversal in flow direction which occurs at a given latitude in the midnight and noon sectors.These are known respectively as the Harang Discontinuity and the Morning Cleft.

The current which flows in the auroral electrojets is primarily due to the high Hall conductivity in the E-layer,since the current flow is in a direction at right-angles to both the electric and magnetic fields.However it has been shown that the Pederson conductivity is also increased during auroral activity,resulting in an increase of current flow in the direction of the electric field.

This basic outline of the mechanism of the auroral electrojets will suffice for this review,but it must be noted that general theories of the aurora include an account of a current flow, between the ionosphere and magnetosphere,called Birkeland currents,which affect the balance of energy transfer between the layers in certain sections of the auroral zone.

A further feature of the aurora to be reviewed is the pulsating effect seen in radar signals at certain times,particularly during the development of substorms.Only brief details of this feature of the aurora will be given,since the bulk of this analysis has concentrated on the times when the auroral echoes have been constant for periods of 1 hour or more.

The pulsating effect of the radar echoes is usually of an oscillatory nature,of periodic times ranging from < 1 second to 600 seconds.The geomagnetic field disturbances which produce the longer pulsations are attributable to electrical current fluctuations in the ionosphere and magnetosphere.The shorter time-scale variations are known as pulsations and are attributable to hydromagnetic waves in the magneto-sphere.

A typical SABRE pulsation is illustrated in fig(2.15) but for details of pulsations and disturbances seen in the Stare radar data,the following references should be consulted; Walker and Greenwald,1981,ref(102) and Nielsen and Sofko,1982,ref(103).

A further feature found in radar auroral echoes is the Westward Travelling Surge,which occurs during the expansive phase of a substorm.During the expansive phase,a region of intensified electrojet current spreads from the midnight sector into the evening sector of the auroral zone,and the propagating head of this current is thought to be at the bend of the auroral arc,as displayed in fig(2.5).The Westward Travelling Surge is not considered further in this Thesis but further details can be found in the following references; Akasofu,1968,ref(104) and Inhester et al 1981,ref(105).

2.4 The equatorial electrojets.

The electrojets in the equatorial region have similar aspect-angle sensitivity characteristics when viewed by radar beams,but are produced by a different mechanism even though the same region of high-conductivity (i.e.the E-layer) is being used.This conducting layer is moved across the earth's magnetic field by the influences of the sun and the moon; the moon by means of its gravitational attraction and the sun by producing horizontal air movements caused by heating the ozone layer. The effect of the solar tides is the greater,and generally has a periodic time of 12 hours.

This tidal motion of the earth's atmosphere,in conjunction with the geomagnetic field,generates electric fields in the ionosphere by a dynamo action.These fields cause horizontal electrojet currents to flow in the equatorial E-region. Radar investigation of this electrojet has indicated reversals in current direction at night-time with relatively weak signals,whereas the auroral electrojets often experience stronger signals during the night-time.

2.5 Irregularity Structures---Processes 1 and 2.

SCHEMATIC ILLUSTRATION OF THE WESTWARD TRAVELLING SURGE.
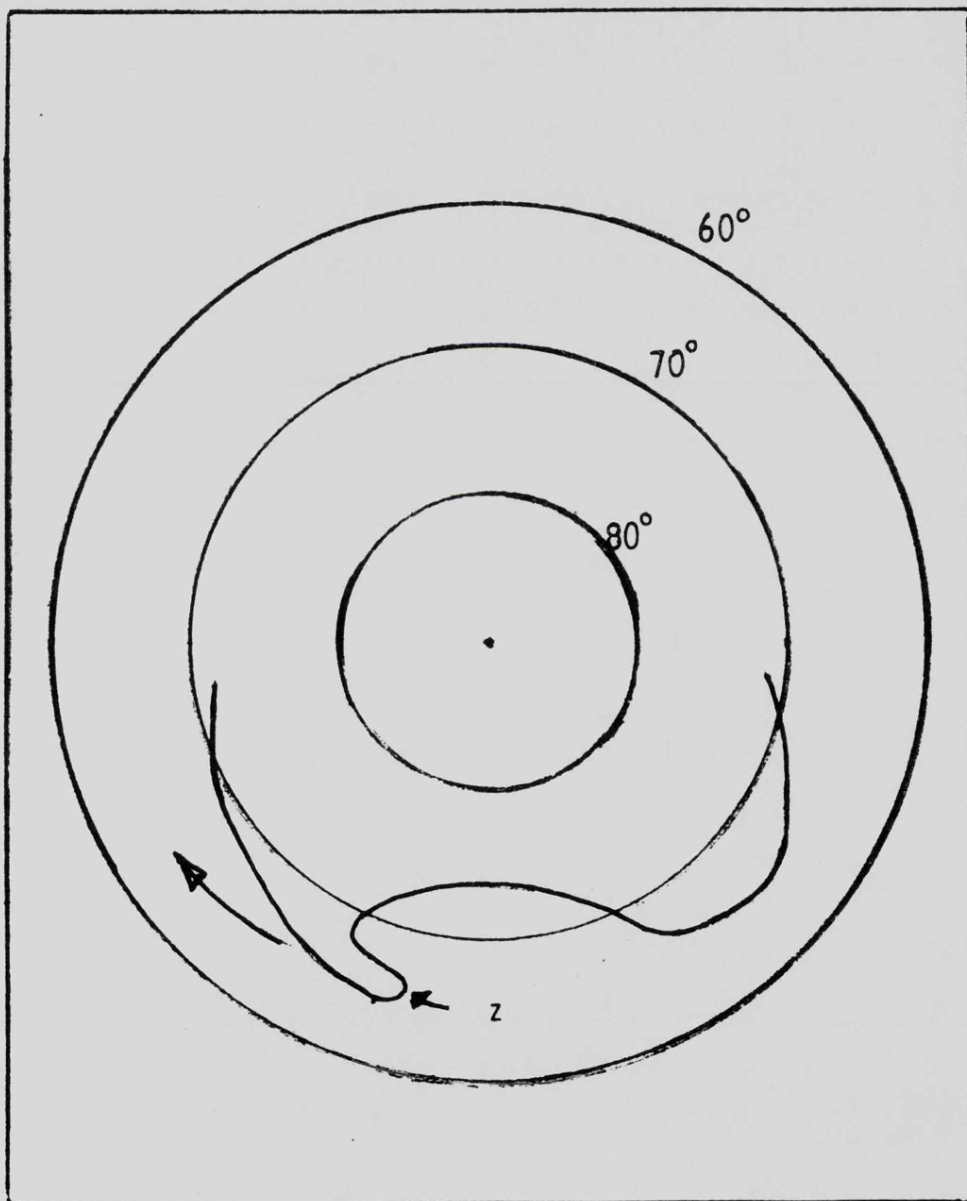
POINT Z IS THE WESTWARD TRAVELLING SURGE.

FIGURE 2.5

There are two main processes which describe the formation of the irregularity structures within the electrojets,both in the auroral zone and at the equator,namely;

a) the two-stream instability process

b) the gradient drift instability process.

The two-stream instability is thought to occur whenever the difference between the electron drift velocity and the ion drift velocity reaches a critical value.At heights of 100 km this critical value is of the order of 350 metres per second.The effect upon the plasma is the production of ion-acoustic waves which are longitudinal,compressional waves which build up in strength at the expense of the kinetic energy of the electrons which move with the wave.As the electron drift increases beyond the critical value,irregularities will grow in those directions in a plane perpendicular to the magnetic field,where the electron drift velocity,V_D,is given by;

$$V_D \cos(A) > \text{the critical velocity},C_S \qquad (2.1)$$

where (A)=angle between electron current and irregularity propagation direction.

In ref(117),1963,by Farley,the ion-acoustic velocity is related to the electron temperature,T_e,as follows;

$$C_S \propto \sqrt{((T_e+T_i)/M_i)} \qquad (2.2)$$

$$\text{where } T_i = \text{ion temperature}$$

$$M_i = \text{ion mass}$$

Fejer and Farley,1975,ref(118),developed a general fluid theory for the instabilities within the electrojet which included the effects of recombination and gradients in the electron and ion densities.The waves were assumed to be electrostatic and refraction effects and propogation effects were ignored.The relevant equations were the continuity equations for electrons and ions,the equations of motion and Poisson's equation;

$$\frac{\partial N}{\partial t} + \nabla \cdot (N \underline{V}) = Q - (\alpha N^2) \qquad (2.3)$$

$$m\frac{D\underset{\sim}{V}}{Dt} = q\left(-\nabla\Phi + \underset{\sim}{V}\times\underset{\sim}{B}\right) - \frac{\Delta P}{N} - m\underset{\sim}{V}(\underset{\sim}{V}-\underset{\sim}{U}) \qquad (2\cdot4)$$

$$\nabla^2\Phi = e(N_e - N_i)/\epsilon_o \qquad (2\cdot5)$$

where Q and $(\propto N^2)$ are the production and recombination rates,$\propto$is the

recombination coefficient,D/Dt is the convective derivative,U is the neutral

particle velocity,$\tilde{V}$ is the particle collision frequency,P is the pressure,

Φ is the electric potential, q is the electronic charge, $\underset{\sim}{V}$ is the drift

velocity.

Ignoring the ion drift velocity in comparison with the electron drift

velocity,$\underset{\sim}{V}_{ed}$,then the angular frequency ω,of the irregularity was shown to

be $\qquad \omega = \underset{\sim}{k}\cdot\underset{\sim}{V}_{ed}/(1 + A_{LP}) \qquad (2.6)$

where $A_{LP} = (\tilde{V}_e \tilde{V}_i)/(\Omega_e \Omega_i)$ $\qquad \underset{\sim}{k}$ = wavevector $\qquad \Omega =$ gyrofrequency

The variation of angular frequency with aspect angle is analysed in chapter

5.Typical values of the auroral parameters at height of 110 km are,as in ref

(85),1983,by Andre,as follows;the equatorial parameters are from ref(119),

1979 by Keskinen et al.

	AURORAL ELECTROJET	EQUATORIAL ELECTROJET
Electron gyrofrequency	$9.5\ 10^6$ rads/sec	$5.3\ 10^6$ rads/sec
Ion "	170 rads/sec	96 rads/sec
Electron collision frequency	9000/sec	40000/sec
Ion " "	1500/sec	2500/sec

A typical value of magnetic field strength at these auroral heights would be

54000 nanoTesla.The variation of echo strength with magnetic field strength

is analysed in Chapter 5.

The aspect of the two-stream instability process which is of particular

relevance to the SABRE spectral analysis section of this Thesis,is the

variation with height of the threshold electric field necessary for the

production of the irregularities.A complete analysis of this variation may

be found in ref(54),1970,by McDiarmid or ref(109),1979,by Moorcroft,but the

SCHEMATIC ILLUSTRATION OF THE HEIGHT DEPENDENCE OF THE THRESHOLD
ELECTRIC FIELD FOR THE TWO STREAM INSTABILITY.

AURORAL HEIGHT IN KILOMETRES.

ELECTRIC FIELD STRENGTH IN MILLIVOLTS/M
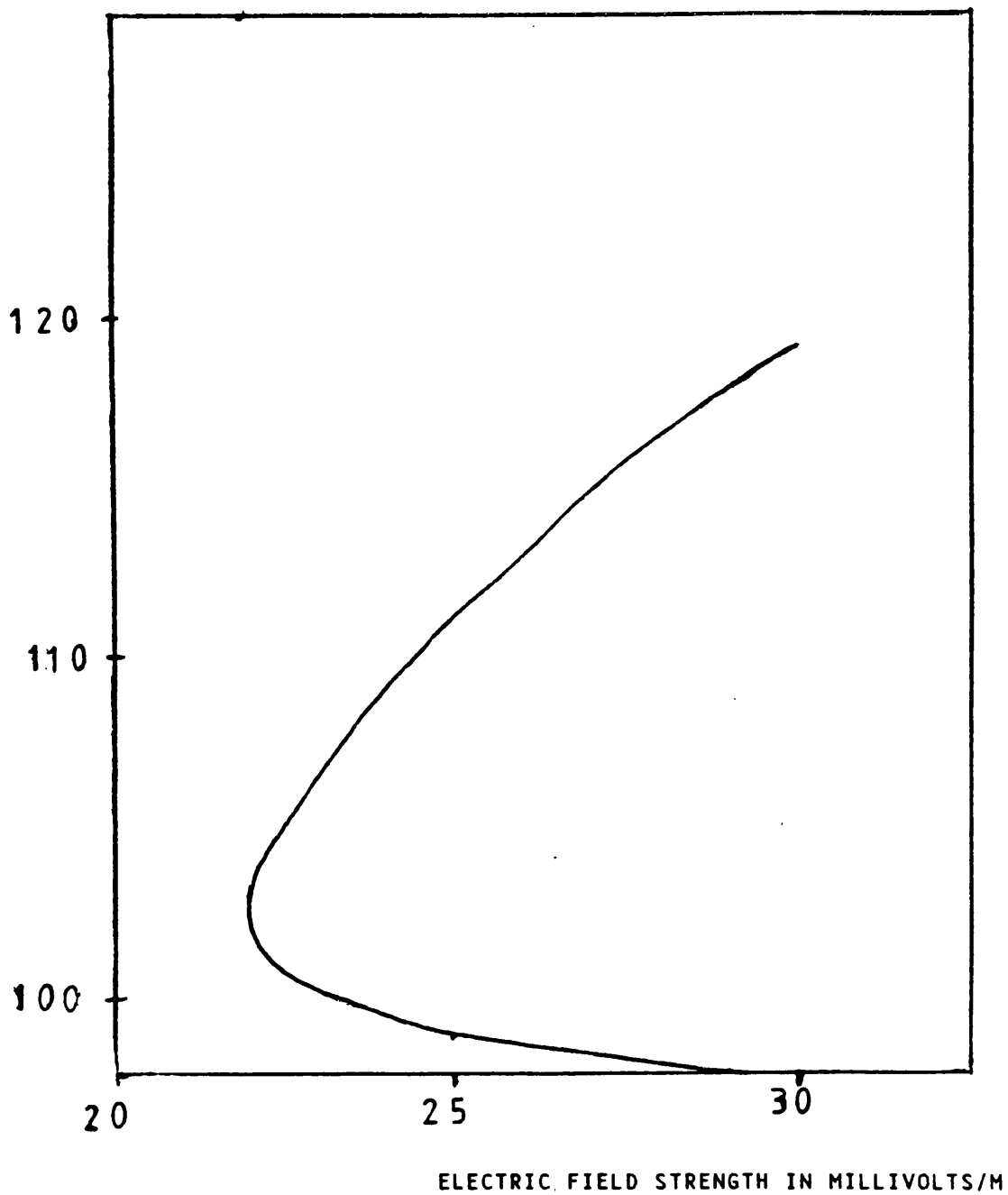
FIGURE 2.6

height characteristics are illustrated schematically in fig(2.6),for 150 MHz operation. Sudan et al,ref(110),1973,also predicted that growth rate of the irregularities and auroral backscatter intensity would maximise near 105 km.

A spectrum of a typical two-stream instability process is displayed in fig(2.7),and is sometimes referred to as Type 1.

The gradient drift instability has been proposed as being capable of producing electron density irregularities within the electrojet plasma,whenever a strong density gradient exists (i.e. between one band of ionization and another band which is less ionised),in the direction of the electric field and at right angles to the magnetic field . Electrons and ions will drift together along the direction of the electric field,with the electron velocity being greater than the ion velocity.If a perturbation disturbs the boundary then it is possible for the polarization fields associated with the perturbation to interact with the electron flow to produce an enhancement of the perturbation.

Fejer and Kelly,ref(111),1980,have derived an expression for the gradient drift irregularity threshold velocity,V_{D1},as follows;

$$V_{D1} > (L_N/\cos(I)) ((2 \, \alpha N_e/5.5) + 8.2/\lambda^2) \qquad (2.7)$$

where I=magnetic dip angle

α=recombination coefficient

N_e=electron density

L_N=vertical gradient scale length

λ^2=the square of the operating wavelength.

A spectrum of a typical gradient drift instability is illustrated in fig(2.7) and is sometimes referred to as Type 2 spectrum. With this type of instability,plasma waves can be created at drift velocities below the ion-acoustic velocity,as well as above,perpendicular to the magnetic field. Generally,the theoretical analysis of radar auroral irregularities has been based upon electric fields for the generation and growth of the plasma wave backscatterers. None of these theories have produced a definition of the

SCHEMATIC ILLUSTRATION OF TYPICAL RADAR AURORA DOPPLER VELOCITY

POWER SPECTRA.
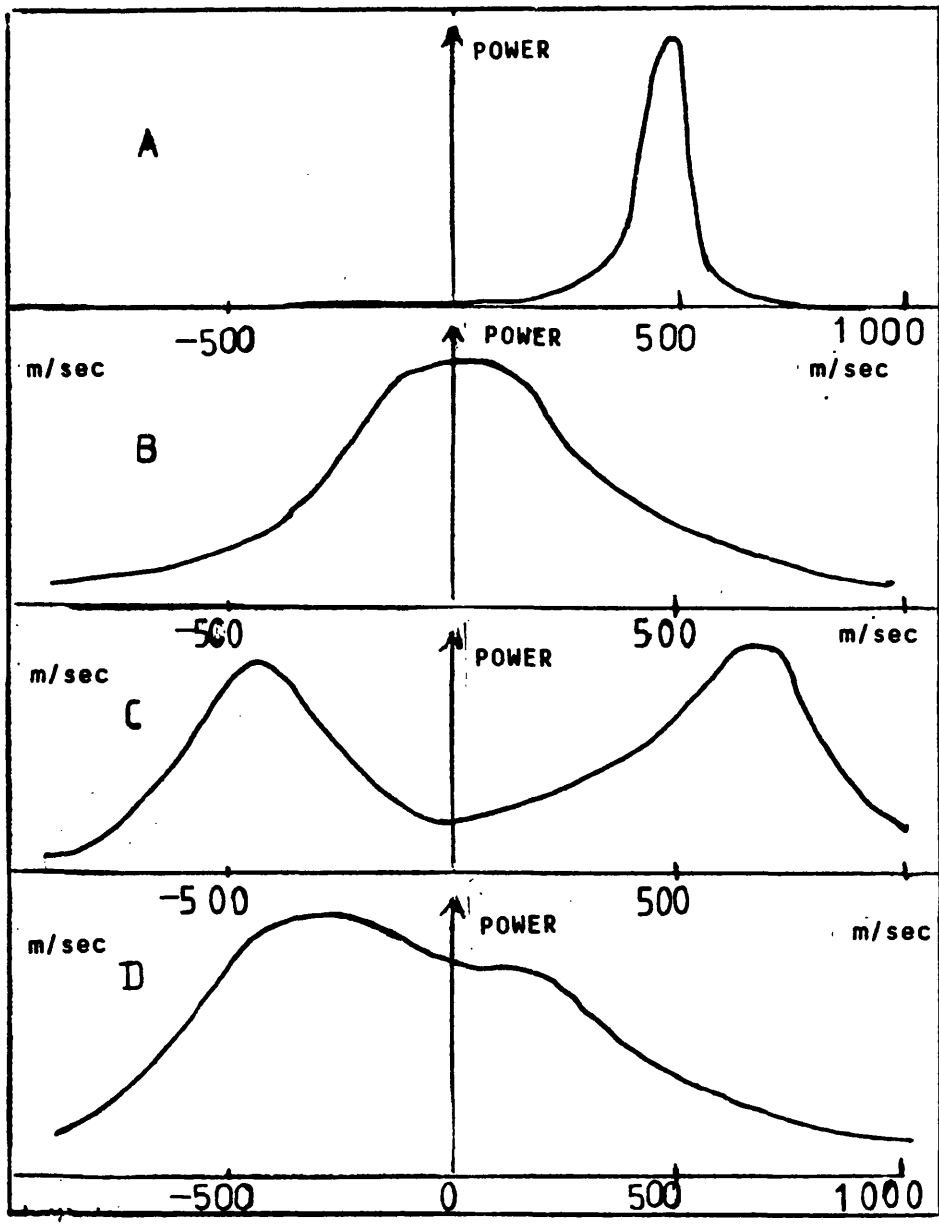
FIG(A) : TYPE 1 SPECTRA   DOPPLER VELOCITY

FIG(B) : TYPE 2 SPECTRA   m/sec

FIG(C) : DOUBLE-PEAKED SPECTRA

FIG(D) : DOUBLE-PEAKED SPECTRA,UNEQUAL.

FIGURE 2.7

back-scatter cross section of the irregularities,however.Farley,ref(132),
1971,predicted that the average radar cross section is proportional to the
square of the absolute value of D_N,where D_N is the difference between the
local electron density and the mean electron density.Ferch and Sudan,ref
(128), 1977,predicted that the relationship between the propagation
angle,P_A, and the electron density fluctuation,D_N,for a frequency of 100 MHz
was as follows;

$$\log \left| D_N \right|^2 \propto 1 + 0.2 \cos(2\, P_A)\tag{2.8}$$

Haldoupis et al, 1982, ref(133),however,indicated that the back scatter
cross section may be directly related to the conductivity.

The backscatter cross section of 2-stream irregularities has been studied by
Ierkic et al,1977,ref(107),for the equatorial electrojet and by Haldoupis
and Nielsen,1984,ref(86),for the auroral electrojet.Generally, 2-stream
irregularities have a narrow spectrum and relatively high velocity, (> 350
m/sec),and have a minimum cross-section at flow-angles of $\pm$ 90
degrees.Gradient Drift irregularities have a broad spectrum and an isotropic
back-scatter cross section,as illustrated in schematic form,in fig (2.8).
The variation of the cross-section amplitude with flow-angle as displayed in
fig (2.8) is for illustrative purposes only, and will vary with auroral
activity; as will be seen in chapter 5, some gradient drift irregularities
may provide very large echoes.

Both types of instability process require a relative drift of the
electrons and ions and in both processes the most unstable irregularities
will propagate in the direction of the electron drift at approximately the
electron drift velocity. If this electron drift velocity is denoted V_D,in a
direction perpendicular to the electric and magnetic fields,E and B,then the
following relationship can be assumed;

$$\underset{\sim}{V}_D = \frac{(\underset{\sim}{E} x \underset{\sim}{B})}{B^2}\tag{2.9}$$

In practice,once gradient drift irregularities are generated,non-linear

SCHEMATIC ILLUSTRATION OF THE THEORETICAL VARIATION OF
BACKSCATTERED POWER WITH FLOW-ANGLE FOR THE TWO MAIN
INSTABILITY PROCESSES.
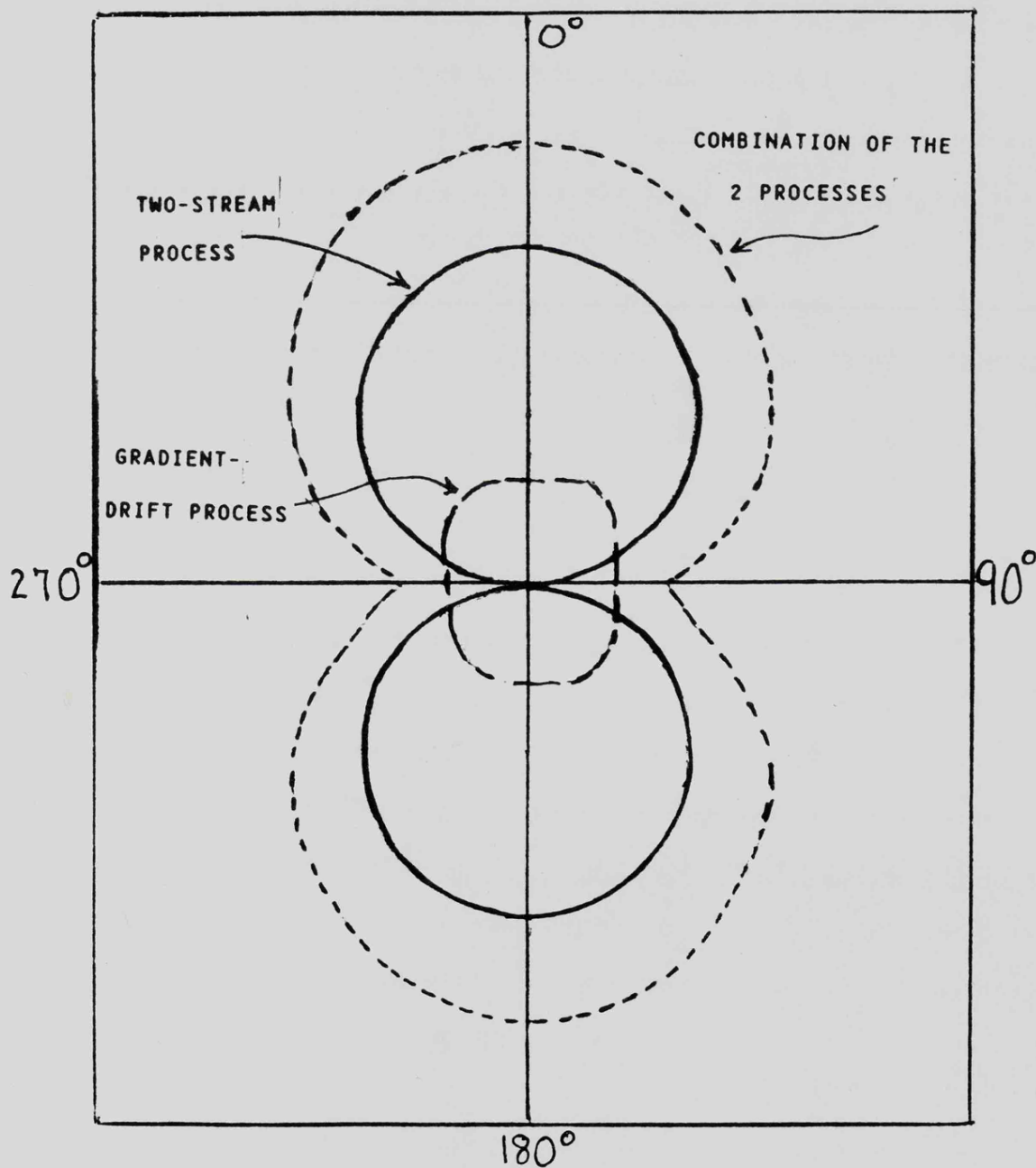
FIGURE 2.8

processes can generate further irregularities that will propagate at all angles in the plane perpendicular to the magnetic field.

Generally,gradient drift irregularities have been observed to be more strongly excited at the larger wavelengths,of the order of tens of metres and these are assumed to be the initially formed instability,from which other structures of shorter wavelength are developed.

For the purposes of this survey it will be assumed that a general spectral analysis of the auroral signals may be undertaken using the concepts of Type 1 and 2 spectra and the simple relationship between the drift velocity,electric and magnetic field strength in equation (2.9) .

2.6 Previous work in auroral radar relevant to this Thesis

In order to examine the measured radar signal characteristics a brief general review of auroral radar systems and results which have been reported in recent years,will now be undertaken.This summary concentrates upon the main features and techniques relevant to the analysis of the SABRE data.

Early investigators of the ionosphere who recorded the reflection of radio signals from the auroral ionosphere included Harang and Stofftegen,1938,ref(38) and Q.S.T.,volume 23,1939,ref(39).Early experimenters were concerned with the reflecting properties of the aurora for VHF and HF propagation,which enabled radio amateurs to communicate over great distances. Most of the early radar investigators employed relatively long pulse-widths,very basic spectral analysis systems and,often,wide beam widths. The high time and spatial resolution necessary for the detailed investigations were not available in the early work and hence this review has concentrated on relevant developments since 1975.

The results of recent work in radar aurora which are relevant to this Thesis can be subdivided as follows:

a) Auroral height b) Aspect-angle loss c) Electrojet velocity spectra

d) Electric field strength e) Anisotropy of backscatter cross-section.

a) Recent published results for auroral height.

The determination of the altitude of the auroral irregularities is fundamental in establishing the region of the ionosphere in which the current flows.Unwin and Johnston,ref(84),1981,have reported their investigations of the height dependence of the diffuse aurora power spectrum,by means of a 50.5 MHz auroral radar in New Zealand,latitude $46^{\circ} 40'$ South. This radar provides height information by means of a multi-lobed narrow beam antenna radiation pattern which is obtained as a result of interference fringes in a Lloyd's mirror technique. The Lloyd's mirror effect (due to the presence of a strong reflector in front of the radar) is produced by mounting the radar antenna on top of a cliff with the sea-surface 136 metres below.Their measurements showed that the Eastward electrojet echoes were centred at 106 km and 112 km in the Southern hemisphere.

Similarly Kamide and Brekke,ref(76),1977,reported height measurements at Chatanika (latitude 64.9° North) of 101 km for the eastward electrojet,119 km for the westward. The radar employed was the Chatanika incoherent-scatter facility operating at 1300 MHz.Height measurements were derived by accurately monitoring slant range whilst the narrow pencil-beam was tilted at a known angle from the vertical.

Timofeev and Miroshnikov,ref(112),1982,obtained auroral height measurements by means of a double interferometer operating at 90 MHz above a lake surface in order to produce the Lloyd's mirror interference pattern at a latitude of 63° North.They reported auroral heights of between 103 km to 117 km. The westward electrojet had an average height which was approximately 2 km higher than the eastward.

In this Thesis,measurements have been made of the altitude of the auroral irregularities of 1 metre scale length,with the SABRE radar system,and these

have been compared with the results of previous workers.

b)Recent published results for aspect-angle loss.

The measurement of aspect-angle loss provides an indication of the extent of the auroral viewing area of a radar system because of the loss in echo power to be expected whenever the radar beam is not orthogonal to the magnetic field line. Ecklund et al,ref(73),1975,reported using two widely-spaced 50 MHz Doppler radars to examine simultaneously an area of diffuse aurora.One radar was located at Anchorage,Alaska,and the other radar was a portable system located at Aniak.The two narrow beams crossed in an area of side 40 km and their angular separation was approximately 43 degrees.The aspect angle so derived was 8 dbs per degree. However,earlier researchers have derived aspect angle losses of up to 10 dbs per degree.

Leadabrand,et al,1967,ref(64),had derived aspect angle losses of up to 10 dbs per degree for radar frequencies in the range 50 MHz to 3000 MHz,whilst McDiarmid,1972,ref(63),determined the value to be less than 2 dbs per degree.

By careful examination of the radar equation magnetic field model for the SABRE radar latitudes,it was considered possible to derive a more exact aspect-loss figure for operational frequencies of 150 MHz.

c)The polar electrojet velocity spectrum.
Analysis of the electrojet velocity spectra can provide an insight into the plasma physics and irregularity processes within the aurora.Evidence of radar echoes at 143.5 MHz due to the two-stream instability,and of double-peaked spectra was reported by Comnitz et al,ref(50),1969.In the same year Abell and Newell,ref(51),reported evidence of both the two-stream instability and of velocity "plateaux",as displayed schematically in fig (2.9), whilst operating a 1295 MHz radar in Massachusetts. The same radar was employed in 1971 by Hagfors,ref(56),with a double-pulse spectral

analysis technique,who found evidence of both broad (ie Type 2) and two-stream (ie Type 1) spectra, as illustrated in fig(2.7).

In more recent years the auroral power spectra have been determined by the Stare radars,at VHF. The Stare radar is the direct fore-runner of the SABRE radar and is fully described in ref(77),1978 by Greenwald et al.Of particular interest is the recent modification to the velocity measuring system which enables 11 values of double-pulse-pairs to be incorporated into the spectral analysis,which allows the power spectrum to be obtained. Whitehead et al,ref(88),1983,found that this 11-pulse pair spectral analysis revealed an asymmetry of the evening velocity spectrum which was attributed to the probable existence of two auroral waves,at different heights,but having different line-of sight-velocities.

Nielsen et al,ref(89),1984,also employed this 11 pulse-pair analysis and found two auroral radar types;

1. Broad spectra:of width up to 1200 m/sec,observed only for flow angles of,typically,greater than 70 degrees.The width increased with increase of drift velocity.

2. Narrow spectra:of width up to 400 m/sec,observed at small and at large flow angles.The width was insensitive to variation of flow angle or drift velocity.

The observed spectral asymmetry was attributed to back-scattering from regions of different heights,and the variation of spectra with flow angle was associated with auroral flow turbulence.

Although types 1 and 2 spectra (as displayed in fig (2.7), have been seen in the radar aurora of VHF radars,certain other spectral shapes have also been seen which do not fit so well with the basic two-stream or gradient drift theories.It was thus evident that a detailed analysis of the SABRE echo and velocity data might add to the overall spectral picture,especially if height information could be included.

d) Measurements of electric field strength.

The assessment of electric field strength within the auroral electrojet is essential in compiling an overall picture of the plasma physics characteristics in the auroral regions.

The values of electric field strength most applicable for comparison with the SABRE radars would be those of the Stare radars.For example,Greenwald,et al,ref(77),1978,have reported values of 30 to 50 millivolts per metre,as derived from the Stare velocity data.The Stare auroral velocity measuring technique has been compared with the results of the Eiscat velocity measuring system,as reported in ref(87),by Nielsen and Schlegel,1983. The Stare velocity vector directions were in good agreement with those of the Eiscat velocities, but the accuracy of the estimated velocity was dependent upon the flow angle and the velocity magnitude. The accuracy was highest for velocities below 700 m/sec. Suggestions for improving the velocity measuring technique of the SABRE radars are presented in chapter 9, but generally the electrojet velocities examined in this Thesis are below 700 m/sec and will not require the small corrections described in this reference.

Most recently,(1983), the high latitude incoherent scatter radars,Eiscat,Millstone Hill,Chatanika,together with the Stare radars have made a series of coordinated measurements of the global structure of the high latitude plasma convection,and a review may be found in ref(106), 1983, by Greenwald.

The electric field vectors can be determined from the SABRE measurements of irregularity flow. These are of considerable interest since they relate to the sub-auroral region,(L=4 to L=6).Recent theories of the magnetospheric processes suggest that large E-fields can exist at these latitudes, a prediction that has been partly confirmed by satellite measurements. A review of such measurements may be found in ref (125),by Heelis,1982.

e)Anisotropy of auroral back-scattering cross-section.

Investigation of the variation of the radar auroral back-scatter cross-section with viewing angle can lead to a better understanding of the geophysical processes involved in the generation of irregularities.

Previous workers in this field include Haldoupis and Nielsen, ref(86), 1984.Their results showed the auroral back-scatter cross-section to be highly anisotropic,with the largest value in the direction of the electron drift velocity.The direction perpendicular to this drift velocity showed a broad minimum.

Similarly,Ierkic et al,ref(107),1977,found that the Type 1 irregularity cross-section of the equatorial electrojet peaked when the radar beam was almost parallel to the electron flow.

In the analysis section of this Thesis,the effect of the variation of electrojet cross-section with flow-angle is deduced from analysis of the digital signal data.The variation is then compensated when assessing the values of aspect-angle loss, as described in chapter 4.

2.7 A summary of Radar investigations of the Equatorial Electrojet.

The characteristics of the plasma irregularities in the equatorial electrojet have been investigated with radar techniques by several research teams.The Jicamarca,Peru,radar systems have been extensively employed and have provided information concerning the radar spectra which is of interest as a comparison with the auroral radar spectra discussed in this Thesis.

The Jicamarca incoherent scatter radar system,operating at 50 MHz,with vertical beams,was originally utilised to study the equatorial electrojet by researchers including Balsley,1969,ref(90),and Farley and Balsley, 1973,ref(91). A modification to the radar system in the form of a narrow-beam antenna,pointed 25 degrees east of vertical enabled investigation of the spectra at different heights within the electrojet,by accurate measurement of the slant-range.This modification was reported by

Fejer et al,1975,ref(92).   The altitude resolution achieved was 1.1 km,and

day-time observations revealed that the Doppler shift maximized at a height

of 104 km. Rocket experiments in the Indian zone of the equatorial

electrojet,as reported by Prakash et al,1971,ref(93),had indicated that the

maximum drift velocity occurred at about 105 km,which supported the radar

observations at Jicamarca,as did the rocket measurements at Peru,reported by

Richmond,1973,ref(94).   The spectra of the radar echoes were found to

change drastically with altitude,especially when echoes were strong and

velocities high.   Type 1 irregularities were observed only in the upper

portion of the electrojet,above about 105 km. No daytime echoes were

observed at heights of a few kilometres above 107 km which was the height of

maximum Type 1 power. The maximum Type 1 Doppler velocity detected was about

500 metres per second,with stronger echo power in the morning.

One basic difference between radar spectra measured in the aurora and in

the equator is the variation of Doppler velocity with flow-angle (i.e. the

angle between the mean irregularity drift direction and the radar beam

vector).Balsley,1969,ref(90),has reported that the Doppler velocity varies

as the cosine of the flow-angle for Type 2 irregularities at the equator,but

not for Type 1 events.   Type 1 irregularity velocities exhibit

plateau-like structures as the flow-angle is varied,with constant velocities

separated by transition regions,as in fig(2.9). These Type 1 irregularities

appear to propagate at approximately the ion-acoustic velocity in the

equatorial electrojet,suggesting that the electron drift velocity does not

greatly exceed the ion drift velocity.

Similar velocity plateaux have been observed in the auroral region,when

employing UHF radar systems,by Moorcroft and Tsunoda,1978,ref(95).

But,noticeably higher Type 1 velocities have been reported by the Stare

radars in the auroral regions,employing VHF radars. Greenwald,et

al,1978,ref(77),measured velocities as high as 2000 metres per second,with

no plateaux.

SCHEMATIC ILLUSTRATION OF DOPPLER VELOCITY PLATEAU.
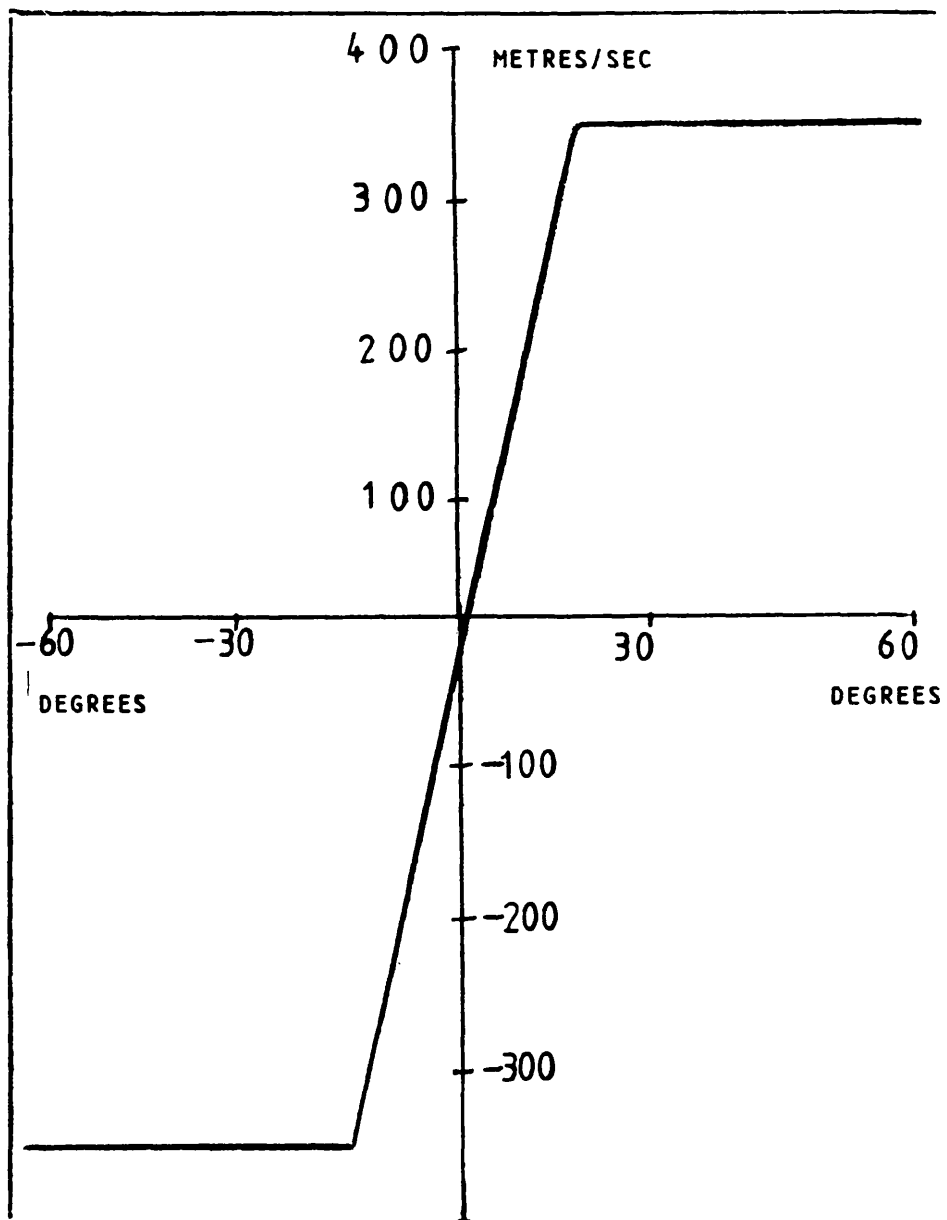
HORIZONTAL AXIS : ANGLE IN DEGREES BETWEEN RADAR VECTOR AND

THE MERIDIAN

FIGURE 2.9

At the time of writing this Thesis,(1984),no detailed explanation of the differences in radar spectra between the auroral signals and equatorial signals has been proposed.

2.8 A summary of the features of the radar aurora.

The conclusions of the radar studies of the aurora which have been outlined in this general review can be summarized as follows:

1. The auroral electrojets are confined to heights between 100 to 120 km.

2. For the stronger levels of magnetic activity,the electrojets may extend as far equatorwards as L=4, and,occasionally, to < 4.

3. The direction of the electrojet irregularity flow in the northern hemisphere will be westward in the afternoon period (local time) and eastward in the midnight period (local time).These two periods will be separated by the Harang Discontinuity and Morning Cleft events,as in fig(2.3).

4. The maximum Doppler velocities attained within the electrojet will be of the order of 2000 metres per second.

5. The echo signal strength and velocity will be dependent upon the viewing angle of the radar beam with respect to the directions of the electrojet.

6.The general order of magnitude of the velocities and electrojet directions as deduced from radar data,particularly Stare,is in agreement with those values deduced by other techniques,including rockets.

7. Stronger auroral echoes indicate only a small change in polarization direction,whereas weaker echoes show a large change. This topic is examined in more detail in refs(61),1971 and(62),1974,by Sofko and Kavadas.

8. Some auroral echoes can be associated with visual auroral patterns,but not all.Greenwald et al,ref (68),1973,found association between discrete auroral echo forms and some visual aouroral patterns.

9. Radar frequencies of up to 3000 MHz(but generally not below about 30 MHz) can be used to study the aurora and the signals are generally stronger

at the lower frequencies. At the higher frequencies,(ie UHF),the variation

of Doppler velocity with viewing angle may differ from the variation when

employing VHF

10. The radar beam must be directed so as to be orthogonal (to within about

five degrees) to the line of magnetic force at the aurora, since the plasma

irregularities propagate at right angles to the magnetic field.

This general review of the features of radar aurora will now be followed

by a description of a VHF auroral radar which employs the most modern

techniques and has been in operation since 1981, the SABRE radar.

2.9 <u>A description of the SABRE auroral radars.</u>

The Stare and SABRE radars are the most advanced coherent radar

facilities yet constructed for studies of the radar aurora.They consist of

two phased-array radars which are capable of high time and spatial

resolution. The SABRE radars are located at Wick (Scotland) and Uppsala

(Sweden) and their viewing areas (L-values 4 to 6) are illustrated in

fig(2.10). The SABRE radars are based upon the Stare radars which are

fully described in ref(77) 1978,by Greenwald et al,and which have been

employed to investigate radar aurora in the region of L-value 6 to 8. The

system features of the SABRE and Stare radars are as follows:

LOCATION	FREQUENCY	WAVELENGTH	IRREGULARITY SCALE

<u>SABRE</u>

Wick	58.27^{o} N	153.2 MHz	1.958 m	0.979 metres
	3.6^{o} W			
Uppsala	59.41^{o} N	142.585 MHz	2.104 m	1.052 metres
	17.4^{o} E			

<u>STARE</u>

Malvik	63.1^{o} N	140.0 MHz	2.143 m	1.071 metres
	11.8^{o} E			
Hankasalmi	62.0^{o} N	143.8 MHz	2.086 m	1.04 metres
	26.2^{o} E			

SABRE VIEWING AREAS.

Illustrating the viewing areas of the SABRE radars in relation to magnetic L-shells.
Coordinates are geographic.

- Auroral radar site.
- ○ Magnetometer site (I.G.S)

FIGURE 2.10

Each of these radars have fixed horizontal-dipole arrays which provide a relatively broad transmitter beam and 16 narrow receiver beams. Each radar system array comprises a transmit array and a receive array,both tilted backwards 6 degrees from the vertical in order to reduce ground-plane effects,as displayed in fig (2.11).The transmitter array consists of two vertical stacks of four 8-element Yagi antennae fed in-phase from an eight-to-one power divider.The vertical separation between the Yagi antennae is 2 metres and the horizontal separation between stacks is 0.75 wavelength.The value of 0.75 wavelength was chosen so as to minimise the gain of the transmitter array in the direction of the receiver array.The receiver array consists of 64 8-element Yagi antennae arranged in 16 vertical stacks,with spacing between antennae in each vertical stack being 2 metres,and with separation between stacks of 1 wavelength.Signals from the Yagi antennae of each vertical stack are combined and then amplified by 30 dbs gain,low-noise preamplifier situated on the mast supporting the stack.

The outputs of the 16 pre-amplifiers are connected to a 16-port Butler matrix as displayed in the block diagram of the SABRE radar in fig (2.12).This unit is a passive network which provides the necessary phase-lag combinations between the 16 inputs to simultaneously form 16 antenna beams.A full description of the couplers and phase-shifters which comprise a Butler matrix can be found in ref(96),1972,by Skolnik,page 11-68.Each of the beams,or lobes, formed by this matrix has a half-power beamwidth of 3.2 degrees,an angular separation of 3.6 degrees. By producing 16 radar beams simultaneously,it is possible for the radar system to investigate 16 different directions simultaneously. However,because of the reduced sidelobe isolation of the outer beams,only the central 8 are used in practice. To reduce the sidelobe levels of these beams,the gain of the pre-amplifiers on the outermost stacks have been slightly reduced,until in practice,sidelobe levels of about 20 dbs have been attained.The Stare radar antenna polar

THE SABRE RECEIVER ARRAY
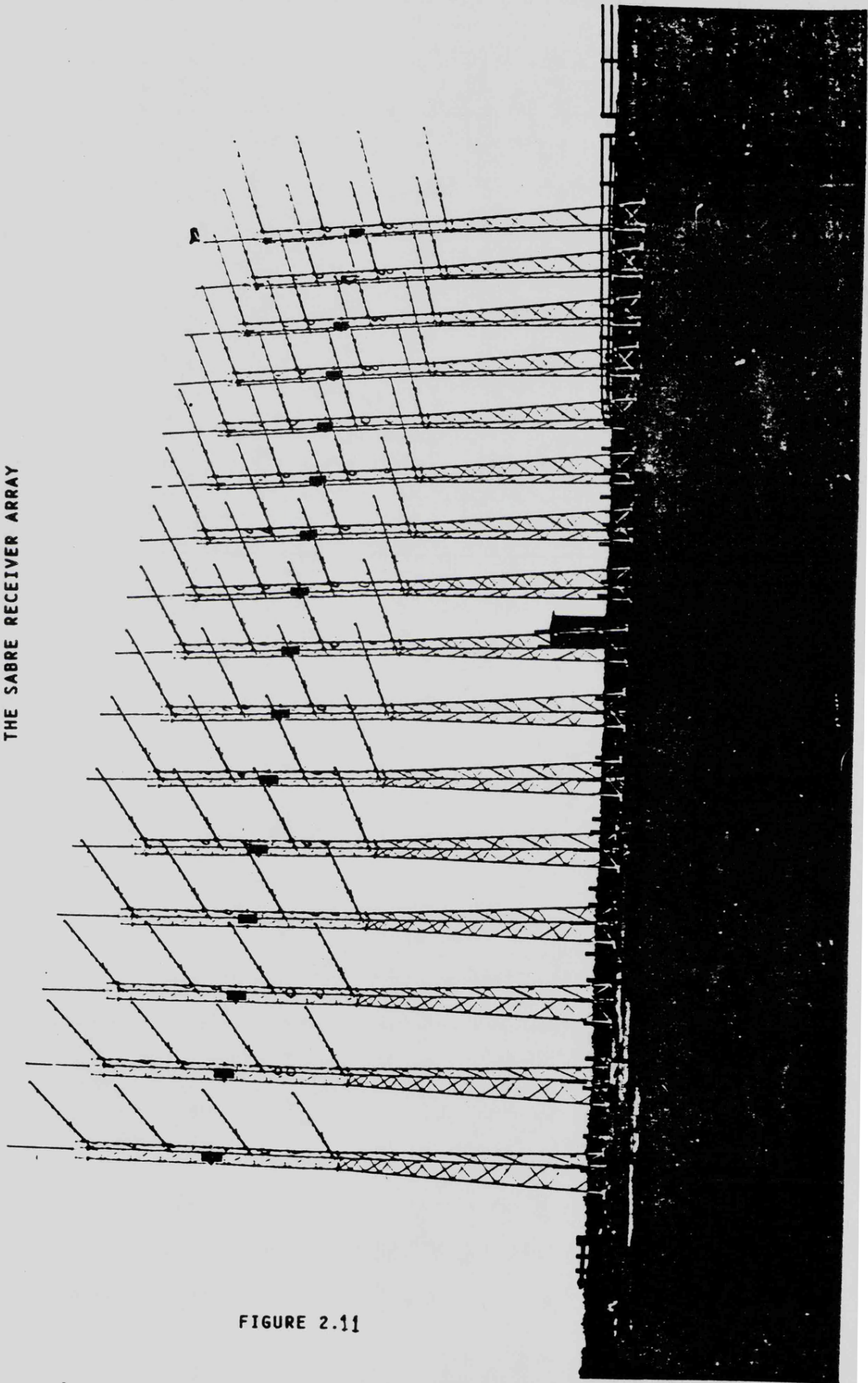
FIGURE 2.11

BLOCK DIAGRAM OF SABRE RADAR.

FIGURE 2.12
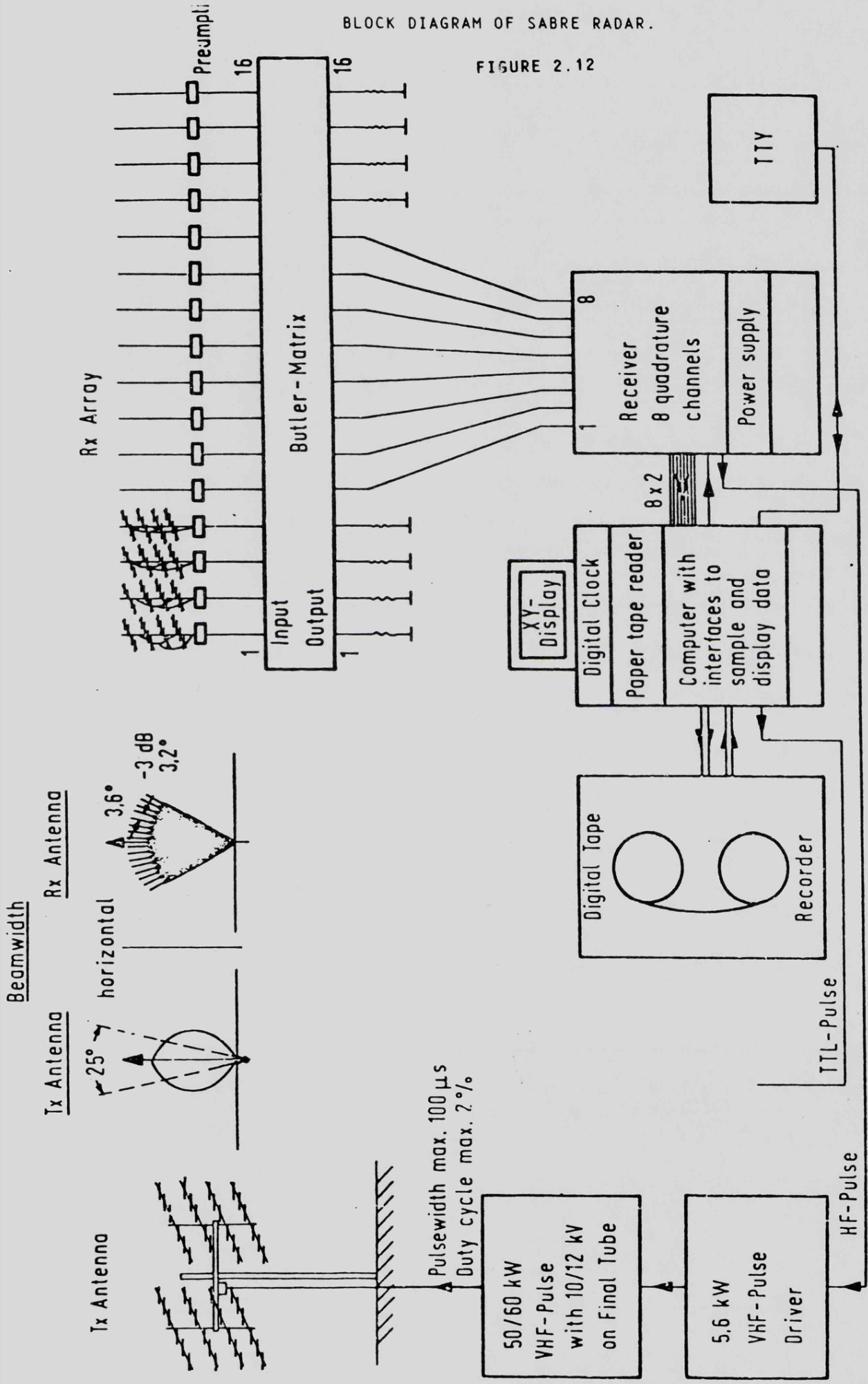
diagrams have been calibrated using airborne transmitters,and full details are available in ref(108),by Nielsen et al,1983.

The 8 outermost beams from the Butler matrix are terminated in 50 ohms,and the inner 8 beams are connected to an 8-channel phase-coherent receiver.Each channel has a noise figure of 3.5 dbs which includes the effects of the pre-amplifier,Butler matrix and cable losses. The receiver down-converts the echo signal to the intermediate frequency,(IF),and the signal amplitude and phase is determined by pairs of in-phase and quadrature phase-sensitive detectors. The output stages of each channel are low-pass active filters matched to either 50 or 100 microsecond transmitter pulse, and the amplification is controlled by the on-line computer.A schematic block diagram of the SABRE receiver is displayed in fig(2.13),but more complete information can be found in ref (77),1978,by Greenwald et al.

The on-line computer,a Nova 3.12,controls the transmitter,receivers,and all system timing.The transmitter is controlled so as to produce a single-pulse,double-pulse sequence,as illustrated in fig(2.14),with each pulse length normally being 100 microseconds.For investigation of the shorter range returns,however,50 microsecond pulse lengths can be employed. The pulse-pair separation is normally 300 microseconds,but for certain spectral investigations it is possible to arrange for the variation of pulse pair separation,on both Stare and SABRE radars as described more fully in ref(89),1984,by Nielsen et al or ref(88),1983, by Whitehead et al.

The outputs of the quadrature phase detectors are sampled by a pair of high-speed multiplexed 8-bit bipolar A to D converters; one for the 8 in-phase channels,one for the 8 quadrature channels.The digital samples of the single pulse signals backscattered from the aurora are taken at times corresponding to radar ranges of between 495 km to 1230 km,with spacing between samples equal to the transmitted pulse length.Normally 49 ranges are sampled after a delay of 3.4 milliseconds and an additional sample is taken at range beyond the maximum range for auroral backscatter. This additional

BLOCK DIAGRAM OF SABRE RECEIVER.
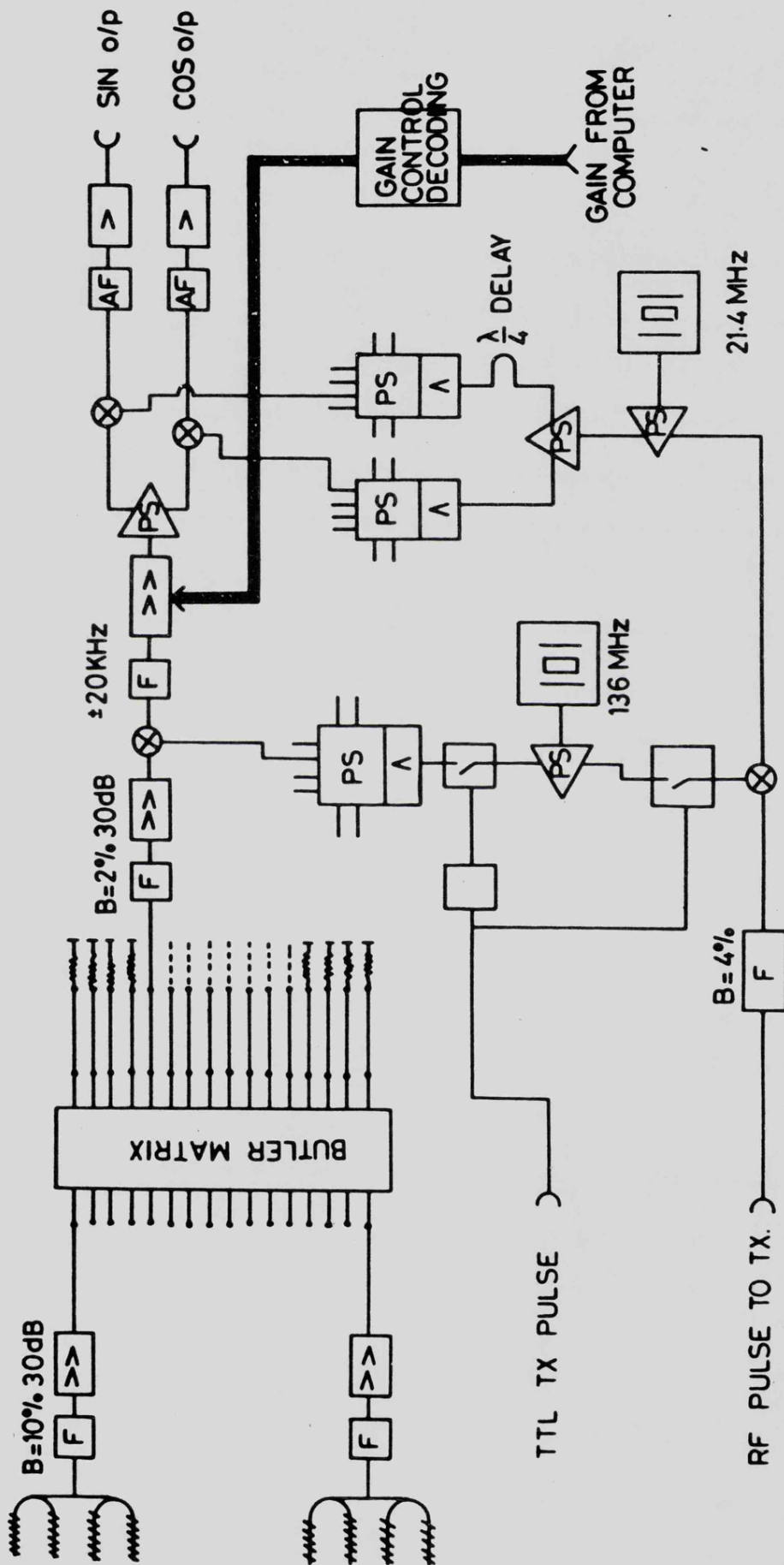
FIGURE 2.13 BLOCK DIAGRAM OF SABRE RECEIVER.
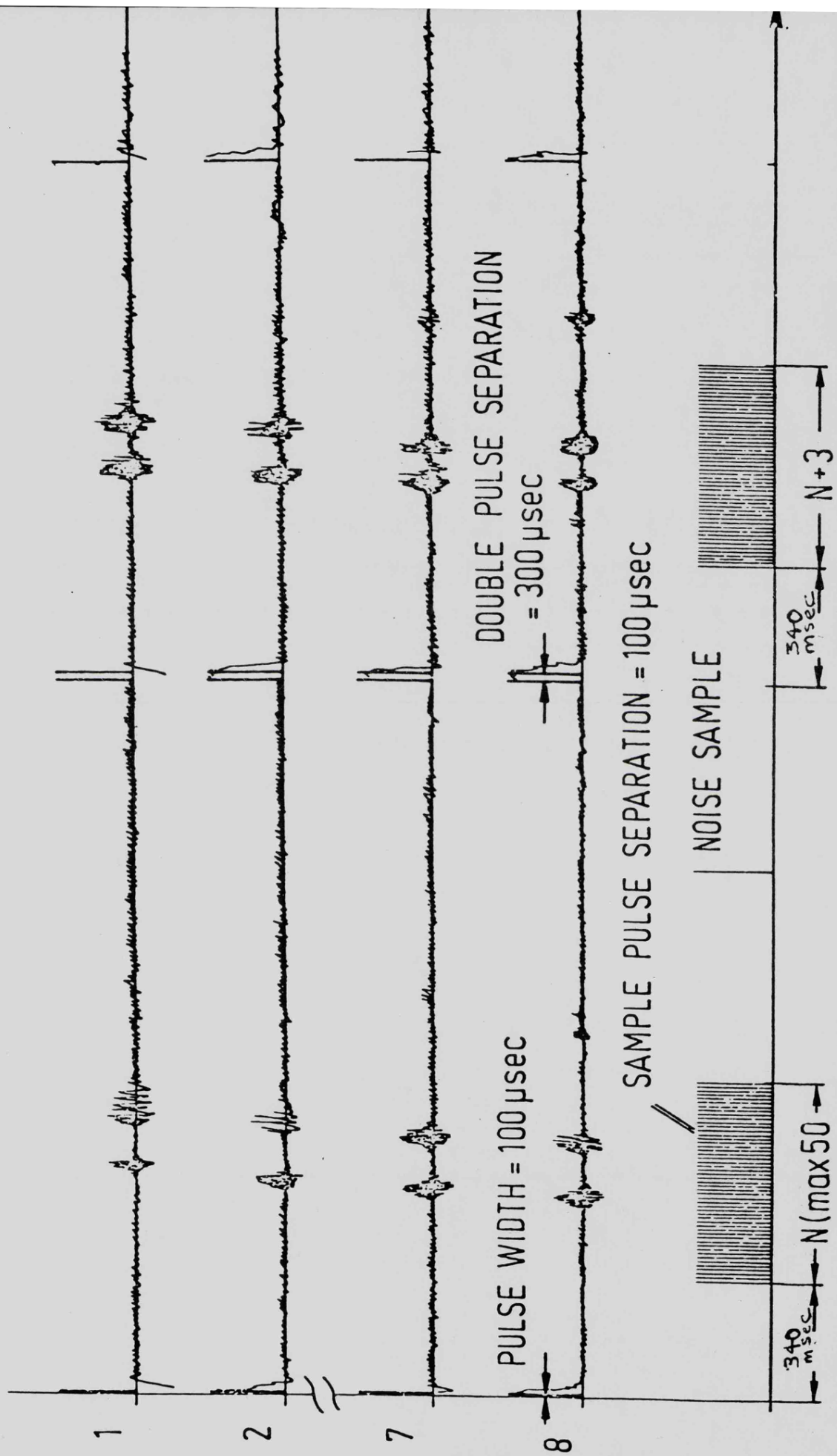
FIGURE 2.13

Figure 2.14 SABRE pulse sequence.

sample provides an accurate noise level for each of the receiver channels and its associated radar beam.

The backscattered power level from a given range and beam is given by:

$$P(N,r) = I^2(N,r) + Q^2(N,r) \tag{2.10}$$

where $I(N,r), Q(N,r)$ are the in-phase and quadrature outputs for beam N, at range r.

The double-pulse data samples are used to calculate the following expressions:

$$R(N,r) = I(N,r)\, I(N,r+3) + Q(N,r)\, Q(N,r+3) \tag{2.11}$$

$$I(N,r) = I(N,r+3)\, Q(N,r) - I(N,r)\, Q(N,r+3) \tag{2.12}$$

where $R(n,r)$ and $I(N,r)$ are the real and imaginary parts of the double-pulse autocorrelation coefficient, normally taken for 53 ranges.

The 3-pulse sequence repetition frequency is approximately 20 Hz and is limited by the computing time required to carry out the necessary calculations. The power values and the autocorrelation coefficients for the 50 ranges in each of the 8 beams are integrated and averaged over a period of 20 seconds in order to improve the statistics of the backscattered signal. At the end of each 20-second integration period the mean power levels are used to adjust the gain of the receiver, if necessary, as in fig(2.13). The SABRE receiver has a dynamic range of gain control of 50 dbs, adjustable before each integration period.

The Doppler velocity, V_D, of the backscattered signal is calculated from the expression:

$$V_D(N,r) = \mathrm{atan}\left| \frac{\overline{I(N,r)}}{\overline{R(N,r)}} \right| \frac{\text{wavelength}}{(4\pi\ (\text{pulse separation}))} \tag{2.13}$$

where (N,r) refers to beam number N, at range =r.

Each of the SABRE radars is capable of automatic operation and during one day of data recording the Doppler frequencies and backscatter power for each of the 50 range-cells of each of the 8 beams is stored on magnetic tape, amounting to a total of typically 6 megabits per day. Each block of data corresponding to a 20-second integration period is preceded by a set of

parameter data,as in Table (2.1),which specifies all of the relevant radar system parameters.These would include,for normal operation,the transmitter peak power of 50 kilowatts,pulse width of 100 microseconds,and amplifier gain. The Wick SABRE radar has had an additional system feature included,in that the system parameters can be monitored and modified,and data transferred,by means of a communications link via the public telephone network. This facility,called "Midnight Line",allows telephone subscribers unlimited data transmission time between midnight and 6 am,and permits the transfer of each day´s radar auroral data from Wick to Leicester University.By using this link,system parameters can be altered remotely without the need for personnel to undertake the 1300 mile round trip.

A typical data output from a single SABRE station is displayed in fig(2.15), in which the received signal strength for a single beam is plotted as a function of time and range.This type of data display is referred to as an "RTI" plot,i.e. Range,Time,Intensity plot.

A typical data output from the 2 radar systems (with the data merged for positions of radar beam overlap in order to determine auroral disturbance velocity),is illustrated in fig(2.16).This type of output is referred to as a "Stareplot". Further details of Stareplots can be found in ref(77),1978,by Greenwald et al.

One feature of the SABRE radar construction is the manner in which the transmissions have been designed to produce a minimum of interference to the surrounding areas.The transmitter employed at Wick SABRE site has been based upon a design described at length in ref(113),by Meade,1973.The output stage is a VHF triode,type 3CPX-1500-A7,and produces about 50 kilowatts peak power at a duty cycle of 0.6%,at a voltage of 8 to 9 kilovolts. The shape of the output transmitted pulse is computer-controlled so that the edges are not sharp,but approximate to a truncated Gaussian shape. In this manner the spectrum of the transmitted pulse is reduced and interference effects

PARAMETER	MEANING

TABLE 2·1

PARAMETER	MEANING
1	Length of parameter block in words
2	Year
3	Day (Julian calander)
4	Hour
5	Min Time this block was taken
6	Sec
7	Integration time in seconds
8	Number of averages taken
9	Nominal Tx power in KW
10	Pulse width in 10's of micro-seconds
11	Double pulse separation in 10's of micro-seconds
12	Number of ranges sampled
13	Delay to first range in 10's of micro-seconds
14	Inter sample gap in 10's of micro-seconds
15	No. of beams used
16	Most CCW beam
17	Rx attenuation in 10's of dB
18	Rx rise time in microseconds
19	Not used
20 - 33	Text identifying the radar
34	No. of samples in double pulse gap
35	Not used
36 - 46	For Wick radar only - operating parameters
47	Day ⎫
48	Hour ⎬ For Wick radar only -
49	Min. ⎪ time operating parameters written
50	Sec. ⎭

THE SLANT RANGES IN THIS FIGURE ARE BETWEEN 495 KM AND 1230 KM IN 60 KM STEPS
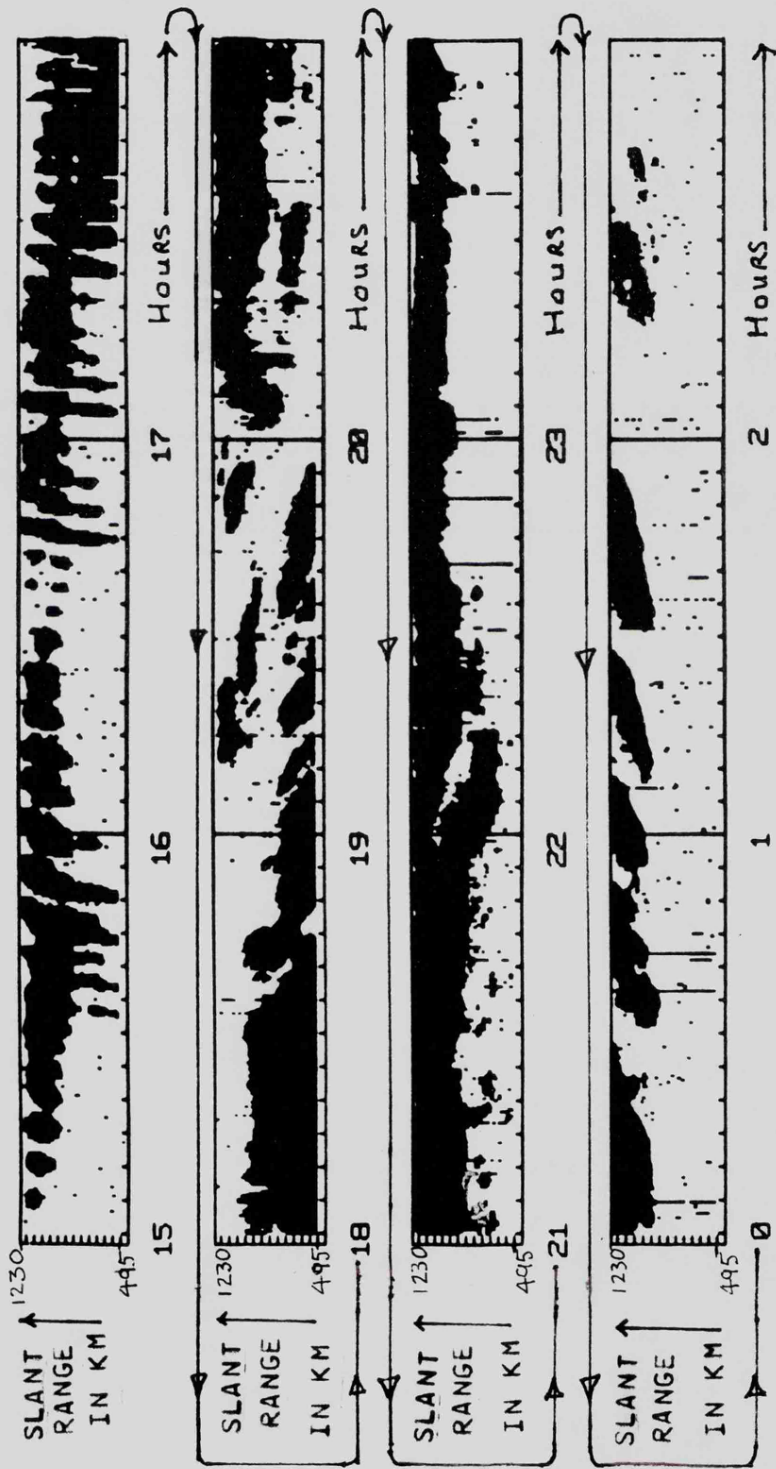
RTI PLOT FOR WICK   YEAR 1982   DAY 252-253   BEAM NUMBER 5

Figure 2.15
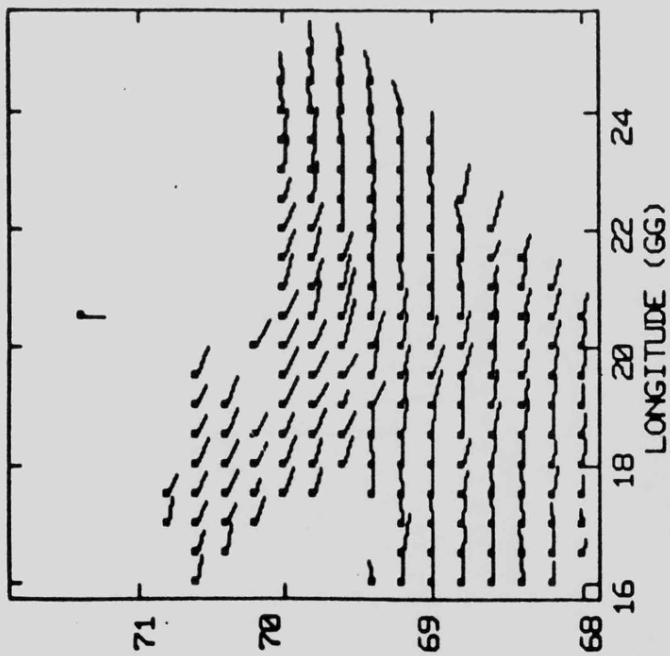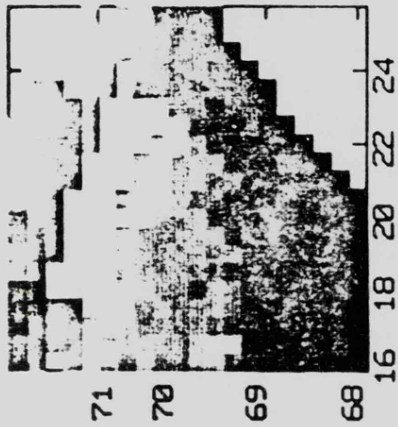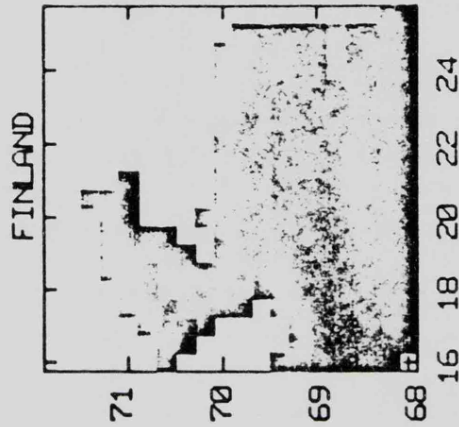
FIGURE 2.16

lessened.Further details of the principles of wave-shaping and hence spectrum-reduction can be found in ref(96),1972,by Skolnik,page 29-18.Typically,a truncated Gaussian waveform can be shown have about 100 dbs less relative power at the frequency equal to the reciprocal of the pulse-width than a rectangular pulse.

Finally,the SABRE radar system can be described as a relatively low-cost radar,with a 1983 cost for a single station being approximately £150,000.

The analysis of the echo data obtained from the SABRE radars will be described in the following chapters.

CHAPTER THREE

3. EVALUATION OF SABRE DATA AND THE RADAR EQUATION.

3.1 Introduction.

The main objectives of the present analysis of the SABRE radar data are as follows:

a) To ascertain the sources of the "Short Range Signals",which were received at ranges between 90 km and 350 km.

b) To derive the basic radar equation for the SABRE radar when receiving auroral echoes from diffuse aurora.

c) To investigate the temporal statistical characteristics of auroral signals as received by each radar,and their combined velocity and power distribution.

d) To estimate the height of the diffuse aurora echoes from the data and subsequently to propose methods of modifying the SABRE radars in order to determine height.

e) To develop a graphical display of the diffuse auroral echo signals which were fully compensated for all of the loss-factors derived from the radar equation.

f) To investigate the variation of the fully-compensated auroral echo signal with time of day,magnetic field strength,height and electrojet flow angle.

The form of the radar equation derived from the radar data assumed the diffuse aurora to be a uniform layer or canopy of back-scatterers which filled each radar range-cell.From measurements of the echo signal to noise ratios a measure of the auroral reflectivity (in square metres per metre square) could be derived for each range-cell,after exact location of the cell's position between L=4 and L=6.The radar equation was derived on the following basis;

1.The power density at the diffuse aurora at elevation angle θ_E,azimuth

angle θ_A and slant range R, from a transmitter of peak power P_T and antenna

gain $G_T(\theta_E, \theta_A)$ is P_{DT} and in a lossless, isotropic medium

$$P_{DT} = \left(\frac{(P_T \, G_T(\theta_E, \theta_A))}{(4\pi R^2)} \right) \tag{3.1}$$

2. The echo power density backscattered from the aurora of area A
illuminated by this radar is P_{DR} and

$$P_{DR} = \left(\frac{P_{DT} \, A \, \sigma'}{(4\pi R^2)} \right) \tag{3.2}$$

where σ' =auroral reflectivity in square metres per metre square.

The expression for antenna gain for a diffuse aurora of wide azimuthal

extent will be dependent upon the variation of gain with elevation angle

since the SABRE azimuth beamwidth is very narrow, but the elevation

beamwidth is broad. Hence,

$$P_{DR} = \left(\frac{(P_T \, G_T(\theta_E, \theta_{AO}))}{(4\pi R^2)} \right) \left(\frac{A \, \sigma'}{(4\pi R^2)} \right) \tag{3.3}$$

where θ_{AO} = zero azimuth angle from antenna

3. The echo power at the receiving antenna is P_R and = P_{DR} x the aperture

of the receiving antenna. The antenna aperture, A_{ER}, is related to the

antenna gain, as derived in ref(96), 1972, by Skolnik, as follows:

$$A_{ER} = \left(\frac{(\text{antenna gain}) \, (\lambda 2)}{4\pi} \right)$$

where λ=operating wavelength.

$$\text{Hence} \quad P_R = \left(\frac{(P_{DR} \, G_R(\theta_E, \theta_{AO}) \, \lambda^2)}{4\pi} \right) \tag{3.4}$$

where θ_{AO} = zero azimuth angle

SCHEMATIC ILLUSTRATION OF THE RANGE-EXTENT OF A RADAR PULSE

AT THE AURORA

$c \cdot \dfrac{\tau}{2} \cdot \sec(\theta_G)$

AURORA

θ_G

θ_E
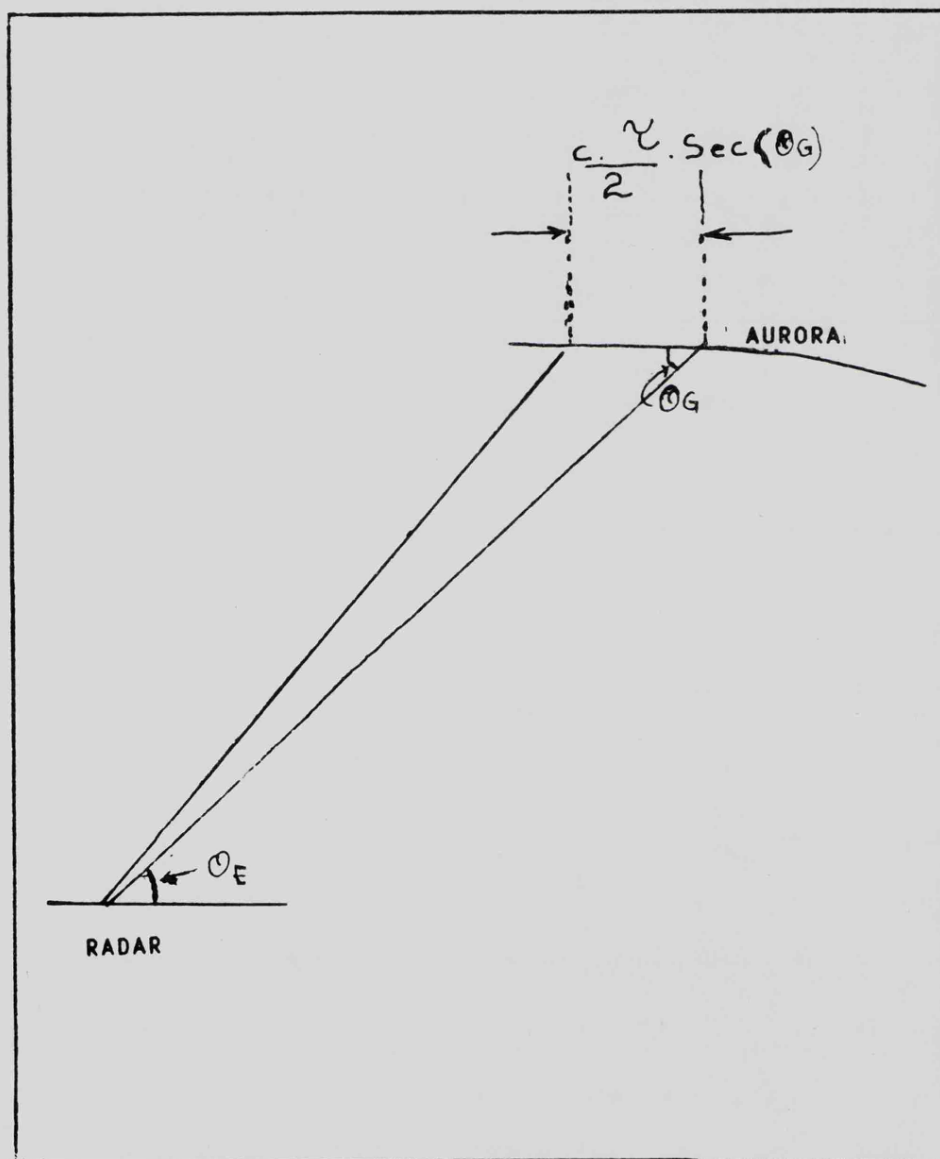
RADAR

τ IS THE RADAR PULSE LENGTH c IS THE VELOCITY OF LIGHT

θ_E IS THE ELEVATION ANGLE θ_G IS THE GRAZING ANGLE

FIGURE 3.1

4. The area A_A, illuminated by the radar, assuming a wide azimuthal extent of the aurora as well as an extended range, will, as in fig(3.1), be

$$A_A = \left(\frac{(T\ \Theta_{BW}\ c\ R)}{(2\ \cos(\Theta_G))} \right)$$
(3.5)

where T = pulse width, Θ_{BW} = azimuthal beamwidth, Θ_G = grazing angle between radar beam and the aurora, c = speed of light.

Hence, in a lossless, isotropic medium the backscattered echo power at the receiving antenna is;

$$P_R = \left(\frac{P_T\ G_T(\Theta_E, \Theta_{AO})}{4\pi\ R^2} \right) \left(\frac{\sigma'\ T\ \Theta_{BW}\ c\ R}{4\pi\ R^2\ 2\cos(\Theta_G)} \right) \left(\frac{G_R(\Theta_E, \Theta_{AO})\ \lambda^2}{4\pi} \right)$$
(3.6)

5. The echo signal power P_R, from a diffuse aurora is thus inversely proportional to the cube of the slant range. The echo signal power from a point target such as an aircraft will be inversely proportional to the fourth power of the slant range, and will be dependent upon its azimuth angle with respect to the radar beam, as well as its elevation angle.

6. The system noise power, N_r, was measured (for each beam), in range-gate 50, (i.e. at such an extreme range that no echoes were present), and the ratio $(P_R - N_r)/N_r$ determined for each integration period.

The radar equation and the investigation of the SABRE parameters and losses which affect the derivation of reflectivity will be considered in more detail, as will the velocity measurements. By combining the resultant velocities of the 2 radars at positions of overlap, the variation of electrojet speed (and hence electric field strength) will be examined. Firstly, the system criteria for the data analysis had to be established in order to determine signal thresholds and operational parameters.

3.2 <u>The criteria for data analysis.</u>

The radar data which are analysed in the bulk of this report covered the years 1981 to 1984 inclusive, but data was not always available from both of

the SABRE radars,due to periods of radar breakdown or inoperability.

Similarly,only brief periods of radar data were available for the short range signal analysis since the measurements necessitated the presence at the Wick radar site of the Leicester University scientists.

The radar equation criteria establishment will now be described.The signal criteria are those of signal thresholds,pulse-pair spacing,echo power measurement and averaging period.

Because of limitations in the capacity of the SABRE Nova computer it was not possible to increase the Pulse-Repetition-Frequency (PRF) of the SABRE radar,nor to change the pulse-width during the investigations of the diffuse aurora.Similarly,the peak transmitter power could not be increased because of limitations in the power supply.

The loss criteria are those of aspect-loss,vertical polar diagram loss, beam pointing loss and filter loss.

The form of the radar equation for a layer of back-scattering reflectors which are distributed in both range and in azimuthal extent,such as to fill each radar beam,is detailed in chapter 4,section 4.10.This equation provides a measure of the auroral reflectivity at each range-cell,but requires an evaluation of the signal,noise and velocity thresholds and associated loss factors before a derivation of reflectivity can be made. The first step in converting the radar data into the radar equation form was to change the format of the data tapes received from the radar site,to allow them to be used on the University mainframe computer.This conversion was achieved via a Fortran IV programme and the format of the data output is as shown in Table (2.1).This format allowed direct access to the system parameters which are featured in the radar equation,particularly peak transmitter power,wavelength,pulse-width and integration time.The subsequent examination of the data and assessment of the criteria were as follows;

3.2.1 Examination of the Doppler velocity measuring criteria.

An analysis programme (COEANA),was then written to obtain auroral echo signal power in each of the 8 beams,which had been compensated for the variation of signal strength with range; i.e. the range-cubed compensation as in the radar equation.   Two simple tests were then performed upon this range-compensated signal data; a) to compare the velocity of the irregularities determined by the double-pulse method,with the velocities determined by a range-rate method,and b) to examine the effect of varying the pulse pair-spacing.The range-rate analysis is based on the measurement of the movement of identifiable features in the backscattered signal power: The range was identified at which the signal strength was greatest,for example on day 108,1982,16.51 hours,in beam 6 at 960 km.

The variation in range of the leading edge of this signal was then monitored over the following 300 seconds and the range-rate,or radial velocity,was derived. Because of the signal-level fluctuation,the value of range-rate was considered accurate to only about 20 %,but typical range-rate values of about 500 metres per second were obtained. These compare with values of the order of 370 metres per second from the double-pulse method.

A simple comparison was then made of the effect upon Doppler velocity measurement of varying the separation of the double-pulses adopted for the SABRE radar system,as was illustrated in fig(2.14).A series of double-pulse delay times were transmitted on day 24,1982 at the Wick site.The observed variation of radial velocity measurement with double-pulse separations of between 200 and 1300 microseconds and for a signal to noise ratio of greater than 20 db in range-cell 32 of beam 5 was less than 8%. The analysis of chapter 4 indicates that the sign of the Doppler velocity will change when the pulse spacing corresponds to half the velocity wavelength.Hence,since Doppler velocities of the order of 1600 metres per second were to be expected in some later measurements,the shorter pulse gaps would have to be employed. A 300 microseconds gap was selected,corresponding to that of the Stare radar system.

RANGE COMPENSATED SIGNAL TO NOISE RATIO.

THE VARIATION OF THE ECHO SIGNAL WITH TIME   Day 214 1982

1400 hour

Time in steps of one minute   BEAM 8
Day 214 1982

15:39 hours UT

1215 km

Slant range in 15 Km steps

495 km

1400 hour
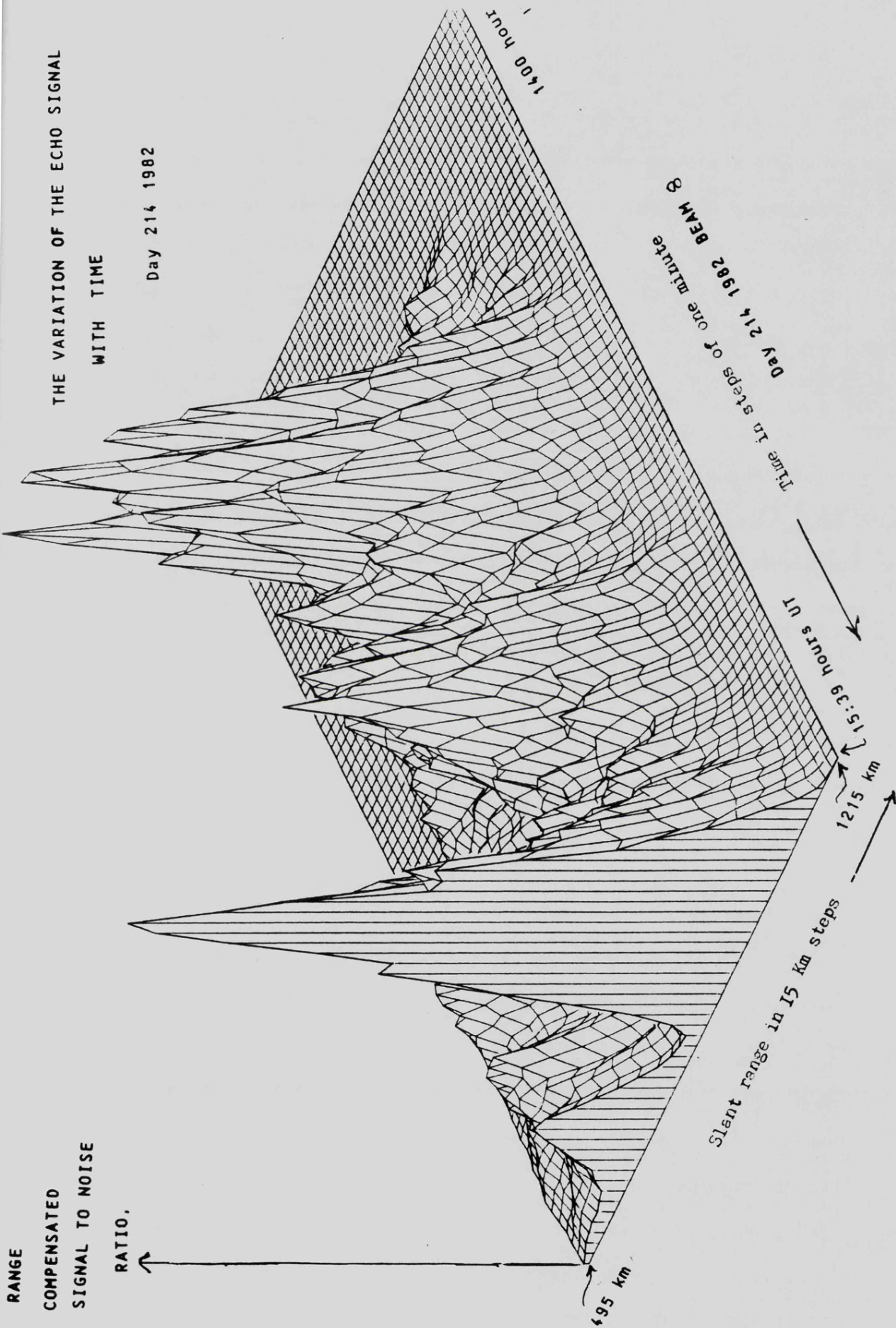
FIGURE 3.2

3.2.2 Examination of the echo signal power measurement criteria.

A comparison was made of the value of the echo signal power obtained from the normal single-pulse (i.e. zero lag) method and the amplitude of the autocorrelation function first lag for a given value of pulse pair separation.The first lag amplitude was derived from the Real and Imaginary outputs,R and I,since its value from each double-pulse measurement,every 20 seconds will be P_{DP} where:

$$P_{DP} = \sqrt{(R^2 + I^2)}$$

P_{DP} was calculated for pulse separations of between 200 and 1300 microseconds for day 24,1982,beam 5,range-cell 32 and compared with the signal power values derived from the single pulses at the corresponding times.The comparison revealed that the two amplitudes differed by less than 1.6 db for signal to noise ratios of greater than 20 db. However,it was also noted that discrepencies in velocity sign and value, and in signal power,occurred for very low signal to noise values.

Further evidence of the need for signal averaging in both power and in velocity was found in the degree of signal fluctuation with time,as displayed in fig(3.2). Eventually,as will be seen in chapter 5,signal fluctuations of as low as 1 db were detected,dependent upon magnetic activity,but initially in order to determine the minimum values of signal to noise ratios for the analysis,the fluctuations of the noise levels were studied:

3.2.3 Examination of the noise level threshold criteria.

On day 298,1982,between 1000 and 1200 (local time) the transmitter radiated into a dummy load,as part of the tests for the short range experiments, described in chapter 7. During the dummy-load tests,the maximum and mean noise levels of each radar beam was measured over a two-hour period. The receiver attenuator setting was at zero,so as to achieve maximum

THE VARIATION OF MEAN NOISE LEVEL FROM DAY TO NIGHT IN EACH WICK BEAM.

ATTENUATOR SETTING IN THE RECEIVER = 10 DB   DAY 214, 1982
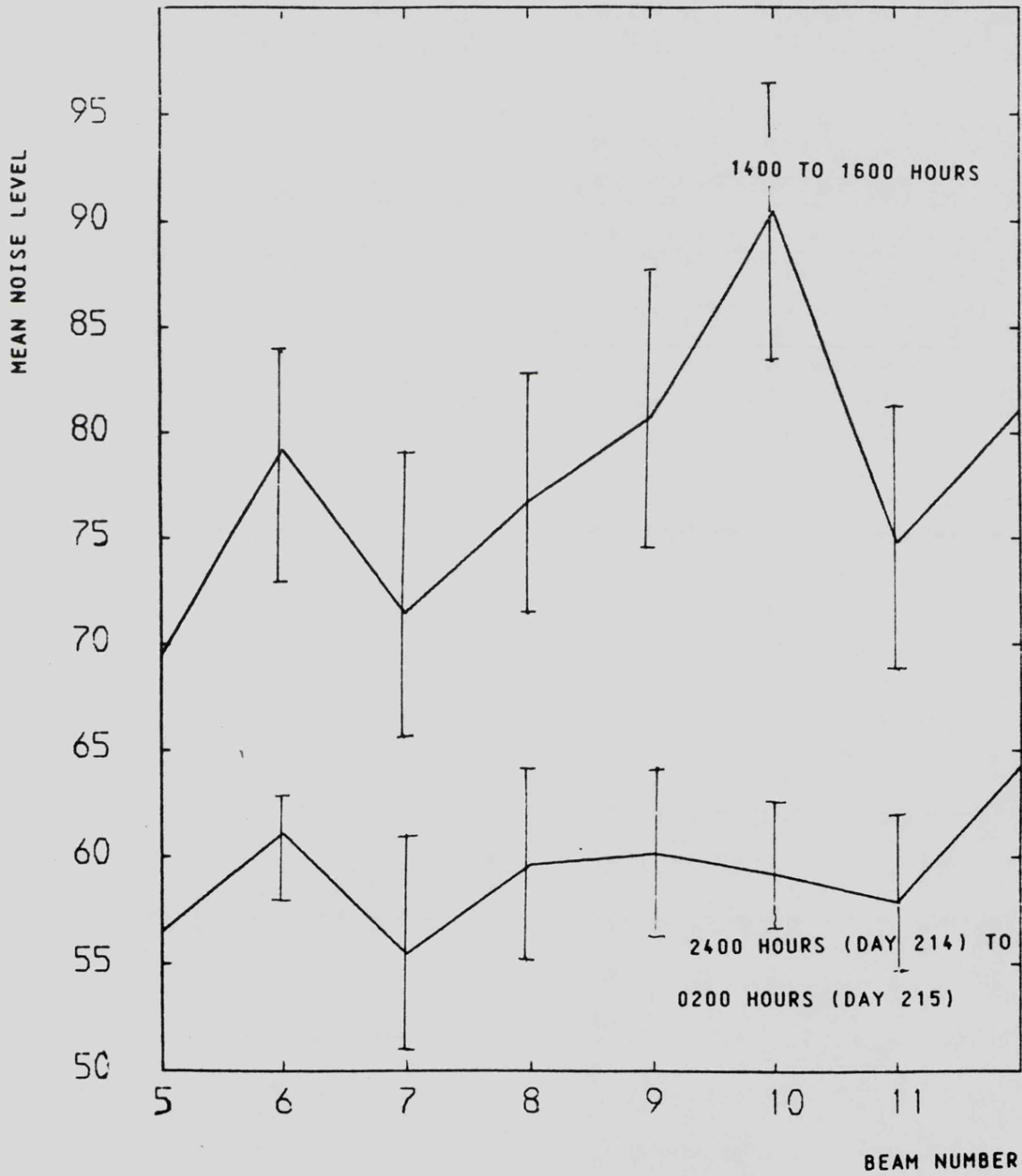
FIGURE 3.3

receiver gain and hence maximum noise amplification. The results of this test were as follows:

BEAM NUMBER	(MAXIMUM NOISE/MEAN NOISE)
5	1.06
6	1.145
7	1.58
8	1.19
9	1.24
10	1.24
11	1.25
12	1.24

It was evident that a signal to noise threshold of only 3 db was sufficient to eliminate the effects of noise upon the velocity measurements, over a two hour period.

3.2.4 Examination of the difference between day and night-time noise levels

In the normal mode of operation of the SABRE radars, the noise level is monitored at a range well in excess of the auroral echo ranges. The differences between noise levels during day-time and those during night-time are illustrated in fig(3.3), for day 214,1982. The noise is approximately 1.3 db greater during the times of the afternoon electrojet, than during the night-time electrojet, for any beam. A mean value of noise power was derived as in chapter 4.8.3, of value 9.62 x10^{-17}watts.

As a result of these initial observations, the data analysis was restricted to the periods satisfying the following criteria:

      i) Pulse-separation gap of 300 microseconds

      ii) An averaging period of at least 30 minutes

WICK SABRE DATA   BEAM 9   Day 249 1982 0100 to 0200

EXAMPLE OF THE GRAPHICAL DISPLAY EMPLOYED IN THE DERIVATION OF ELEVATION POLAR DIAGRAM. SIGNAL AMPLITUDE, DOPPLER VELOCITY AND NUMBER OF OCCURRENCES ARE PLOTTED AGAINST SLANT RANGE.

MAX. REF DB= 51-150DB M/SQ.M
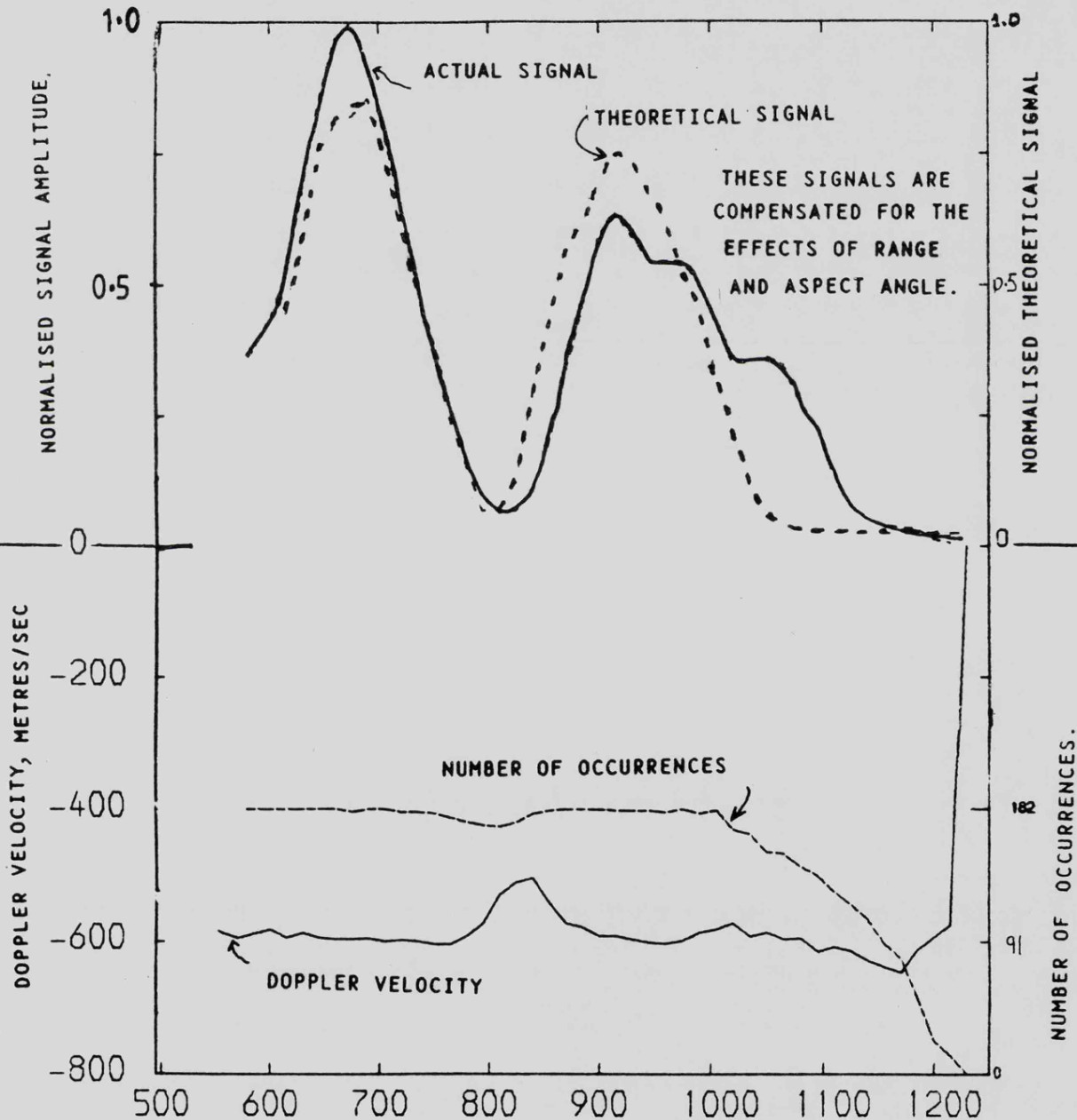
WAVELENGTH= 1.958METRES
TXR PEAK POWER= 40KILOWATTS
INTEGRATION PERIOD= 20SECONDS
DOUBLE-PULSE SEPARATION= 300MICROSECONDS
SIGNAL THRESHOLDS SET AT 6DB ABOVE NOISE
VELOCITY STEP WIDTH=50 METRES/SEC
LERWICK MAGNETIC INDEX= 8

FIGURE 3.4

iii) A signal to noise ratio of at least 3 db per pulse

iv) Echo power measurement derived from the single-pulses.

3.2.5   Examination of the loss-factor criteria in the radar equation.

Once these criteria had been established,and the differences between night and day noise values measured, graphs were plotted of signals (range-cubed compensated),against slant range,together with the number of times that the signals were greater than the noise thresholds. By examining such graphs,as displayed in fig(3.4), for each of the 8 beams the angular extent and range extent of the auroral signal and its general pattern across the beams were established. Such examination revealed 4 main features of the aurora,between L-values of 4.5 to 6,when viewed from the Wick site:

a) Signals were generally strongest in beam 11

b) Signals were generally stronger in range cells 29 to 31 in any beam.The Doppler velocity in range-cell 29 was generally higher for beam 12 and decreased approximately cosinusoidally to beam 5

c) The influence of the vertical polar diagram of the antenna was most clearly evident in beams 9,10,11.The null occurred at about 800 km.

d) The most common distribution of the stronger auroral signals was diagonally across the 8 beams.

Because of feature (d) the range-cells of beams 11,12, at the ranges below 600 km did not often contain strong echo-signals.

As a result of this examination of the data it became apparent that separate studies should be undertaken,of the influence of the antenna

EXAMPLE OF THE GRAPHICAL DISPLAY EMPLOYED IN THE DERIVATION

OF ELEVATION POLAR DIAGRAM FOR DIFFERENT AURORAL HEIGHTS.

NORMALISED VALUES OF THEORETICAL SIGNALS AND RANGE-COMPENSATED

SIGNALS ARE COMPARED, TOGETHER WITH THE MEAN DOPPLER VELOCITY,

FOR EACH RANGE-CELL.

SABRE WICK POLAR DIAGRAMS FOR 2 AURORAL LAYERS   BEAM 9
BROKEN LINE IS FOR 115KM, FULL LINE 90KM LAYER HEIGHT
● ● ● ● ● ● ● ● ● LINE SHOWS ACTUAL R-CUBED DATA
PART-BROKEN LINE SHOWS ACTUAL MEAN VELOCITY

NORMALISED SIGNAL AMPLITUDE (y-axis): 1.0, 0.75, 0.5, 0.25, 0.0

MEAN DOPPLER VELOCITY, M/SEC (right y-axis): 550, 500, 400, 100, 0

Labels within plot: actual mean echo; velocity; 90km; Theoretical patterns, 115km

SLANT RANGE IN KILOMETRES (x-axis): 500, 600, 700, 800, 900, 1000, 1100, 1200
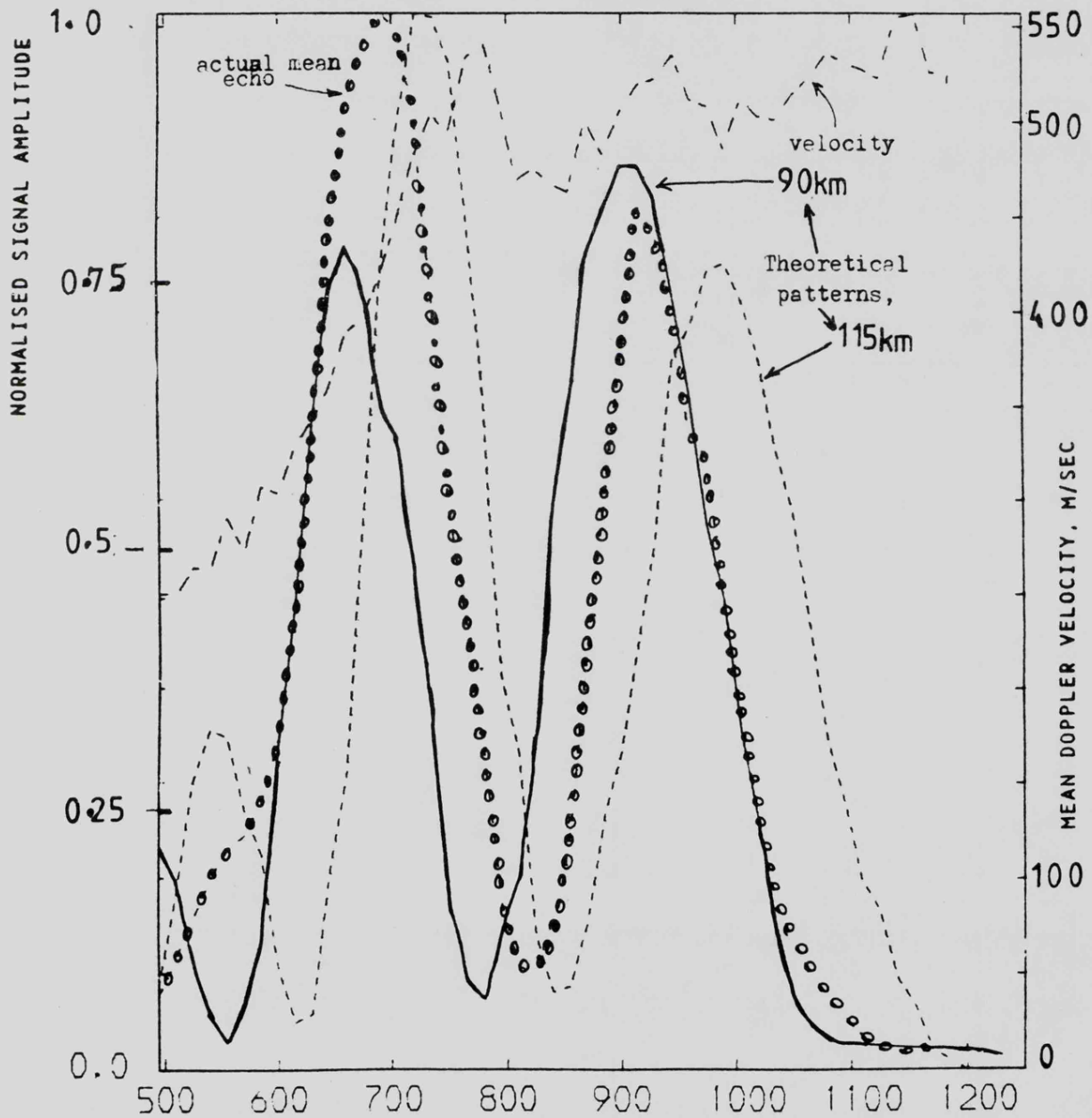
ASPECT-ANGLE LOSS=4.DB PER DEGREE   SLANT RANGE IN KILOMETRES
THEORETICAL ARRAY HEIGHT= 7.7WAVELENGTHS
GROUND REFLECTIVITY= 0.6

MEAN SIGNAL DATA OF DAY 249   15HOURS TO 16 U.T.

FIGURE 3.5

vertical polar diagram and the aspect-angle loss,within the radar equation:
These studies were:

i) An analysis of the exact latitude and longitude of each range-cell of each SABRE radar beam in order to determine the aspect-angles and positions of overlap of the two radars.This was achieved by means of a Radio Star noise source and a study of the effects of atmospheric refraction.

ii) A graphical analysis of the vertical polar diagram loss as determined from the data of Wick beam 9. Two such graphs are displayed in figs (3.4),(3.5). The assumption was made that the auroral backscatterers were uniformly distributed in a layer at a height of about 100 km and were of wide azimuthal extent. Compensation was made for the losses due to aspect-angle and range.

iii) An analysis of the aspect-angle loss.This was separated from the polar diagram loss by selecting the range-cell in each beam in which at which the vertical polar diagram was at a peak and in which echo-signals were normally strongest: i.e.Wick range-cell 29.The aspect angle for each of the radar beams was evaluated at that point from the IGRF Magnetic Field Model and aspect-angle loss was derived from examination of the relative echo signal strengths in range-cell 29 of each beam,after compensation for beam-pointing loss.   The losses between the beams due to the beam-pointing loss (as described in chapter 4) were derived by a separate study;

iv) An analysis was made of the variation in echo signal power in Wick range-cell 29 with flow-angle i.e. the angle between the radar beam and the electrojet direction.

A further analysis was also made of the variation of echo signal

WICK SABRE DATA

COMPARISON OF THE DISTRIBUTIONS OF DOPPLER VELOCITIES IN

STEPS OF 50 METRES/SECOND.

THE DASHED CURVES ARE THE NORMALISED REFLECTIVITIES AT EACH

DOPPLER VELOCITY.

NO. OF COUNTS V. VELOCITY, IN BEAM 9 FROM 630KM TO 1215KM

	Year	Day	Hour	Min		Day	Hour	Min
	1982	249	1	0	TO	249	17	8

FIGURE 3.6

UPPSALA SABRE DATA   Day 250 1982 0100 to 0200
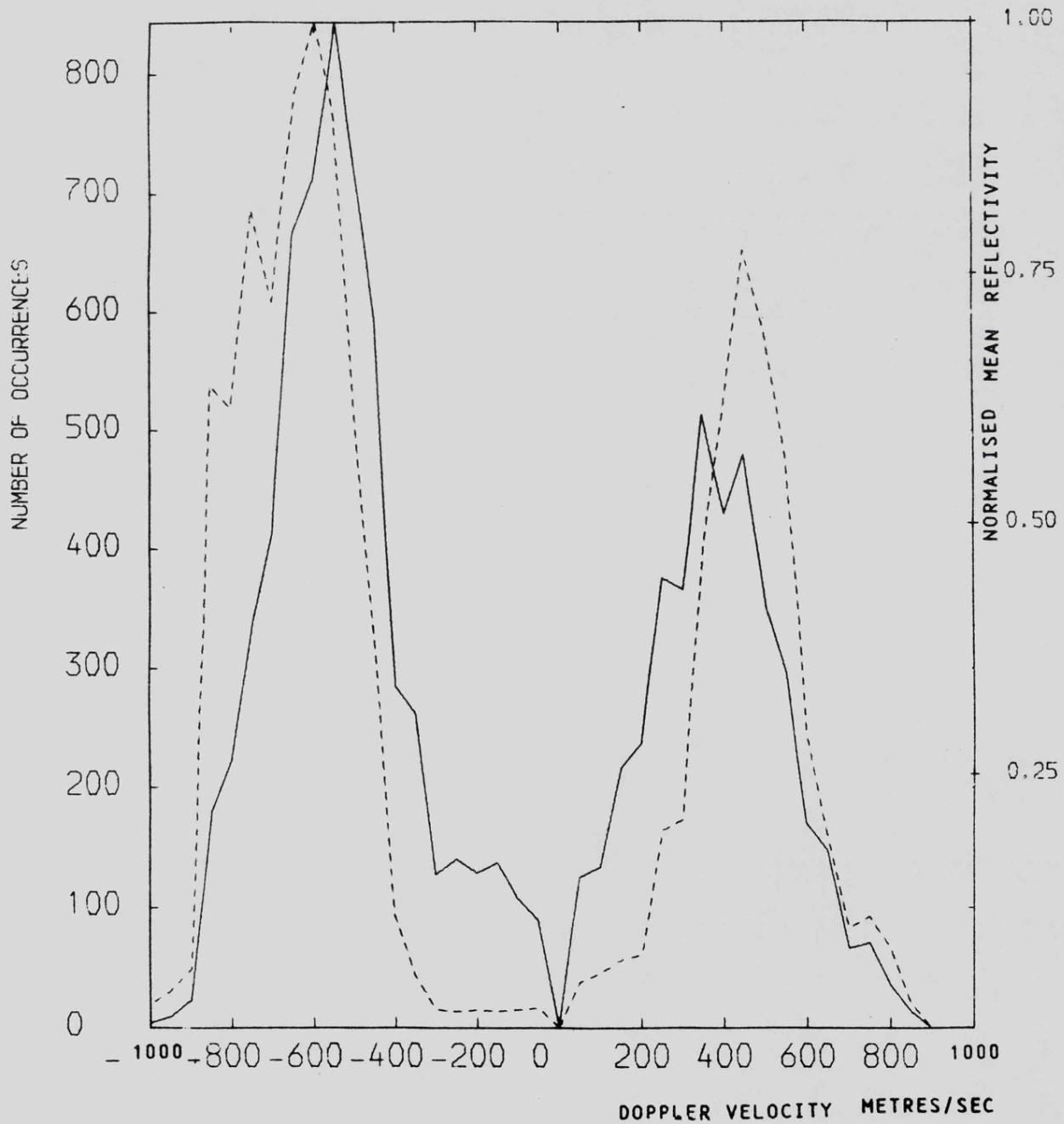
THE DISTRIBUTION OF DOPPLER VELOCITIES IN STEPS OF 50 METRES/SECOND.

THE DASHED CURVES ARE THE NORMALISED REFLECTIVITIES AT EACH DOPPLER VELOCITY.

BEAM 9 FROM 630KM TO 1215KM
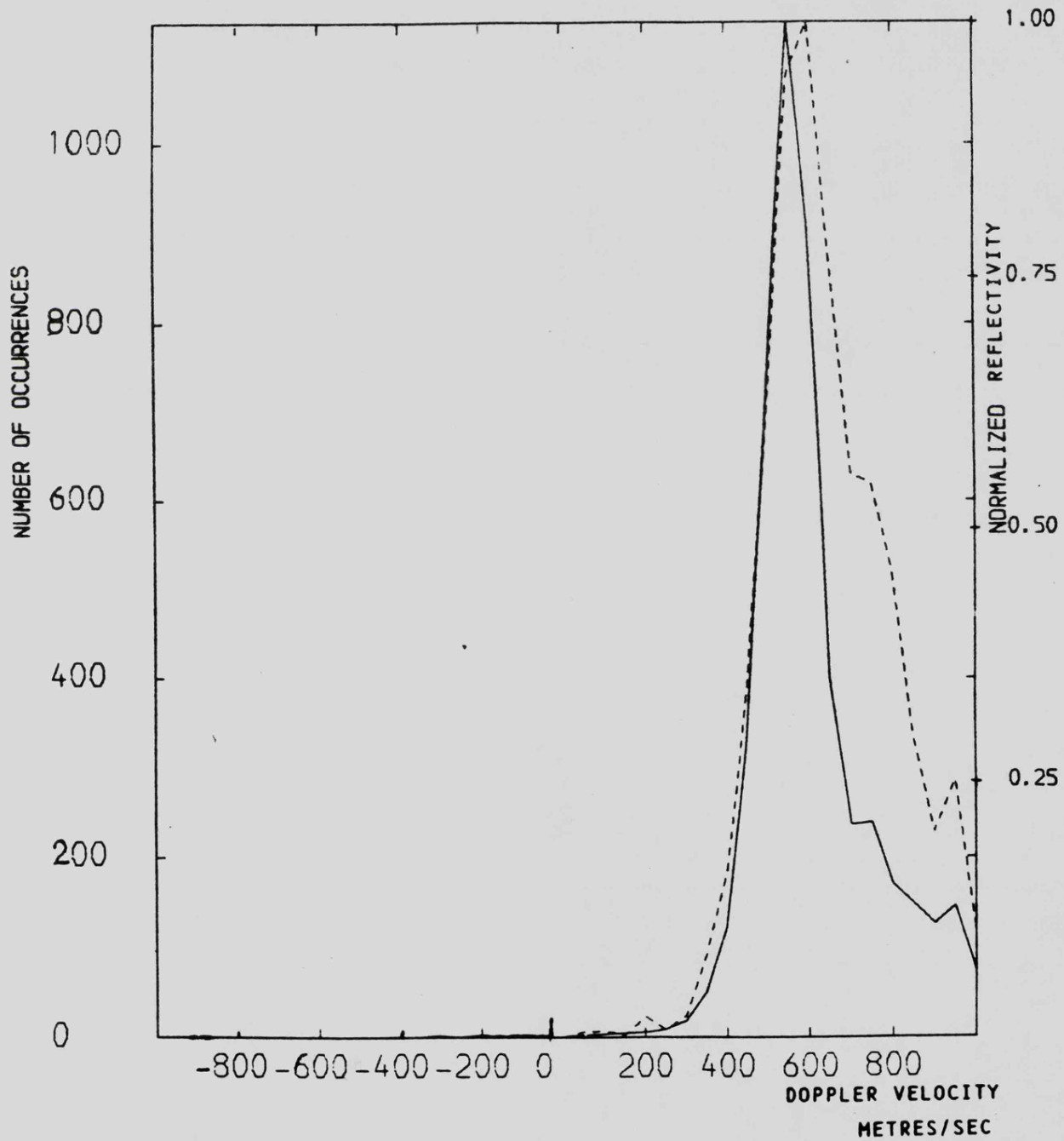
FIGURE 3.7

SABRE WICK RADAR

AURORAL REFLECTIVITY AGAINST DOPPLER VELOCITIES

540 KM SLANT RANGE

1982 FROM DAY 249 HOUR 0 MINS. 0 TO 249 14 7 U.T.
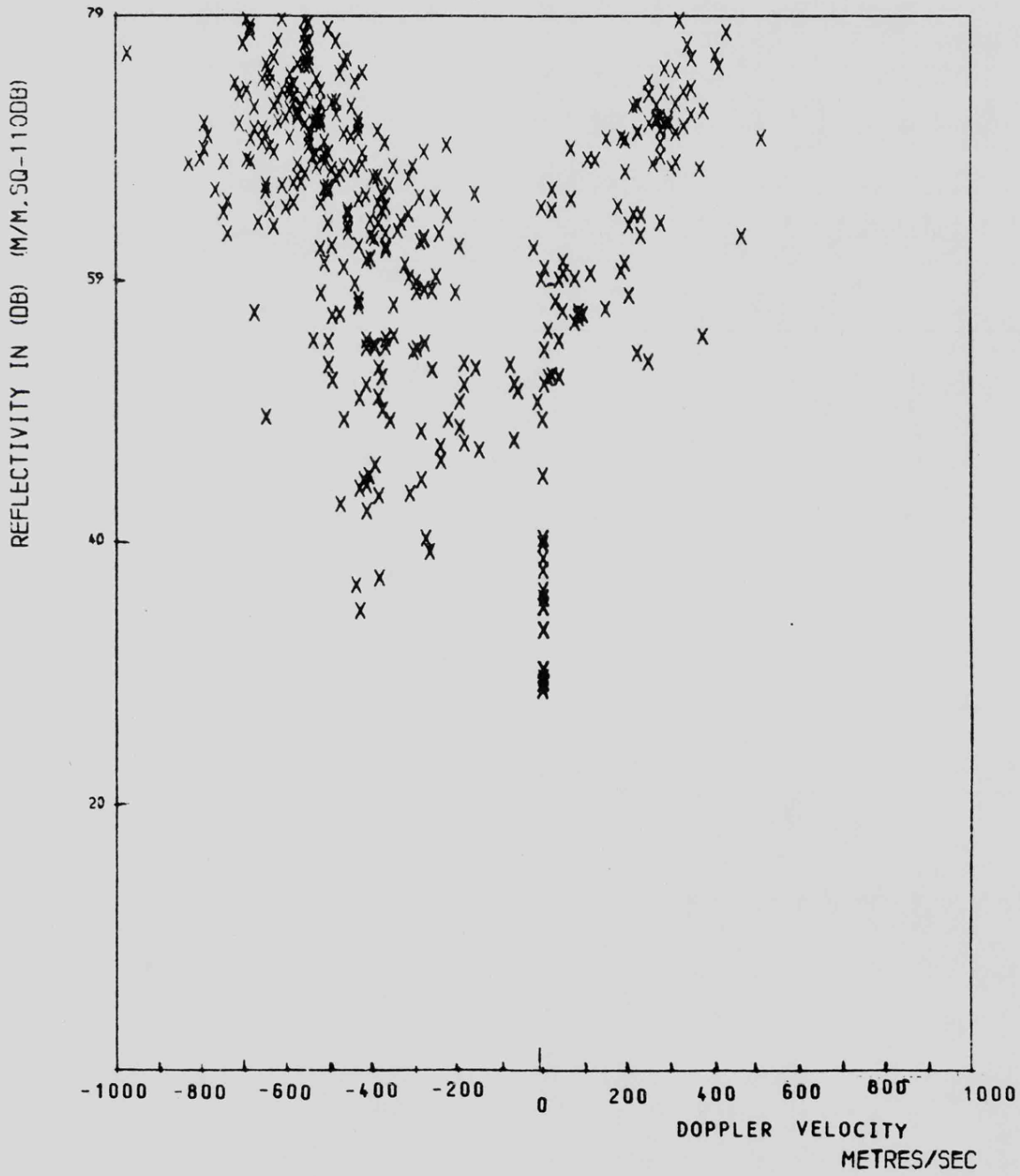
FIGURE 3.8

strength with Doppler velocity:

v) For each time period over which a mean value of echo signal strength was derived,the number of occurrences of each velocity increment was plotted,together with the averaged echo power associated with that increment.Fig(3.6) is an example of such a plot for the Wick radar,for a time interval of 16 hours,for beam 9 for ranges of 630 km to 1215 km. Fig(3.7) is a similar plot but for a different time interval,and is for the Uppsala radar.In both plots the right-hand axis represents the averaged echo power normalised to the maximum value. For both the Wick and Uppsala radars a non-linear relationship was found between echo power and Doppler velocity.

When analysing the variation of echo power with Doppler velocity at a fixed range,as plotted in figs(3.8),two range-cells were selected,one at a relatively short range of 540 km and the other at range-cell 29.This type of plot is also known as a "scatter diagram" and is a display of the auroral reflectivity (a measure of the echo power) against Doppler frequency for a 14 hour period.

At this stage of the analysis it became evident that a further criterion could be added to the list,when establishing the radar equation; namely that comparisons of echo powers at different ranges or beams (such as in the derivation of polar diagram null-depths) should be only be made when the Doppler velocities of the 2 positions corresponded.The variation of mean Doppler velocity with beam azimuth angle at a fixed range (i.e. range-cell 29) did not exhibit the distinctive,peaked pattern of the echo signal variation,but approximated to a cosine relationship.No sharp variation of Doppler velocity with aspect angle was detected at this stage.

With these echo-signal and noise criteria established as shown above,it was possible to determine the operating parameters for each SABRE radar. In order to derive the losses due to beam-pointing (i.e. variation of

flow-angle),it had been necessary to analyse the combined velocity data of the 2 radars.The criteria for the derivation of the combined radar velocity data will now be described;

3.2.6 Examination of the criteria for electrojet speed and flow angle.

When data from both radars are available the vector-velocity of the electrojet can be established.The data was obtained from Wick range-cell 29 of beam 11,since this had the smallest aspect-angle loss of all 8 beams of the Wick radar and coincided with polar diagram peak.Furthermore,the aspect angle loss for the Uppsala radar at this point was small. The results of this analysis,as will be shown in chapter 5,revealed distinct Type 1 spectral features,and permitted the derivation of an averaged value of beam-pointing loss.

Finally,in order to determine the uniformity of flow of the electrojet,three points of coincidence of the 2 radar systems were located and their flow angles examined.

At this stage of the data examination it became necessary to assess the variation of electrojet speed with auroral height,and the criteria for such height analysis were examined as follows;

3.2.7 The examination of the criteria for estimating mean auroral height.

As will be shown in more detail in chapter 5,3 methods of estimating mean auroral height are proposed in this analysis;

    a) From the slant-range of the position of the NULL in the vertical polar diagram of the Wick radar

    b) From the pattern of the echo signal strengths at the MAXIMA in the radar beam polar diagrams,compared with that of the theoretical aspect-loss.

    c) Examination of the slant-range to the Radar Horizon.

In method (a),the Null position of beam 9 of the Wick radar was selected

since in general,signals were present in more of the range-cells (including the Null and Peak of the vertical polar diagram),than in the other beams. The range-cell in which the null occurred most commonly was cell 21,the peak in cell 29.

In method (b) the peaks of each beam vertical polar diagram corresponded to range-cell 29 and the aspect-angle losses were derived from the IGRF magnetic field model.

In method (c),the radar horizon generally occurred at range-cells greater than 42.

3.2.8 Examination of the criteria for spectral analysis.
The spectral analysis in chapter 5 consists of an examination of the distributions of auroral velocities and their associated values of reflectivity over periods of at least 1 hour.The distinction between spectral types 1 and 2 are as follows;

Type 1 : Doppler velocity >350 m/sec,of narrow half-power spectral width ,and with a minimum value of reflectivity at + 90 degrees flow angle.

Type 2 : of wide spectral width and isotropic reflectivity.
The variations of reflectivity with absolute field strength and with magnetic field strengths were also examined.

3.2.9 Summary of criteria

The criteria employed for the selection of data for this analysis were:

1. Pulse-pair separation of 300 microseconds.

2. Averaging times to be at least 30 minutes.

3. The averaged signal-to-noise ratio to be at least 20 db.

4. Wick vertical polar diagram to be derived from the data of beam 9.

5. Aspect angle loss to be derived from data of cell 29 in each Wick beam.

6. Velocity spectral analysis to be derived at short and at long range.

7. Electrojet speed analysis to be obtained from Wick beam 11,Uppsala beam 5.

8. Electrojet flow direction to be derived for 3 different locations at which the 2 radar beams most closely overlapped.

9. All echo-power comparisons to be made when both signals are at essentially the same Doppler velocity and flow angle.

When these criteria had been established, an analysis was undertaken of the system features which affected the evaluation of the radar equation, including refraction effects, radar beam azimuth and atmospheric losses as follows, in chapter 4;

CHAPTER FOUR

4. Theory of operation of the SABRE radars.

This chapter will provide a derivation of the radar equation, from basic radar theory and examination of the SABRE echo data for the diffuse aurora. The loss-factors will be considered, (particularly the loss due to aspect angle), and the sources of noise will be examined. The electrojet speed and Doppler velocity equations will be analysed and the SABRE double-pulse velocity measuring technique will be compared with other similar techniques.

4.1 Evaluating the effect of refraction.

Before deriving the full expression of the radar equation for the SABRE radars, the effect of refraction upon the slant range of the auroral signals, (and upon the true elevation angle of these signals), must be evaluated. If a radar beam is propagated through free space where there is no atmosphere, the path followed by the beam is a straight line. However, a beam that is propagated through the earth's lower atmosphere encounters variations in atmospheric refractive index along its trajectory that cause the ray path to become curved.

Fig(4.1) illustrates the geometry of the refraction of the radar beam as it travels towards the auroral irregularity, and the angle τ_B represents the bending of the radar beam, between the tangents at the point of launch and point of incidence. From a knowledge of the refractive index, n, the angle τ_B can be deduced as follows:

it is assumed that the refractive index reduces for an increase of height above the surface of a smooth, spherical earth and that the path of a radar beam will obey Snell's law:

$$n_2 \ (R_E + h) \ \cos(\theta_3) = n_1 \ R_E \ \cos(\theta_2) \quad \text{as in fig(4.1)} \qquad (4.1)$$

As shown in ref(96), by Skolnik, 1972, τ_B can be approximated by:

$$\tau_B = (n_1 \ \cot(\theta_2) - n_2 \ \cot(\theta_3)) \times 10^{-6} \quad \text{in radians, and the}$$

error angle, E_R, the difference between θ_2 and θ_1 by:

SCHEMATIC ILLUSTRATION OF THE EFFECT OF REFRACTION
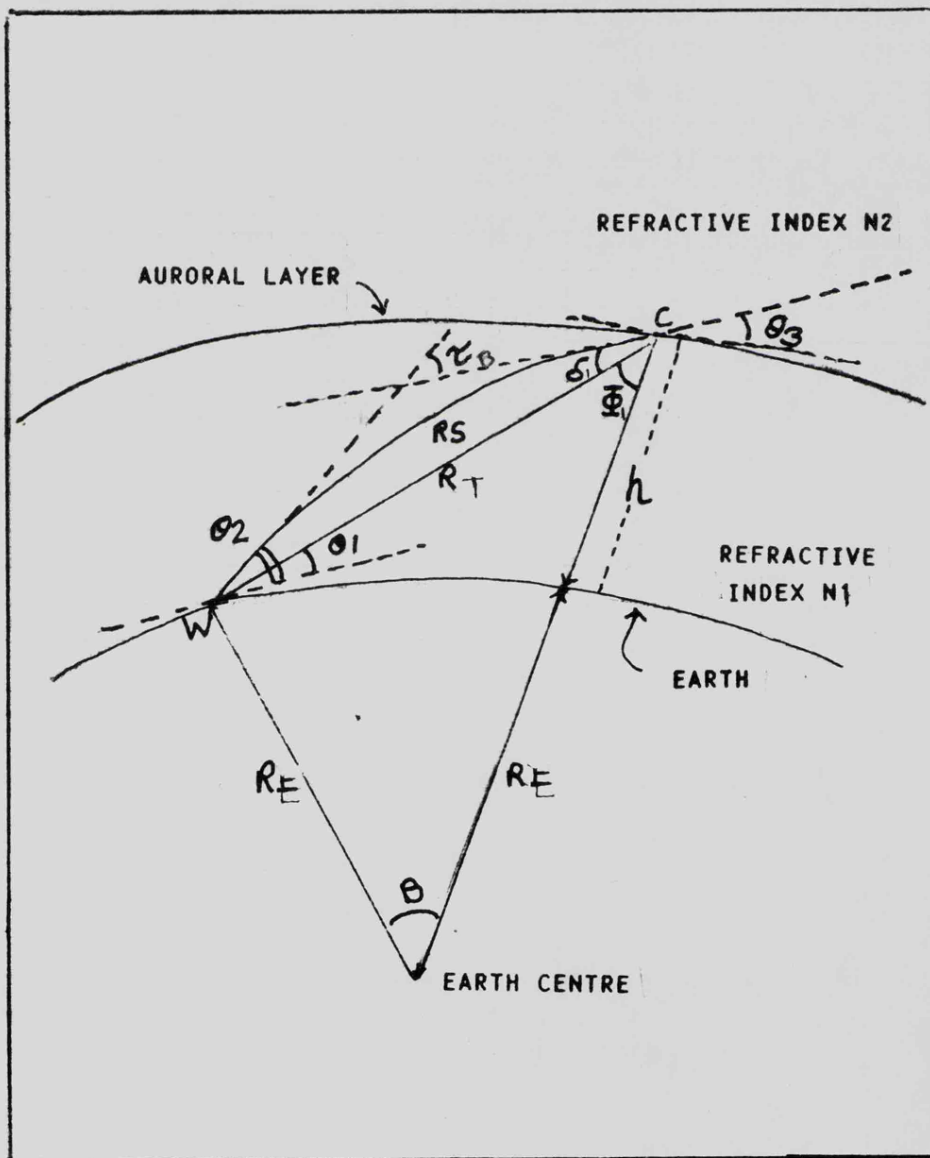
W IS THE POSITION OF THE RADAR
C IS THE POSITION RADAR BEAM ON THE AURORA
   AT SLANT RANGE RS
h IS THE HEIGHT OF THE AURORA
R_E IS THE MEAN RADIUS OF THE EARTH
θ_2 IS THE APPARENT ELEVATION ANGLE
θ_1 IS THE TRUE ELEVATION ANGLE.

FIGURE 4.1

$$E_R = \arctan\left(\frac{\cos\gamma_B - \sin\gamma_B \tan\theta_3 - n_1/n_2}{(n_1/n_2)\tan\theta_2 - \sin\gamma_B - \cos\gamma_B . \tan\theta_3}\right) \qquad (4.2)$$

These formulae and refraction effects are frequency-independent below 100 Ghz and affect all radar systems whose beams traverse the troposphere.

Before assessing typical values of error angles, it is necessary to derive exact values of refractive index at the auroral altitudes. Refractive indices are generally expressed in terms of atmospheric exponential models, or CRPL exponential reference atmosphere:

$$n(h) = 1 + (N_S \ 10^{-6}) \ e^{-uh} \qquad (4.3)$$

where N_S=313 and u=0.143859 and h is height in km.

The atmospheric radio refractive index, n, has a typical value of 1.0003 at the earth's surface and approaches unity with increasing height.

As shown in ref(96) by Skolnik, and ref (97) by Blake, 1968, charts of true elevation angle against slant range are available, based upon ray-tracing techniques and numerical integration, using refraction formulae. Fig(4.2) represents a plot of true elevation angle against slant range for different auroral heights, derived from such charts.

Ref(98), 1958, by Millman, quotes typical refraction errors in the elevation angles due to refraction effects as follows:

For altitudes of 33,000 metres and elevation angle of 5 degrees,

a) for 100% relative humidity, error=2.3 milliradians =0.132 degrees

b) for 0%   "   "   " =1.7   "   =0.098   "

For altitudes of 33,000 metres and elevation angle of 25 degrees,

a) for 100% relative humidity, error=0.5 milliradians =0.029 degrees,

b) for 0%   "   "   " =0.39   "   =0.0224   "

The error angle increases with height for a given elevation angle and extrapolation of the graphs in ref (98) indicates that that the expected error angle for 100 km altitude, and elevation angle of 5 degrees (as in the SABRE system), to be of the order of 2.8 milliradians for 100% humidity. Below

TRUE ELEVATION ANGLE AGAINST SLANT RANGE

FOR AN AURORAL HEIGHT OF 100KM
DASHED LINE IS FOR A HEIGHT OF 110KM
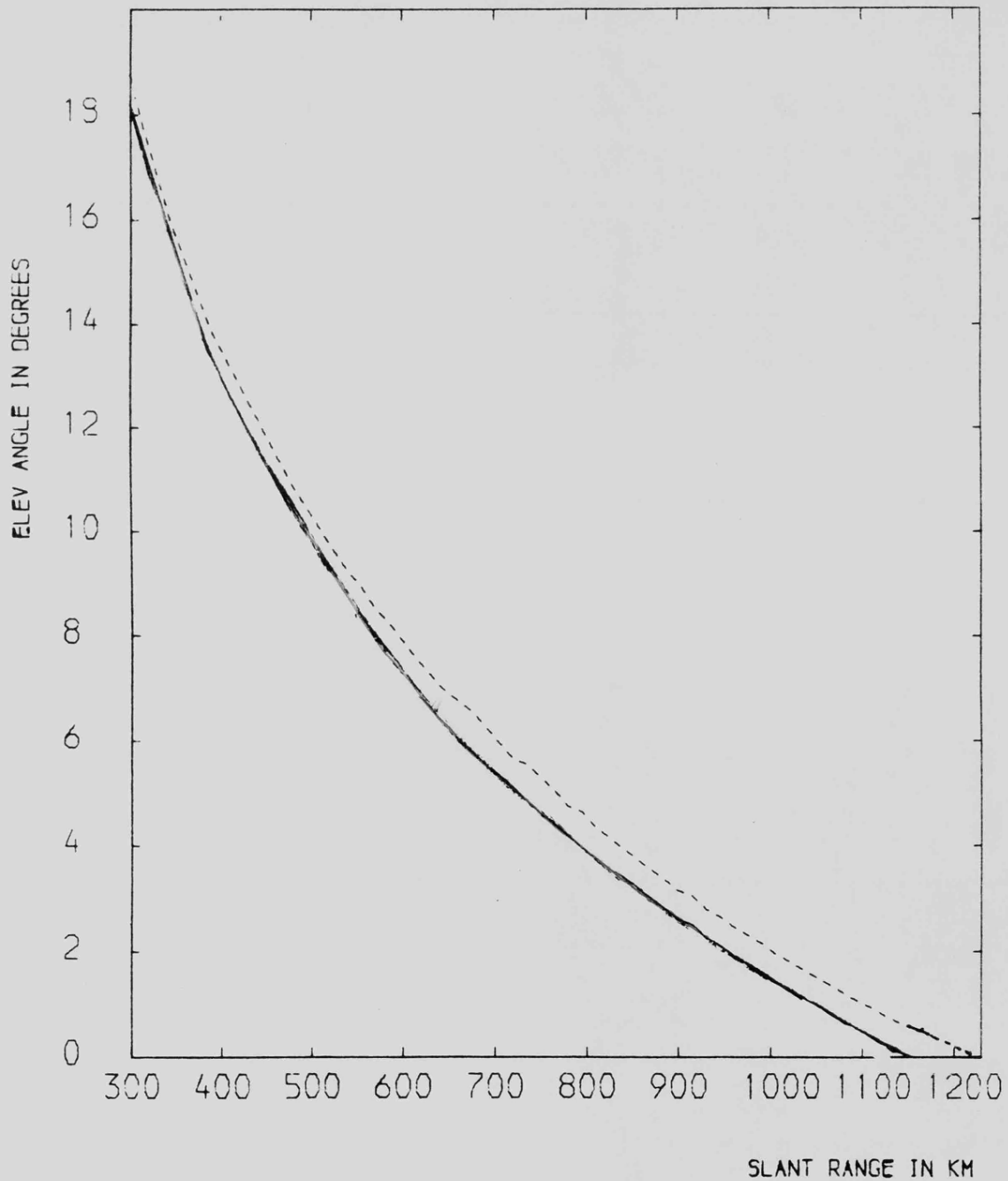
REFRACTION EFFECTS EVALUATED USING CRPL
EXPONENTIAL REFERENCE ATMOSPHERE

FIGURE 4.2

5 degrees elevation the error will probably increase to the order of 0.2 degrees maximum,for 100% humidity,or 0.15 degrees for 60% humidity.In order to derive more exact values of error angles,an investigation of the variation of elevation angle with change of refractive index was undertaken,using standard refraction techniques,but for two different atmospheric reference models,as follows;

4.1.1 Analysis of refraction effects for 2 atmospheric reference models.

Millman,ref(98),1958 derived values of elevation angle errors due to refraction effects by assuming the atmosphere to consist of a series of layers or stratifications, and thence obtaining the changes in the angles of incidence at each layer from Snell's law. A similar analysis employing 2 models of refactive index and the schematic illustration of atmospheric layers in fig(4.3) is:

Let h = spacing between each layer. θ_E=elevation angle of radar beam

R = distance from layer to Earth's centre. W=position of radar

R_E = Earth's radius. i = angle of incidence of radar beam at a layer.

$n_1,n_2,n_3,---n_N$ = refractive index of layers. N = number of layers.

For each layer the angle of incidence,i,can be derived from the expression;

$\sin(i)$ = $\cos(\theta_E)(R/(R+h))$. Applying Snell's law for a spherically symmetrical surface: n_1 R $\cos(\theta_E)$ = n_2 (R+h) $\cos(\theta_{E1})$ and the angle subtended at the Earth's centre,B,for each layer will be

B = 90 - $(\theta_E + i)$ degrees.

By calculating the angles of incidence,elevation and the angle subtended at the earth's centre for each of the layers,the error angles were derived from their summations. The values of refractive index at each layer was derived form the 2 mathematical models of the variation of refractive index with height;

a)The CPRL exponential reference atmosphere

SCHEMATIC ILLUSTRATION OF REFRACTION OF A RADAR BEAM AS IT
PASSES THROUGH ATMOSPHERIC LAYERS
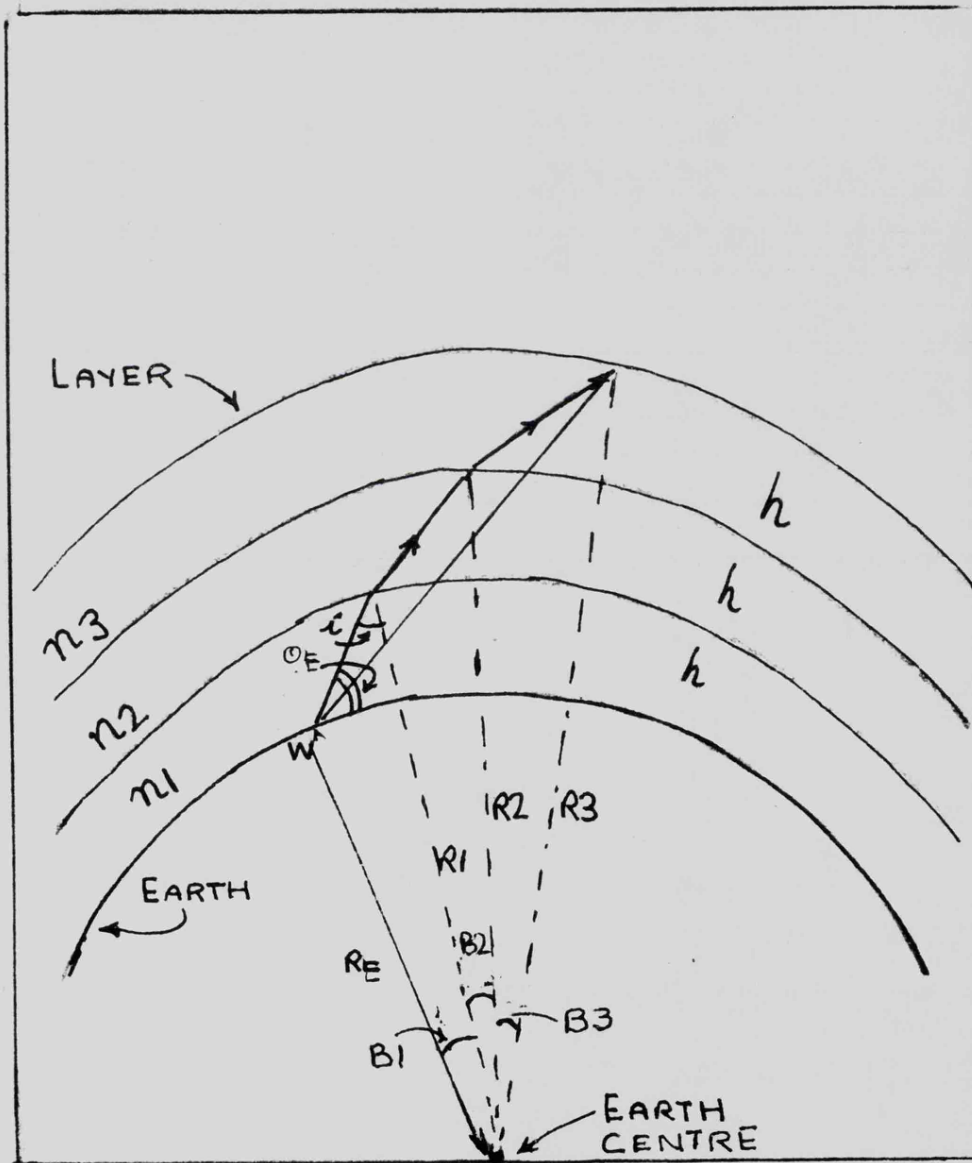
h is the spacing of each layer. W is the position of the radar

R_E is the mean earth radius. i is the angle of incidence of the beam

θ_E is the elevation angle of the beam

B   is the angle subtended at the earth centre

n1,n2,n3, are the refractive indices of the layers.

FIGURE 4.3

$$n(h) = 1.0 + 0.000313 \; e^{(-0.143859 \; h)}.$$ where h=height in kilometres. This model is described in ref(96) by Skolnik.

b) The "Cool-weather exponential model"

$$n(h) = 1.0 + 0.000320 \; e^{(-0.1217 \; h)},$$ where h=height in kilometres. This model is described in ref(97),1968,by Blake.

A second method of evaluating the elevation angle errors due to refraction effects was to evaluate the integral relating radar slant range R_s, elevation angle Θ and refractive index n(h):

$$R(h,\Theta) = \int_{0}^{h} \frac{n \; dh}{\sqrt{1 - \left(\frac{n_{(o)} \; Cos(\Theta_o)}{n(1 + h/R_E)^2} \right)}} \qquad (4.4)$$

Where h = height of the aurora. n(o) = refractive index at ground level

Θ_o = elevation angle at ground level.

This integral and its derivation is described in more detail in ref(131), 1958,by Bauer et al. For the present investigation the integral was evaluated using Simpson's Rule,for elevation angles of 1 to 10 degrees. The elevation angle errors were derived by comparing these values of slant range with those derived from calculations with curved earth theory neglecting the effects of refraction.

The results of these 2 methods of evaluating refraction effects at elevation angles below 10 degrees are in table(4.1),and reveal that the effects are most pronounced below values of 2 degrees,or in terms of SABRE radar slant-range measurement,range-gates greater than 33.For range-gates greater than 39 the angular error will be 0.3 to 0.5 degree.

In the derivation of aspect-angle loss in this chapter range-gate 29 is employed in each of the Wick beams. The elevation angular error at this range will be 0.2 to 0.25 degrees which represents a range-error of about 4 kilometres,which is less than the error in the range-measurements,ie 7.5 km.

TABLE OF ELEVATION ANGLE ERRORS, IN DEGREES
TABLE 4.1

Ground Elevation Angle	Error Angle, Using Increments		Error Angle Using Integration		Slant Range Using Integration		Slant Range Using Curved Earth Theory	SABRE Radar Range Cell
-	Hot	Cold	Hot	Cold	Hot	Cold	-	-
1^0	0.48	0.49	0.37	0.32	1065.8	1060.6	1070.78	39-40
2^0	0.26	0.27	0.27	0.25	958.2	955.9	960.81	32-33
3^0	0.175	0.18	0.21	0.198	865.5	864.4	867.39	25-26
4^0	0.13	0.13	0.17	0.16	785.4	784.8	786.86	20-21
5^0	0.11	0.11	0.14	0.13	715.8	715.4	717.04	15-16
6^0	0.098	0.098	0.11	0.11	655.2	654.9	656.28	11-12
7^0	0.092	0.092	0.098	0.09	602.4	602.1	603.27	8-9
8^0	0.089	0.089	0.084	0.08	556.1	555.9	556.08	5-6
9^0	0.089	0.084	0.071	0.07	515.5	515.4	515.46	2-3
10^0	0.09	0.09	0.062	0.06	479.7	479.6	476.69	

Refractive Index Model used to calculate "Hot" column:

$$n(HT) = 1.0 + 0.000313 \; Exp(-0.143859 \times HT)$$

Refractive Index Model used to calculate "Cold" column:

$$n(HT) = 1.0 + 0.000320 \; Exp(-0.1217 \times (Km))$$

The columns of error angles labelled "using increments" refer to the method of Ray-tracing using incremental atmospheric layers, technique (1) in this chapter.

The columns of error angles labelled "using integration" refer to the method of Ray-tracing using integration, Technique (2) in this chapter.

4.1.2 The conclusion of the analysis of refraction effects.

For the values of radar slant-range that are employed in this chapter in the derivation of aspect-angle, auroral height and antenna height, the effects of refraction need not be compensated. However, for calculations of auroral reflectivity at slant-ranges of greater than 1060 kilometres the effects should be catered for by correction of the elevation angle.

In order to allow for this error, the values of elevation angle derived as shown above can be employed in radar systems of high range-resolution. When the elevation angle, θ_1, has been deduced the angle B at the earth's centre subtended between the radar site and the auroral section at slant range R_S, can be derived as follows:

$$\sin(B) = (R_E/(R_E+h)) \sin(90+\theta_1) \quad \text{where} \quad R_E=\text{mean earth}$$

radius, 6371.2 km, and h=height of aurora in km.

If the elevation angle is not known, and refraction effects are to be considered negligible, then the angle B can be derived as follows:

$$\text{let } S=0.5 \ (R_E+(R_E+h)+R_S)$$

$$\text{then} \quad \tan(B/2) = \sqrt{\frac{(S-(R_E+h))\ (S-R_E)}{S\ (S-R_S)}} \quad\quad (4.5)$$

Once angle B has been evaluated, the elevation angle θ_2 can be derived from:

$$\left(\frac{R_E+h}{\sin(90+\theta_2)}\right) = \left(\frac{R_S}{\sin(B)}\right) \quad\quad (4.6)$$

When values of the angle B have been derived for the slant ranges 300 km to 1200 km, then it is possible to derive the latitude and longitude of each range-cell of the SABRE radar range measuring system, for a given value of auroral height, and radar beam direction.

4.2 <u>Derivation of the latitude and longitude of each range-cell.</u>

4.2.1 Derivation of geographic latitude and longitude.

The geographic position of each section of the diffuse aurora which back-scatters the radar beam at a slant range of R_T can be derived from the parameters in fig(4.4):

In this figure Θ_4=longitude of the radar, Θ_5=latitude of the radar

a=angle subtended between the irregularity at slant range R_T,and the geographic north.

b=angle subtended between radar and north.

Then
$$\cos(a)=(\cos(b)\ \cos(90-\Theta_5)) + (\sin(B)\ \sin(90-\Theta_5)\ \cos(A)) \qquad (4.7)$$
$$\sin(b)=(\sin(B)\ \sin(A))/\sin(a) \qquad (4.8)$$

and the latitude of the section of the aurora at slant range R_T is then given by (90-a) degrees and the longitude is given by (Θ_4+b) degrees.

4.2.2 Derivation of magnetic latitude and longitude.

The relationship between geographic coordinates (latitude Θ_5,longitude Θ_4) and the corresponding geomagnetic coordinates (latitude Θ_7,longitude Θ_8) for an earth-centred dipole field is,in degrees;

$$\sin(\Theta_8) = (\sin(\Theta_5)\ \sin(78.3)) + (\cos(\Theta_5)\ \cos(78.3)\ \cos(\Theta_4-291)) \qquad (4.9)$$
$$\sin(\Theta_7) = (\cos(\Theta_5)\ \sin(\Theta_4-291))/\cos(\Theta_8) \qquad (4.10)$$

These equations are detailed in ref(126),1966,by Davies.

When the values of latitude and longitude have thus been evaluated for each of the 49 range-cells of the SABRE range-measuring system,the aspect-angles can be derived,assuming some magnetic field.

4.3 <u>Derivation of the aspect angles using the IGRF magnetic model.</u>

4.3.1 The derivation of aspect angle.

The aspect angle,beween radar beam and magnetic line of force,is displayed schematically in fig(4.5),for a section of the aurora at slant range R_T.Although the radar beam is drawn as a straight line from radar antenna to the magnetic field line,it is in fact curved downwards very slightly due to the effect of atmospheric refraction. However,the analysis of section(4.1) revealed that this curvature will be negligible at ranges below 1060 kilometres.

SCHEMATIC ILLUSTRATION OF POSITION OF RADAR AND POSITION OF ONE

SECTION OF THE AURORA AT SLANT RANGE RT
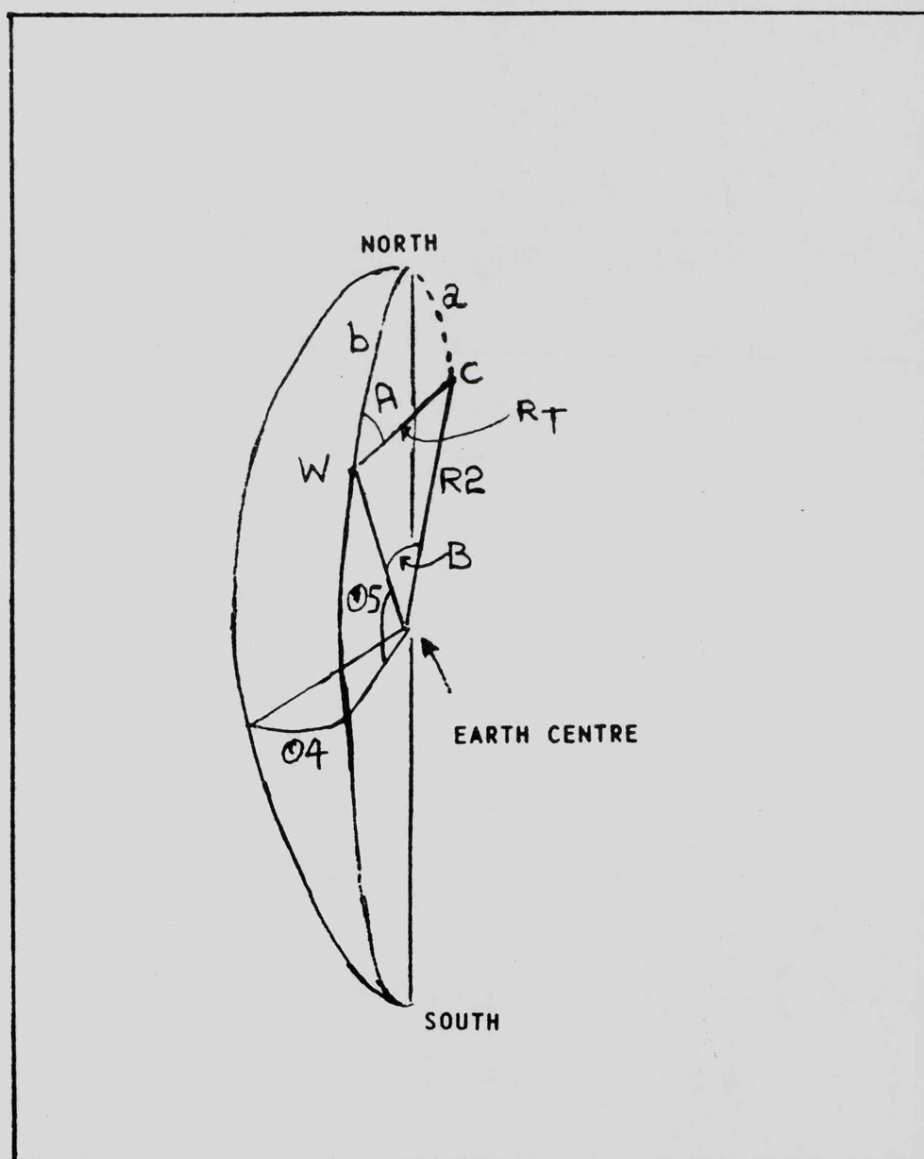
W IS THE POSITION OF THE RADAR
θ4 , θ5 ARE THE LONGITUDE AND LATITUDE OF THE RADAR
C IS THE POSITION OF AURORA AT SLANT RANGE RT
B IS THE ANGLE SUBTENDED AT EARTH CENTRE, BETWEEN
  RADAR AND AURORA
a IS THE ANGLE SUBTENDED BETWEEN AURORA AND POLE
b IS THE ANGLE SUBTENDED BETWEEN RADAR AND POLE

FIGURE 4.4

SCHEMATIC ILLUSTRATION OF THE ASPECT ANGLE BETWEEN A RADAR BEAM

AND THE MAGNETIC FIELD LINE.
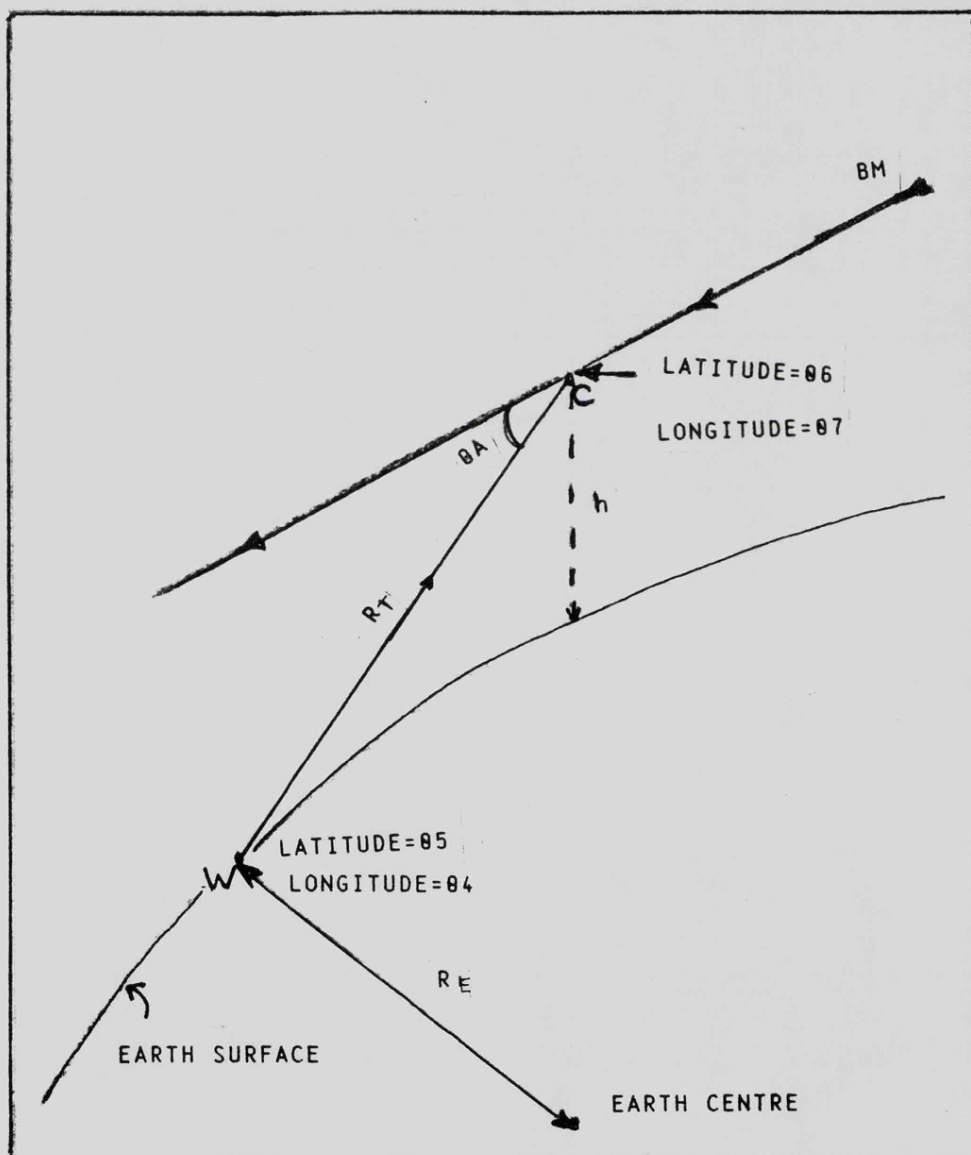
W IS THE POSITION OF THE RADAR.   C IS THE POSITION OF THE AURORA.

R_T IS THE SLANT RANGE.   h IS THE HEIGHT OF THE AURORA.

BM IS THE MAGNETIC FIELD LINE.

θ_A IS THE ASPECT ANGLE BETWEEN RADAR BEAM AND MAGNETIC FIELD.

R_E IS THE MEAN EARTH RADIUS, 6371.2 KM.

FIGURE 4.5

The angle between the radar beam vector and the geomagnetic field line can be derived as follows: it is assumed that the radar beam can be represented by R_T in fig(4.5),at latitude θ_5,longitude θ_4,and that the auroral section at point C has latitude θ_6,longitude θ_7. The polar coordinates can be converted to rectangular coordinates,in order to derive the direction cosines as described in ref(100),1968,by Brown and Manson, as follows: The radar rectangular coordinates,X_R,Y_R,Z_R,are:

$$X_R = (R_E \sin(90-\theta_5) \cos(\theta_4))$$

$$Y_R = (R_E \sin(90-\theta_5) \sin(\theta_4))$$

$$Z_R = (R_E \cos(90-\theta_5))$$

and the rectangular coordinates at point C, X_A,Y_A,Z_A, are:

$$X_A = (R_E \sin(90-\theta_6) \cos(\theta_7))$$

$$Y_A = (R_E \sin(90-\theta_6) \sin(\theta_7))$$

$$Z_A = (R_E \cos(90-\theta_6))$$

Hence the radar beam can be described by the direction cosines:

$$C_X = (X_A-X_R)/d \ , \ C_Y = (Y_A-Y_R)/d \ , \ C_Z = (Z_A-Z_R)/d \tag{4.11}$$

where $d = \sqrt{(X_A-X_R)^2 + (Y_A-Y_R)^2 + (Z_A-Z_R)^2}$

$$\tag{4.12}$$

The magnetic field line at point C is described by the coordinate system of the IGRF magnetic model where

B_{MX} = Northerly component B_{MY} = Eastward component

B_{MZ} = vertical component B_{MF} = total magnetic component.

A full description of the IGRF magnetic field model and its coordinate systems can be found in ref(134),1981,by Malin and Barraclough.

Converting these coordinates to rectangular coordinates provides direction cosines for the magnetic field line of:

$$D_X = ((M_Z \sin(T) \cos(P)) + (M_X \cos(T) \cos(P)) - (M_Y \sin(P)))/M_F$$

$$D_Y = ((M_Z \sin(T) \sin(P)) + (M_X \cos(T) \sin(P)) + (M_Y \cos(P)))/M_F$$

$$D_Z = ((M_Z \cos(T)) - (M_X \sin(T)))/M_F$$

where $T = (90-\theta_6)$ and $P = \theta_7$. $M_Z = -B_{MZ}$, $M_Y = B_{MY}$, $M_X = -B_{MX}$

Hence the aspect angle, Θ_A, is given in

$$\cos(\Theta_A) = (C_X \, D_X) + (C_Y \, D_Y) + (C_Z \, D_Z) \qquad (4.13)$$

The parameter of most interest in assessing aspect-angle loss is the orthogonallity of the radar beam to the magnetic line of force.

The values of aspect angle were calculated using these equations and the extent to which they differed from 90 degrees is displayed in fig(4.6),for auroral heights of between 90 and 110 km,for range-cell 29 of Wick radar,beams 9 to 12. Fig(4.7) is a similar display for Uppsala radar, range-cell 10,beams 6,7 and 8.

Initially the aspect-angles were determined from the POGO magnetic field model but these were not consistent with the actual experimental results since they indicated that maximum echo signal returns should occur in beam 9 of the Wick radar. The aspect angles were then recalculated adopting the IGRF magnetic field model. These calculations indicated that maximum signals should occur in beam 11 which is consistent with experimental observations,as was revealed in chapter 3.The values of aspect-angle change between the Wick radar beam positions at range-cell 29 as calculated via the IGRF and the POGO models were in agreement to 0.01 degree. It is this change in aspect-angle between the beams that is important in this derivation of aspect-angle-loss.Subsequent analysis of aspect-angle loss is confined to the ranges below 1000 km in order to avoid problems associated with weak signals or refraction effects,and also to ranges greater than 600 km because of the shortage of data at these short ranges.

In order to assess the variation of aspect angle with time of year,the mean power levels in cell 29 of each of the 8 Wick radar beams,(corrected for beam pointing losses as in section (4.7)),were plotted as fig(4.8),with averaging times of 30 or 60 minutes.The days selected for this analysis were those when echo signals were present in most of the range-cells of all 8 beams: 1982 days 214,249,250; 1984 day 35.

The Wick echo signal data in fig (4.8) has one common feature,namely

THE VARIATION OF THE OFF-ASPECT ANGLE WITH HEIGHT.

THESE VALUES ARE DERIVED FROM THE IGRF MAGNETIC FIELD MODEL.

WICK RADAR RANGE CELL 29
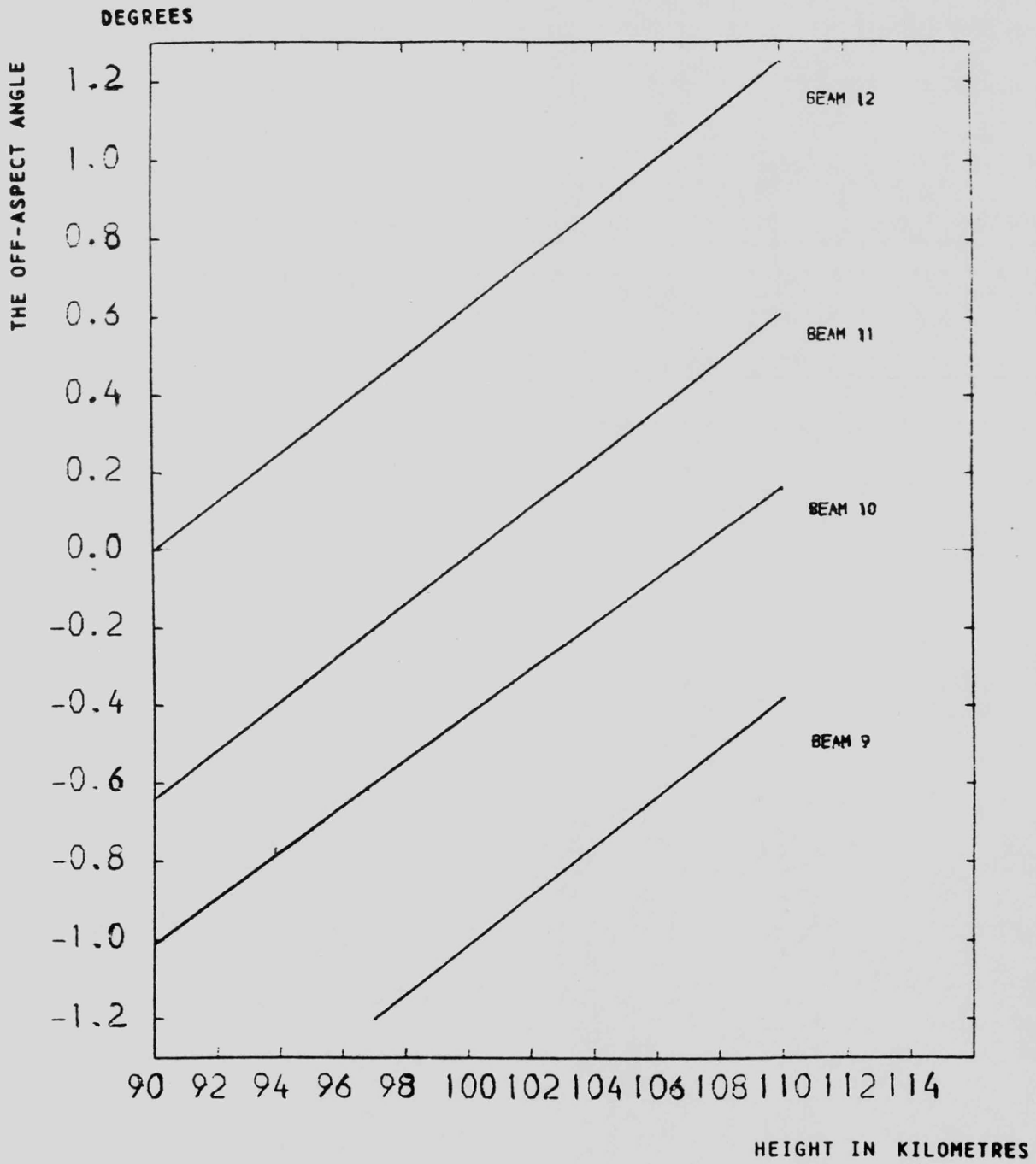
FIGURE 4.6

THE VARIATION OF THE OFF-ASPECT ANGLE WITH HEIGHT.

THESE VALUES ARE DERIVED FROM THE IGRF MAGNETIC FIELD MODEL.
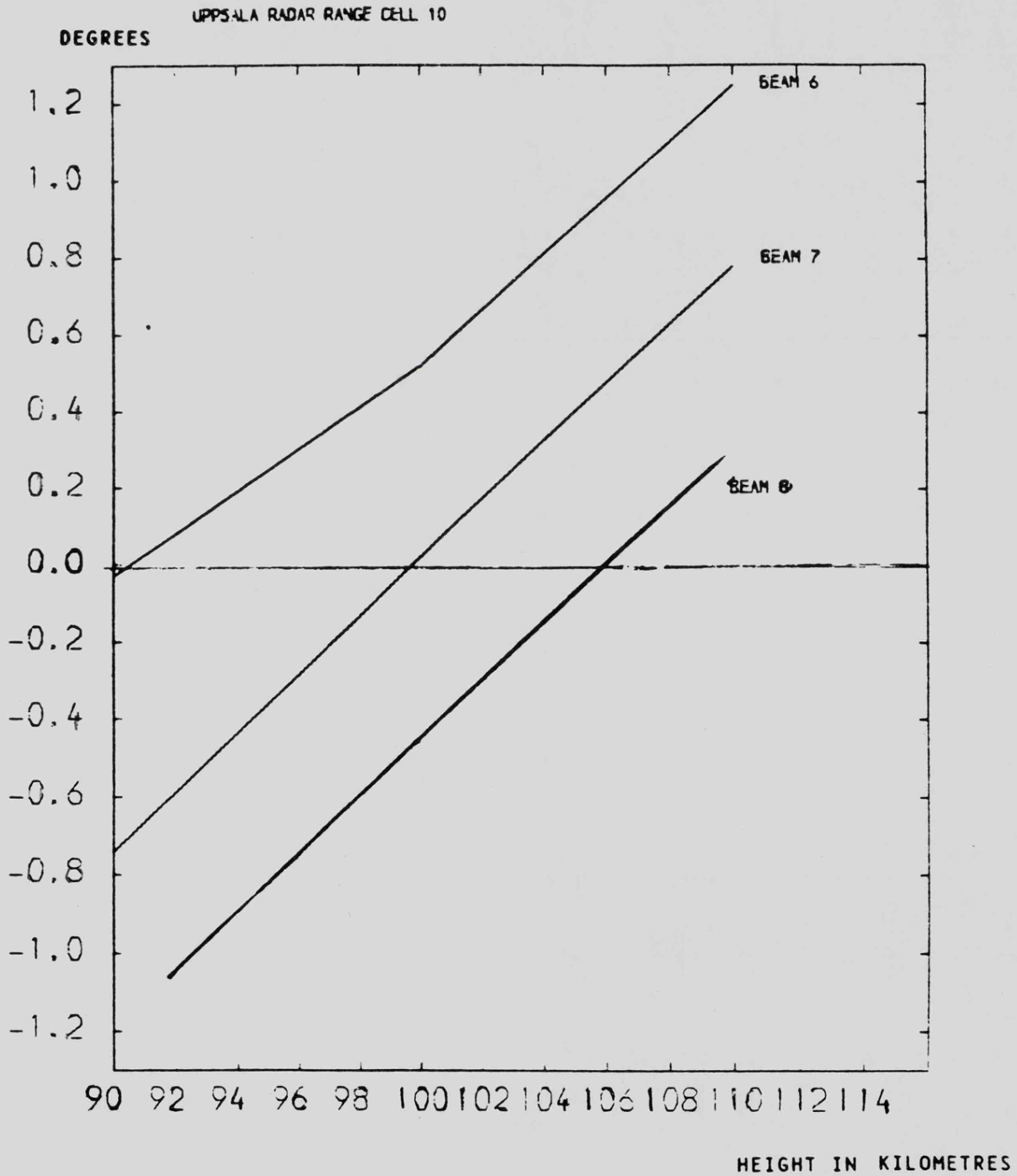
FIGURE 4.7

that beam 11 has the strongest signal,consistently,over the time period selected,at cell 29.Also,the general shape of the curves of power against beam number varies only slightly for signal to noise ratios of greater than 20 dbs. However,this shape is not retained for signal to noise ratios below about 20 dbs.The values of Lerwick magnetic field index,K_L,are plotted in fig(4.8) and generally it was found that the characteristic shape of fig (4.9), in which beam 11 range-cell 29 had the strongest echo-signals,was true for values of K_L greater than 6. For example,when $K_L=4$,on day 264,1982,14:00 to 14:30 hours,the signal curve peaked at beam 9,as in fig(4.8).Since the aim of the analysis was to derive a radar equation applicable when the signals were present in all range-cells,no further investigation of the variation of aspect-angle loss for magnetic indices below 6 was undertaken,apart from noting that the loss was less pronounced for K_L less than 6. Generally,signal strength in range-cell 29 of beam 11 was found to increase with an increase in magnetic index.

The mean signal to noise ratios in each wick radar beam at range-cell 29 were seen to be of a consistent pattern,for relatively strong echoes,in the days of data for 1982,1984.The theoretical values of aspect-angle were then derived for each of the 8 beam positions at this range,using the IGRF model,after calibration of the beam positions with Cygnus ´A´,and calculation of the true range as in section (4.1). The computer programmes developed for this analysis,COERANG and COEREF,are described in chapter 8.

The aspect-angle change with increase of auroral height is plotted in fig(4.6),(4.7),for the three strongest-signal beams of each radar.The aspect-angle variation with beam position is plotted in fig(4.9),for an auroral height of 100 km,for day 249,1982. The calculated aspect-angle pattern agrees well with that determined from the mean of the experimental data. This prompted a more detailed study of the aspect-angle pattern for individual days of the year. The calculated aspect-angle was not expected to vary significantly from day to day and typical values are reproduced below

MEAN SIGNAL TO NOISE RATIO, COMPENSATED FOR BEAM POINTING LOSSES, IN CELL 29 OF EACH BEAM AT WICK, FOR DIFFERENT VALUES OF MAGNETIC INDEX KL
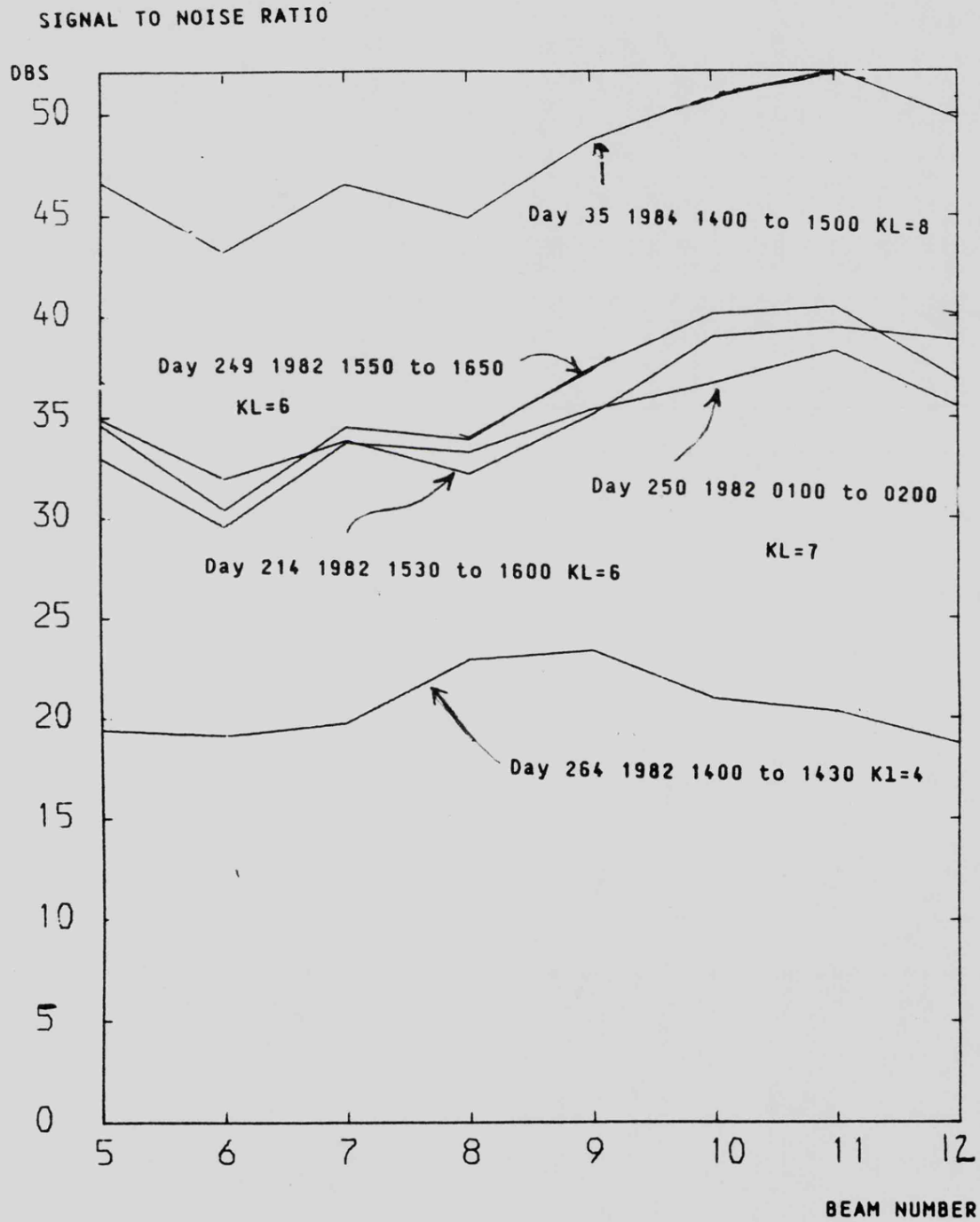
FIGURE 4.8

MEAN SIGNAL REFLECTIVITIES IN CELL 29 OF EACH WICK RADAR BEAM

THE DOTTED CURVE REPRESENTS THE OFF-ASPECT ANGLE (ie 90° - ASPECT ANGLE)

MEAN REFLECTIVITY (NORMALISED)
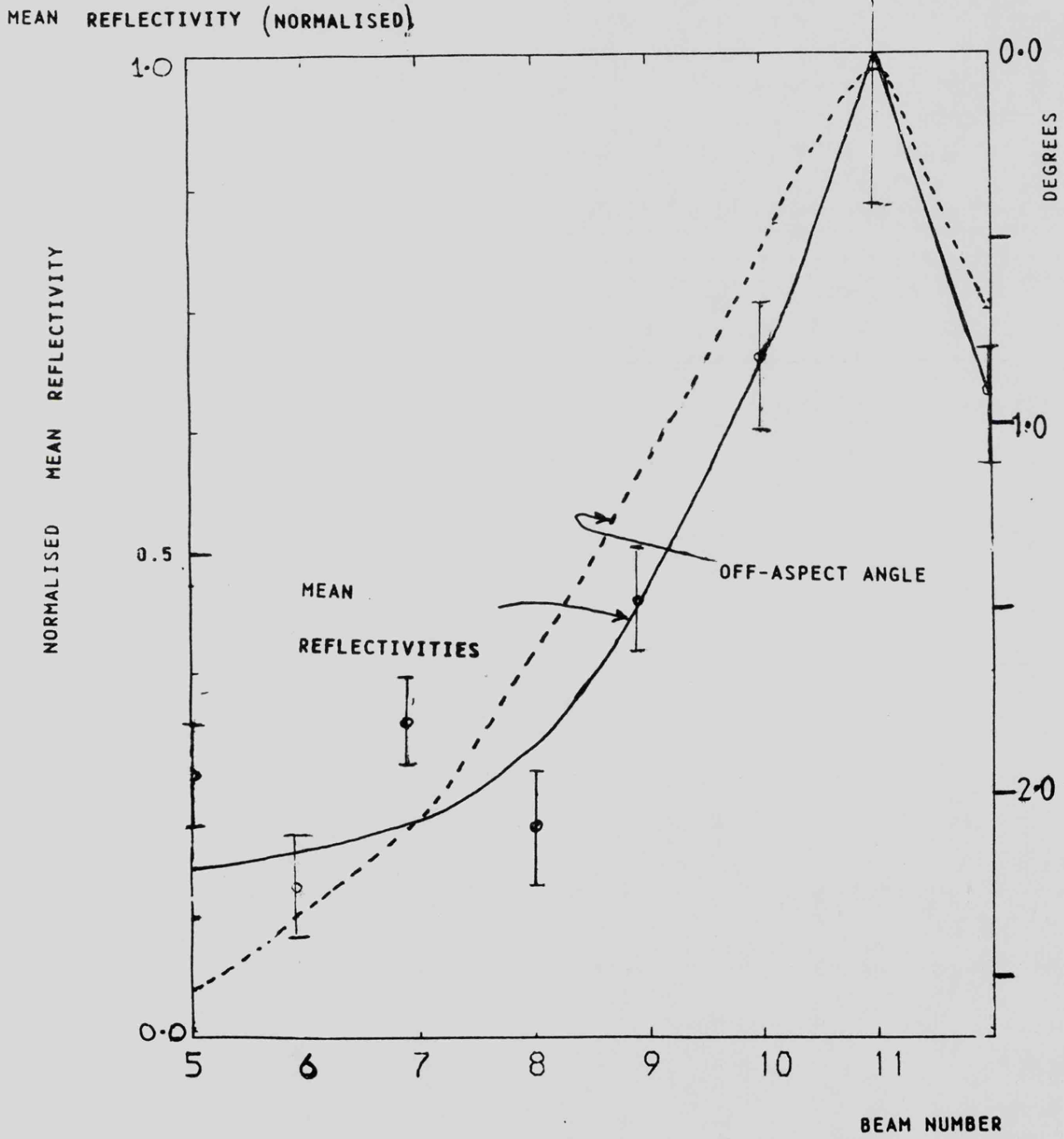
FIGURE 4.9

for both Wick and Uppsala; (it is of interest to note that the observed experimental data distributions across the beams were also consistent)

Wick beam number: 5   6   7   8   9   10   11   12

Aspect-angle   : -2.57 -2.27 -1.91 -1.15 -1.01 -0.46 -0.01 +0.63

These values,in degrees,for range-cell 29 were consistent to within 0.01 degree for days 214,264,249 of 1982 and day 35 of 1984,as were these values of aspect-angle for range-cell 10 of the Uppsala radar;

Uppsala beam   : 5   6   7   8   9   10   11   12

Aspect angle   : 1.14   0.52   0.03 -0.52 -0.66 -1.06 -1.48 -1.73

The IGRF model yielded aspect-angle patterns which closely matched the measured Wick patterns for an auroral height of 100 km.As a further check,the Uppsala echo-signal pattern was examined for day 249 of 1982,at a fixed range-cell in each beam.The Uppsala radar's relatively simple antenna polar diagram,as in fig(4.21),exhibit no deep nulls in the vertical plane.Thus two values of range-cell were selected at which the echo-signals were greatest,(numbers 10 and 20),and the signal to noise distributions across the beams were compared with the theoretical distribution pattern as predicted by the IGRF model for a height of 100 km.The theoretical values,in degrees were as follows;

Beam number   : 5   6   7   8   9   10   11   12

Range-cell 10   : 1.14   0.52   0.03 -0.52 -0.66 -1.06 -1.48 -1.73

Range-cell 20   : 0.44 -0.15 -0.62 -1.14 -1.28 -1.66 -2.01 -2.23

The measured values of signal to noise ratio were as follows;

Range-cell 10   :29.17 33.96 37.60 36.12 33.67 30.04 26.80 26.31

Range-cell 20   :34.56 37.11 36.59 32.12 28.56 24.36 20.75 21.24

It was evident that for both values of slant-range the IGRF model had correctly predicted the beam numbers that would have the strongest echo signal.A mean value of aspect-angle-loss as determined from fig(4.9),(4.10) for signal to noise ratios of greater than 30 dbs is 5.5 dbs per degree for off aspect angles of less than 1.8 degrees;for ratios below 20 dbs this loss

A DISPLAY OF THE LOSS IN RECEIVED ECHO POWER (IN DBS) AGAINST THE OFF-ASPECT ANGLE.
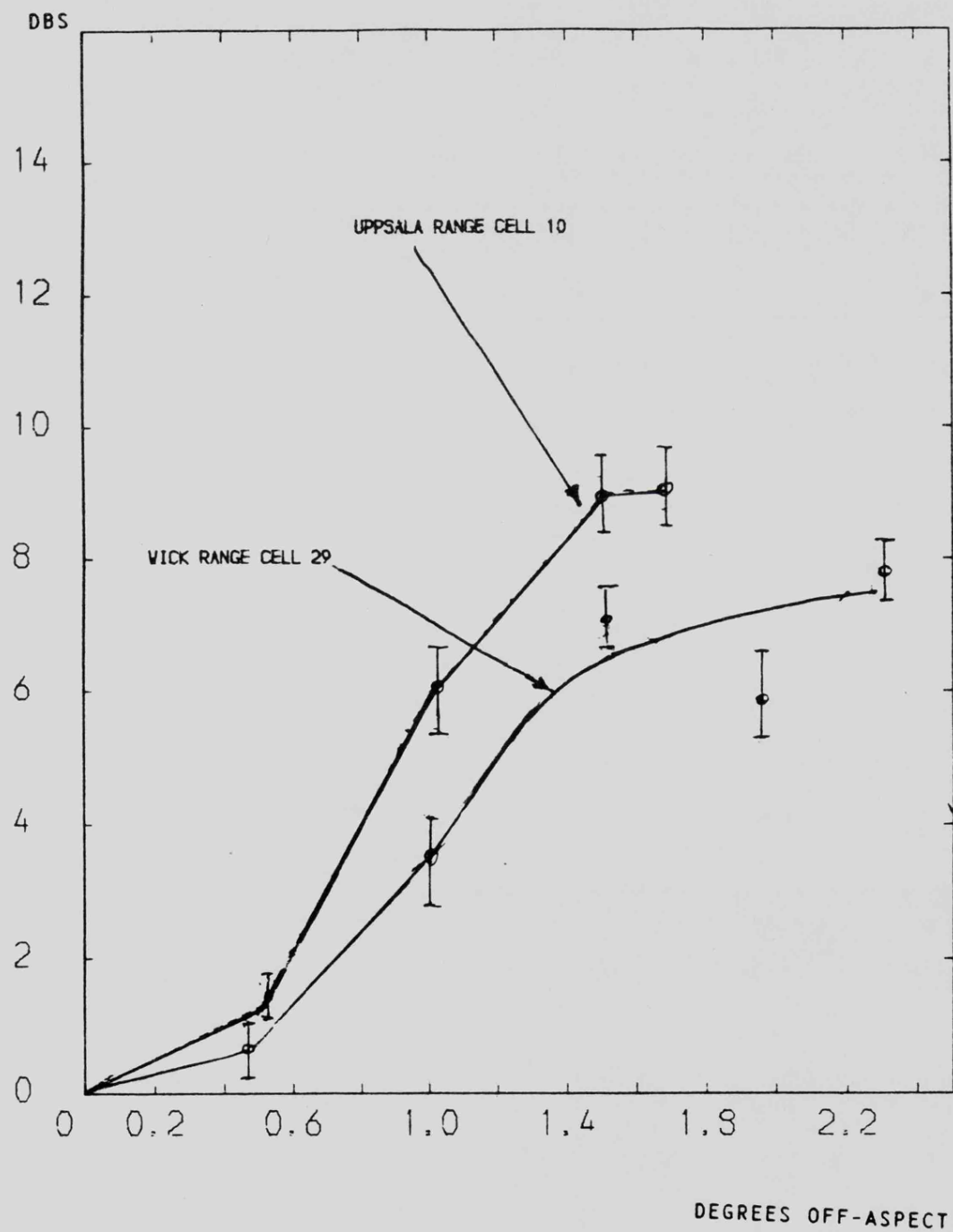
FIGURE 4.10

reduces to about 4 dbs per degree.

Although a very close match between theoretical aspect angles (using IGRF model) and actual echo-signal values is obtained for both radars,one difference exists between the aspect-angle pattern of the 2 radars. Fig(4.10) indicates that the Wick radar pattern of power level loss against off-aspect angle does not increase uniformly above 1.5 degrees as is the case for the Uppsala radar.Examination of the antenna azimuthal polar diagram revealed that the sidelobe levels were of the order of -25 dbs for the Uppsala radar but only about -10 dbs for the Wick radar,as detailed in chapter 7.It is possible that echo-signals received in the radar beam sidelobes are responsible for the non-linear trend in the Wick pattern reproduced in in fig (4.10),and hence the Uppsala data was used in determining the mean value of aspect-angle loss.

4.3.2 The accuracy of measurement of the aspect-angle loss.

The magnitude of the auroral back-scatter signal fluctuations in Wick radar beams 10,11,12 was evaluated by examining the variation with time of the echo signal levels at range-cell 29.Fig (4.11) displays such signals for a period of 1 hour for day 250,1982. The correlation between the signals is clearly evident. Similar correlation was found during the afternoon period of day 249,1982. Fig (4.12) illustrates the variation with time of the signal levels at the point of overlap for best orthogonality between the 2 radars as employed in the analysis of beam-pointing error,namely 64.26^{o} N,6.0^{o} E.In this figure,the dotted curve represents the Uppsala signal variations.For the afternoon period of day 249,1982 (in the analysis of aspect-angle loss) the signal fluctuations lay within a band of + 1.5 dbs,and fig(4.13) indicates that the electrojet was consistently eastwards,with no sudden reversals of flow,(which often occurred during night-times).Furthermore,the data of day 249,1982, contained no evidence of pulsating auroral echo signals,as in day 355,1982,fig(4.14).

A COMPARISON OF THE VARIATIONS OF REFLECTIVITY WITH
TIME IN RANGE-CELL 37 FOR WICK BEAMS 10,11,12.
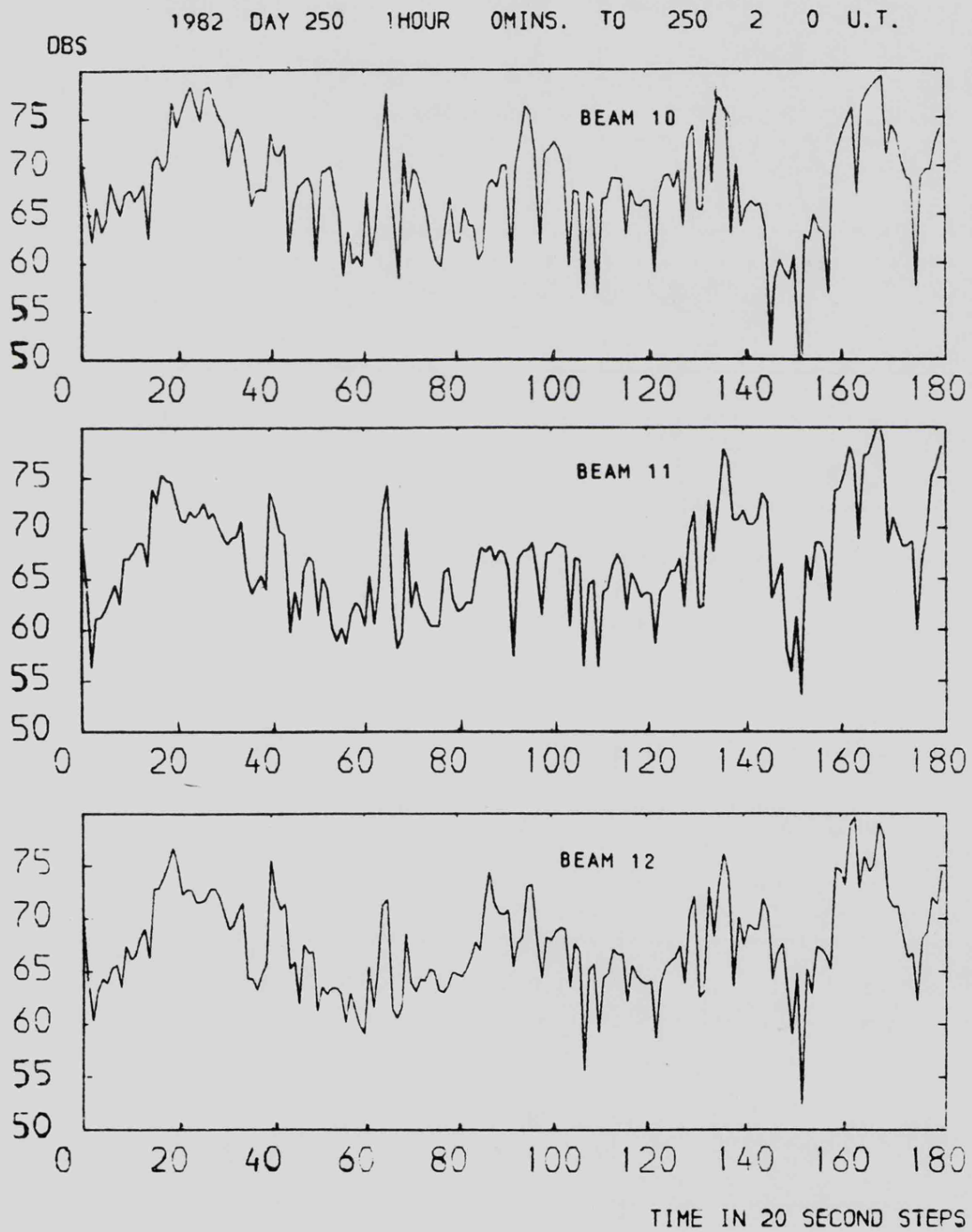
FIGURE 4.11

COMPARISON OF AURORAL REFLECTIVITIES AT 64.26° N, 6.00° E, AGAINST TIME

DASHED LINE IS UPPSALA DATA.

BOTTOM GRAPH SHOWS THE RESULTANT ELECTROJET VELOCITY VARIATION
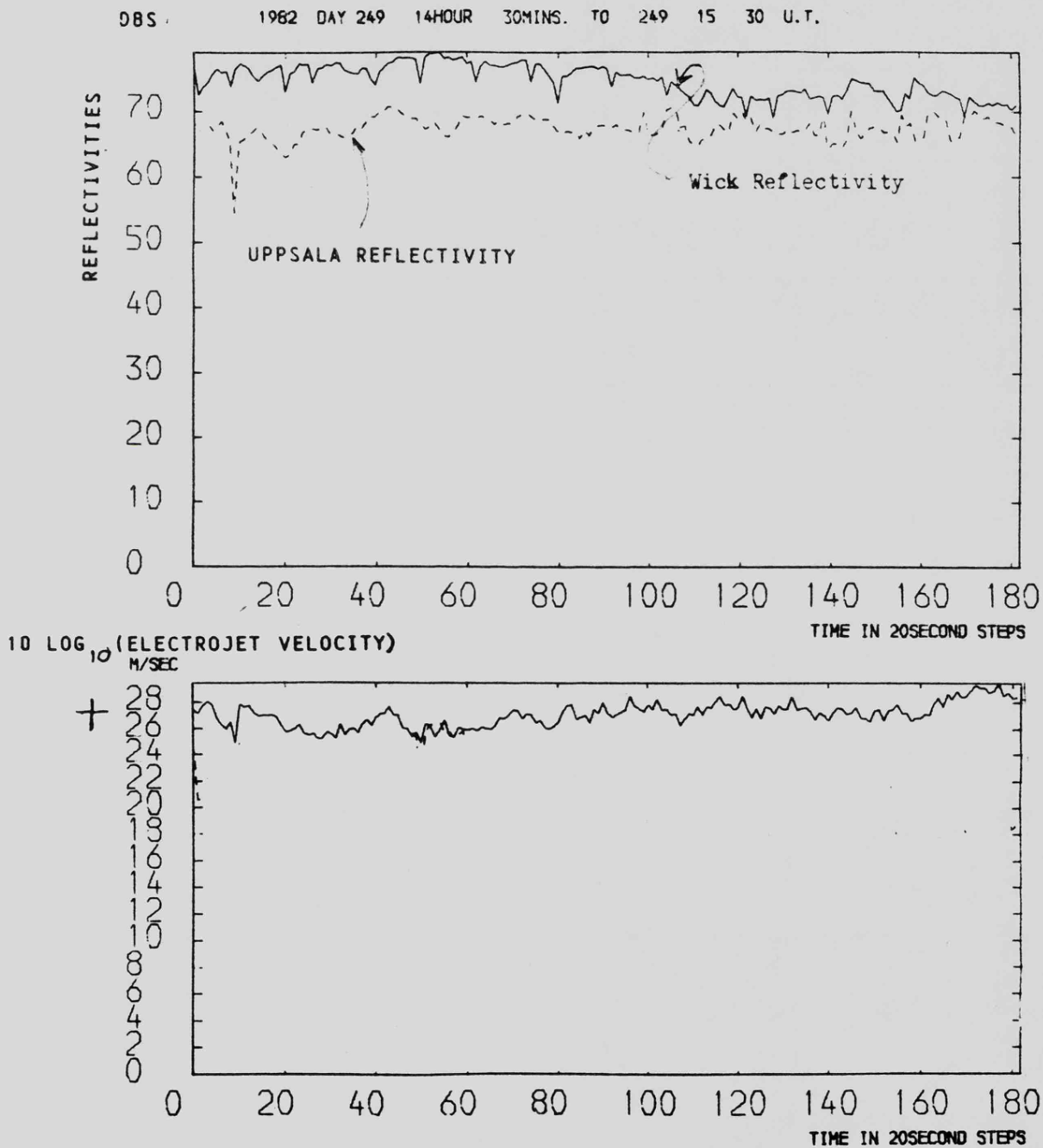
FIGURE 4.12

PLOT OF RESULTANT FLOW –ANGLE WRT BEAM 11 AGAINST TIME
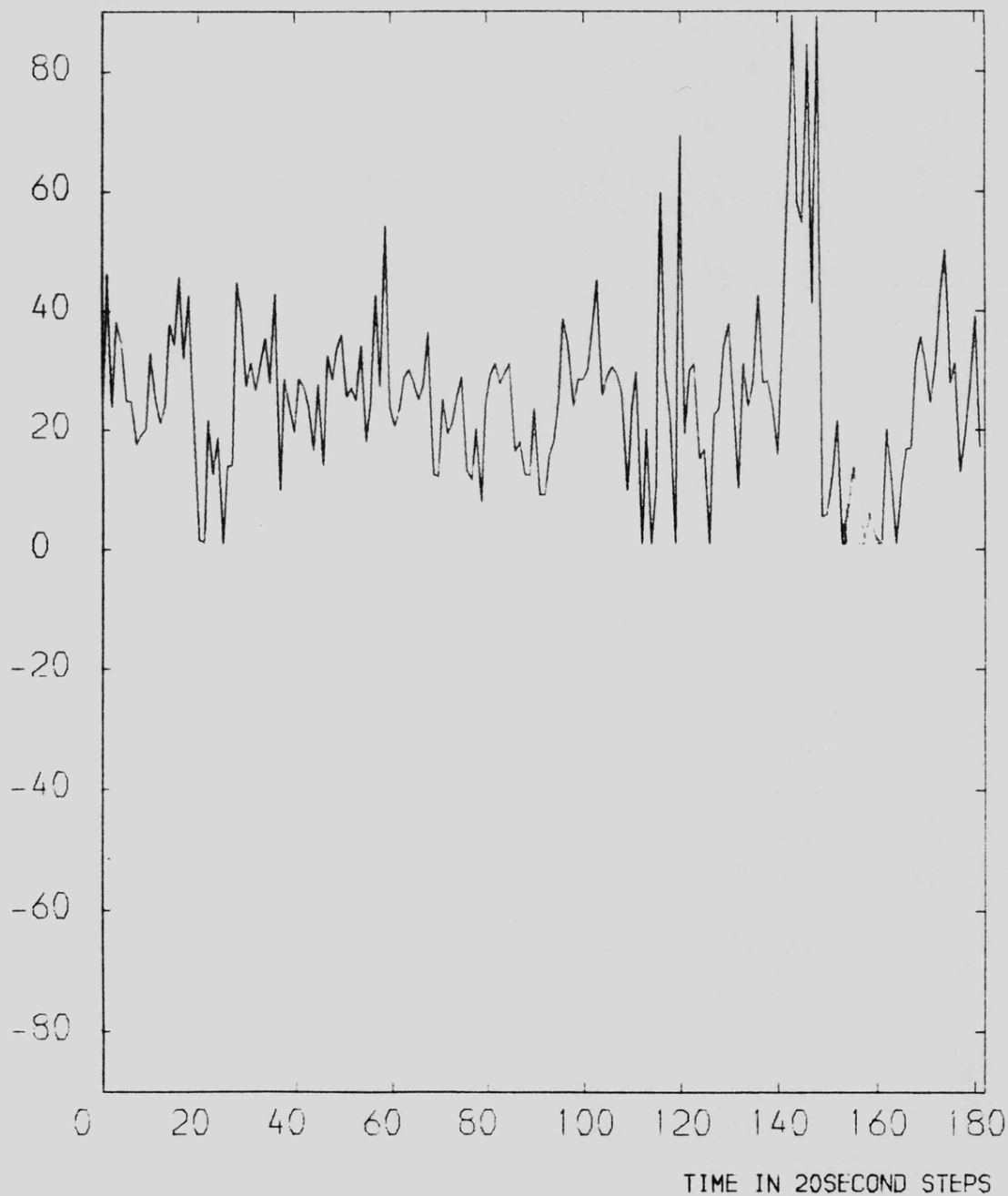
FIGURE 4.13

COMPARISON OF AURORAL REFLECTIVITIES AT 64.26° N, 6.00° E, AGAINST TIME

DASHED LINE IS UPPSALA DATA.

BOTTOM GRAPH SHOWS THE RESULTANT ELECTROJET VELOCITY, VARIATION
(POSITIVE VELOCITIES ONLY)
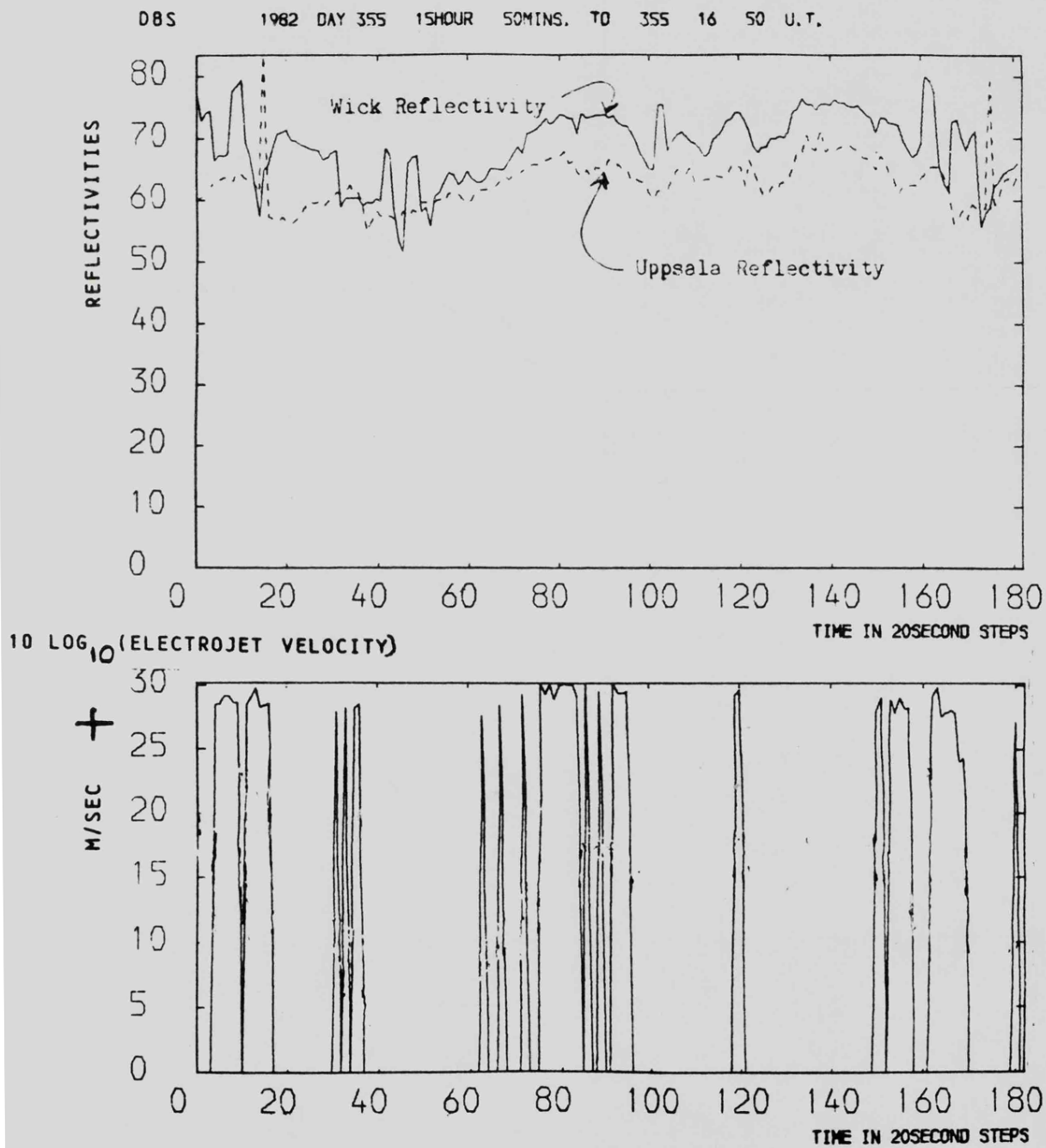
FIGURE 4.14

This analysis of Wick beams 10,11,12 and Uppsala beam 5 data indicated that during the times employed in the assessment of aspect-angle loss for angles below about 1.5 degrees,the data fluctuations from the mean were;

a) echo-signal power levels   -1.5 dbs to +1.5 dbs.

b) Electrojet velocity levels   -2 dbs to +2 dbs.

c) Electrojet flow-angle   +10   to -10 degrees.

The signals were present for each integration period,for 1 hour.The backscatter intensity varied with time;however,this variation was well correlated for each beam position employed in determining the aspect angle losses.Thus it is possible to compare the values of this parameter obtained in all the beams at any instant.The computer programme developed for this analysis is COEMER,described in chapter 8.

A band of accuracy of $\pm$ 2 dbs was thus assumed for the measurement of aspect angle loss employing the techniques described in this chapter. A more general method of deducing this loss,incorporating the radar equation,for other values of slant-range will now be described.

4.3.3 Determination of the averaged aspect-angle loss,for all ranges.

The averaged aspect-angle loss was obtained by comparing the mean echo-signals in neighbouring range-cells of all 8 radar beams,after suitable compensation for the effects of range,beam-pointing losses and antennae polar diagram. The aspect-angle change between each neighbouring pair of range-cells was derived from the IGRF model and the averaged value of aspect-angle loss determined for slant-ranges 630 km to 1050 km,over both a 1-hour and a 10-hour period.The beam-pointing losses corresponding to these times and the aspect-angle losses were as follows;

DAY in 1982	Mean beam-pointing loss	Mean aspect-angle loss	
		WICK	UPPSALA
249 for 10 hours	0.14 dbs/degree	6.47	5.7 dbs/degree
249 " 1 "	0.16 " "	5.8	5.6 " "
250 " 1 "	0.16 " "	6.3	5.5 " "

The days of data employed in this analysis were those when the Lerwick Magnetic Indices were always greater than 6 and the auroral backscatter signals were consistently high,(greater than 20 dbs signal to noise ratio). Under these conditions,employing the Uppsala data for off-aspect angles of up to 1.8 degrees,the mean value of aspect angle loss is 5.6 ± 2 dbs per degree.For weaker echo signals the loss figure will be lower,but would require a more thorough investigation.

The method of determining the radar beam positions will now be described.

4.4 The derivation of beam position using a radio star.

The technique of employing Radio Stars as point sources of wide-band noise for calibration of antennae has been used for many years and is described in ref(120),1966,by Smith,ref(121),1982,by Czechowsky and ref(122) 1981,Marconi Review. This method was employed during the data analysis in order to locate the azimuthal positions of the SABRE radar beams and to detect errors in the beam-forming matrix.

The SABRE radars consist of an array of fixed antenna beams whose azimuthal directions are constant with respect to geographic north and whose elevation angle coverage is limited to less than 20 degrees. Each beam is relatively narrow in azimuth,of about 3.2 degrees at the half power beam width. Hence,in order to detect a radio star in the SABRE receiver system,the time at which the radio star crosses each radar beam (at the appropriate elevation angle and azimuth angle) must be accurately predicted. The movements of four such radio stars were examined; Cassiopeia ´A´,Cygnus ´A´,Virgo ´A´ and Taurus ´A´. The one most suitable as an azimuthal calibration point source was Cygnus ´A´ and its position relative to the radars was determined as follows;

4.4.1 Radio star coordinates.

Radio star locations are generally defined using the Equatorial Coordinates RIGHT ASCENSION (α),and DECLINATION (δ),as illustrated schematically in

fig(4.15), whereas radar sites are generally defined in Horizon Coordinates,LATITUDE,(Θ_L) and LONGITUDE (L).

The values of RIGHT ASCENSION and DECLINATION for Cygnus ´A´ for the years following 1950 must be corrected for precessional effects to achieve highest accuracy;

Right Ascension (corrected)=((Right Ascension) (0.008625 Y_Y)) where Y_Y=number of years since 1950.

Declination (corrected) =(Declination 0.0027361 Y_Y)

The horizontal coordinates ,a,A,of a radio star at any given time t, can be derived from the equatorial coordinates as shown in ref(99),by McNally, "Positional Astronomy" as follows:

Let A = azimuth of radio star using horizontal coordinates

let a = elevation of " "   "   "   "

let Z = 90-a   be the zenith distance of the radio star

Then $\cos(Z) = (\sin(\Theta_L) \sin(\delta)) + (\cos(\Theta_L) \cos(\delta) \cos(H))$ (4.14)

where H = hour angle of the radio star and is related in time to the right ascension, $\aleph$, by:

H = Local sidereal time - right ascension.

The local sidereal time,L_{ST},can be derived from:

L_{ST} = Greenwich mean sidereal time + (longitude/15)

where Greenwich mean sidereal time,G_{MST},is calculated from:

G_{MST}= 6.645833 + ((8640184.542) (number of Julian centuries))

The derivation of these formulae is shown in some detail in ref (114), "American Ephemeris and Nautical Almanac".

When the elevation angle,a,has been derived,the azimuth angle A,can be derived from the following expression:

$\sin(\delta) = (\sin(\Theta_L) \cos(Z)) + (\cos(\Theta_L) \sin(Z) \cos(A))$ (4.15)

Elevation and azimuth angles for Cygnus "A"and Cassiopeia "A" against time for day 76 of 1982 are displayed in fig(4.16). The times of day in 1982 when Cygnus "A" could be received in Wick beam 12 are plotted in figure (4.17).

SCHEMATIC ILLUSTRATION OF EQUATORIAL COORDINATES.
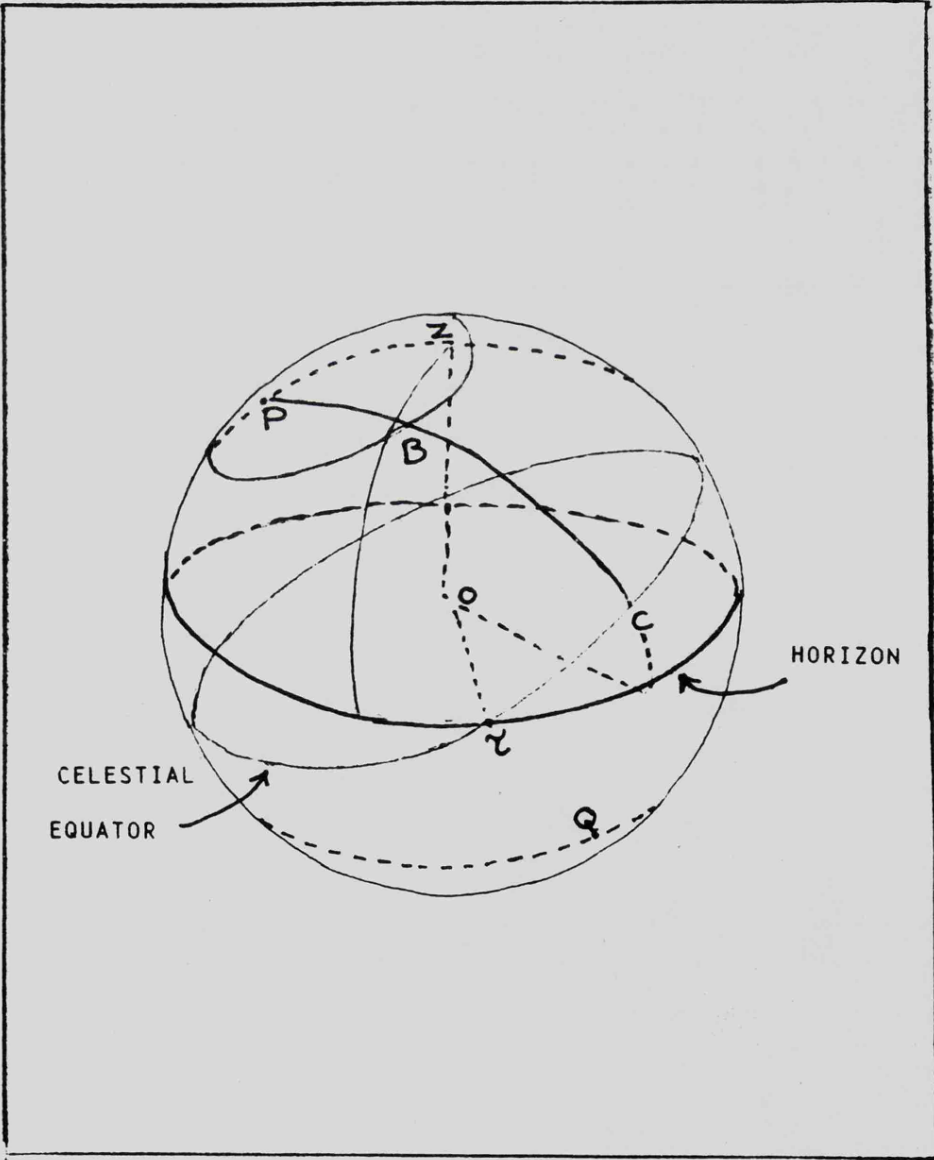
P AND Q ARE THE CELESTIAL POLES.

ANGLE (ZPB) IS THE HOUR ANGLE.

BC IS THE DECLINATION. ♈ IS THE RIGHT ASCENSION

FIGURE 4.15

PLOT OF ELEVATION AND AZIMUTH ANGLES AGAINST TIME FOR CYGNUS "A".

ON DAY 76,1982.

DASHED LINES ARE FOR CASSIOPEIA "A"
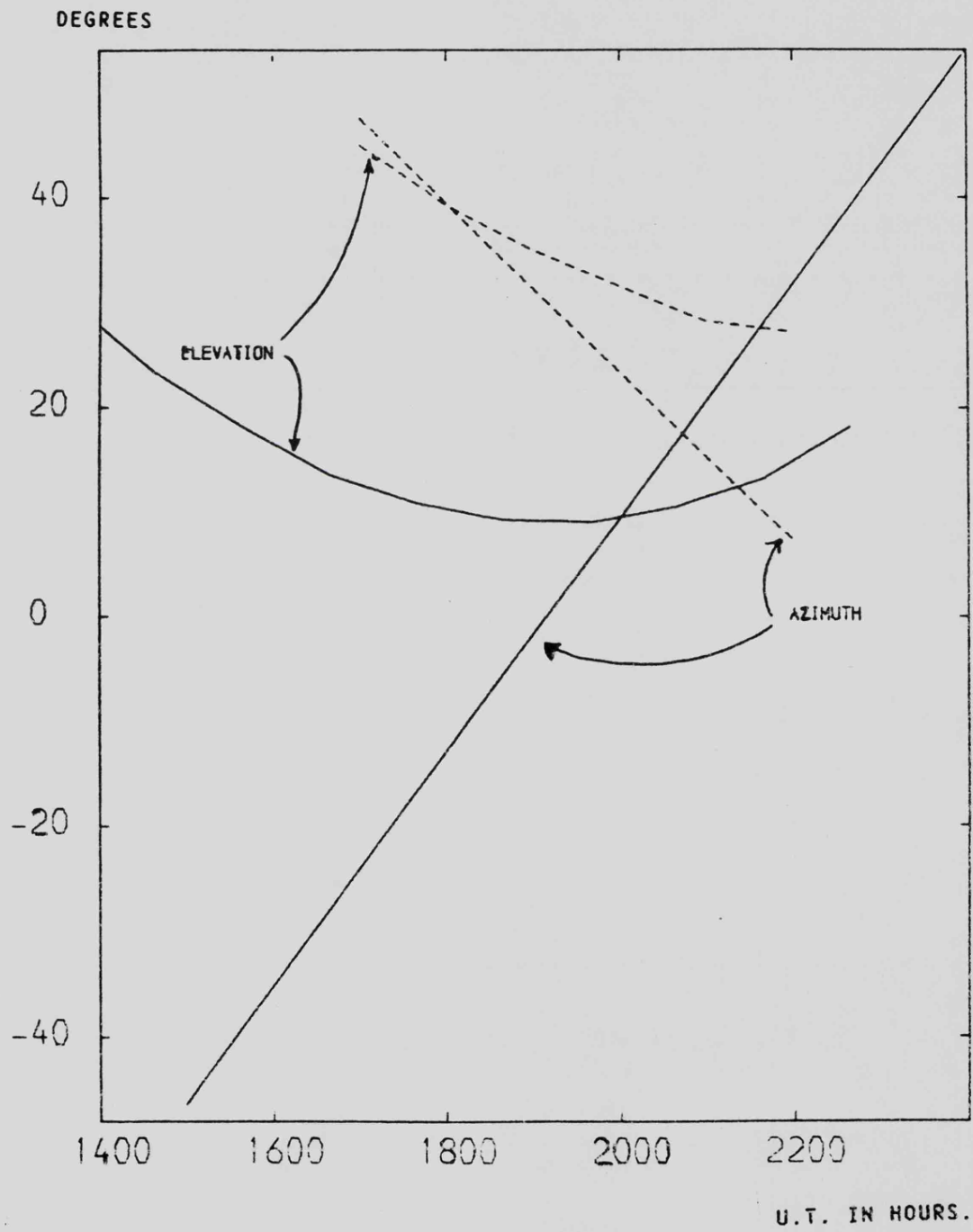
DEGREES

U.T. IN HOURS.

FIGURE 4.16

TIME OF DAY WHEN CYGNUS "A" COULD BE RECEIVED IN WICK BEAM 12

U.T. IN HOURS.

DAYS OF YEAR 1982.
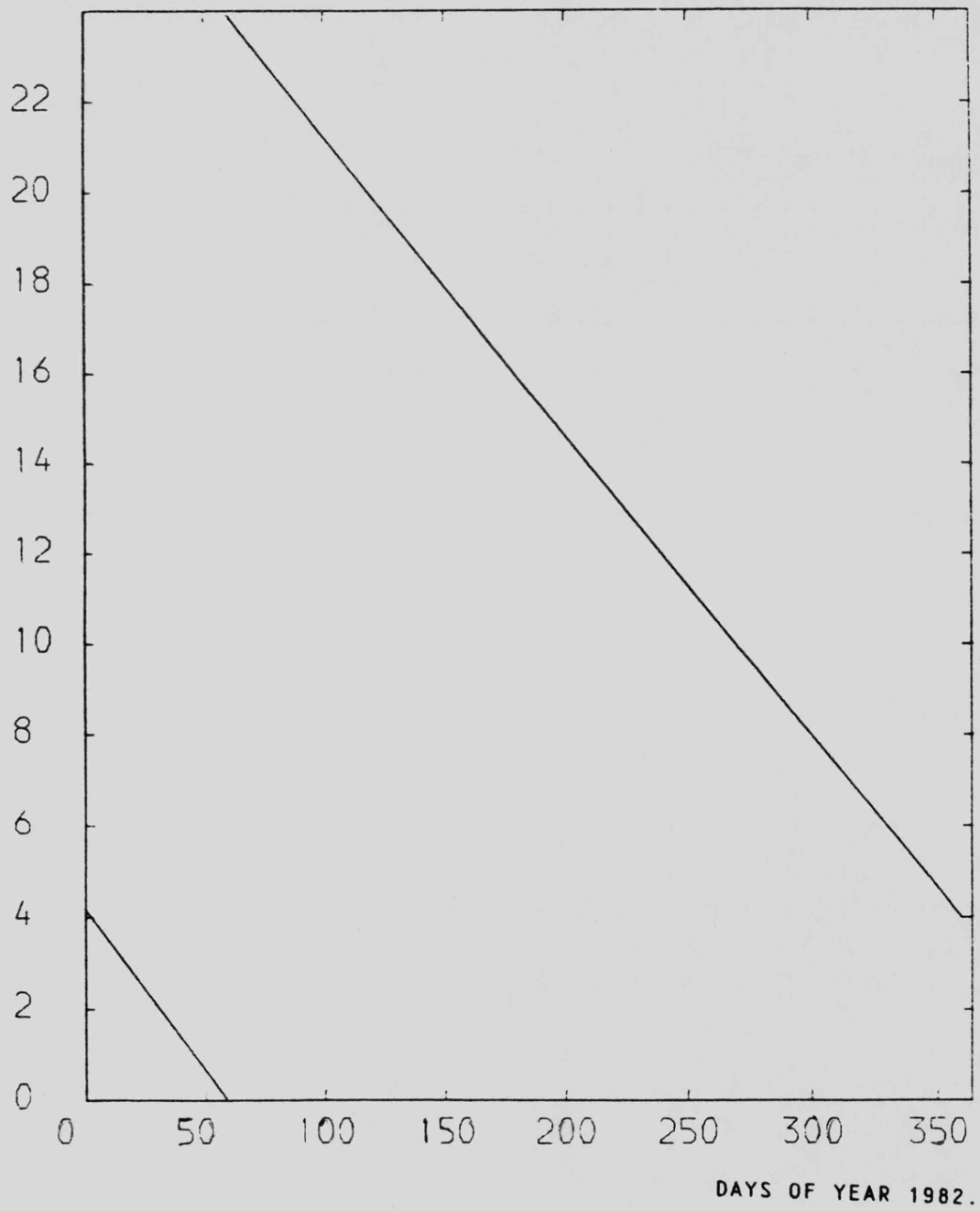
FIGURE 4.17

4.4.2 Results of the calibration.

The azimuthal angular crossing rate of Cygnus´A´ was 11.3 degrees per hour or approximately 23 minutes per radar beamwidth.During the time of passage of the radio star across each beam its elevation angle change was relatively small and the elevation angle did not fall below 12 degrees.Hence the change in signal level from the radio star due to change in elevation angle was not significant since the only major null occurred at 4.2 degrees,and only in the Wick radar.

The elevation and azimuth angles of the radio star noise source were calculated and its position relative to the azimuth polar diagram of each radar beam was determined.The passage of the stellar noise source across each beam was measured by recording the change in output level of the noise-gate for each of the 8 beams.From this information the azimuth polar diagram peak was ascertained. The normal SABRE receiver pulse frequency of 20 Hz and integration time of 20 seconds were employed,but on certain days of the year,(when no auroral signals were present),the noise-signals from all 50 range cells in a beam were added,to increase the data output.In order to resolve the beam-shape from the noise signal fluctuations a 5-point running mean was employed.

The search for days of Wick data containing signals applicable to this azimuthal calibration were complicated by the occurrence of very low-level interference signals,as displayed in fig (4.18).These signals were thought to emanate from local industrial sources and were of a regular frequency and power level.

When suitable days of data had been analysed for both radars,the resultant signal to noise ratios proved to be sufficient to enable a calibration of the beam positions,but not the antenna sidelobes. Modifications to the SABRE operating parameters,(integration times and P.R.F),to improve these ratios are considered in chapter 7.

The results of this analysis of the SABRE radar beam azimuth maxima are;

WICK SABRE DATA   BEAM 11

ILLUSTRATION OF TYPICAL LOW-LEVEL NORMALISED INTERFERENCE SIGNAL.
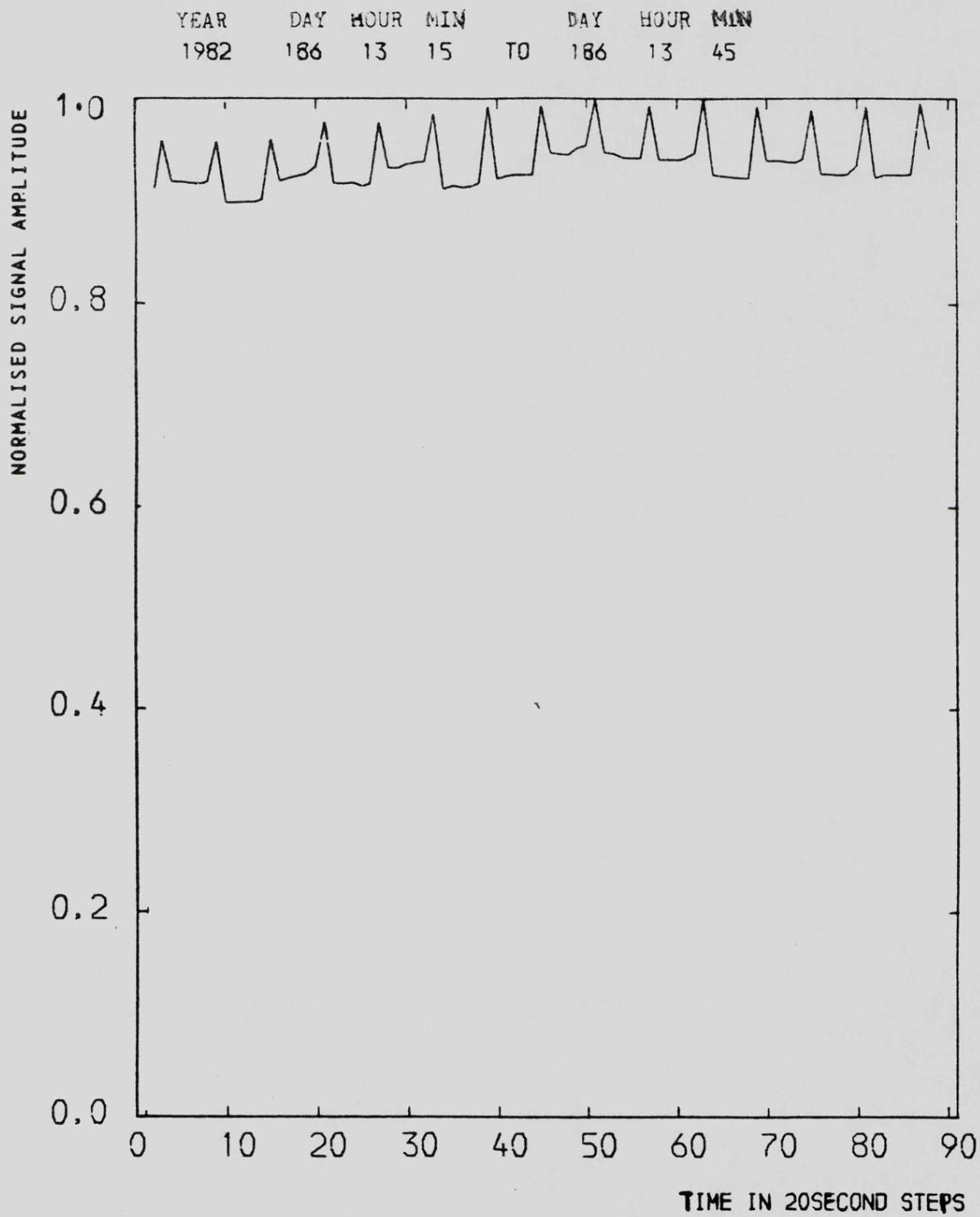
FIGURE 4.18

	WICK RADAR		UPPSALA RADAR	
Beam number	Theoretical	Actual	Theoretical	Actual
5	12.4	12.71	-45.6	-43.72
6	16.0	15.93	-42.0	-40.11
7	19.6	19.31	-38.4	-37.02
8	23.2	22.73	-34.8	-33.22
9	26.8	26.55	-31.2	-32.10
10	30.4	30.33	-27.6	-28.97
11	34.0	33.20	-24.0	-25.19
12	37.6	36.97	-21.4	-22.72

The theoretical values are derived from the known positions of the antenna on the assumption that the Butler matrix will produce a pattern of beams separated by 3.6 degrees in the azimuth plane.As can be seen from this table of results,the differences between theoretical and actual values are relatively small and are probably attributable to slight misalignment in the Butler matrices.The computer programme developed for this analysis,Coenak,is described in chapter 8.

4.5 <u>Calibration of the radar system filters using a radio star.</u>

An examination of the output of each receiver of the 2 SABRE radars was made by means of the radio star Cygnus ´A´,employed as a wide-band noise source.

The averaged value of the output noise power was calculated for measurements of Doppler frequency in the range -1600 to +1600 Hz. The results indicated that the output filters were correctly adjusted to within 5%.Hence the filter loss, L_{FIL}, in the radar equation can be neglected,in comparison with the other losses.

4.6 <u>Derivation of the Antenna polar diagram and antenna height.</u>

During the times of strongest geomagnetic activity when the diffuse
aurora is distributed in azimuth and in latitude,it may be considered as a
layer or canopy of fairly uniform height. Under these conditions the
elevation polar diagram will influence the variation of echo strength with
slant range.Examination of the auroral backscatter signals received at the
Wick radar revealed the presence of nulls (i.e. minima) in the signal
amplitude at certain slant ranges.After compensating these signals for the
variation in signal strength with slant range and aspect-angle the positions
of the nulls and of the peaks were determined and mean values of the null
depths were derived.On many days all of the range-cells did not contain echo
signals.However,the variation of amplitude with range,(ie cell-number),was
always in the same sense irrespective of the absolute magnitude of the echo
signal.Thus the underlying elevation polar diagram gain pattern was evident
in all of the data examined.Because of the variation of signal power with
Doppler velocity,(as diplayed in fig(3.8)),measurement of peak and null
amplitudes were taken when each was at the same Doppler velocity and the
electrojet flow angle was most uniform.In this way a mean value of null
depth was obtained,generally over a half-hour averaging period.

From the measurement of null depth in the elevation polar diagram,the
value of ground reflectivity was estimated and from the position in slant
range of the nulls and peaks the effective height of the antenna above the
reflecting plane was derived,as follows:

4.6.1 The Wick radar antenna elevation polar diagrams.

The vertical polar diagram of the Wick radar was expected to be
relatively wide and free of ground reflection effects,because of the 6
degree backwards tilt of the array from the vertical.Due to the appearance
of the nulls,ground reflection effects were investigated,using the
configuration illustrated in fig(4.19).The reflecting surface need not
actually be the ground level beneath the array,but might be a more

SCHEMATIC ILLUSTRATION OF THE EFFECTS OF REFLECTION FROM A GROUND
PLANE.
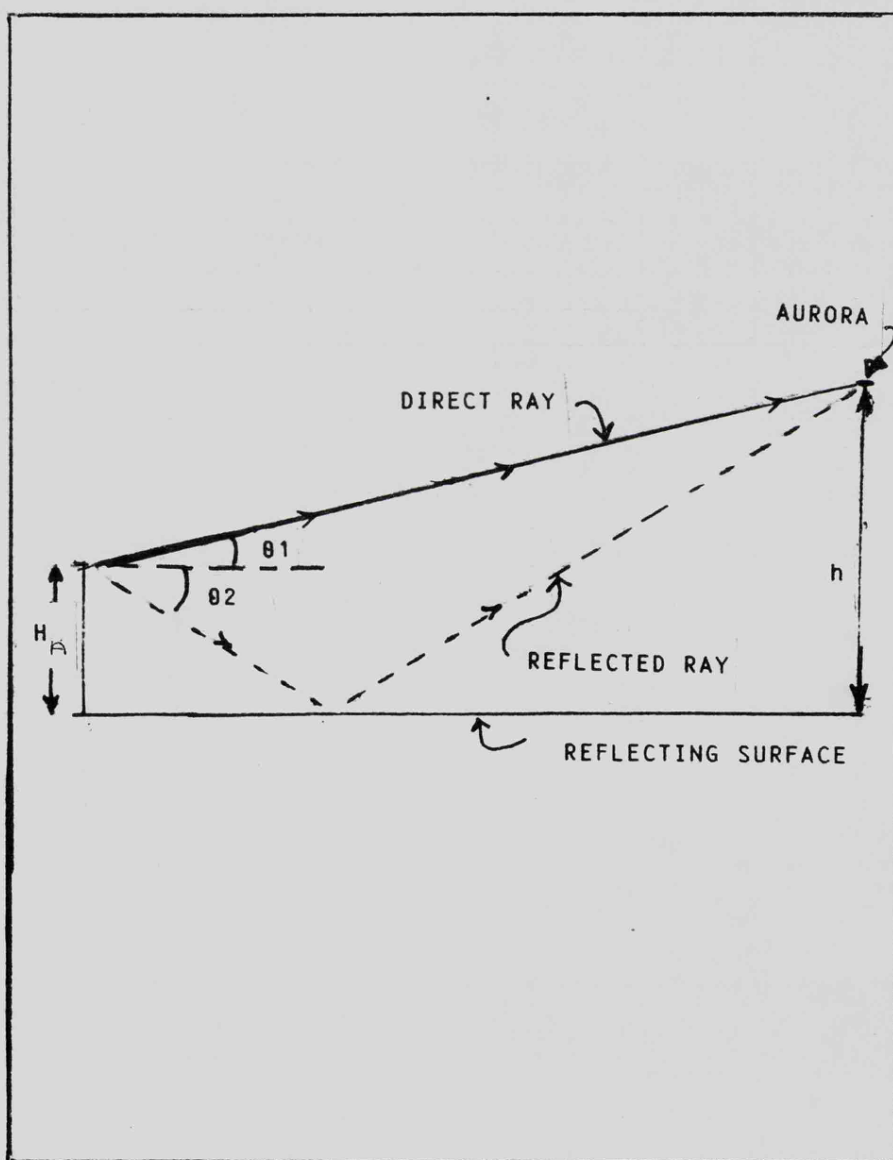
h IS THE HEIGHT OF THE AURORA H_A IS THE HEIGHT OF THE ANTENNA

FIGURE 4.19

fluid-like structure beneath ground level.As shown in ref(96),Skolnik,this configuration and the basic analysis which follows is applicable for situations where

$$\tan(\theta_1) > \sqrt{(H_A)/1000} \qquad \text{where } \theta_1 = \text{elevation angle and } H_A$$

is the array height in feet.Actual values of H_A were found to be of the order of 36 feet hence $\tan(\theta_1)$ must be >0.06,or (θ_1) must be > 0.35 degrees.

Because of the uncertainty of the refraction effects below about 1 degree the bulk of the analysis in this Thesis will concentrate on slant ranges to the aurora for which $(\theta_1) > 1$ degree.Hence the schematic diagram of fig(4.18) will be applicable to the Wick radar analysis.

Now for slant ranges which are very much greater than the antenna height,H_A, it can be shown,as in ref (96),that $(\theta_1)$is approximately equal to (θ_2) and that the phase difference ,D_{EL},between the direct ray and the reflected ray will approximate to:

$$D_{EL} = (2\ H_A\ \sin(\theta))\ \text{where } (\theta) = \text{elevation angle,at the}$$

point of reflection from a smooth surface. For horizontal polarization the reflected wave undergoes a phase change of almost 180 degrees at ground reflection and has an amplitude of R_C x incident wave amplitude,where R_C is the ground plane reflectivity coefficient.Hence,as derived more fully in ref(96),the expression for the field strength,E,at an elevation angle (θ_E),will be given by:

$$E(\theta_E) = E_1 \sqrt{1 + R_C^2 - (2\ R_C\ \cos(4\ \pi\ H_A\ \sin(\theta_E)/\lambda))} \qquad (4.16)$$

where λ=operating wavelength, $\pi = 3.14159$

and E_1 = field strength without ground reflection.

In order to evaluate the expression for $E(\theta_E)$ for the polar diagram of the SABRE array alone,without the effect of the ground plane,it is necessary to examine the polar diagram equation for each element of the vertical array,then the equation for all four elements acting together,when tilted 6 degrees from vertical.As shown in ref (96) by Skolnik,the expression for the

field strength E_T at angle $= T$ degrees, due to a linear array of elements all supplied uniformly and in phase will be :

$$E_T = \frac{\sin(N \pi (s/\lambda) \sin(T))}{N \sin(\pi (s/\lambda) \sin(T))} \qquad (4.17)$$

where N=number of elements, s=element spacing in metres, λ=wavelength, and T=angle from the normal to the array, $= (\theta_E - 6)$.

The power gain, P_G, of a Yagi element, as used in the SABRE arrays, can be derived from the polar diagram and beamwidths as supplied by the manufacturers and is expressed as:

$$P_G = P_{GB} \ e^{(-pT^2)} \qquad (4.18)$$

where P_{GB}=antenna gain at boresight and $p = \log_e(2)/((B_W^2/4))$

and B_W=half power beamwidth, and T=angle from boresight.

The theoretical expression for the antenna elevation polar diagram power gain is thus proportional to

$$(E_T E(\theta_E))^2 \ P_G$$

and is plotted in fig(4.20) for an antenna height, H_A, of 6.5 wavelengths, number of elements, N=4, and element spacing, s of 1 wavelength, with ground reflectivity coefficient of 0.5. These values of antenna height and reflectivity coefficient were derived as follows;

4.6.1.1 Derivation of Wick antenna height, H_A, ground reflectivity and first null angle.

The predominant equation in determining the polar diagram peak and null is equation(4.16). Analysis of this equation reveals that null positions occur at elevation angles θ_N, given by:

$$\sin(\theta_N) = \left[\frac{(n-1) \ \lambda}{2 \ H_A} \right]$$

where λ=wavelength, and n=1,2,3,4

RELATIVE GAIN OF SABRE ARRAY WITH ELEVATION--THEORY
DASHED LINE IS FOR UPPSALA ARRAY
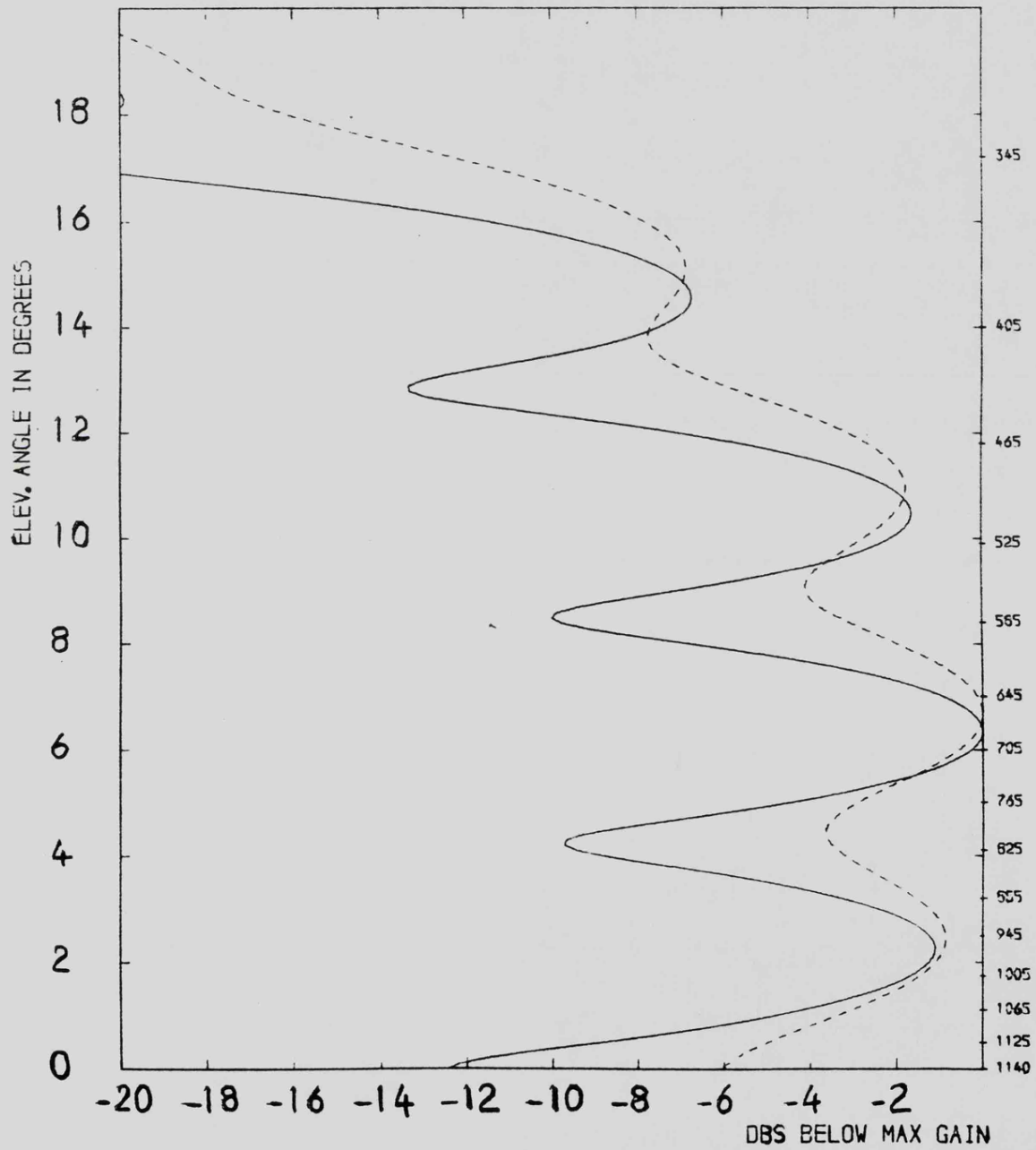
RIGHT HAND SCALE IS SLANT RANGE IN KM FOR AN AURORAL HEIGHT OF 100 KM

FIGURE 4.20

Peak positions in the polar diagram occur at elevation angles,θ_p,given by:

$$\sin(\theta_p) = \left[\frac{(2n-1)\ \lambda}{4.H_A}\right]$$

The angles θ_N and θ_p can also be derived from the analysis of section 4.1 and in particular from figure (4.2).

From the mean of many days of observation of the signal level (after compensation for the effects of range,and by assuming a fixed height for the auroral backscatterers), the antenna effective height above the reflecting plane was deduced by locating the null and peak angles.Similarly the ground reflection coefficient,R_c,was deduced from the mean signal levels at the positions of null and peak,as derived from figure (4.21).An effective height of 6.75 wavelengths and reflection coefficient of 0.5 were obtained for the Wick radar.In comparison,the physical height of the Wick SABRE antenna arrays was found to be approximately 6 wavelengths above the ground level. The ground area consisted of relatively soft,marshy soil in contrast to the hard rocky area at the Uppsala site.The ground reflection effects which are encountered at the Wick site are probably due to the interface between the marshy soils and the earth, below ground level. The effective half-power beamwidth of the main lobe of the polar diagram in figure (4.21) was found to be $\sim$ 3 degrees in elevation.

4.6.2 Wick radar antenna Azimuth polar diagrams

The azimuth polar diagram of the SABRE receiving array was deduced as follows,using the antenna analyses of ref(96),1972,by Skolnik:

The half-power beamwidth in the azimuth plane for the receiving array of 16 elements spaced 1 wavelength apart can be approximated by:

$$B_{WA} = \left[\frac{0.886\ \lambda}{N\ s}\right] \qquad \text{radians}$$

(4.21)

where N=number of elements,s=spacing of elements,λ=wavelength,and hence the

RELATIVE GAIN OF SABRE ARRAY WITH ELEVATION--ACTUAL
DASHED LINE IS FOR UPPSALA ARRAY

EACH GRAPH IS DERIVED FROM ANALYSIS OF SABRE DATA FOR 1982 TO 1984
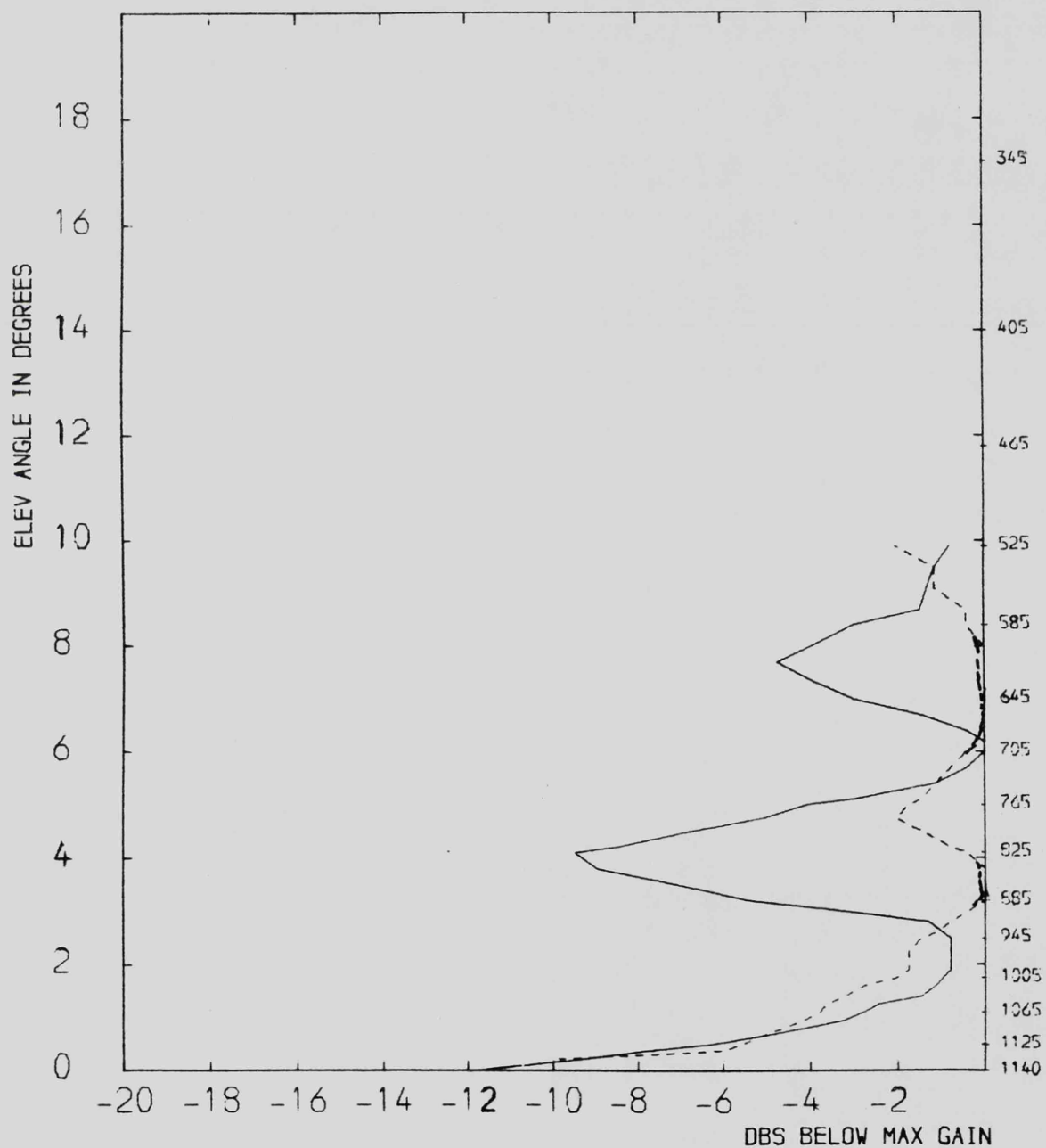
RIGHT HAND SCALE IS SLANT RANGE IN KM FOR AN AURORAL HEIGHT OF 100 KM

FIGURE 4.21

THEORETICAL WICK ANTENNA BEAMSHAPE IN AZIMUTH, WITHOUT TAPERING

DOTTED CURVES ARE THE UPPSALA SIDELOBES ACHIEVED WITH TAPERING
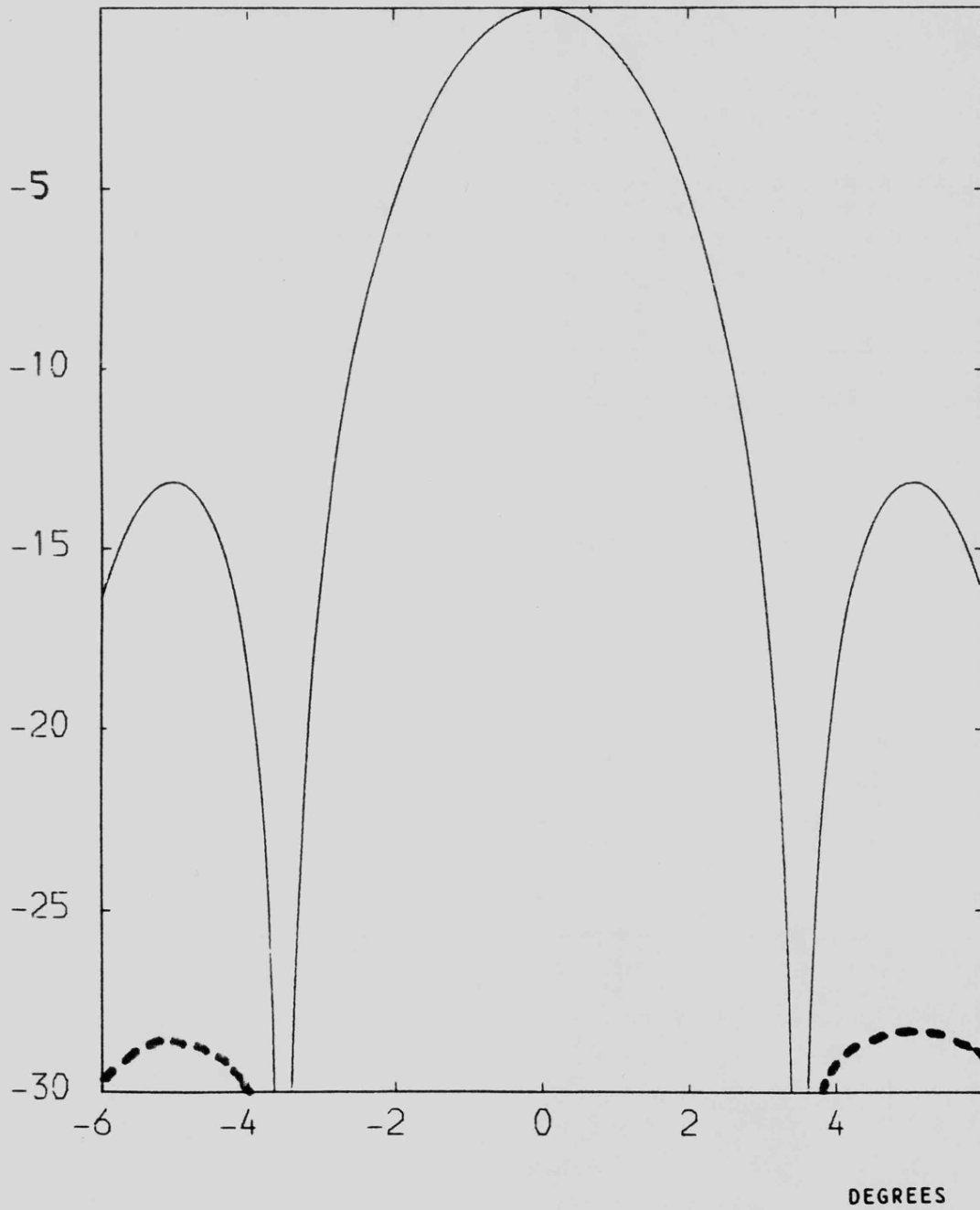
FIGURE 4.22

beamwidth will be about 3.16 degrees.

However, an unspecified amount of amplitude tapering is applied to the outside elements of the array,which will tend to increase this beamwidth. According to a calibration performed upon the Uppsala radars, a beamwidth of 3.2 degrees is achieved in practice,with sidelobe levels of about -30 dbs. Now the theoretical azimuthal polar diagram for the receiver 16-element array should be represented by equation(4.17) with N=16 and s=1. The antenna power gain,represented by the square of this expression is plotted in fig(4.2),and would be applicable to either Wick or Uppsala receiver arrays if no tapering were applied. The effect of tapering, which has been applied to both SABRE arrays in order to reduce the sidelobe levels, is indicated in fig(4.2) as dotted curves and is derived from the Uppsala calibration data.

4.6.3 Antenna maximum gain values and apertures.

With the values of calculated receiver array beamwidth,B_{WA} in azimuth,B_{WE} in elevation,being 3.2 degrees and 3.0 degrees respectively,the Wick receiver array maximum gain value can be derived,assuming an antenna efficiency,n,of 78% as :

$$\text{Wick receiver array gain} = \left[\frac{32000}{(B_{WA} \; B_{WE})} \right] = 35.2 \text{ dbs}$$

The antenna aperture,A_p,can be derived from the value of antenna gain,as:

$$\text{array gain} = \frac{(4 \, \pi \, A_p \, \eta)}{(\lambda^2)} \qquad (4.22)$$

where A_p = antenna aperture,η = antenna efficiency. λ = WAVELENGTH

Hence if the antenna efficiency,η,is assumed to be 78%,because of the uncertainty of the small amplitude tapering across the array,then Wick receiving array aperture is approximately 1305 square metres.

Similarly,the Wick radar transmitting array directive gain ,G_T,can be

derived,using an antenna efficiency of 78%,as follows:

The Wick transmitter azimuthal half-power beamwidth,T_B,will be given by

$$T_B = \left[\frac{(0.886\ \lambda)}{(N_2\ s_2)} \right] \tag{4.23}$$

where N_2 = number of elements, and s_2 = element spacing and λ = wavelength.

Hence T_B = 33.86 degrees.

The Wick transmitter array directive gain ,G_T,is thus approximated by:

$$G_T = 32000/(3.0 \times 33.86) = 25\ \text{dbs}.$$

4.6.4 The Uppsala radar antenna polar diagrams.

The Uppsala vertical polar diagram,as displayed in fig (4.21) was similarly derived from the mean values of many days of data and shows little evidence of ground plane reflection effects.The theoretical value of half-power vertical beamwidth,B_U,will be given by:

$$B_U = 50.8/4 \quad \text{or approximately } 12.7 \text{ degrees}.$$

Hence the Uppsala receiver array directive gain,G_{DU},may be approximated by:

$$G_{DU} = 32000/(12.7 \times 3.2) = 29\ \text{dbs},$$

and its effective antenna aperture,A_{EU},will be approximately 326 square metres. Similarly the Uppsala transmitter array directive gain,G_{TU}, may be approximated by

$$G_{TU} = 32000/(33.86 \times 12.7) = 18.7\ \text{dbs}.$$

The relative gain variation with slant range to the aurora is displayed in fig(4.23),for each SABRE array and was derived from the mean of many days of data.

4.6.5 A comparison of the SABRE receiving array apertures.

In order to establish the accuracy of these theoretically derived antenna parameters,a comparison was made of the difference in receiving array cross-section of the Wick and Uppsala radars as follows:

RELATIVE GAIN OF SABRE ARRAY WITH ELEVATION
DASHED LINE IS FOR UPPSALA ARRAY

EACH GRAPH IS DERIVED FROM ANALYSIS OF SABRE DATA FOR 1982 TO 1984
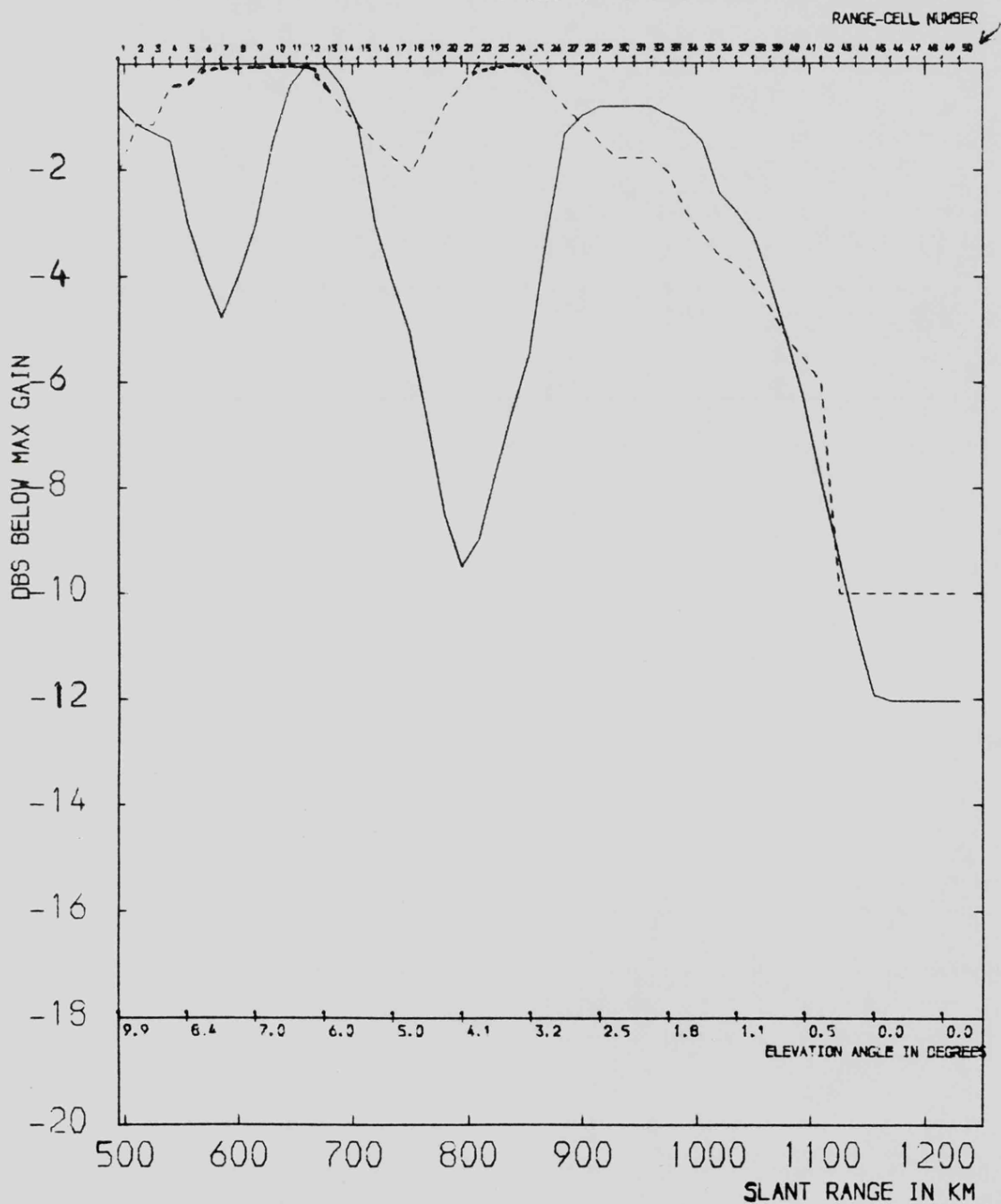
FIGURE 4.23

SCHEMATIC ILLUSTRATION OF SABRE RADAR BEAM POSITIONS
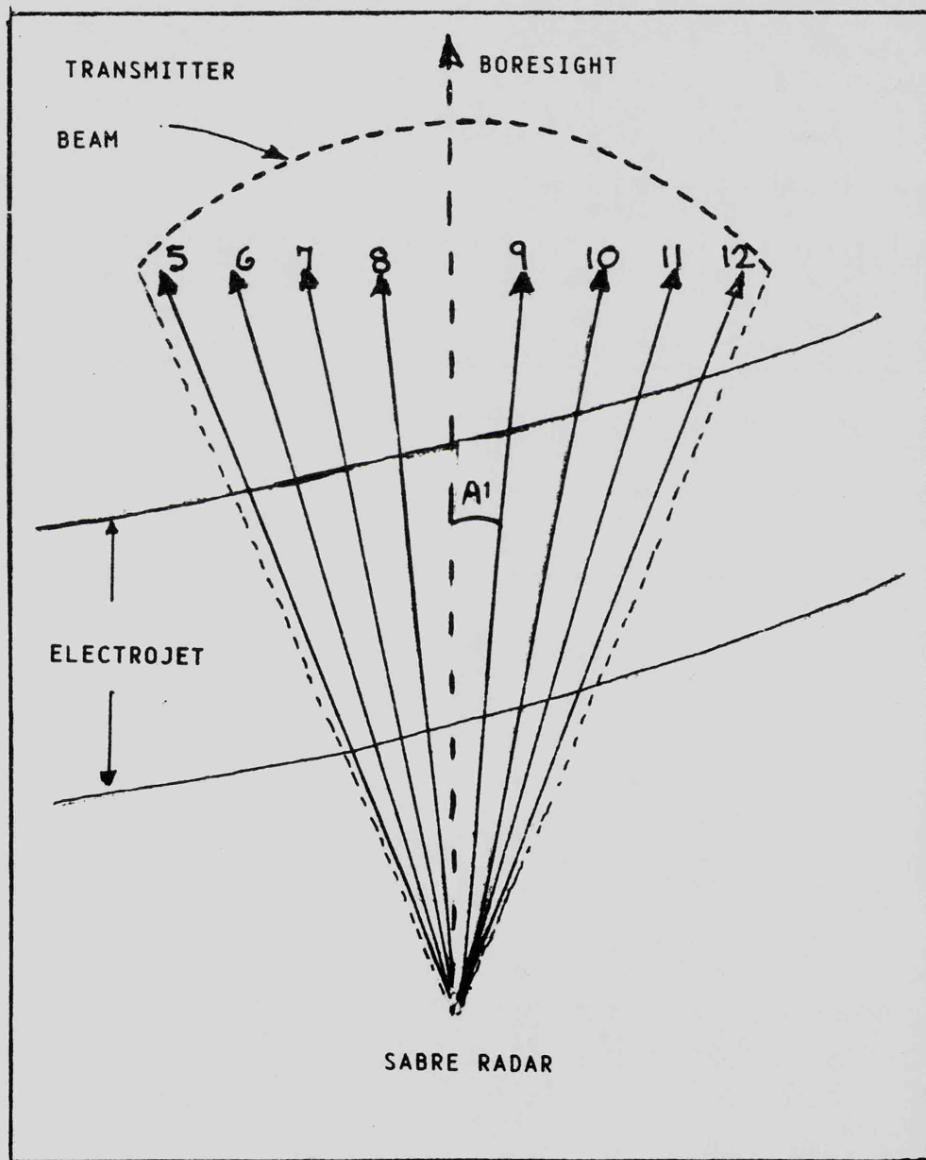
THE NUMBERS 5 TO 12 REFER TO THE SABRE RECEIVER ARRAY

BEAM POSITIONS WITHIN THE BROAD TRANSMITTER BEAM.

A1 IS THE ANGLE FROM THE BORESIGHT.

FIGURE 4.24

The theoretical difference in receiving array cross-section between the two SABRE arrays is approximately 6 dbs. A comparison of the two SABRE receiver signals was made,over an 8 hour period,at an auroral position common to both radars,in the main lobe of the Wick array,and at minimum aspect angles.   After compensation for the differences in transmitter power and range,the mean difference in receiver signal power (and hence array cross-section) was found to be 5.7 dbs.

4.7 The derivation of beam-pointing losses.

The SABRE radar system incorporates a Butler matrix which forms a total of 16 radar beams simultaneously,the centre 8 of which are employed,as displayed in fig(4.24). Analysis of this schematic diagram reveals that the signal strength of an auroral echo may be dependent upon beam-pointing or direction,as follows:

4.7.1 The loss due to the transmitter antenna polar diagram.

The transmitted power incident upon any fixed point of the aurora will be dependent upon the transmitter polar diagram with respect to that point.Hence the back-scattered signal will be dependent upon the transmitter antenna polar diagram.It will also be dependent upon the receiver antenna polar diagram,and the variation of signal strength will be dependent upon each of the beam positions as follows:

Let the transmitter polar diagram be approximated by the Gaussian expression for power gain

$$G(A) = G(\theta_b) \; e^{(-y \; A^2)} \qquad\qquad (4.24)$$

where $G(\theta_b)$ = transmitter gain at boresight

   (A)   = azimuth angle from boresight

   y   = $(\log_e 2)/(b_w^2/4)$ and beamwidth,b_w,=33.8 degrees.

Hence,if the 4 receiving array beams to the left and to the right of the transmitter boresight are at angles

1.8,   5.4,   9.0,   12.6   degrees,then the loss in incident power at each of these angles will be

0.034   0.31   0.85   1.67   dbs.

4.7.2 The loss due to variation of viewing area at the aurora.

The effective gain of each of the 8 receiving array beams will be dependent upon the azimuth angle with respect to the receiver antenna array,and also to the elevation angle of the beam.The variation of polar diagram with elevation angle is analyzed in the previous section but the variation of auroral area as viewed by each radar beam is displayed schematically in fig(3.1). From this figure it is seen that the auroral area viewed by each receiving beam varies as $\sec(\theta_G)$ where (θ_G) is the grazing angle.   This grazing angle will vary with elevation angle and hence slant range,but can be calculated for a diffuse aurora as follows:

let R_E=earth's radius,6371.2 km.

let $R_2=R_E+h$ where h=height of aurora,100 km

let R_S=slant range to the aurora

then $(\theta_G)=90-(\theta_E)$ where $(\theta_E)=2$ atan $\left(\dfrac{(S-R_2)\ (S-R_S)}{(S)\ (S-R_E)}\right)$ (4.25)

where $S=0.5(R_E+R_2+R_S)$

4.7.3 The loss due to variation of receiving-array cross-sectional area.

The variation of receiver antenna array cross-section with azimuth angle for each of the 4 beams to the left and to the right of boresight,as in fig(4.24), will be proportional to the cosine of the that azimuth angle,as follows:

Beams 8 and 9 will be reduced in gain to cos(1.8)

"   7 " 10 "   "   "   "   "   " cos(5.4)

"   6   11 "   "   "   "   "   " cos(9.0)

"   5   12 "   "   "   "   "   " cos(12.6)

SCHEMATIC ILLUSTRATION OF THE SABRE RADARS' POSITION OF OVERLAP.
THE ELECTROJET SPEED IS DERIVED AT THIS POINT.
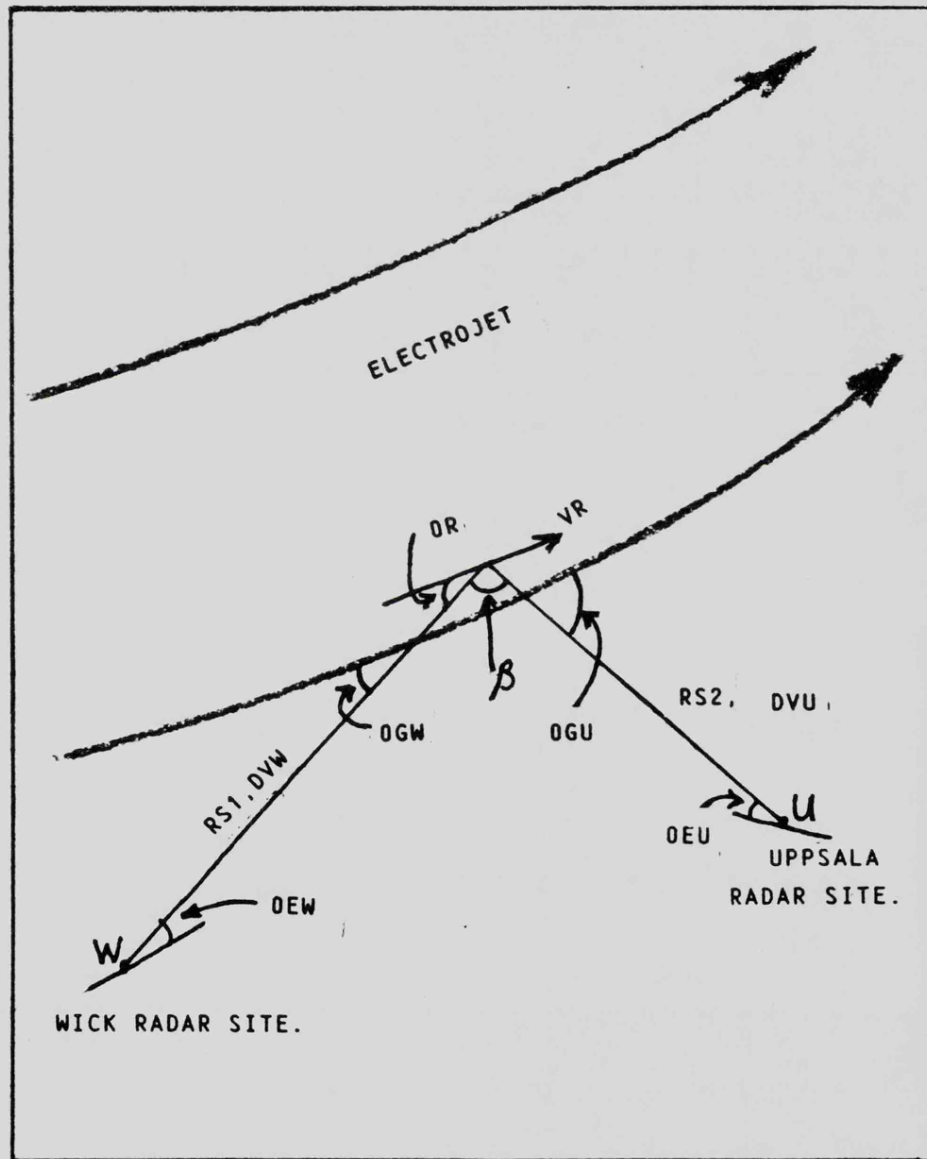
RS1 IS THE SLANT RANGE TO WICK.   RS2 IS THE SLANT RANGE TO UPPSALA.

OEW,OEU ARE THE ELEVATION ANGLES AT WICK AND UPPSALA.

   IS THE ANGLE BETWEEN THE RADAR BEAMS AT THE AURORA.

OR IS THE RESULTANT VECTOR ANGLE.   VR IS THE RESULTANT SPEED.

DVW,DVU ARE THE DOPPLER VELOCITIES AT WICK,UPPSALA.

FIGURE 4.25

Hence the reduction in effective antenna gain due to receiver beam positions will be:

    Beams 8 and 9   0.036 dbs

    Beams 7 and 10   0.329 dbs

    Beams 6 and 11   0.9   dbs

    Beams 5 and 12   1.775 dbs.

4.7.4 The loss due to variation of electrojet cross-section.

Analysis of the combined data of the 2 SABRE radars revealed that the cross-section of the auroral disturbances viewed by each of the 8 radar beams was dependent upon the angle between the radar beam and the direction of auroral flow.Andre,ref(85),1983,has also reported that the auroral cross-section is largest in the direction of the drift velocity.The direction of flow of the eastward and westward electrojets is approximately as drawn in fig (4.25). Hence,for the times of day that the electrojet is streaming uniformly at an angle across the beams the cross-section seen by a radar beam will increase from beam 5 to a maximum at beam 12,for both Wick and Uppsala radars.   The actual values of this variation of cross-section with viewing angle were determined,from radar data for those times of streaming electrojet flow,as follows;
The day selected for the analysis was that employed for the derivation of aspect-angle loss,day 249 1982,since the auroral echo signals were consistently strong and the Lerwick magnetic index was between 6 and 9. In order to determine flow angles,it was necessary to combine the velocity data of the 2 radars,as derived in section(4.11.4),at the point of closest overlap of the Wick and Uppsala beams. The point selected was 64.26^{o} N,6.0^{o} E,where Wick beam 11 overlaps with Uppsala beam 5. Both radars contained strong echoes at this point,and both had minimal aspect-angle loss.

PLOT OF REFLECTIVITY AGAINST FLOW-ANGLE WITH RESPECT TO WICK BEAM 11
AT 64.26 N,6.00 E.   DATA IS AVERAGED OVER 30 MINUTE INTERVALS
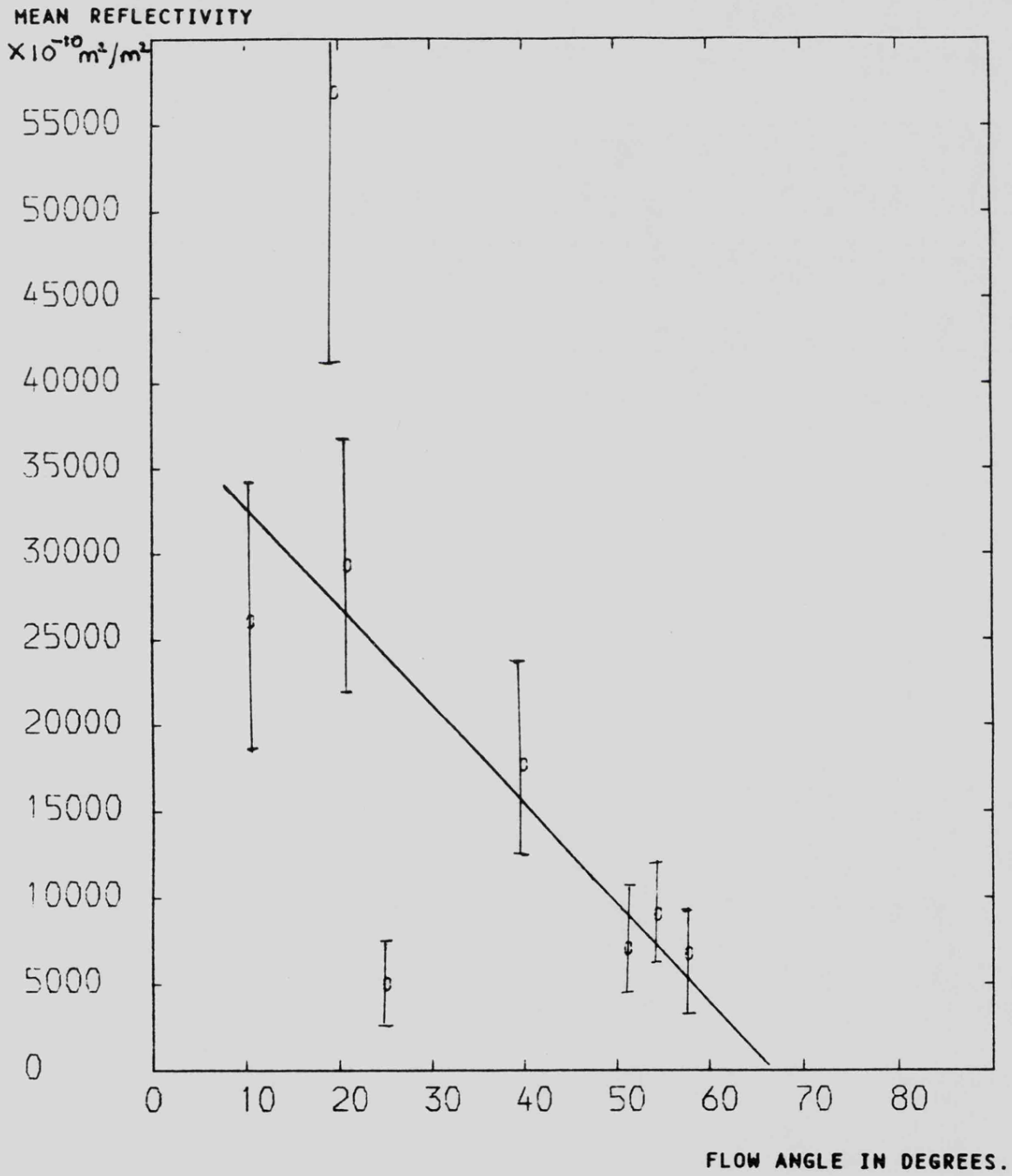
FIGURE 4.26

PLOT OF WICK MEAN DOPPLER VELOCITY AGAINST FLOW ANGLE FOR BEAM 11.
DATA IS AVERAGED OVER 30 MINUTE INTERVALS.
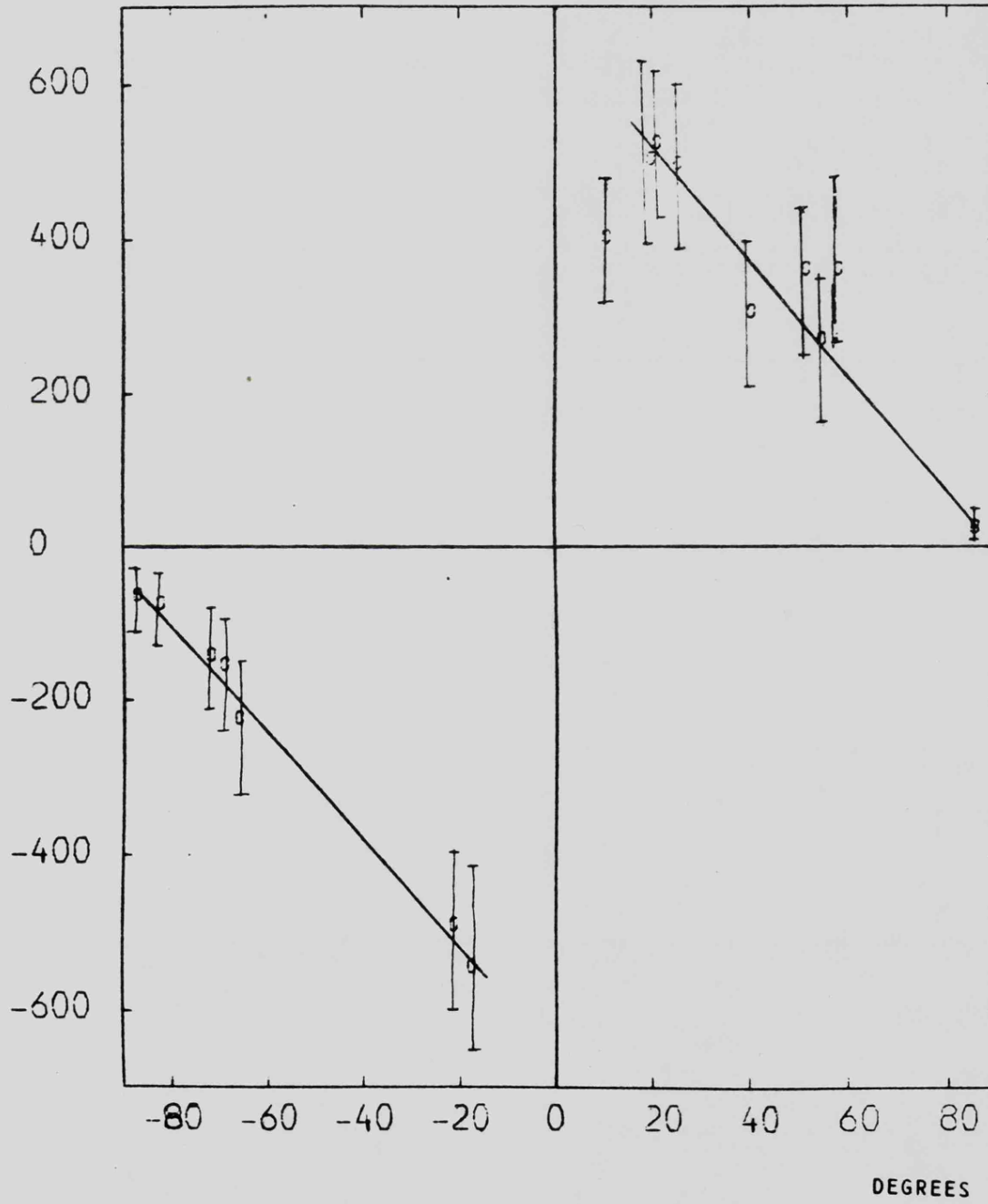
FIGURE 4.27

A series of 30-minute mean echo signal power levels and velocities were recorded and the resultant electrojet speed and flow angles derived. Fig(4.26) is a plot of auroral echo signal against electrojet flow-angle for Wick radar and fig(4.27) is a plot of the Wick Doppler velocity against flow-angle. These 2 graphs do not include any values for the periods of time when the Harang Discontinuity or Morning Cleft were present.

The value of beam-pointing loss due to flow angle as derived from these graphs is 0.14 dbs per degree for the echo signal and the Doppler velocity change with flow angle is 6.2 metres per second per degree.The variation of the absolute value of the mean Doppler velocity with flow-angle is approximately proportional to the cosine of the flow-angle.

A study of fig(4.24),the schematic position of all 8 beams of both SABRE radars,indicates that Wick beam 12 will have,on average,smallest beam pointing loss for the Wick radar,and the loss will gradually increase in value from beam 11 to beam 5.The reverse is true for the Uppsala radar where beam 5 will have the least beam-pointing loss,beam 12 the most.This schematic diagram particularly applies to the analysis of day 249,1982,when the strong auroral electrojet was flowing in the direction indicated.Hence the beam pointing loss for each radar was taken to be 0.14 dbs per degree or 0.5 dbs per beam position.

4.8 <u>The evaluation of system noise.</u>

The level of noise output from the SABRE radar receiving system can be considered to be a summation of the following sources of noise:

   i) Antenna noise--comprising galactic,sun and man-made noise

   ii) Receiver electronics noise

   iii) computer processing noise

   iv) internal interference.

Each of these sources will now be evaluated.

4.8.1 Antenna noise and man-made noise.

The noise power output from the antenna can be expressed in terms of a "Noise Temperature", T_A, where

$$T_A = P_N/(k\ B_N) \hspace{4cm} (4.26)$$

where P_N=noise power, k=Boltzmann's constant, B_N=frequency bandwidth. Antenna noise temperature will generally depend upon:

a) Average galactic noise at the radar frequencies,which in turn depends upon the direction of the radar beam.

b) Sun noise temperature,which can vary greatly with time of year and will also depend upon which antenna sidelobe receives the sun's radiation.

c) The noise temperature of the troposphere.

d) The uniform 2.7 degrees Kelvin cosmic blackbody radiation.

e) The noise temperature of the warm ground if an antenna lobe or sidelobe is pointing groundward.

f) The noise contribution of man-made electrical sources,usually predominant below 50 MHz.

Generally antenna noise temperature is dependent upon the frequency of the radar system,and graphs of antenna noise versus frequency (in the range 100 MHz to 100 GHz) are available in ref(96) by Skolnik,1972.

The change of antenna noise characteristics wih radar frequency is discussed in this ref(96),but for the SABRE operating frequency of 150 MHz the predominant sources of antenna noise are galactic and solar.Typical values of antenna noise at 150 MHz are quoted as:

Absolute maximum: 6000 degrees Kelvin,for a sun noise of 100 times the quiet level,for zero elevation angle. In practice the effects of the Earth's atmosphere will be to reduce this value considerably.

Absolute minimum: 200 degrees Kelvin,for zero sun noise and 90 degree elevation angle.

Further details of antenna noise temperature and its variation with

position in the sky can be found in ref (135), 1973, by Taylor.

In practice the SABRE antenna noise temperatures have been measured by the research scientists and have been quoted as:

Maximum: 1100 degrees Kelvin, minumum: 220 degrees Kelvin, and the average value: 300 degrees Kelvin.

These values will be used in the analysis of the SABRE radar system,but an actual figure for the total system noise will,as shown in section (4.8.3),be derived from a study of the change in noise power from mid-day to mid-night.

4.8.2 Receiver electronics noise.

The receiver electronics system output noise power is usually expressed in terms of the "Noise Factor",N_F.The receiver noise factor accounts for the degradation of the signal to noise ratio at the output,in comparison with the signal to noise ratio at the receiver input:

$$N_F = (S/N)in / (S/N)out \qquad (4.27)$$

The 8-channel receiver has a noise factor quoted by the research scientists,of 2.37.

The antenna noise temperature,T_A,at the receiver input will effectively be added to the noise contribution of the receiver,referred to its input terminals,as derived in ref(96),Skolnik,1972,as follows:

The equivalent input noise,$N_I = T_A$ + equivalent receiver input noise

or $N_I = k(T_0(N_F-1) + T_A) B_N$ \qquad (4.28)

where k = Boltzmann's constant ,T_0 = 290 degrees Kelvin,B_N=frequency bandwidth.

4.8.3 Analysis of the SABRE noise level data.

A study of the SABRE ouput noise revealed the presence,on certain days of the year,of very low-level man-made interference,as displayed in fig(4.18). These interference signals could easily be identified by monitoring the noise output levels of the SABRE data,but were usually of too low a level to

influence the auroral signals.

An example of the increase in SABRE output noise levels from night-time to day-time,on days free from interference, is illustrated in fig(3.3).This increase (of about 1.3 dbs)is probably an indication of the influence of the sun´s noise on the day-time antenna noise levels,via an antenna sidelobe or backlobe.The times of day selected for this comparison were those corresponding to the peaks in the afternoon and night-time electrojet current flow.

If a mean antenna noise temperature of 300 degrees Kelvin is assumed,then the equivalent input noise power is:

$$N_I = (1.38/10^{23}) \ (290 \ (2.37-1) + 300) \ 10,000$$
$$= -130.2 \ dbm, \quad i.e. \ -160.2 \ dbW, \ or \ 9.62.10^{-17} \ watts.$$

If the mean antenna noise temperature were to increase to 1000 degrees Kelvin,then the equivalent noise input power is:

$$N_I = (1.38/10^{23}) \ (290(2.37-1) + 1000) \ 10,000$$
$$= 19.1 \ x \ 10^{-17} \ watts, \ which \ an \ increase \ of \ 2.97 \ dbs \ on \ the \ 300$$

degrees Kelvin value. If the night-time noise temperature is assumed to be 220 degrees Kelvin then the afternoon temperature corresponding to an increase of 1.3 dbs in noise level,would actually be 454 degrees Kelvin. A mean value of about 300 degrees Kelvin can therefore be assumed for the purposes of this analysis,for both day and night-time data.

4.8.3.1 Computer processing noise.

Computer processing noise was found in the SABRE data output to be of two types:

a) Faulty digital data output in which,very occasionally,the digital power levels indicated values of greater than 50 watts,or signal to noise ratios of greater than 90 dbs.This was attributed to computer processing

error,probably during the telephone linkage between Wick and Leicester. Such excessive values were eliminated from the analysis in the computer programming.Similarly,Doppler velocity values of greater than 1600 metres per second were eliminated by suitable programming.

b) For very low levels of signal to noise ratio,certain values of Doppler frequency were found to be output from the processor far more frequently than any other.Because of this characteristic,the analysis of the SABRE data was undertaken only for signal to noise ratios of greater than 6.

4.8.3.2 Internal interference.

Internal interference effects were found only in the "very short range signal" investigations,in which transmitter breakthrough(i.e. leakage from transmitter pulse into the receiver) was encountered when attempting to measure ranges of less than 90 km.This problem is described in more detail in chapter (7).

4.8.4 Conclusion of the noise-analysis.

A mean noise power value of 9.62×10^{-17} watts in Wick beam 11 was selected for the radar equation in the day-time analysis of auroral reflectivity. A comparison of the noise power levels in each of 8 beams was made during a day's analysis and suitable,small adjustments made,referenced to beam 11.

Methods of improving the signal to noise ratios will now be considered:

4.9 The effect of integration.

Generally,most pulsed radar systems employ a form of signal integration in order to improve the signal to noise ratio at the output of the receiving system. Integration improves the signal to noise ratio because signals combine additively,whereas the result of added noise samples has a

fluctuation that is not the direct sum of the added fluctuations.The sum of M signal voltages,each of unit amplitude,is M,whereas the sum of M added noise samples (each having unit standard deviation before the addition),have a standard deviation equal to the square root of M. Therefore the signal to noise voltage improvement is :

$$M/\sqrt{M} = \sqrt{M}$$

and the signal to noise power improvement is = M.

Integration can be performed either before or after detection and fuller details of the different techniques and advantages can be found in ref(96),by Skolnik,1972. For the SABRE radar system,the value of M,the number of additions of signals in one integration period will be:

M = (pulse repetition frequency) x integration period.

= 400.

At this stage of the analysis the basic radar equation can be produced, incorporating the radar parameters derived in this chapter,as follows;

4.10 The basic radar equation for SABRE radars.

The basic radar equation for the SABRE radar system can be derived for two different auroral states:

i) Diffuse aurora in which the auroral echoes are returned from a wide azimuthal area and over an extended range,i.e. 495 km to 1250 km.

ii) Discrete aurora,in which the auroral echoes are returned from an area of small azimuthal extent and small range extent.

The bulk of this Thesis deals with radar echoes from the diffuse type of aurora and the subsequent derivation of the radar equation is as follows,based upon the schematic configuration of fig(3.1) and the analysis of chapter 3.1

The backscattered signal power received from an area of backscattering reflectors which fill the radar beam in both range extent and azimuth extent,at range R, elevation angle θ_E will be,for each single radar pulse:

$$P_R = \left(\frac{(P_T\, G_T(\Theta_E, \Theta_{AO}))}{4\pi\, R^2}\right)\left(\frac{\mathcal{T}'\Theta_{BW}\; c\; R\; \delta'}{4\pi\, R^2\; 2\cos(\Theta_G)}\right)\left(\frac{(G_R(\Theta_E, \Theta_{AO})\,\lambda^2)}{4\pi}\right)\Bigg/ \left(\frac{1}{(L_S\, L_{AS}\, L_{SYST}\, L_{FIL})}\right)$$

$$(4\cdot29)$$

The first pair of brackets represents the power density at the aurora; the product of the first 2 pairs of brackets represents the power density returned to the radar. The third pair of brackets represents the receiving aperture and the fourth pair of brackets represents the losses.(More detailed derivations of Radar Equations are fully described in ref(96), by Skolnik, 1972).

where P_T =peak transmitter power, $G_T(\Theta_E, \Theta_{AO})$=transmitter antenna gain

$G_R(\Theta_E, \Theta_{AO})$=receiver antenna gain, λ=operating wavelength

Θ_{BW} =azimuthal beamwidth, $\mathcal{T}'$=radar pulse width

Θ_G=grazing angle, between radar beam and irregularity at the aurora, Θ_{AO} = zero azimuth angle from the antenna,

L_S=system losses due to beam pointing angle, as derived in 4.7.

L_{AS}=aspect angle loss, as derived in section 4.2.

L_{FIL}=losses due to filter characteristics.

L_{SYST}=losses due to the two-way passage through the atmosphere, plus cable losses.

δ'= auroral reflectivity   c= speed of light

The last two losses, L_{FIL} and L_{SYST}, are less than 0.4 db. L_{SYST} is displayed as a function of elevation angle in fig (4.28) and is derived from ref (96) by Skolnik. Further details of atmospheric losses at 150 MHz can be found in this reference.

As derived in section(4.8), the noise power output from the receiver system, referred to the input, for each pulse will be given by:

$$N_R = k\,(B_N)\,(290\,(N_F - 1) + T_A) \tag{4.30}$$

where k=Boltzmann's constant, N_F=noise factor, T_A=antenna noise temperature and (B_N)=bandwidth.

The true signal to noise ratio for a single pulse will hence be :

PLOT OF 2-WAY ATMOSPHERIC TRANSMISSION LOSS AGAINST ELEVATION

ANGLE FOR THE SABRE RADARS.

THIS DATA IS DERIVED FROM REFERENCE 96,BY SKOLNIK,1972.
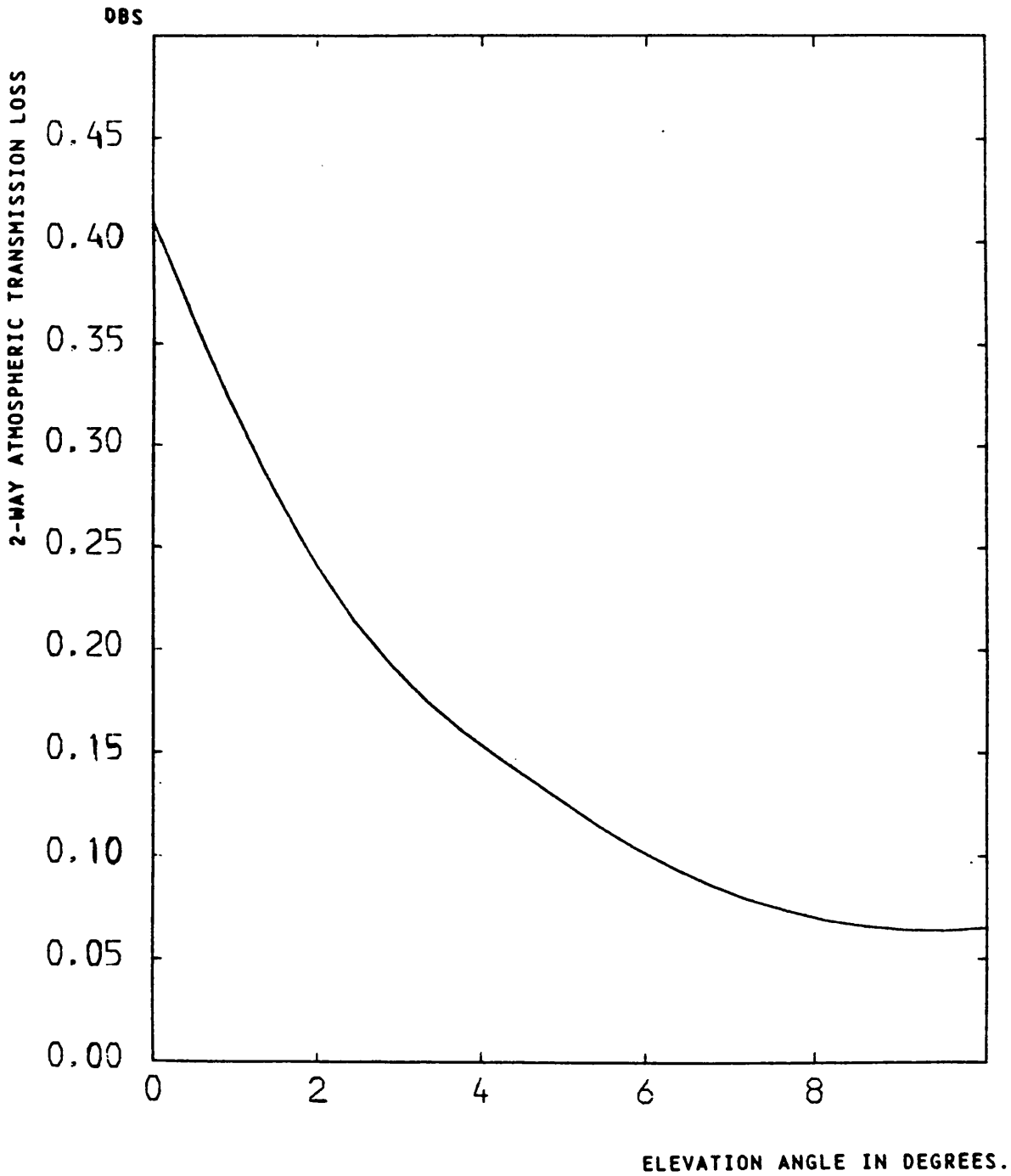
FIGURE 4.28

$$\frac{(\text{actual signal}) - \text{noise}}{\text{noise}} = \left(\frac{P_R}{N_R} \right) \qquad (4.31)$$

and the signal to noise power ratio after integration and averaging will be:

$$(P_R/N_R) \text{ (integration improvement factor,M)} \qquad (4.32)$$

where M=(pulse repetition frequency x integration period).

At this stage,it has been shown possible to derive the basic radar equation for the SABRE radars from examination of the diffuse auroral echoes and hence to examine the variation of reflectivity with range and azimith angle. The next step in analyzing the SABRE data is to derive the basic equations for the auroral Doppler velocities and electrojet speed.

4.11 Derivation of the Doppler velocity and electrojet speed.

4.11.1 Introduction.

As will have been evident from the survey of atmospheric radar systems in chapter 1, a Doppler velocity measuring technique frequently employed is that of pulse Doppler radar.

This technique is also reviewed in this Thesis because of its possible application to future investigation of the Short-Range-Echoes examined in chapter 9.The pulse-Doppler radar technique is used in many fields of research,both scientific and military,whenever the detection of relative motion between target and radar is desired.These radars operate by detecting the Doppler shift in frequency caused by the relative movement of a target which has a radial velocity component with respect to the radar. Most Doppler radars detect the amount of frequency shift rather than the actual frequency of the returned signal.The equation for the Doppler frequency shift,F_D,as shown in ref(96),by Skolnik,1972,is:

$$F_D = 2 \text{ (relative radial velocity)}/\text{(wavelength)}$$

For example, a typical Doppler shift in a pulse-Doppler system operating at a wavelength of 3 cm is about 34 Hertz per knot of relative radial velocity.

Generally, the pulse Doppler carrier frequency is pulse-modulated such as to cause transmission of a series of regular pulses. If the pulse-repetition frequency, (PRF), or as it is sometimes called "the chopping frequency", is continuous, then the spectrum of the transmitted frequency is as in fig(4.29). This spectrum consists of frequency components that form a grouping of spectral lines about the carrier frequency. The received signal spectrum, as reflected or back-scattered from the target, is essentially the same as this transmitted spectrum except that each spectral line is shifted by the amount of the Doppler frequency, F_D.

Usually the received echo signal is heterodyned down to an intermediate frequency, which produces a Doppler signal above and below each spectral line: i.e. carrier frequency $\pm$ Doppler frequency.

Hence, as can be seen in fig(4.30), the Doppler shift must not be allowed to exceed half of the value of the PRF, otherwise Doppler signals from adjacent spectral lines will overlap. Therefore the maximum Doppler frequency shift that can be detected unambiguously is limited by the PRF to: 0.5 x PRF.

The output of the intermediate-frequency mixer is generally passed through a band-pass filter so as to eliminate all but the desired spectral line and then amplified. A second stage of mixing is usually performed to translate the frequency spectrum to such a low value that either analogue or digital filtering may then be employed to determine the Doppler shift. In modern pulse-Doppler radar systems digital frequency filtering would be employed. The receiver would provide 2 outputs in phase-quadrature, (as in the SABRE receiver of fig(2.13)), into a Fast-Fourier Transform (FFT) system.

Examples of this FFT spectral analysis method may be found in ref(96), by Skolnik, 1972, or, in particular:

SCHEMATIC ILLUSTRATION OF THE FREQUENCY SPECTRUM OF A TRANSMITTER
MODULATED BY A SERIES OF PULSES.
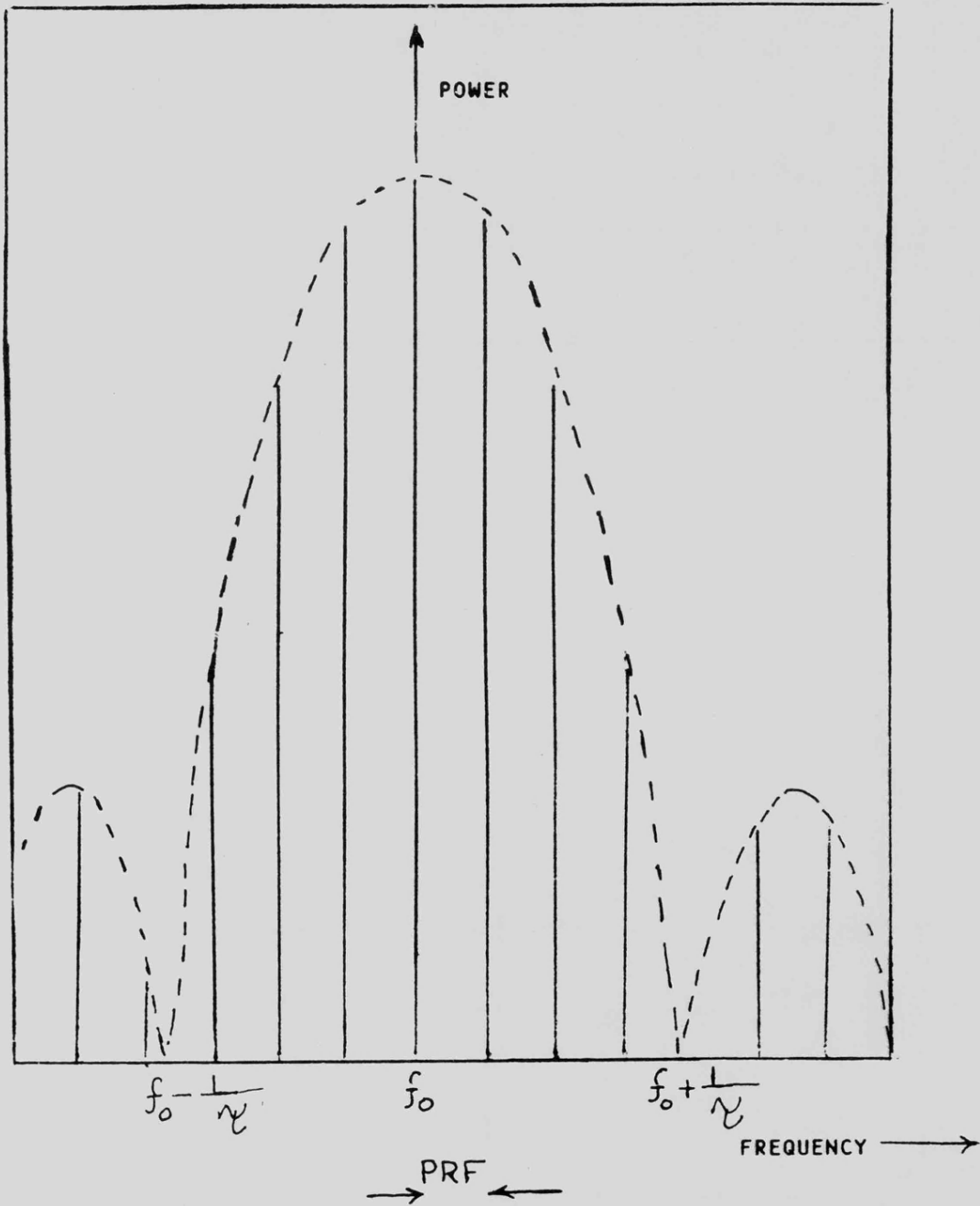
FIGURE 4.29

SCHEMATIC ILLUSTRATION OF THE RECEIVED DOPPLER SPECTRUM AFTER THE
INTERMEDIATE FREQUENCY MIXER.
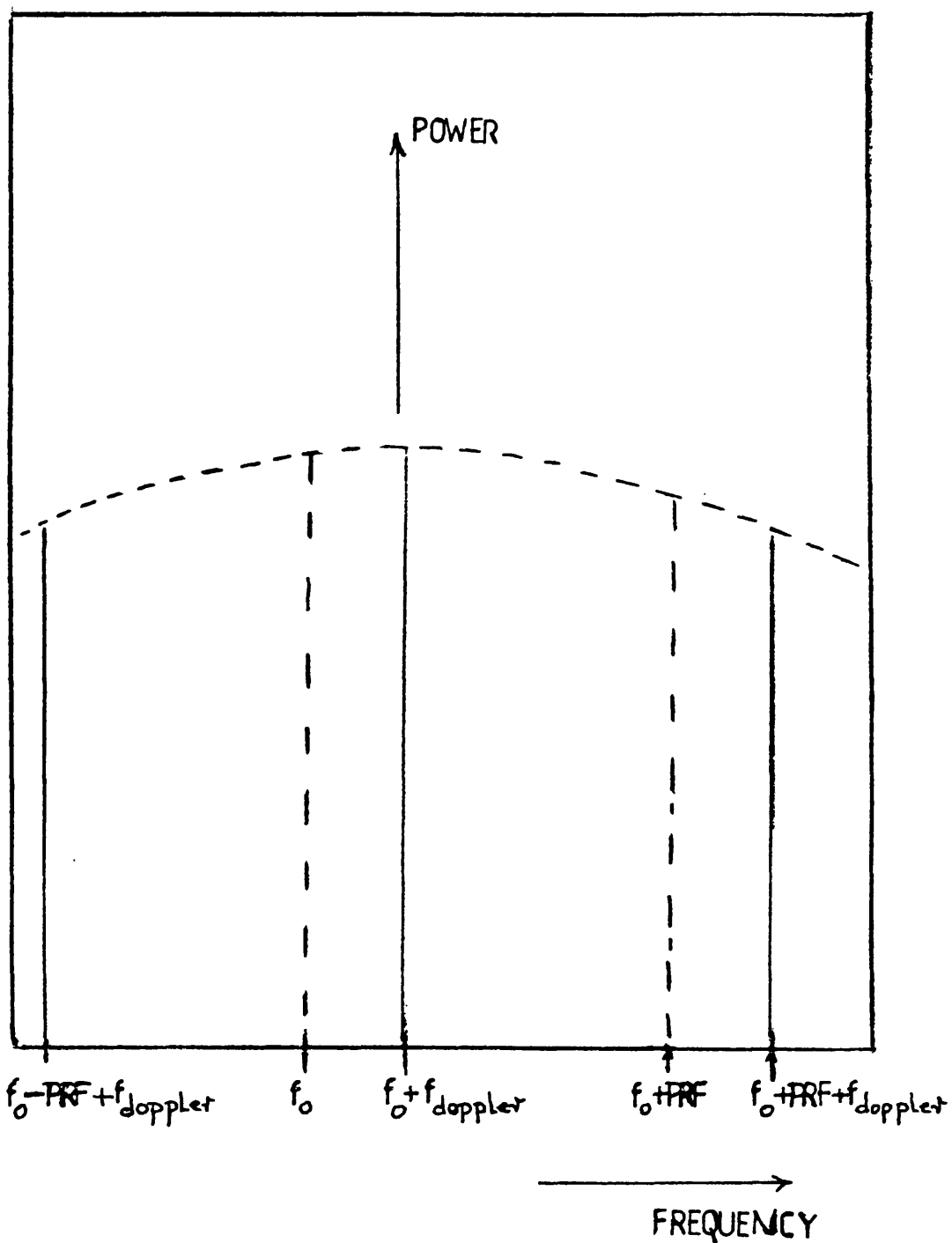
FIGURE 4.30

a) In HF pulse-Doppler radars,see ref(17),1979, by Shearman,et al.

b) In VHF "   "   "   " ref(24),1979,by Green et al.

c) In auroral radars,see ref(84),1981,by Unwin.

The major problem in employing the pulse-Doppler radar technique in the SABRE radars would be that of ambiguous ranging.The PRF for normal operation in pulse-Doppler mode must,by the Nyquist criterion,be at least twice the maximum expected Doppler shift.Hence,for a wavelength of about 2 metres,and electrojet velocities of about 2 km per second,the PRF must be at least 4 kHz. Now the maximum value of the PRF for which the value of the target range can be determined unambiguously(i.e.the echo signal is received before the next pulse is transmitted),is given by:

maximum PRF = 0.5 (velocity of light)/(range)   (4.33)

Hence,if the PRF were 4 kHz,the maximum range would be about 37 km.

Since the usual SABRE auroral targets are distributed over the ranges 490 km to 1250 km,at velocities of up to 2 km per second,this pulse Doppler technique is not generally applicable,but it may be considered for the short-range discrete target signals,which are investigated in chapter (7).The velocity measuring system currently employed in very-long range radars,including some incoherent-scatter radars and the SABRE radars is the double-pulse system,which will now be examined.

4.11.2 <u>The derivation of Doppler velocity using a double-pulse system.</u>

The SABRE velocity measuring system consists of two transmitted pulses,each of width 100 microseconds,and separated in time by 300 microseconds.

The echo pulses from the auroral irregularities are processed in the SABRE receiver to produce sine and cosine output functions of the echo signals,and each output is integrated for 20 second intervals.After each integration interval a mean value of sine and cosine is formed,and the velocity is deduced as follows:

Let pulse number one(of the pulse pair),be represented by P_1 where

$$P_1 = E(T_0)\ e^{(j\omega T_0)}$$

where $E(T_o)$ =receiver output voltage at time T_o and $\omega = (2$

π frequency). $\pi = 3.14159$ Let pulse number two (of the first pulse pair) be

represented by P_2 where $P_2 = E(T_1) e^{(j\omega T_1)}$

where $E(T_1)$=receiver output voltage at time T_1,and $T_1 - T_o = 300$

microseconds,the inter-pulse spacing.

These separate pulse voltages could be either the mean values after 20

seconds integration period,or the values derived from one pulse-pair if the

signal to noise ratio were high.

P_1 can be written as $E(t_o) (\cos(\theta_o) + j\sin(\theta_o)) = R_o + jI_o$ (4.34)

P_2 " " " " $E(t_1) (\cos(\theta_1) + j\sin(\theta_1)) = R_1 + jI_1$ (4.35)

where θ_o=instantaneous phase of pulse P_1,with sin and cos outputs=R_o,I_o

θ_1= " " " " P_2, " " " " " =R_1,I_1

The phase difference,θ_d,between the two pulses is $\theta_d = \theta_1 - \theta_o$

hence,θ_d = arctan$((I_1/R_1)$ - arctan(I_o/T_o)

or $\tan(\theta_d) = \tan(\theta_1 - \theta_o) = \left[\dfrac{\tan(\theta_1) - \tan(\theta_o)}{1 + \tan(\theta_1)\tan(\theta_o)} \right]$

$$= \left[\dfrac{(I_1/R_1) - (I_o/R_o)}{1 + I_1 I_o/(R_1 R_o)} \right]$$

or $\theta_1 - \theta_o$ = arctan$((I_1 R_o - I_o R_1)/(R_1 R_o + I_1 I_o))$ (4.36)

Now the Doppler frequency,F_D,as shown in ref(96),by Skolnik,can be shown to

be = 2 (relative velocity/wavelength). Hence the radial velocity,V_F,will be

= ((phase-difference/(2 π pulse separation))(wavelength/2)

Or V_F = $((\theta_1 - \theta_o)/(t_1 - t_o))$(wavelength/(4$\pi$))   (4.37)

In practice,the SABRE receiving system computes the values of

$(I_1 R_o - I_o R_1)$ and $(R_1 R_o + I_1 I_o)$ for each pulse-pair

received,and averages the values after 20-second integration periods.

Further details of the double-pulse technique can be found in ref (74),

by Greenwald and Ecklund,1975.

4.11.3 The derivation of velocity spectrum using Multiple-Pulse systems.

The Stare radar system has employed multiple-pulse transmissions in order to determine the velocity spectrum of the auroral radar echoes,as described in ref(88),1983 by Whitehead,et al. Pulse-pairs are transmitted at various time spacings,or lags,between the pulses,and for each value of spacing,T_G,the mean of the products of the amplitude at time t,and the complex conjugate at time $(t + T_G)$ is used to provide the auto-correlation function:

$$\text{i.e. } (R_O + jI_O) \ (R_1 - jI_1) \tag{4.38}$$

$$\text{and phase-shift } = \arctan((I_1 \ R_O - I_O \ R_1)/(R_1 \ R_2 + I_1 \ I_O)) \tag{4.39}$$

By using 11 values of T_G and averaging over 100 samples of the 11 pairs of pulses,the full autocorrelation function is obtained,and the Fast Fourier Transform of this function provides the full power spectrum.

A full description of the FFT can be found in ref(115), 1967,by Cochran,et al and details of the usage of autocorrelation functions can be found in ref(116), by Blackman and Tukey.

A further method of multiple-pulse spectral analysis is the "Maximum Entropy" technique employed by Moorcroft,ref(78),1978,in the Homer radar,in which 3-pulse transmissions are utilised.Although these techniques of multiple-pulse spectral analysis are not analysed in this Thesis,the problem inherent in such techniques,namely "overlapping echo returns" is considered in chapter 9,as a proposed future work project. The overlapping of echo signals occurs whenever echoes are received simultaneously due to different pulse transmissions,as a result of the extended range covered by the aurora.

4.11.4 The derivation of resultant vector-velocity from the SABRE radars.

The technique for deriving the actual speed of the auroral irregularity from the velocity data of the two SABRE radars will now be derived.

Fig(4.31) illustrates schematically the geometry of the two SABRE radars

SCHEMATIC ILLUSTRATION OF THE GEOMETRY OF THE SABRE RADARS
AND THE AURORAL ELECTROJET.

FIGURE 4.31

when viewing a point of the auroral electrojet at the same time.Because of the different locations of the two radars the elevation angles,grazing angles and slant ranges will all differ.The grazing angle is defined as the angle between the radar beam and the electrojet,at the aurora.

Fig (4.32) displays the areas of overlap of the 2 sets of radar beams. The Doppler (i.e. radial) velocity,V_D,measured by each radar beam will be given by:

$$V_{D(Wick)} = V_{DW} = V_T \cos(\theta_R)$$

$$V_{D(Uppsala)} = V_{DU} = V_T \cos(\theta_R + B)$$

or θ_R = arcos($(V_{DW}/V_{DU}) \cos(\theta_G + B)$) (4.40)

where V_T = resultant velocity,θ_R= flow angle between electrojet and the Wick radar,as in fig(4.31),and β = angle between the two radar beams.

The angle β between the two radar beams can be derived using the values of latitude and longitude for the two radars and for the electrojet:

Let A_{LOW},A_{LOU} be the longitudes of Wick and Uppsala,and let A_{LAW},A_{LAU} be their latitudes.Let A_{LOE},A_{LAE},be the longitude and latitude at the electrojet,as in fig(4.31).Then:

Angle B_1 = arcos(cos($A_{LOU}-A_{LOE}$) cos($A_{LAE}-A_{LAU}$))

" C_1 = arcos(cos($A_{LEO}-A_{LOW}$) cos($A_{LAE}-A_{LAW}$))

then angle B_{B2} = arcsin(sin($A_{LOU}-A_{LOE}$) sin(B_1)) (4.41)

and " C_{C2} = arcsin(sin($A_{LOE}-A_{LOW}$) sin(C_1)) (4.42)

and " β = (B_{B2}) + (C_{C2})

When these angles have been evaluated,the flow angle θ_R can be derived and the resultant speed of the electrojet can be calculated as follows;

let V_{DW}/V_{DU} = k_r = cos(θ_R)/cos($\theta_R + \beta$)

or cos (θ_R) = k_r cos($\theta_R + \beta$)

= k_r (cos(B) cos(θ_R) - sin(β) sin(θ_R))

or cos(θ_R)(1 - k_r cos(β)) = -k_r sin(β) sin(θ_R)

or tan(θ_R) = (k_r cos(β) - 1)/k_r sin(β)

or θ_R = atan ((cos(β) - (V_{DU}/V_{DW}))/sin(β)) (4.43)
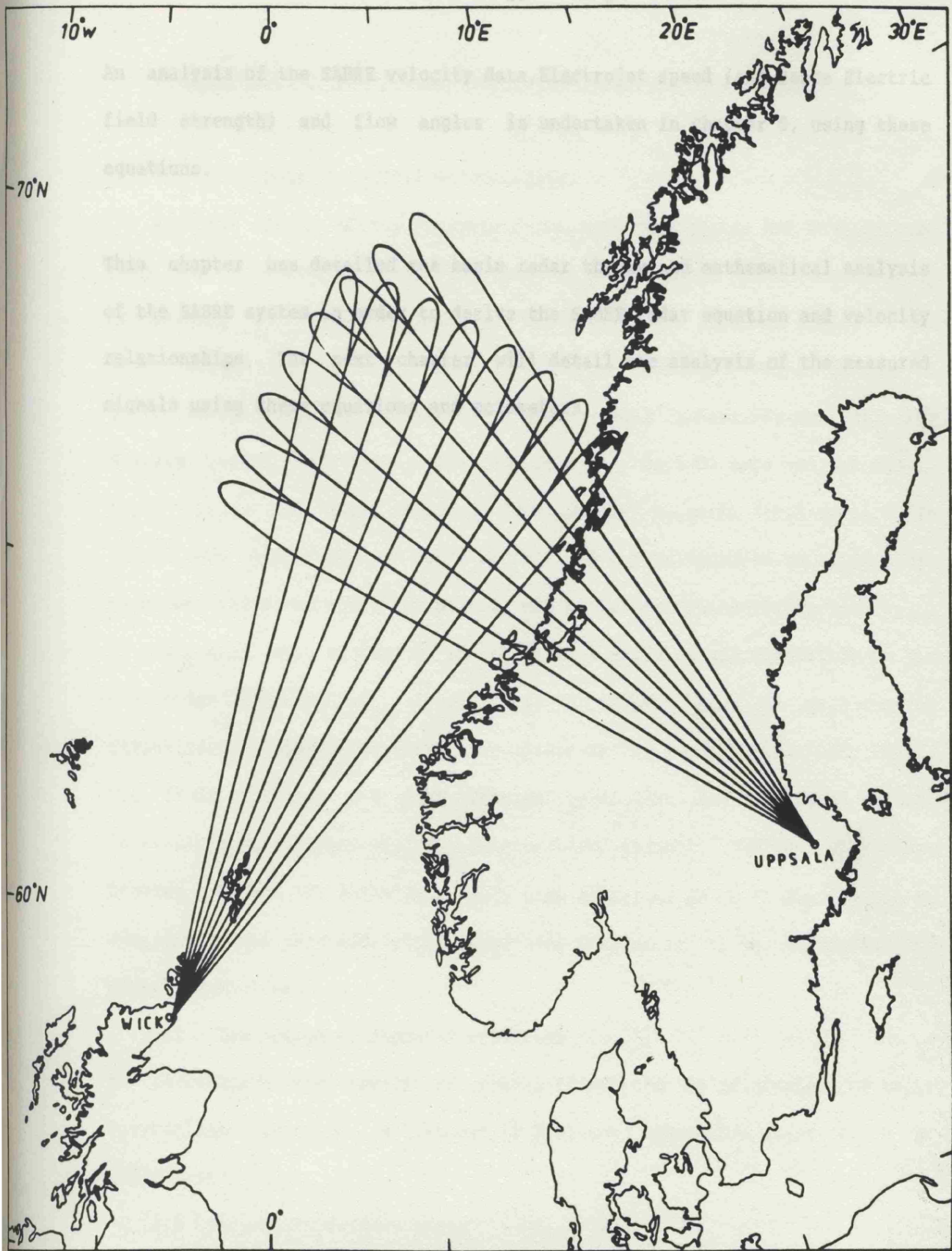
Beam Geometry of the Wick and Uppsala Radars

FIGURE 4.32

and hence Electrojet speed, $V_T = V_{DW}/ \cos(\theta_R)$

An analysis of the SABRE velocity data, Electrojet speed (and hence Electric field strength) and flow angles is undertaken in chapter 5, using these equations.

This chapter has detailed the basic radar theory and mathematical analysis of the SABRE system in order to derive the SABRE radar equation and velocity relationships. The next chapter will detail the analysis of the measured signals using these equations and parameters.

5. <u>Derivation of the Auroral parameters using the radar equation.</u>

5.1 Derivation of Auroral Reflectivity.

At this stage of the analysis sufficient information had been derived from the experimental data to form a basic SABRE radar equation.By calculating the system losses,(as detailed in the previous chapters) for slant ranges between 640 km and 1050 km,in each beam, values of auroral reflectivity could be derived for both SABRE radars.The antenna polar diagram losses had been evaluated from many days of data and the aspect angle losses had been assessed from the IGRF magnetic field model.These losses are displayed in table (5.1), and may be employed to convert the measured signal to noise ratio to values of auroral reflectivity.This table is most applicable to days of strong auroral activity,and especially to the electrojet flow periods. Fig(5.1) is a typical plot of mean auroral reflectivity in db(square metres per square metre) for the Wick SABRE radar. Fig (5.2) displays the mean Doppler velocities for the same period. Generally,mean values of reflectivity for magnetic indices of >6 were between - 34 and -80 dbs(m^2/m^2), with peak values of up to 11 dbs greater.An examination was then made of the degree of fluctuation of the back-scattered signals,as follows;

5.1.1 The degree of signal fluctuation.

To investigate the levels of signal fluctuation an examination of their "percentage standard deviation",(P.S.D),was undertaken,where P.S.D is defined as

P.S.D=(standard deviation/mean value) x 100

where standard deviation$=\sqrt{(\sum((S - Smean)(S - Smean))/number)}$ (5.1)

where Smean = mean value of samples,of total = number

Three separate geographic locations were selected for this signal

TABLE 5.1

WICK SABRE DATA

THE LOSS IN RECEIVED ECHO POWER (IN DBS)

WICK BEAM NUMBER

5 6 7 8 9 10 11 12

SLANT RANGE IN KILOMETRES

THE ANTENNA + ASPECT ANGLE LOSS (DBS)

RANGE CELL

TABLE 5.1

AURORAL CORRECTED REFLECTIVITY IN (DBS-120 M/M)²
FOR ASPECT LOSS=5.5 DBS PER DEGREE
AND MEAN AURORAL HEIGHT=100KM

DEGREES LATITUDE

1982 DAY 249   12HOUR   0MINS. TO 249   12   30 U.T.
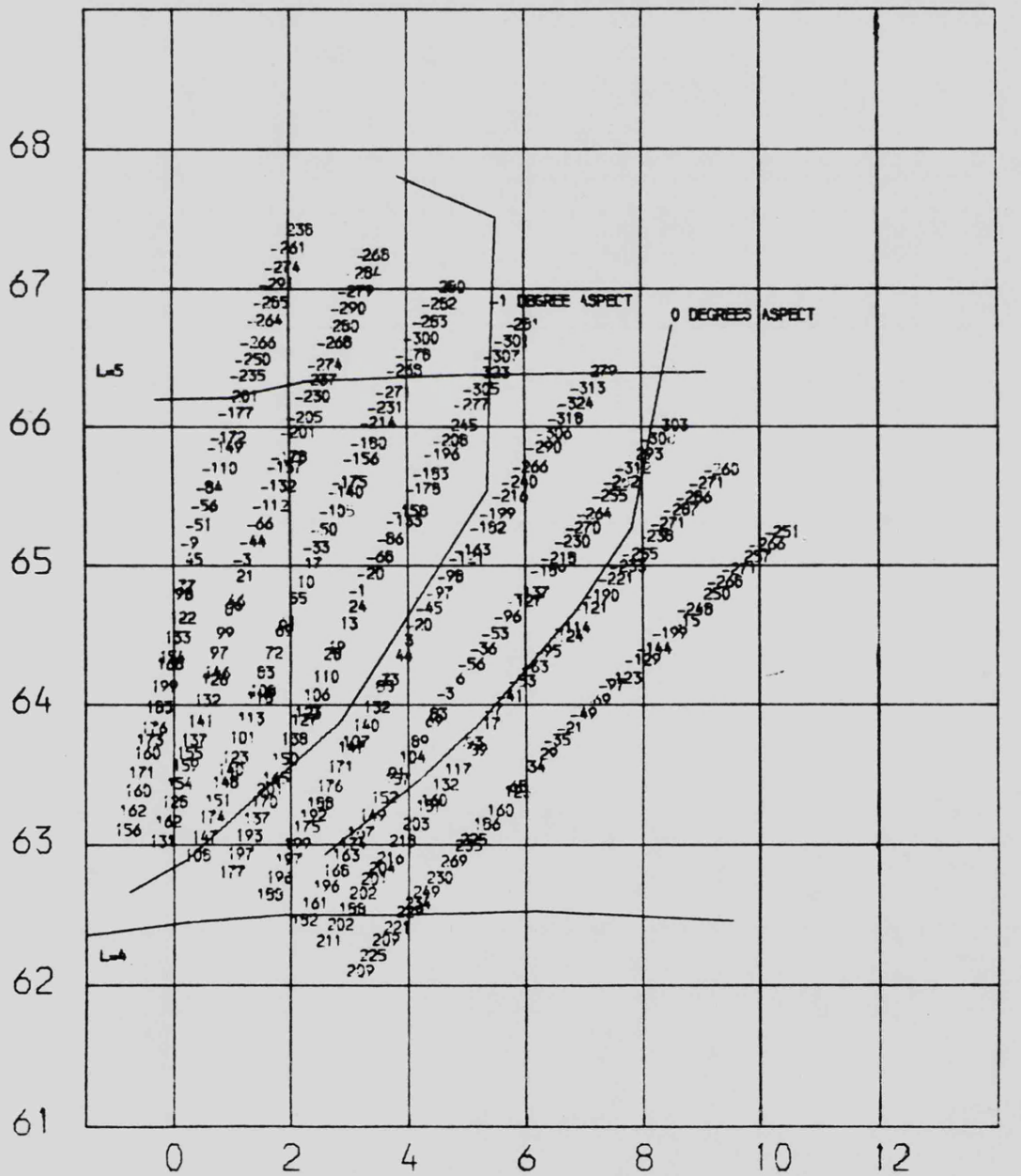
LERWICK MAGNETIC INDEX= 8   DEGREES LONGITUDE

WICK SABRE RADAR DATA
GEOGRAPHIC COORDINATES CALIBRATED USING CYGNUSA

FIGURE 5.1

AURORAL MEAN VELOCITY IN M/SEC

FIGURE 5.2

analysis,where the 2 SABRE radars overlapped most closely.For each set of radar echo signals the corresponding values of auroral reflectivity were calculated with the radar equation,and a comparison was made of their fluctuations for the days of most consistently strong echoes,as in Table(5.2).The order of magnitude of the standard deviation for these days ranged from 0.35 to 2.12 times the mean value.The order of magnitude of the differences in Wick echo power levels between the three positions of overlap was 1 to 7 dbs and are displayed in table (5.2).With the degree of signal fluctuation established,an examination was then made of the variation of reflectivity with Magnetic field strength.

5.1.2 The variation of Auroral reflectivity with Magnetic field strength

The point of overlap of the 2 SABRE radars which was chosen for this analysis was $64.26N,6.0E$,where both radars had very low aspect-angle loss and the Wick radar had a low polar-diagram loss. The day chosen was 249,to 250,1982,because of the consistently strong values of reflectivity and the relatively high (>6) values of magnetic index at Lerwick,$(60.9N,1.8W)$. The resultant plot of auroral reflectivity for each radar from this point on the electrojet is in fig(5.3).Data for the Uppsala radar was not available from 0600 to 0900 hours,whereas Wick data was available at all times.A comparison of the 2 radar signals can be made from 0830 to 1600 hours,as in fig(5.3).The hours between 0900 and 1130 represent the times of auroral activity associated with the "Morning Cleft" and the signal fluctuations during this time will be too unstable and weak to perform a reliable comparison between the 2 radars.For the times of day 249 when the electrojet flow was most uniform,(i.e. the afternoon period) two characteristics became apparent;

a) The largest signal returns occurred during the periods of highest magnetic activity,H,in the horizontal plane.Generally,a correspondence was noted between echo strength and the strength of the horizontal magnetic component, but not of the vertical magnetic component.

TABLE (5.2)

	ELECTROJET		Mean signal fluctuation dBs		Mean Reflectivity (-120) dbs m²/m²	
	Mean Speed, M/sec.	Mean Flow Angle, degrees	UPPSALA	WICK	UPPSALA	WICK
1982 Day 249 1430-1530						
Beam 7 (A)	679	27.9	1.5	2.0	63.6	71.6
Beam 9 (B)	694	27.8	0.4	1.5	70.1	74.3
Beam 11 (C)	518	23.1	4.5	2.8	67.7	75.2
1982 Day 249 1550-1650						
Beam 7 (A)	464	49.7	1.8	2.4	58.0	60.9
Beam 9 (B)	471	40.4	1.1	1.3	61.7	60.17
Beam 11 (C)	523	27.3	0.9	1.1	63.82	68.0
1982 Day 250 0100-0200						
Beam 7 (A)	-667	55.7	2.3	1.0	57.5	65.2
Beam 9 (B)	-627	51.1	0.4	1.8	62.45	68.83
Beam 11 (C)	-633	44.6	0.3	0.9	56.4	66.6
1984 Day 35 1500-1600						
Beam 7 (A)	858	38.2	1.1	3.1	60.5	72.8
Beam 9 (B)	693	24.8	3.3	0.4	67.2	70.4
Beam 11 (C)	680	14.8	0.2	3.3	56.64	70.76

Position (A) is 66.24° North, 3.56° East

Position (B) is 66.16° North, 6.66° East

Position (C) is 64.26° North, 6.00° East

PLOT OF HORIZONTAL MAGNETIC COMPONENT FLUCTUATION AT LERWICK AGAINST TIME FOR DAY 249, 1982

DOTTED LINE REPRESENTS THE REFLECTIVITY SIGNAL AT UPPSALA

THICK LINE REPRESENTS THE REFLECTIVITY SIGNAL AT WICK
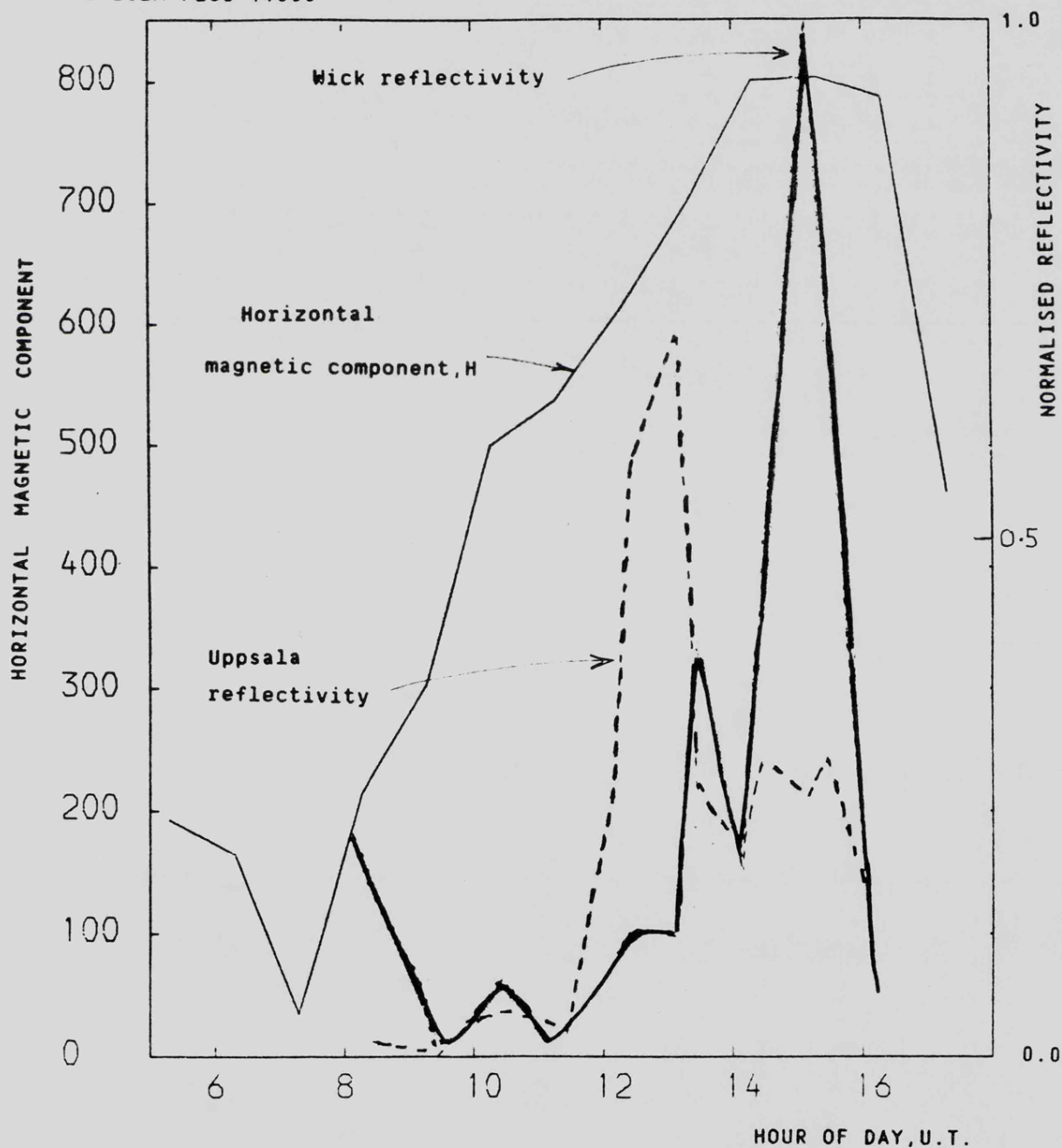
FIGURE 5.3

b) The signal strengths of the 2 SABRE radars reached a peak at different times,approximately 2 hours apart.

The variation of the Wick reflectivity data for a 27 hour period commencing 0000 hours on day 249 is displayed in fig(5.4) for the same location.The time periods 0930 to 1130 and 1900 to 2100 hours correspond to the Morning Cleft and Harang Discontinuity respectively.During these times weak backscattered signals are to be expected due to the absence of scattering instabilities.These 2 events can also be detected by analysis of the plot of the corresponding Wick Doppler velocity signals,in fig(5.5).The periods of velocity fluctuation and change of direction,(i.e. reversal of electrojet flow from eastward to westward) can clearly be seen in this graph.The dotted graph represents the change in direction of the Uppsala velocity signals.

During the remainder of day 249 peaks in horizontal magnetic activity correspond to peaks in reflectivity signals at Wick.This correspondence is to be expected since auroral electrojet activity is closely related to geomagnetic activity.If it is assumed that the horizontal magnetic component is mainly due to ionospheric Hall currents,then the peak values of reflectivity occur during the peaks in these currents; ie the maximum echo strengths are proportional to the auroral conductivity.As will be evident from fig(5.6),the variations in echo strength do not correlate with the variations of electrojet speed (ie Electric field strength).

The 2-hour displacement in peak reflectivity signals observed at Wick and at Uppsala were noted on several occasions.In order to explain this difference in signal level at the point of radar overlap,two studies were undertaken of auroral features which might be responsible;

   i) Mean auroral height of the echoes backscattered to each radar

   ii) The flow-angle of the electrojet for each radar.

5.1.3 Analysis of the Reflectivity data in order to estimate mean height

   Three possible methods of estimating mean auroral height were outlined

PLOT OF WICK MEAN REFLECTIVITY AGAINST TIME FROM
MIDNIGHT ON DAY 249,1982

BEAM 11, RANGE CELL 25, AT 64.26 N, 6.0 E.
DATA IS AVERAGED OVER 30 MINUTE INTERVALS,
DASHED LINE IS NORMALISED MAGNETIC FIELD STRENGTH AT LERWICK,60.9N,1.8W
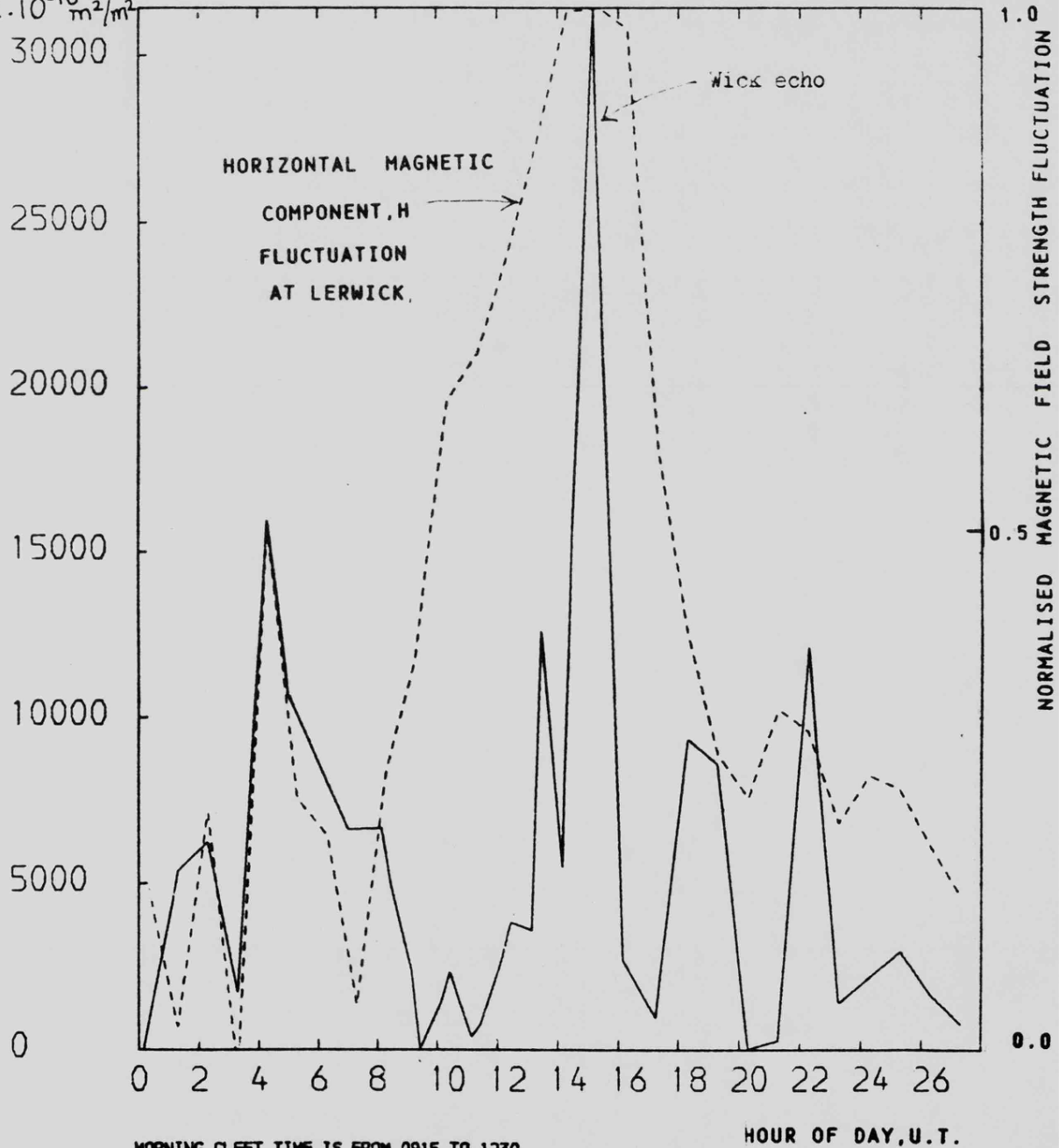
MORNING CLEFT TIME IS FROM 0915 TO 1230
HARANG DISCONTINUITY TIME FROM 2000 TO 2430

FIGURE 5.4

PLOT OF MEAN DOPPLER VELOCITIES AGAINST TIME OF DAY, FOR DAY 249, 1982.

WICK BEAM 11, RANGE CELL 25, AT 64.26 N, 6.0 E.
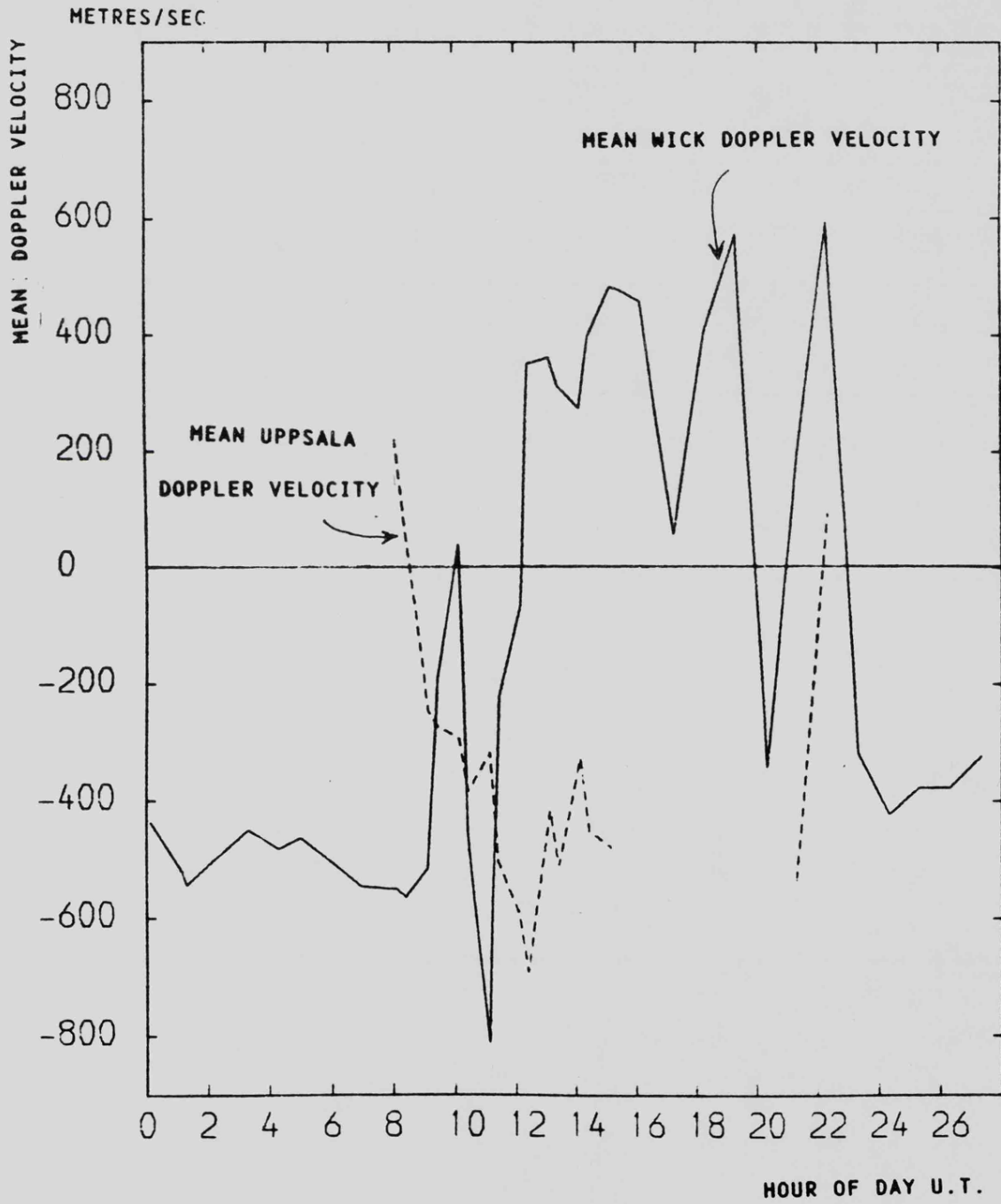
FIGURE 5.5

A COMPARISON OF ELECTROJET SPEED,WICK REFLECTIVITY,LERWICK

MAGNETIC INDEX (KL) AND AURORAL HEIGHT AGAINST TIME OF DAY.

DAY 249, 1982, AT 64.26 N,6.00 E
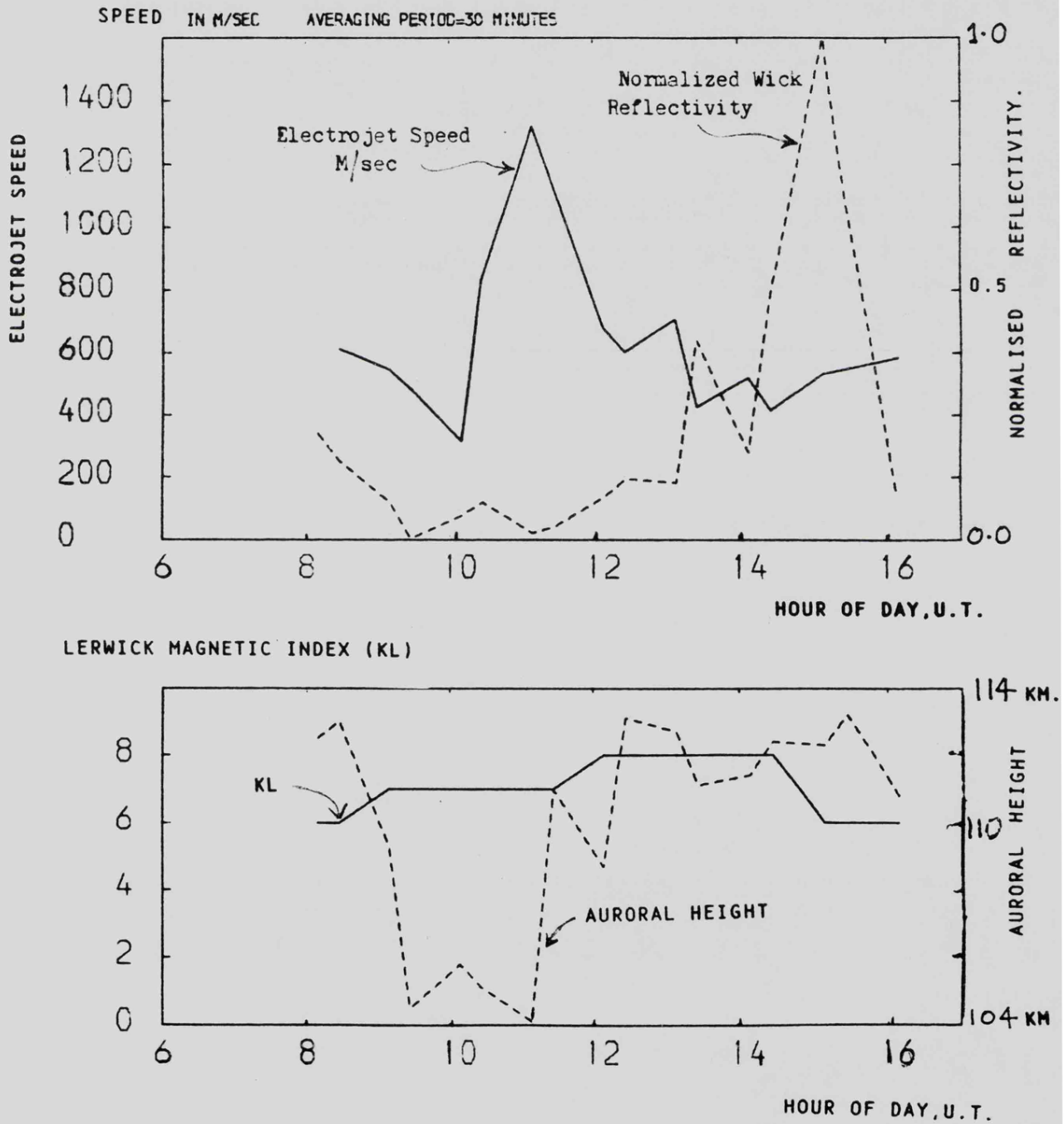
FIGURE 5.6

in chapter (3) as analysis of A) the Wick elevation polar diagram null position,B)the radar horizon slant-range and C) the ratio of the signals in each of the 8 beams of both radars at a given range.

5.1.3.1 Derivation of mean auroral height from the Wick elevation Null. Examination of equation(4.16) derived in chapter (4)for the Wick elevation polar diagram revealed that the first null (i.e.minimum),occurred for an elevation angle,θ_{E1},given by;

$$\theta_{E1} = asin((\lambda/2) \ H_A)$$

where λ = operating wavelength and H_A = antenna height above the ground plane.Two methods of determining the angle θ_{E1} were adopted;   i) A mean antenna height was derived as in chapter (4)from many days of reflectivity data and θ_{E1} found to be 4.2 degrees.

ii) A simple calibration was performed at the Wick site by means of a helicopter-borne VHF transmitter,(as described in chapter(7)),and θ_{E1} determined to be 4.2 $\pm$0.1 degrees.

With the angle θ_{E1} established,then accurate measurement of the slant-range at which the null in the auroral echo signal occurs enables the estimation of auroral height,assuming a mean value of the Earth's radius.The beam chosen for a study of the null position in slant-range was Wick beam 9,because of its relatively strong echo signals and low aspect losses,and because the auroral echoes occurred most frequently at the higher latitudes. The nulls of beams 10 and 11 occurred at lower latitudes,and the nulls of beams 5 to 8 contained weaker signals because of their larger values of aspect-angle loss.The mean value of auroral height was deduced as follows;

Let the slant range to the null = R_s,of accuracy $\pm$ 7.5 km,and let the null angle,θ_{E1} be 4.25 $\pm$ 0.1 degrees,and assume a mean Earth's radius of 6371.2 km.Then if errors in ranging measurement due to refraction effects, (as examined in chapter (4)),can be assumed to be 2 km at a slant range of between 785.5 and 800.5 km,then the mean auroral heights for null positions in range-cell 20,21,22 are as follows;

RANGE-CELL NUMBER	MEAN height	MINIMUM height	MAXIMUM height
20	104.3 km	101.5 km	107.1 km
21	107.2 km	104.4 km	110.1 km
22	110.1 km	107.3 km	113.1 km
23	113.2 km	110.4 km	116.1 km

A comparison was made of the echo signals in each of the 4 most common null range-cell positions in slant-range.If,over a 30 minute period of 181 signals,cell 21 signal was smaller than cell 20 signal for 170 counts out of 181,but was also smaller than cell 22 for 170 counts out of 181,then the null position was clearly in cell 21 and the mean auroral height was approximately 107 km.If however,the ratios were of the order 1:170 and 90:90 respectively then the mean auroral height would be nearer to 102 km since the echo signals are appearing in cells 21,22 equally.By employing such ratio measurements,an estimation of the mean auroral heights was made for day 249,1982,as displayed in fig(5.7),and the height values so derived were between 104 km and 113 km. However,the data for the time of the Morning Cleft is best ignored;hence the mean heights are between 107 km and 113 km. This method of height estimation is strictly applicable to the geographic location at range-cell 29,Wick beam 9,unless the diffuse aurora can truly be considered as a uniform layer.The accuracy of this method is limited by the pulse-width of the SABRE radar system. Methods of reducing the pulse-width and hence improving the accuracy are considered in chapter (9).

5.1.3.2 Estimating auroral height from the radar horizon.

The values of mean auroral height,(h),as derived from the value of slant range at the radar horizon can be derived from fig (4.2),or calculated using approximations given in Skolnik,ref(96),1972,as follows;

a)Radar horizon(in statute miles) $= \sqrt{(2\ h(feet))}$ (5.2)

PLOT OF AURORAL HEIGHT AGAINST TIME FROM MIDNIGHT ON DAY 249,1982.

THE HEIGHT IS CALCULATED FROM THE NULL IN THE ELEVATION POLAR

DIAGRAM OF WICK BEAM 9.

MEAN HEIGHT IN KILOMETRES

MORNING CLEFT TIME IS FROM 0915 TO 1230
HARANG DISCONTINUITY TIME FROM 2000 TO 2430

HOUR OF DAY IN U.T.

FIGURE 5.7

b)Radar horizon(in nautical miles)$=1.23(\sqrt{(H_A)}+\sqrt{(h(in\ feet)))}$ (5.3)

where $H_A=$ height of antenna in feet. Values of the radar horizon so calculated are in Table (5.3),in comparison with those quoted in ref (77),by Greenwald et al,1978,but without reference to the method of derivation.The two equations include the effects of refraction by assuming a "four-thirds" value of the earth's effective radius.This technique is generally employed to approximate the radar horizon,and as can be seen from Table (5.3) produces values of slant-range which are significantly higher than those derived from fig(4.2),which was based upon the CRPL reference atmosphere.A comparison between heights estimated from the value of slant-range to the radar horizon as derived from fig(4.2),and those estimated from the Wick null position can be made from Tables (5.4),(5.5).Also included in table (5.5) are the values of height calculated using the method of echo-signal ratios,as follows;

5.1.3.3 Estimating auroral height by the aspect-angle pattern.

As described in chapter (3),a fixed pattern of echo-signal strengths exists between the radar beams for a given auroral height,at a fixed slant-range.The major influence in deciding this pattern is the aspect-angle variation between the beams,as was revealed in fig(4.9).For example,if for the Wick radar the beam signal pattern at range-cell 29 were analysed,beam 11 would generally have the strongest echo signal on days of strong auroral activity,(i.e.Lerwick magnetic index >6).However,during such a day beams 10 and 12 may have equal mean echo signals;if so,then as can be seen from fig(4.6), the auroral height would be approximately 99 km.Hence,by examining the ratios of the mean signals in the radar beams,an estimate of auroral height may be derived from a knowledge of the theoretical aspect-angle pattern.

The resultant mean values of auroral heights so derived for day 249,1982,are compared with the height values deduced from the 2 previous methods,in Table (5.5).

TABLE 5.3

Auroral height in km	Radar horizon in km:			
	Using (a)	Using (b)	Using Fig (4.2)	Using Ref (77)
80	1165	1167	1055	no data
90	1236	1238	1080	no data
100	1303	1304	1150	no data
110	1367	1368	1200	1180
120	1427	1429	1265	1240

TABLE 5.4

Time (in 1982)	Lerwick Magnetic Index	Height as estimated by null position	Height as estimated by radar horizon
DAY 249 0100-0200	7	110 km	105 km
DAY 249 1030-1100	7	107 km	106 km
DAY 249 1230-1300	8	113 km	106 km
DAY 249 1500-1530	6	≥ 113 km	≥ 110 km
DAY 249 1600-1630	6	100 km	105 km
DAY 250 0100-0200	6	107 km	≥ 110 km

TABLE 5.5

TABLE (5.5)

Time	Mean Height as estimated by null position	Mean Height as estimated by aspect angle pattern (IGRF)		Mean Height as estimated by radar horizon		Estimated layer thickness	
		WICK	UPPSALA	WICK	UPPSALA	WICK	UPPSALA
Day 249 0100-0200	109 km	104 km	no data	105 km	no data	4 km	no data
Day 249 1600-1630	110 km	99 km	96 km	105 km	110 km	5 km	no data
Day 250 0100-0200	107 km	102 km	101 km	≥ 110 km	100 km	≥ 3 km	7 km

An estimate of the thickness of the auroral layer can also be made, based upon the understanding that the measurement of radar horizon would have involved back-scattered signals from the upper-most irregularities of the aurora. Hence an estimate of the layer thickness would be the difference in heights between that deduced from the radar horizon, and that deduced from a measurement of say the null position. If for example, the echo signals in range-cells 20,21,22 were utilised in the measurement of the null position and were predominantly back-scattered from the lower layers of the aurora and the echo signals in range-cells 48,49, employed to derive the radar horizon, were predominantly back-scattered from the upper layers, then the auroral thickness would be at least 10 km. Layer thicknesses estimated in this way for days 249,250, 1982 are displayed in table (5.5).

5.1.3.4 A summary of the estimated auroral heights.

In this section 3 techniques have been outlined for estimating the mean auroral height. These are based upon analysis of;

A) The Wick vertical polar diagram null position

B) The radar horizon slant-range

C) The ratio of the signals at a given range in each radar beam.

Each of these techniques is, however, only applicable to the radar data for a limited period of time and under certain geophysical conditions. Comparisons of mean auroral heights estimated by all 3 techniques for the period 1982 to 1984 are only possible for a few hours of data and strong echoes. An examination of the radar data revealed that the weaker echoes were of limited range extent, generally 5 to 10 range-cells, but were extended across all of the radar beams, to form a band of aurora of very wide azimuthal extent. The latitudinal position of this band varied from day to day but when it was positioned across range-cells 20,21,22 of Wick beam 9 it was possible to estimate the mean auroral height from the polar diagram null position. When the auroral band was positioned across the range-cells 29 at

Wick and the electrojet flow was uniform,it was possible to estimate auroral height from the ratio of signals in each radar beam.However,this technique was also limited to the brief periods of uniform electrojet flow,usually between 1400 to 1700 hours, or 0100 to 0300 hours. When the auroral band was positioned at higher latitudes (i.e. range-cells higher than 40) it was possible to estimate the auroral height from the radar horizon.

For the bulk of the auroral signals analyzed in this Thesis,the signals were selected for those days when auroral activity was so intense that most of the radar range-cells contained strong echoes. Under these conditions it became possible to compare the values of estimated heights as were displayed in figs(5.4),(5.5). However,these conditions were found in only 3 of the 740 days of data examined. A comparison of mean heights estimated from days of data for which the Lerwick Auroral index K_L is >6 is as follows;

TECHNIQUE	NUMBER OF DAYS OF DATA EXAMINED	MEAN AURORAL HEIGHT
A) Null	7	107 ± 3 Km
B) Radar horizon	7	105 ± 3 Km
C) Ratio of signals	3	101 ± 3 Km

The number of days of data which contained echoes strong enough for height estimation analysis programming were;

TECHNIQUE	NUMBER OF DAYS OF DATA AVAILABLE
A)	296
B)	140
C)	222

Technique A) is considered to be the most reliable and convenient method of height estimation since it is based upon an antenna calibration of the null elevation angle and provides a height estimation near the centre of the SABRE viewing area. Technique B) enables an estimation of the height of the top of the auroral layer,but only at the extreme edge of the SABRE viewing area. Technique C) requires an examination of the auroral flow conditions

during electrojet flow periods and relies upon values of aspect angles derived from the I.G.R.F magnetic field model.It also requires considerably longer analysis time than techniques A) and B).

The bulk of the auroral height estimates within this Thesis have been obtained via technique A), the analysis of the Wick elevation null. The mean auroral height so estimated, for the years 1982 to 1984 is approximately 107 Km at the centre of the SABRE viewing area.

The techniques outlined in this section have estimated the auroral mean heights to be between 96 km and >113 km,and have indicated that each radar may be viewing a common volume of the aurora,but may detect irregularities which are at slightly different heights.Furthermore, the auroral height may vary slightly across the SABRE viewing area.However,these techniques of data analysis are not sufficiently accurate to distinguish such height differences at all times. The range of auroral heights estimated in this section are in general agreement with those of other researchers, including Unwin and Johnston, ref(84),1981 and Timofeev and Miroshnikov,ref(112),1982. Further details of the variation of auroral characteristics with height and slant range can be found in these references. Modifications to the SABRE radars which may permit more precise height measurements are considered in Chapter (9).

An examination of the variation of the strongest values of reflectivity with flow-angle for each radar was then undertaken as follows;

5.2 The variation of the strongest reflectivity signals with flow angle.

5.2.1 The uniformity of the electrojet flow

The electrojet flow data was first examined to determine the uniformity of flow at the 3 positions of closest overlap,as were defined in Table (5.2).The most uniform electrojet flow measured was for day 249,1982,1550 to 1650 hours,with uniformity derived with the following criteria;

a) The difference in flow-angle when measured with respect to each radar

beam should be approximately 3.6 degrees per beam.

b) The electrojet velocity should vary as the cosine of the angular differences between the beams.

Hence, the velocity in beams 9 and 7, relative to the velocity in beam 11 should be;

$$V_9 = V_{11} \cos(7.2 + \text{(difference in flow-angles)})$$

$$V_7 = V_{11} \cos(14.4 + \text{(difference in flow-angles)})$$

For day 249, 1982, 1550 to 1650 hours the values for beams 9,7 were;

BEAM NUMBER	MEASURED MEAN VELOCITY	THEORETICAL MEAN VELOCITY
Wick, 7	464 m/sec	419 m/sec
Wick, 9	490 m/sec	471 m/sec

The measured mean velocity in beam 11 was 523 m/sec. Hence, the electrojet flow for this period of time was uniform to within 10 %.

5.2.2 The variation of the strongest values of reflectivity with flow angle.

The variation of the stronger levels of reflectivity with flow-angle for the 3 points of closest overlap during this day, can be derived from table (5.2). Also presented in this Table are data for day 250, 1982, and day 35, 1984, since these days contained consistently strong echoes. Generally, the very strongest echoes occur for flow-angles of less than 40 degrees. For example, the strongest values of reflectivity in the Wick data, for day 249, over a 30 minute period, occurred for flow-angles of 10.5 and 40 degrees, whilst the Uppsala data for the same day had maxima values for flow-angles of 3 and 33 degrees. The examination of the mean echo signals had, up to this point, been for auroral echoes of Doppler velocities of up to 1600 m/sec, and had indicated an approximately cosine dependence of reflectivity upon the flow-angle, with "data scatter" occurring at the higher values of reflectivity. An examination was then undertaken of the variation of reflectivity with flow-angle, but for restricted values of velocity, as follows;

5.2.3 The variation of the strongest values of reflectivity with flow

angle,for a fixed value of electrojet velocity.

The reflectivity values at the 3 closest points of radar overlap were monitored for the Wick radar,for electrojet velocities in the range 400 to 440 m/sec,600 to 640 m/sec and 800 to 840 m/sec,on days 249, 250 1982 and day 35 1984.

The results of this examination were similar to those of the analysis of the data which included all values of electrojet velocities;

i) The stronger echo signals occur at angles of flow < 40 degrees. However,a peak echo signal(of > 70 dbs) may occasionally appear at flow-angles of up to 50 degrees.

ii) The mean variation of reflectivity with flow-angle,as in fig(5.8), is approximately 0.2 dbs/degree,for angles of up to 40 degrees.A roughly cosinusoidal dependence upon flow-angle can be assumed for angles of between $\pm$ 90 degrees for all but the very strongest echoes.As can be seen in fig(5.8), the maximum signal does not occur at 0 degrees.

These results are indicative of an essentially Type 1 spectra,with Type 2 in evidence at the largest flow angles.

Similar anisotropy of the backscattering cross section of 2 stream irregularities has been reported for the equatorial electrojet by Ierkic et al,1980,ref(107),and for the auroral electrojet by Haldoupis and Nielsen,1984,ref(86).Generally,gradient drift irregularities possess an isotropic scattering cross section,as was discussed in chapter 2,fig (2.8) and have a broad spectrum. 2-stream irregularities have a narrow spectrum and relatively high velocity,(> 350 m/sec).

An examination was then made of the variation of reflectivity with Doppler velocity and electrojet velocity,to confirm the presence of 2-stream and gradient drift irregularities and to detect any differences in the characteristics of the Auroral volume "viewed" by each radar.

5.3 Analysis of the Data Distributions.

THIS GRAPH IS APPLICABLE TO ELECTROJET VELOCITIES FROM 600 TO 640 M/SEC

PLOT OF REFLECTIVITY AGAINST FLOW-ANGLE WITH RESPECT TO WICK BEAM 11 AT 64.26 N,6.00 E.

TOP CURVE IS FOR THE AFTERNOON ELECTROJET,BOTTOM CURVE IS FOR THE NIGHT-TIME ELECTROJET.
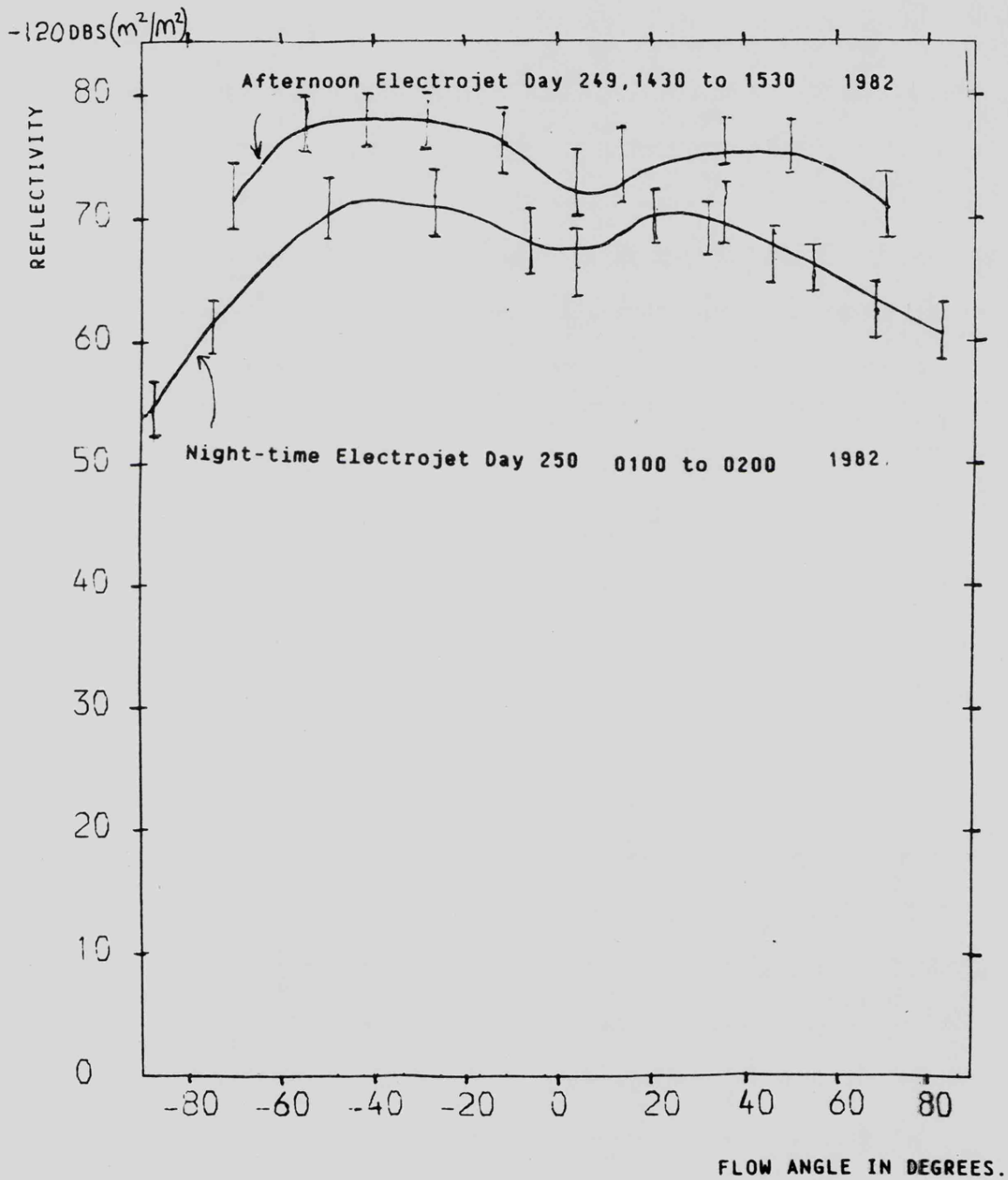
FIGURE 5.8

5.3.1 The distribution of reflectivity with Doppler velocity.

A graphical study was undertaken of the distributions of the Doppler velocities and resultant field strength for periods of 1 hour,via the computer programme COEMER,described in chapter (8).The distribution of the velocities and their associated values of reflectivity were plotted in series of graphs,similar to fig(5.9).Although these graphs are strictly distributions of velocity (in 50 m/sec steps) and mean reflectivity over a 1-hour period,they are presented in a form of spectral-analysis,on the understanding that the analysis is not applicable to a single integration period.The shapes of the distributions (see fig(5.9)) are similar to the spectral shapes obtained by Nielsen et al,ref(89),1984,with the Stare radar when operating in the 11 double pulse spectral analysis mode of 2 minute duration.The spectral parameters monitored in this analysis of the distributions were;

a) The maximum and minimum Doppler velocities and field strengths.The minimum velocity of a Type 1 spectrum,defined in Chapter 2,was to be of the order of 350 m/sec,and of field strength 22 mV/m. Velocities below this value are normally associated with Type 2 (gradient drift) spectra.Generally,the velocity limits were between 350 and 1200 m/sec although one strong echo occurred in the early afternoon at 300 m/sec.The bulk of the spectra for the strongest echoes were of the Type 1.

b) The width of the distributions at the half-power points,i.e. the spectral beam-width.Spectra associated with primary irregularities (2 stream) are generally narrow,ie 300 to 600 m/sec,whilst the spectra of secondary irregularities,(gradient drift) are broad,ie up to 1200 m/sec.The width of the distributions in this analysis were mostly below 550 m/sec.

c) The slope of the graph of mean reflectivity against Doppler velocity and field strength.
The results of this analysis for the 3 points of closest overlap,and for the 3 days of most consistent signals contain 3 types of graph-slope;

COMPARISON OF THE DISTRIBUTIONS OF DOPPLER VELOCITIES IN
STEPS OF 50 METRES/SECOND.
THE DASHED CURVES ARE THE NORMALISED REFLECTIVITIES AT EACH
DOPPLER VELOCITY.

1982 DAY 249 14HOUR 30MINS. TO 249 15 30 U.T.
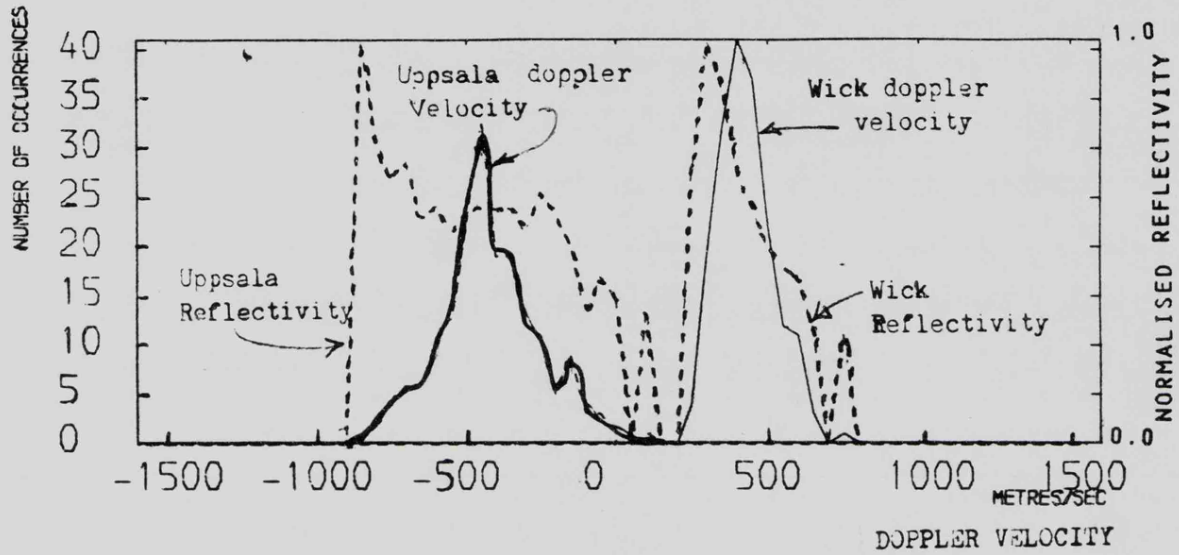
1982 DAY 250 1HOUR 0MINS. TO 250 2 0 U.T.
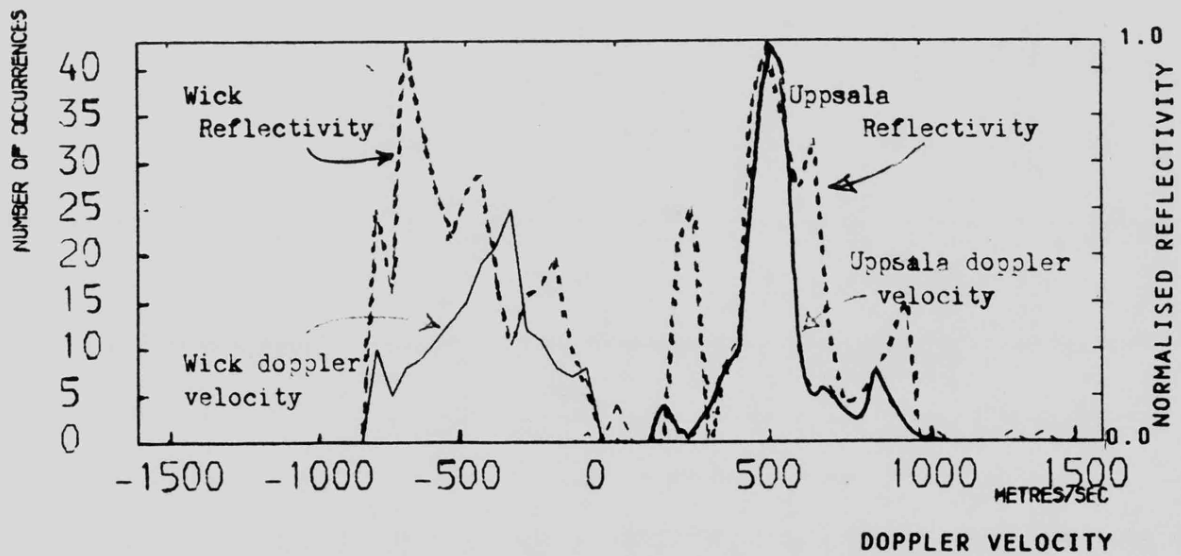
FIGURE 5.9

1) "POS" where the reflectivity increases with velocity up to a peak,then decreases sharply.A 2-stream irregularity spectrum would initiate above 350 m/sec and then increase in echo power and Doppler velocity until damping occurred at about 600 m/sec due to transfer of energy to other non linear processes. This shape occurred in the majority of the analyses.

2) "NEG" where the reflectivity increases sharply with electrojet velocity,up to a peak,then decreases gradually.This spectral shape would be associated with a combination of the two irregularity types and occurred for a peak velocity of 300 m/sec,indicating the presence of gradient drift irregularities.

3) "GAUSSIAN" where the reflectivity is centred about a mean value of velocity,in a roughly gaussian shape.This spectral shape could result from several irregularities of both types.

The differences between "pos" and "neg" velocity graph-slopes could be explained in terms of the variation of reflectivity with flow-angle for all but the highest values of reflectivity,since,(as was described in the previous section),these may occur at any flow angle below about 50 degrees.

5.3.2 The distribution of maximum reflectivity with field strength,E.

The analysis of chapter 2 revealed that Electric field strength,E,may be directly proportional to the electrojet speed for a given value of Magnetic field strength,B. The variation in Magnetic field strength during the days of echo data analysed in this section were less than + 1 % and hence the electrojet Electric field strength will be assumed to be directly proportional to electrojet speed.The relationship between E in millivolts per metre and speed V in metres per second is $E = V/20$ (5.4)

Graph-slope types similar to those in the previous section were detected in the distributions of the maximum values of reflectivity against electrojet speed,as in figs(5.10),(5.11).The mean values of reflectivity,derived for 1 hour periods,were plotted against mean electrojet speed in fig (5.6) for day 249,1982,and no clear correlation is evident.

COMPARISON OF UPPSALA MEAN REFLECTIVITIES AND ELECTROJET SPEED

FOR 1 HOUR PERIODS, AT 64.26 N, 6.00 E.

MAXIMUM REFLECTIVITY = -50.7 DB (M^2/ M^2)
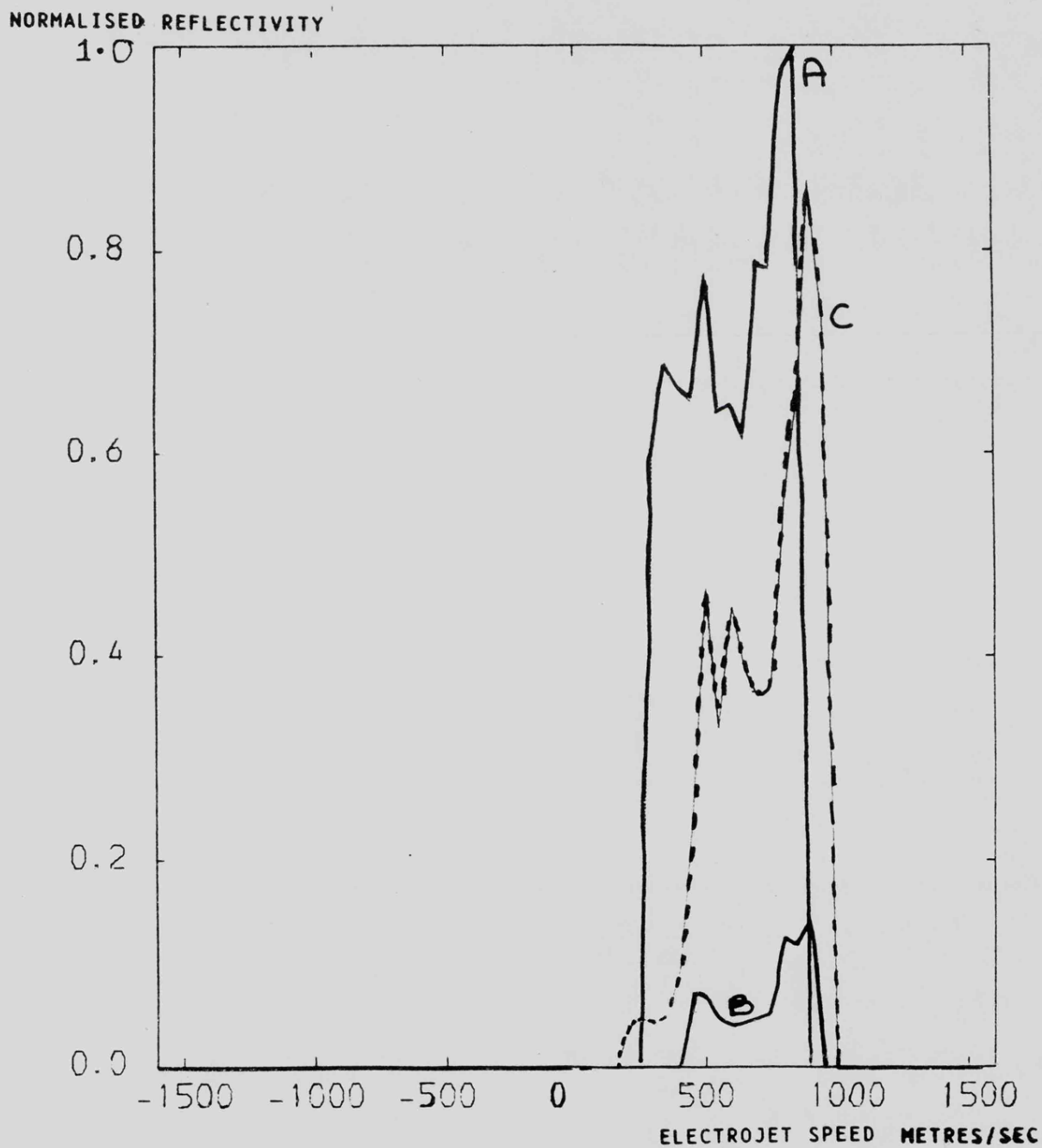
CURVE A IS FOR DAY 249 1982, 1430 TO 1530 HOURS

CURVE B IS FOR DAY 35   1984, 1400 TO 1500 HOURS

CURVE C IS FOR DAY 249 1984, 1550 TO 1650 HOURS.

FIGURE 5.10

COMPARISON BETWEEN WICK MEAN REFLECTIVITIES AND ELECTROJET
SPEED FOR 1 HOUR PERIODS, AT 64.26 N, 6.00 E.
MAXIMUM REFLECTIVITY = -42.8 DB (M^2/ M^2)
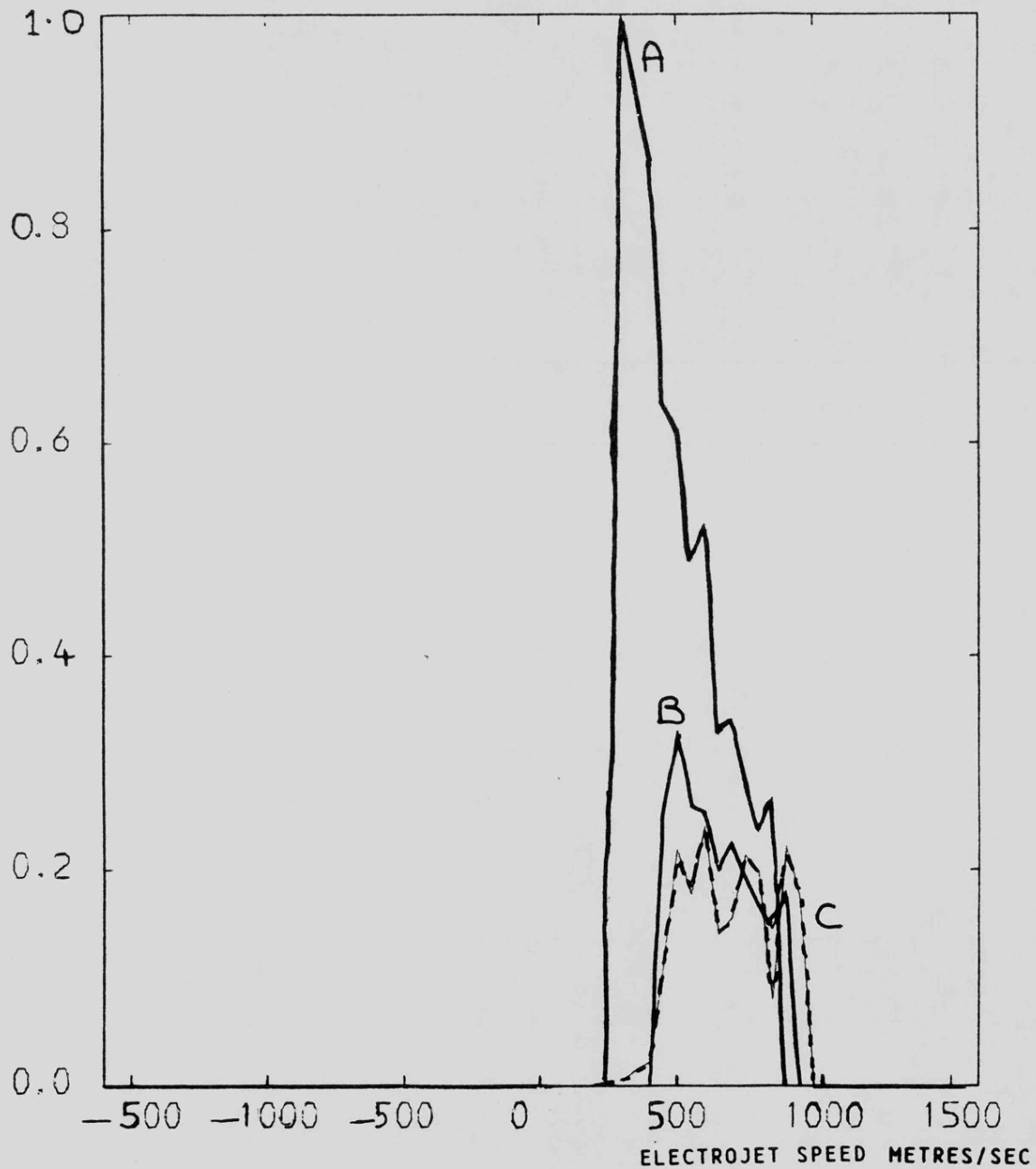
CURVE A IS FOR DAY 249 1982, 1430 TO 1530 HOURS

CURVE B IS FOR DAY 35 1984, 1400 TO 1500 HOURS

CURVE C IS FOR DAY 249 1982, 1550 TO 1650 HOURS.

FIGURE 5.11

The differences between the 3 types of distribution graph-slope could also be explained by the variation of velocity (and minimum field strength for initiation of the 2-stream process) with auroral height,as was outlined in chapter 2. Sudan,et al,ref(110), 1973, indicated that the Doppler velocity (and reflectivity) would increase with height,up to a maximum value at 105 km,then decrease above this height.McDiarmid,1970,ref (54),also predicted a similar pattern,dependent upon the field strength in the electrojet. Accordingly,the distribution shape "POS" would correspond to echoes backscattered mainly from auroral areas of height above 105 km,and "NEG" to echoes backscattered from areas below 105 km.However,for those occasions of the very strongest values of reflectivity,the Doppler velocity fell below 350 m/sec,(and the field strength fell below 22 mV/m)and the gradient-drift irregularity process can be suspected as being dominant.This is most probable since these echoes occurred in the afternoon periods when the Sun's activity would be greatest in enhancing the density of electrons in the E-layer,and producing the density gradients.

The distributions were not always smooth,and contained several minor peaks,suggesting that echoes were being backscattered from several layers within the aurora.

5.3.3 Conclusions of the analysis of the data distributions.

The general conclusion drawn from this analysis was that both SABRE radars exhibited reflectivity-velocity distributions which indicated that echoes could be incoming from irregularities at different auroral heights.

Techniques of improving the spectral-analysis of the SABRE data,and hence investigating the variation of signals with height more thoroughly,are outlined in chapter(9).The analysis of the data up to this point had indicated the importance of height-measurement.The next stage in the analysis was to examine the variation of mean Doppler velocity with aspect-angle;

5.4   The variation of mean Doppler velocity with aspect-angle and height.

Although the IGRF magnetic field model had correctly predicted the variation of echo signal (i.e. reflectivity) with aspect-angle at a fixed range,the measured echo Doppler velocities did not display the same distinctive variation;a roughly cosine(azimuth angle) relationship was detected instead. Investigations were then undertaken into

a) The variation of auroral Doppler velocity with aspect-angle and slant-range.

b) The variation of Doppler velocity with height.

5.4.1   The variation of auroral Doppler velocity with aspect angle and slant range.

The theoretical variation of the Doppler velocity for the 2-stream (Type 1) irregularity process can be derived from the basic equations in chapter 1. The Doppler velocity,V_{DO},of the irregularities when the ion drift velocity is negligible in comparison with the electron drift velocity V_D,and for irregularities which are nearly aligned with the magnetic field B,is given by;

$V_{DO} = V_D/(1 + A_{LP})$

where $A_{LP} = ((\tilde{V}_i \tilde{V}_e)/(\Omega_i \Omega_e))(K_1^2/K^2)) + ((\tilde{V}_i \Omega_e/\tilde{V}_e \Omega_i))(K_2^2/K_1^2)$

where $\tilde{V}_i,\tilde{V}_e$,=collision frequencies of ions,electrons

and Ω_i,Ω_e = gyro   "   " "   "

and K_1,K_2 =components   of   the   irregularities wave-number,K,perpendicular   and   parallel   to   the   magnetic   field,B.For irregularities which are nearly field aligned,$K_2 \ll K_1 \approx K$ and in the E-region for auroral heights of 105 km to 115 km,the expression for A_{LP} reduces to the approximation;

$1+A_{LP} = (1 + 3000 (K_2^2/K^2))$.

The factor (K_2/K) is a measure of the degree of orthogonality of a radar beam which for the SABRE radars is typically less than 2.2 degrees.The aspect-angles for range-cell 29 of each Wick radar beam was evaluated in chapter(4) for different auroral heights.The changes in off-aspect-angle (i.e. 90 degrees -aspect angle),between the beam positions were approximately constant and hence the theoretical variation in V_{DO} due to aspect angle change can be calculated and compared with the measured mean values,normalised to beam 11,as follows;

Wick beam number	5	6	7	8	9	10	11

Off-aspect angle	-2.57	-2.27	-1.91	-1.15	-1.01	-0.46	-0.01 degrees

Calculated Doppler

velocity wrt beam 11	0.15	0.18	0.23	0.48	0.37	0.90	1.0

Measured mean Doppler

velocity wrt beam 11	0.82	0.83	0.85	0.85	0.86	0.99	1.0

The measured mean Doppler velocity distribution was for day 250,1982,0100 to 0200 hours.

Generally,no clear evidence of the theoretical variation of mean Doppler or peak Doppler velocity with aspect-angle at a fixed range was found,for the stronger signals,i.e signal to noise ratios of > 20 dbs.When examining the variation of Wick Doppler velocity with slant-range,however,one feature was detected which prompted further investigation;namely that occasionally the Doppler velocity pattern with slant range followed the antenna vertical polar diagram pattern.

5.4.2 Determining the auroral velocity-height profile.

For the majority of measurements the Doppler velocity either increased or decreased slightly with slant-range,but as in fig(5.12.c) for day

SCHEMATIC ILLUSTRATION OF THE VARIATION OF SABRE DOPPLER VELOCITY

WITH SLANT RANGE IF A VELOCITY GRADIENT EXISTS WITHIN THE AURORA.

GRAPH (B) APPLIES FOR A LINEAR VERTICAL VELOCITY GRADIENT

GRAPH (C) APPLIES FOR A VELOCITY PEAK IN THE CENTRE
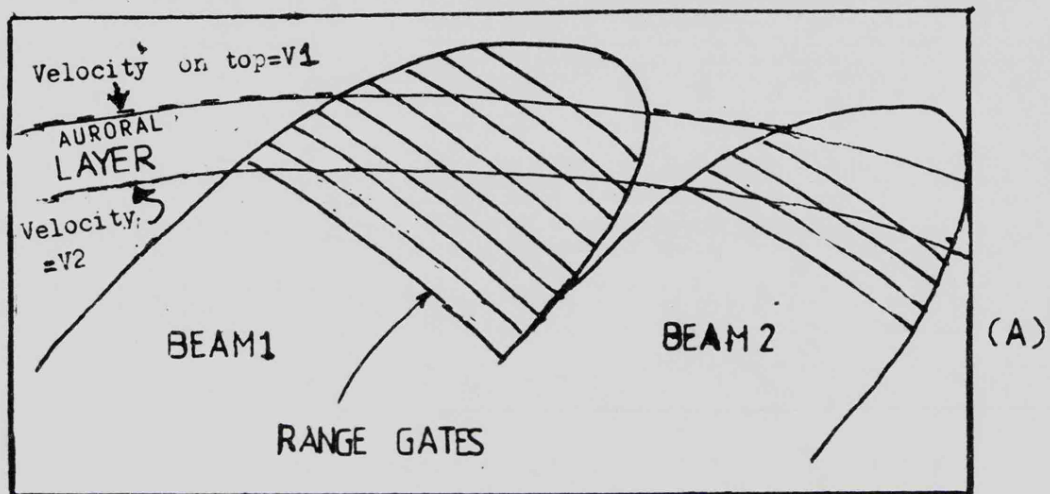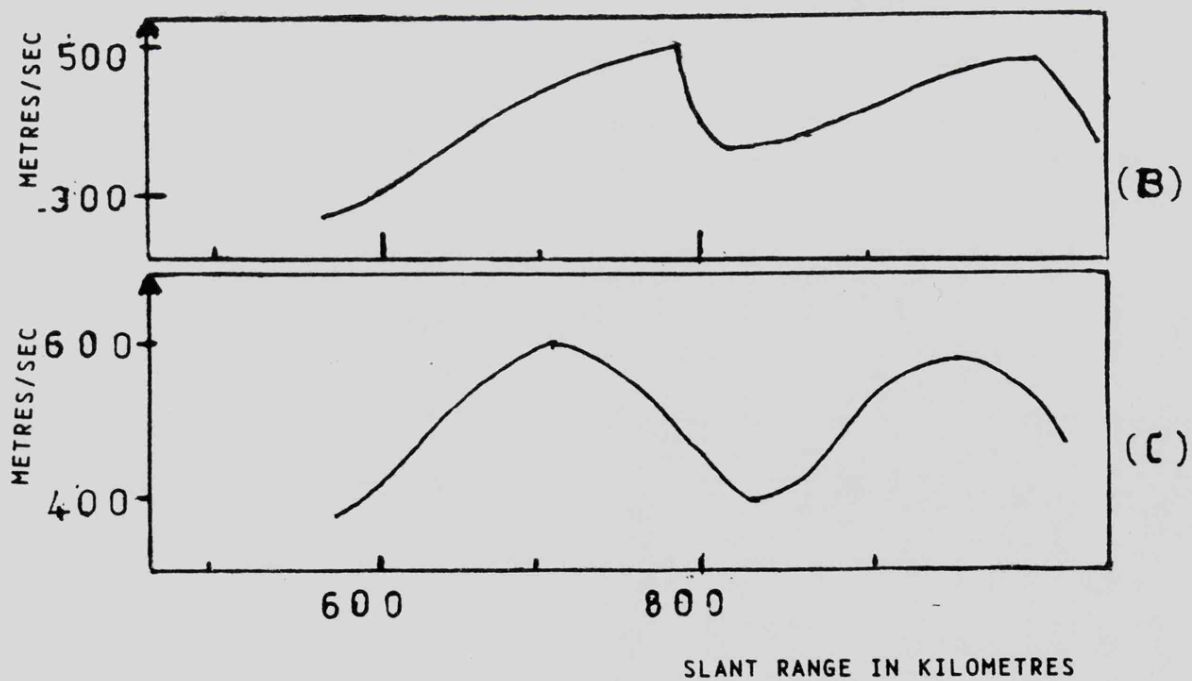
FIGURE 5.12

249,1982,0000 to 0100 hours,the shape of the polar diagram can be seen in the velocity pattern.

The positions of the polar diagram maxima in the velocity occur at slightly greater slant-ranges than do the corresponding maxima in the mean echo-signal pattern.An explanation for this feature was derived from the work of Unwin,ref(84),1981,who reported similar findings with the 53.5 MHz auroral radar in New Zealand.Unwin proposed that the reason for differences in the slant range between the Doppler velocity maxima and the echo-signal maxima was due to the variation in Doppler velocity with auroral height,and the fact that each successive range gate would progressively monitor a higher level of the aurora,as in fig(5.12 a). The velocity profile would therefore be a maximum in the centre of the auroral layer in the pattern of fig(5.12.c).The velocity pattern for the afternoon of day 249,(for which the bulk of the aspect angle and height calculations were made),is displayed in fig (5.12.b),and contains the 2 lobes of the elevation polar diagram.However the velocity increased in a similar manner in each lobe.The velocity-height profile corresponding to this pattern would have a positive velocity gradient,with the highest velocity at the top of the auroral layer.

The differences in slant-range between the velocity-diagram null and the reflectivity diagram null were between 1 and 3 range-gates;ie (15±7.5)km to (45±7.5)km.The corresponding values of estimated auroral layer thickness were therefore (3±1.5) km to (9±1.5) km.The layer thickness for the afternoon of day 249 was estimated to be (6 ± 1.5) Km,which compares favourably with the value of 5 Km as estimated in section 5.1.3.2.The conclusion drawn from this part of the analysis was that the existence of velocity gradients within the aurora further justified the requirement for precise height measurements.From the auroral layer dimensions so derived,it is possible to predict the value of electrojet current,as follows;

5.5 Estimating the value of electrojet current,between L=4 to 6.

A broad estimate of the mean value of electrojet current can be made for day

249,1982,by assuming the values of auroral electron concentration as measured in ref (71),1975,by Banks and Doupnik.

For the uniform electrojet flow of the afternoon of day 249,the mean layer thickness was 6 Km,range extent 700 Km and mean velocity 500 m/sec.The resultant electrojet current for these conditions is 140,000 amps in daytime, 35,000 amps at night.

5.6 Summary of the results of this chapter.

The results and conclusions of this part of the analysis of the general radar equation can be summarised as follows;

1. The mean values of diffuse auroral reflectivity in dbs (square metre per square metre) range between -34 to -80. The peak values are about 11 dbs greater than the means.The strongest values of mean reflectivity generally occur (a) during the times of strongest magnetic activity and horizontal magnetic field strength, and (b) most frequently during early afternoon. Day-time echo signals can be up to 3 dbs greater than night-time and generally increase with L-value and height.The times of day during which the maximum area of aurora appears as radar echoes is from 1600 to 1700 hours.

2. The range of values of mean auroral heights is from 104 km to 113 km and are greater during the afternoon.The value of mean height calculated from the aspect-angle patterns indicated that the 2 SABRE radars may be viewing irregularities at slightly different heights,in the same volume of the Aurora.

3. Some short-lived disturbances may not be seen by both radars,but generally for disturbances of greater than 2 minutes,both radars will register an echo but not necessarily of the same magnitude.The very strongest echoes may be separated by a 2-hour interval between the 2 radars.

4. An average value of the electrojet speed,for the times of strongest reflectivity,may be from 300 to 600 m/sec,corresponding to field strengths of approximately 15 mV/m to 30 mV/m.

5. The times of occurrence of the Morning Cleft would be from 0810 to

1230 hours,and the Evening (Harang) Discontinuity from 1800 to 0300 hours. The times of initiation and termination of these events is marked by severe fluctuation in the velocity measurements.

6. The analysis of the 1-hour distributions of reflectivity and velocity indicates the existence of mainly Type 1 irregularities,and some Type 2.

7. The analysis of the velocity-slant range profile indicates that the velocity may increase with auroral height,and may also maximise in the auroral centre.Typical velocity-height gradients may be 16 m/sec/Km.

8. The mean values of auroral layer thickness,estimated from the reflectivity and velocity data range from 3 to >10 km.

9. The estimated values of mean electrojet current in the SABRE viewing region lie in the range 35,000 to 140,000 amps.

A general discussion of these results,and the calculations of the previous chapters will now be undertaken,in Chapter (6);

CHAPTER SIX

6. Results of the data analysis.

6.1 Introduction.

An examination of the SABRE data over the time period 1981 to 1984 has indicated that only a small percentage of days contained echo signals which covered the entire viewing area.Generally the echoes would extend in azimuth across all the radar beams,but would have limited range-extent.This strip or ribbon-like echo was detected between the L-values of 4 to 5.5.

On the very few days that both radars received echoes which covered the viewing area it was possible to examine the signal to noise ratios and the velocity data and hence to deduce the antenna polar diagrams and the basic features of the auroral backscattering region.Both radars are sensitive to the same scale (1 m) irregularities but because of the different viewing angles,the backscatter cross-section of the auroral density fluctuations seen by either radar may differ at any instant of time.

In the analysis of the mean radar or electrojet parameters it must be stressed that the values were derived from a mean of the strongest echoes and that the averaging times are greatly in excess of an individual disturbance lifetime,but less than that of the major auroral features such as the Morning Cleft or Harang Discontinuity.The values of auroral height which were derived from these mean data might also include height fluctuations of relatively short lifetime.The analysis of the data distributions however,refers to events within the averaging periods,(usually 1 hour),and are based upon integration times of 20 seconds.

6.2 A comparison of the results of this analysis with other publications

This analysis has resulted in the derivation of mean values of parameters which include; Auroral height,antennae polar diagrams,aspect-angle loss,electrojet velocity spectra and electric field strength.These values

were derived for the days of strongest auroral and magnetic activity,for the diffuse aurora and may differ from those of relatively weak activity or discrete aurora.The values so derived can be compared with the results of other researchers as follows;

6.2.1 Mean auroral height in kilometres

This analysis	Unwin and Johnston 1981,ref(84)	Kamide and Brekke 1977,ref(76)
104 to 113	106 to 112	101 to 119

The values derived in this analysis are in general agreement with earlier findings,but methods of improving the SABRE height-measuring techniques are detailed in chapter (9)

6.2.2 Wick antenna vertical polar diagram

	This analysis,1982	Calibration via a helicopter,1984
First Null angle	4.2 degrees	4.25 degrees
Second Null angle	8.4 "	8.5 "

The Wick vertical polar diagram derived from this analysis of many days of data was a very close match with the averaged calibration polar diagram for elevation angles below 8.5 degrees.For angles above this value there were insufficient data available.

6.2.3 The ratio of the Wick and Uppsala receiver array cross-sections.

Theoretically derived ratio	ratio obtained in practice
6 db	5.7 db

6.2.4 Aspect-angle loss in db/degree.

This analysis	McDiarmid 1972,ref(63)	Leadabrand,et al 1967,ref(64)	Ecklund,et al 1975,ref(65)
6.5 ±2	2	10	8

6.2.5 Electrojet velocity spectrum

This analysis derived the spectra from the distributions of reflectivity and velocity,over 1 hour periods,employing the SABRE double-pulse velocity measuring technique.The results indicated the presence of a predominantly

Type 1 spectrum,(2-stream irregularities). Type 2 spectra,(gradient drift irregularities) occurred at large flow-angles and during the early afternoon at highest reflectivity.The results which were analysed in chapter (5) were very similar to those achieved with multiple pulse techniques,as reported in refs(88),1983,by Whitehead et al,and (89),1984,by Nielsen et al.

Methods of improving the SABRE velocity measuring scheme are outlined in chapter (9),and must be considered with the improved height measuring proposals,since evidence of the variation of velocity with height was also detected in the analysis.

6.2.6 Electric field strength in millivolts per metre.

This analysis	Greenwald et al,1978,ref(77)
15 to 50	30 to 50

These values are only applicable to days of strong auroral activity; much lower values would be obtained if the investigations had included analysis of weaker signals and lower velocities.

Similarly the mean values of beam-pointing loss (due to the variation of auroral cross-section with flow angle),of between 0.14 and 0.2 db/degree, are comparable to the values obtained by Ierkic et al,ref (107),1980, when viewing the equatorial electrojet. However, it must be stressed that the investigation within this Thesis has not included a detailed examination of the auroral parameters for conditions of weak echo signals; subsequent investigation may prove that the loss factors differ for auroral conditions of low magnetic activity.

6.3 Discussion

Generally the results of this analysis are in good agreement with those of other researchers and with the calibrations,and confirm the importance of evaluating each factor in the radar equation.This analysis has been undertaken with the minimum of hardware or equipment modification.Instead, it has relied upon computer analysis and radar theory in deriving the

auroral parameters from the SABRE data.It has revealed the need for more accurate height measurements,particularly when monitoring velocity gradients.On certain days the electrojet direction seemed to follow the direction of the L-contour,but on others the motion was diagonal to this contour.Similar variation in behaviour was encountered when examining the record of auroral echoes against magnetic field strength for the years 1981 to 1984; a high value of field strength or Lerwick magnetic index did not always guarantee strong auroral echoes.Similarly,the echo strengths did not always peak at the same time in each SABRE radar,nor at zero degrees flow angle.The probable reason for these effects is that the stronger echoes require a combination of magnetic fluctuation,auroral height,conductivity and radar viewing angle.

The most stable,streamlike flow patterns of auroral electrojets were to be seen during mid-afternoon or mid morning but even then small areas of localised disturbances could be observed in the reflectivity and velocity maps.

It is possible that the derivation of reflectivity described in this analysis,and the general radar equation for diffuse aurora,may be extended to include the effects of height and flow angle such that a more direct link with magnetometer readings may be derived for each day of the year.It is of interest to note that the very strongest values of auroral reflectivities that were encountered in this analysis are of similar order of magnitude to those obtained for some sea echoes, at VHF, with horizontally polarized radiation, as described in ref (96),1972,by Skolnik.

The values of afternoon electrojet current derived in this analysis, for L-values between 4 and 6, represent a portion of the total electrojet. Typical values of total electrojet current quoted in ref(127), by Hargreaves,1979, for example,are of the order of a million amperes.

At this stage of the analysis sufficient information had been derived from

the SABRE data to enable a form of radar equation which would be of value in

the examination of the short-range signals,described in the next chapter.

CHAPTER SEVEN

7. The investigation of short range radar echo signals.

This chapter will describe the analysis of a new class of backscatter echo detected at short ranges by the Wick SABRE radar.Methods of echo location and possible source mechanisms are described.The radar system parameters which were derived in the previous chapters from analysis of the echoes from diffuse aurora will be employed in evaluating these new signals. Similarly the results of the review of atmospheric echo processes in chapter 1 will be utilised in this investigation.

Although the SABRE radar system was designed to examine the backscatter returns from the auroral regions at slant ranges of between 495 Km to 1250 Km, echoes have been detected at much shorter slant ranges ---90 Km to 350 Km. These echoes have characteristics which differ from those of the normal diffuse auroral echoes which were analysed in the previous chapters of this Thesis. The basic features of these short-range echoes are;

a) They appear at slant ranges below 300 Km and have a range-extent of 2 to 3 range-cells,(ie 15 Km to 45 Km).

b) They appear in all 8 beams of the Wick radar simultaneously.

7.1 Initial investigation of the echo signal characteristics.

The investigation of these returns was complicated by a series of system faults including transmitter breakthrough,timing errors,programming errors and antenna component failure.The methods of detecting the system faults and of determining the nature of the echoes were as follows;

7.1.1. Transmitter interference effects.

Examination of the minimum range signals revealed that they were of fixed range, of relatively uniform amplitude in all 8 beams and had rapidly fluctuating Doppler velocities.Such characteristics prompted an investigation of the transmitter timing control programme employed in the short range mode of operation. A timing error was located which had caused the receiver to be switched on prematurely,during transmission time. The error was corrected and this type of interference effect disappeared.

7.1.2 Receiver interference effects.

In order to examine the effects of possible internal interference within the SABRE receivers,the performance was evaluated under laboratory conditions. The experiment was arranged as in fig (7.1(a),(b)). Because of the variety of tuned circuits and filters within the receiver,particularly the head amplifiers,it was suspected that "ringing" or oscillation of these units after being switched on or off by the control computer might produce spurious output signals.These unwanted outputs could be interpreted as radar echoes.

Close examination of the receiver performance revealed that no spurious signals were generated when the receiver was switched at the normal SABRE sequence, as employed at the Wick site.

7.1.3 Doppler velocity measurement errors.

Since a short range echo occupies several adjacent range-cells,its velocity may be determined by its change in range within a given time; a measurement often referred to as the "range-rate".This velocity may then be compared with the Doppler velocity derived from the double-pulse SABRE system.

The range-rates so measured were of the order of 60 to 100 metres/second but the Doppler velocities were between -800 to +800 metres/second. Thus a large discrepency existed.

A method of testing the SABRE Doppler velocity processing system in the short range mode was then proposed, based upon the schematic illustration in fig(7.2).The Doppler velocity is normally derived from measurements of the

SCHEMATIC ILLUSTRATION OF THE EXPERIMENT FOR INVESTIGATING

POSSIBLE "RINGING" OF THE SABRE RECEIVER.
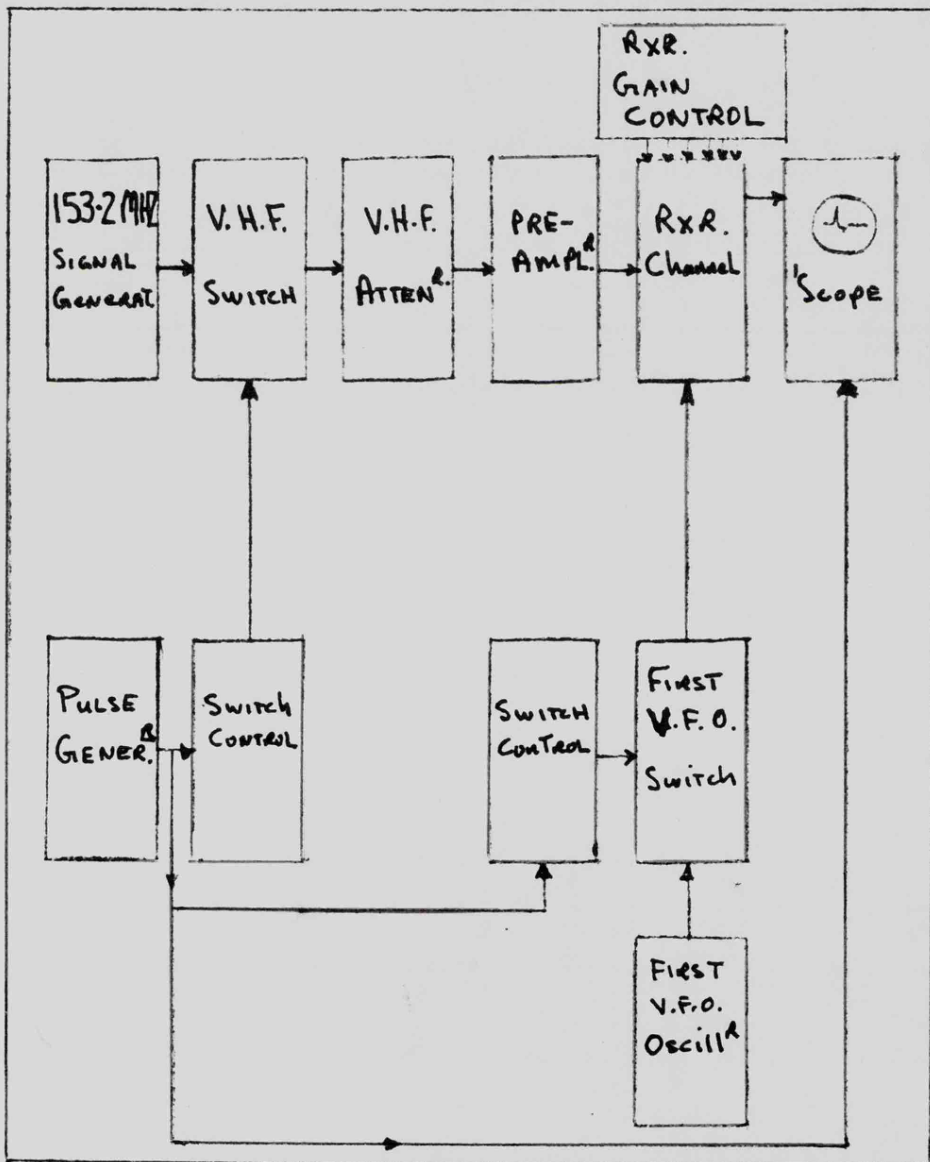
V.F.O. IS THE VARIABLE FREQUENCY OSCILLATOR.

ATTEN=ATTENUATOR   GEN =GENERATOR

RXR = RECEIVER   SCOPE = OSCILLOSCOPE.

FIGURE 7.1(A)

CIRCUIT DIAGRAM OF THE SWITCH CONTROL AND SWITCH EMPLOYED IN
THE EXPERIMENT TO INVESTIGATE POSSIBLE RECEIVER "RINGING".
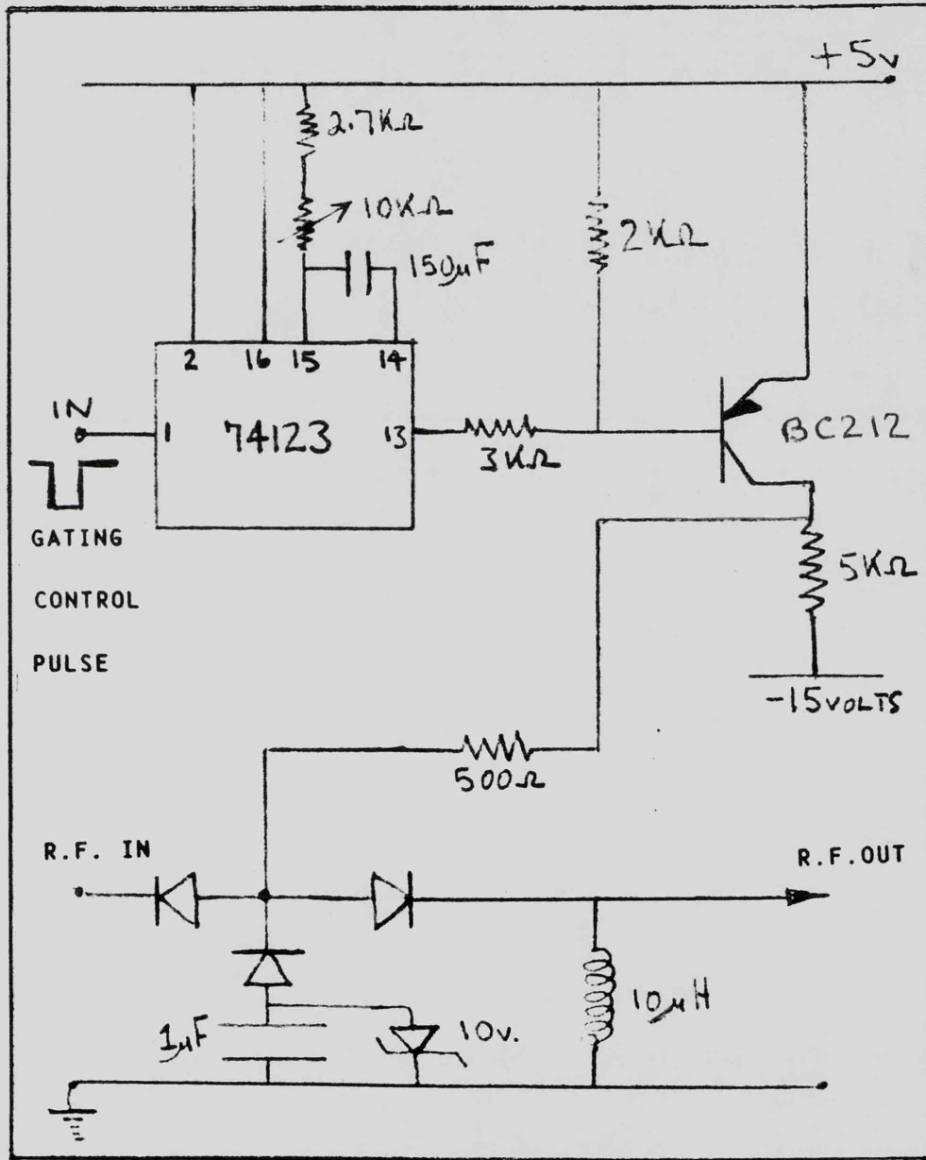
THE THREE DIODES ARE TYPE H.P. 5082--3188

FIGURE 7.1(B)

SCHEMATIC ILLUSTRATION OF THE CIRCUITRY FOR TESTING
THE SABRE SIGNAL PROCESSING SYSTEM.
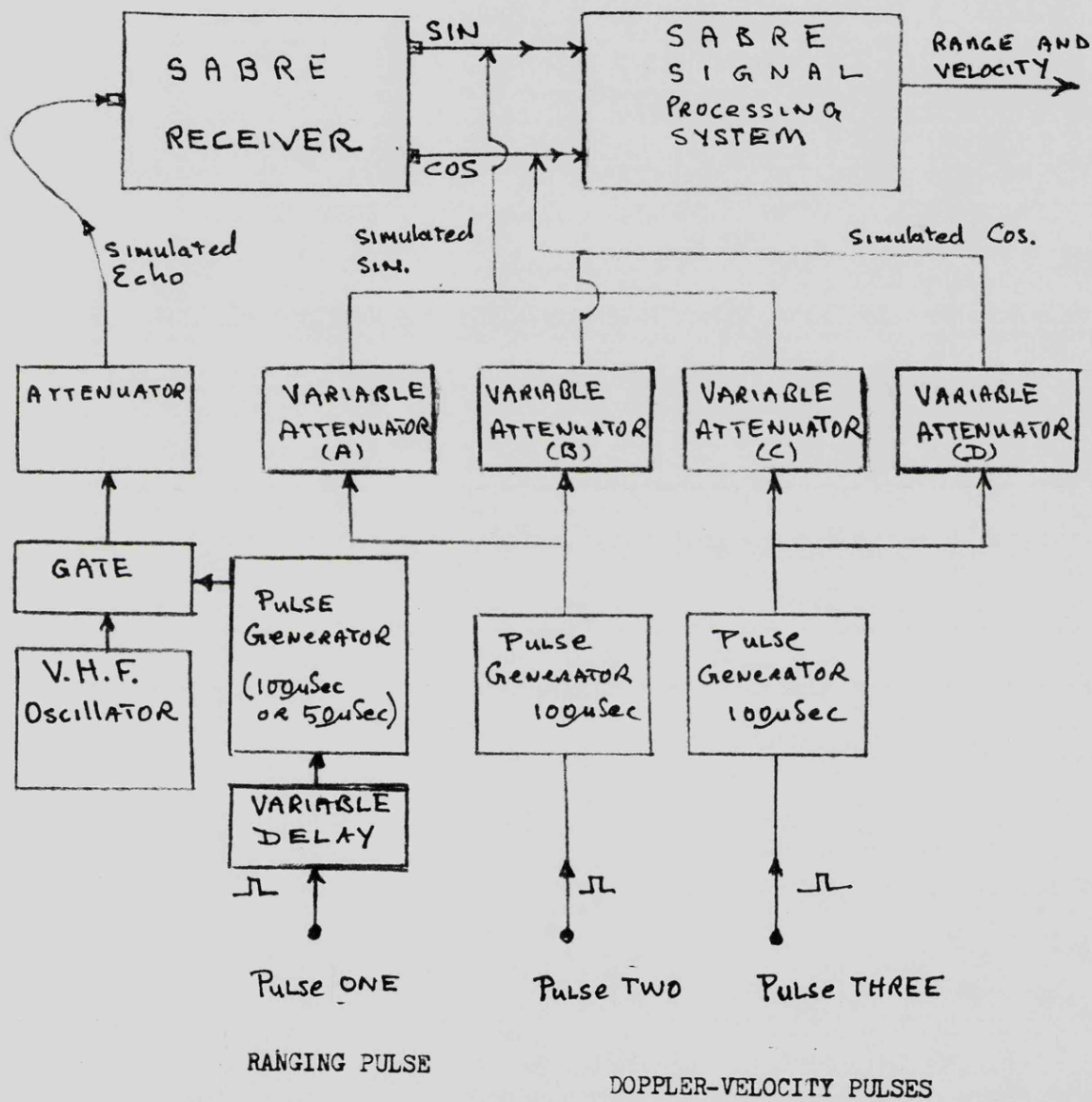
FIGURE 7.2

mean phase difference between the 2 pulses over a fixed time interval,as was described in chapter 2.The phase difference is derived from measurements of the quadrature outputs from the receiver and hence, by inserting low-level test pulses (which simulate the receiver outputs) into the Doppler processor its performance can be monitored. Furthermore,by varying the ratio of the magnitudes of these simulated quadrature output signals the Doppler processor can be evaluated over a wide frequency range.This test system was implemented and the short range mode Doppler processing system was found to contain a fault which was traced to a programming errors.When these errors were corrected,the Doppler velocities and the range-rate velocities were of similar magnitude and direction to within the accuracy of the measurements. This method of testing the Doppler processing system has now been incorporated into the Wick site,under microprocessor control,by the SABRE scientists.

7.1.4 System timing errors.

The transmitter was arranged to be switched on and off,and then into a dummy load, whilst the output signal levels were monitored,during reception of the short range signals. These signals were found to occur only during normal transmission periods,which confirmed that they were of external origin and not caused by SABRE timing errors or by internal interference effects.

After removal of the transmitter and Doppler processor faults,the characteristics of the short-range echoes (which occurred in all 8 beams simultaneously) were;

slant range: 90 Km to 350 Km   range-extent: 2 to 4 range-cells

signal to noise   Doppler velocity

ratio: 3.3:1 to 1500:1   and range-rate: -200 to +200 m/sec

Typical examples of short-range echo signals are reproduced in the RTI plots of fig(7.3), with ranges between 90 Km to 350 Km. A 30 minute sample of typical data is displayed in fig(7.4) which plots signal velocity and normalised signal amplitude as a function of slant range. The number of

THE SLANT RANGES IN THIS FIGURE ARE BETWEEN 90 KM AND 450 KM IN 30 KM STEPS
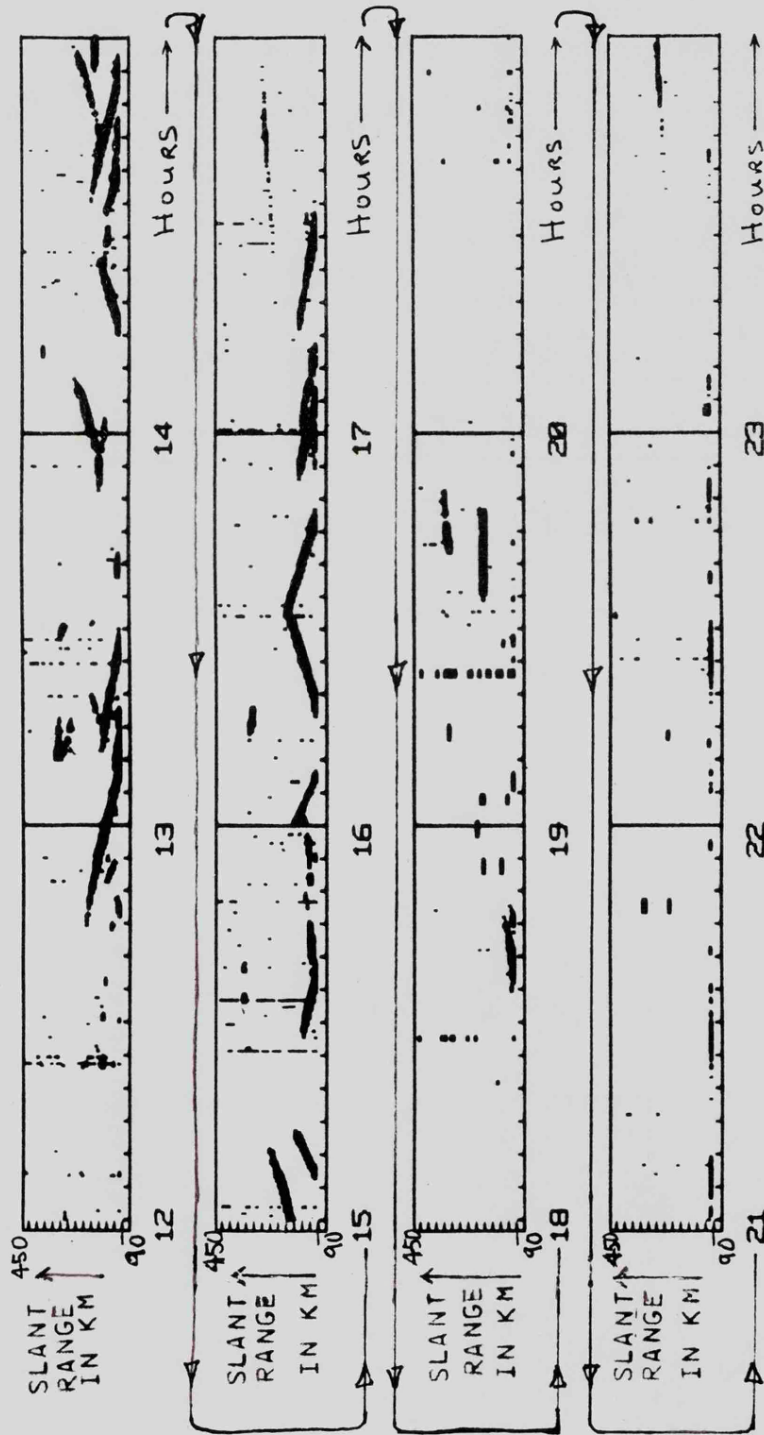
FIGURE 7.3

RTI PLOT FOR WICK   YEAR 1982   DAY 316-317   BEAM NUMBER 5

TIME GMT IN HOURS

WICK SABRE DATA   BEAM 9

EXAMPLE OF THE GRAPHICAL DISPLAY EMPLOYED IN THE ANALYSIS OF THE
WICK SHORT RANGE SIGNALS. MEAN DOPPLER VELOCITY IS PLOTTED AGAINST
SLANT RANGE, TOGETHER WITH THE NORMALISED SIGNAL AMPLITUDE AND, BELOW
THE NUMBER OF SIGNAL OCCURRENCES.
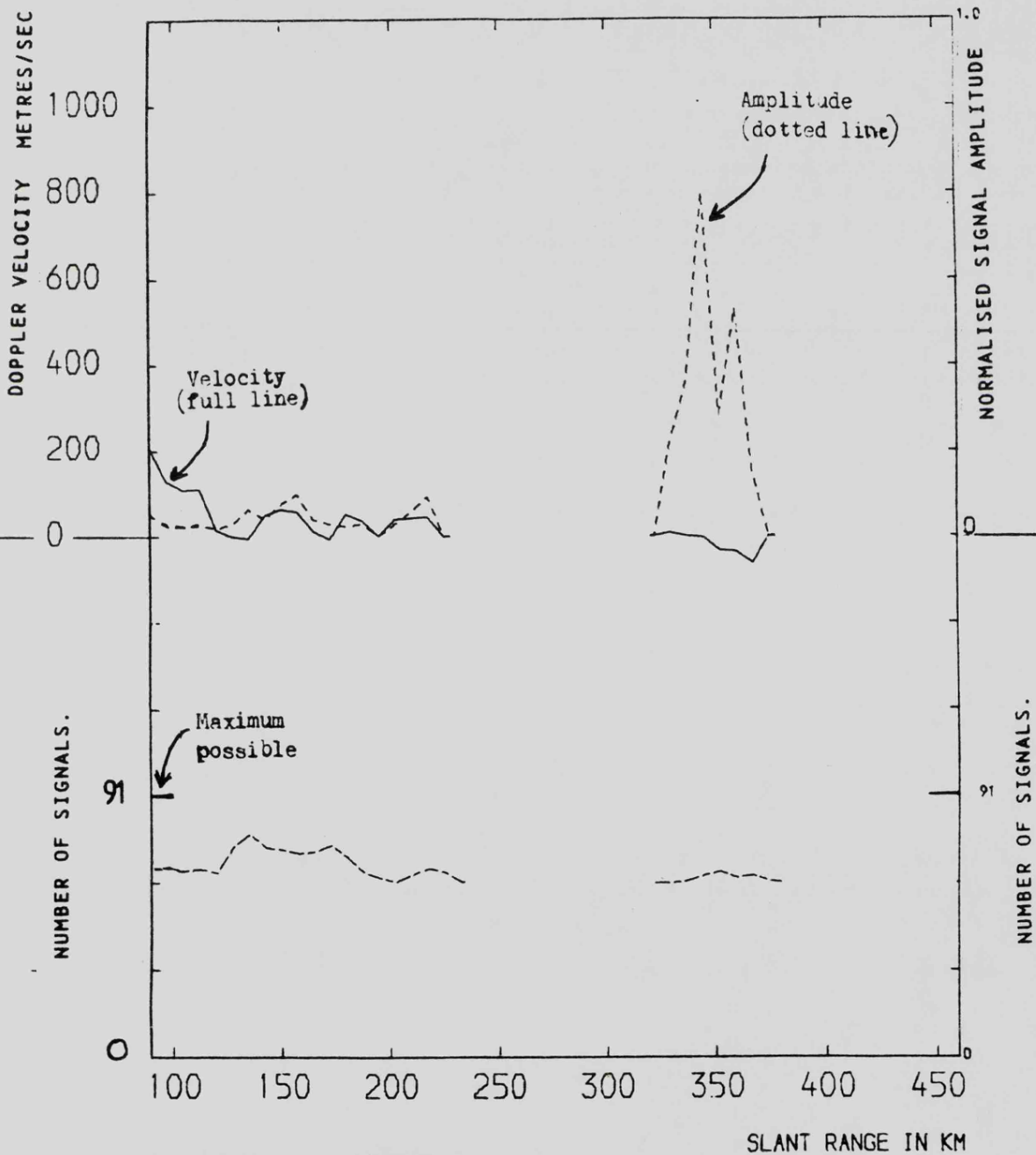
FIGURE 7.4

signal occurrences is also included. The echoes do not appear to be uniformly distributed in range,but were present in all 8 beams in the same range-cells. Such distributions were found in other days of data,at all hours of day and night.

The next step in the investigation was to determine whether the echoes were from the front or rear of the antenna arrays.

7.1.5 Echo signals from behind the antenna arrays.

The Yagi antennae employed in the Wick arrays have manufacturers quoted "backward facing gain" values which are at least 20 dbs below the forward facing values.Hence echo signals may be received from extremely large target areas behind the Wick site.For example the mountains to the south of site could present a large stationary target which would produce echoes at a constant range, with zero Doppler velocity. A study of the Ordnance Survey map for North Scotland revealed that a number of mountain peaks could be illuminated by the rear lobes of the SABRE arrays but no echoes were detected at the requisite range having zero Doppler velocity.Hence it was concluded that the backlobe radiation andd echo signals were not of sufficient strength to affect the radar performance. Similarly,no significant mountain peaks are situated in front of the SABRE antennae that might produce radar echoes at the ranges under investigation.

7.1.6 Conclusion of the initial investigation.

It was apparent at this stage that the echoes were due to external,moving targets in the field of view of the Wick SABRE radar.A closer examination was then undertaken of the echo characteristics and possible sources (including atmospheric turbulence and aircraft) as follows;

7.2 Radar echoes from atmospheric structures.

The short-range echoes were of very wide azimuthal extent (ie they normally appeared in all 8 beams at the same range),were several range-cells

in range extent, but moved together in direction towards or away from the radar site. These characteristics prompted investigation of atmospheric echoes from layered structures,on the understanding that the sidelobe levels of the radar beams had been designed to restrict each beam's azimuthal extent to about 3.6 degrees.Hence,a small target should appear in 1 beam centre at a time,in 1 range cell. Target motion might cause it to appear equally strongly in 2 beams or 2 range-cells but theoretically only a wide target should cause echoes to appear in all 8 beams.

Such wide-azimuth,short range-extent echoes have been reported by Unwin, ref (129),1966 and Nielsen,ref (103),1982 who classified them as "Long Discrete Echoes".However,these echoes were generally weak,with typical signal to noise ratios of a few db, and were associated with auroral activity,at heights of not greater than 100 Km. In contrast,the Wick short-range echoes had signal to noise ratios of up to 33 db and occurred at all hours of day and night. If these echoes were due to atmospheric effects,then as will have been evident from a survey of chapter 1,they will be from altitudes of less than 45 Km.The relationship between irregularity scale length and altitude was displayed in fig (1.4). Similarly,it was indicated in chapter 1 that night-time echoes are generally due to atmospheric effects rather than electronic effects,especially so for altitudes below 45 Km.

An examination was then undertaken of the range of velocities attainable at such altitudes, due to atmospheric motion.

Van Zandt et al,ref(29),1978,have reported a velocity peak of 65 m/sec in the northward wind during a jetstream, at an altitude of 10 Km.In order to determine the nature and direction of the winds at the Wick viewing area, details of the echo signal characteristics were sent to the Meteorological Office at Bracknell.The reply from department MET-03B included details of the variation of the wind velocities and directions with altitude for the area near Stornaway. Mean wind velocities of 51 knots per hour at altitudes

AZIMUTH POLAR DIAGRAM
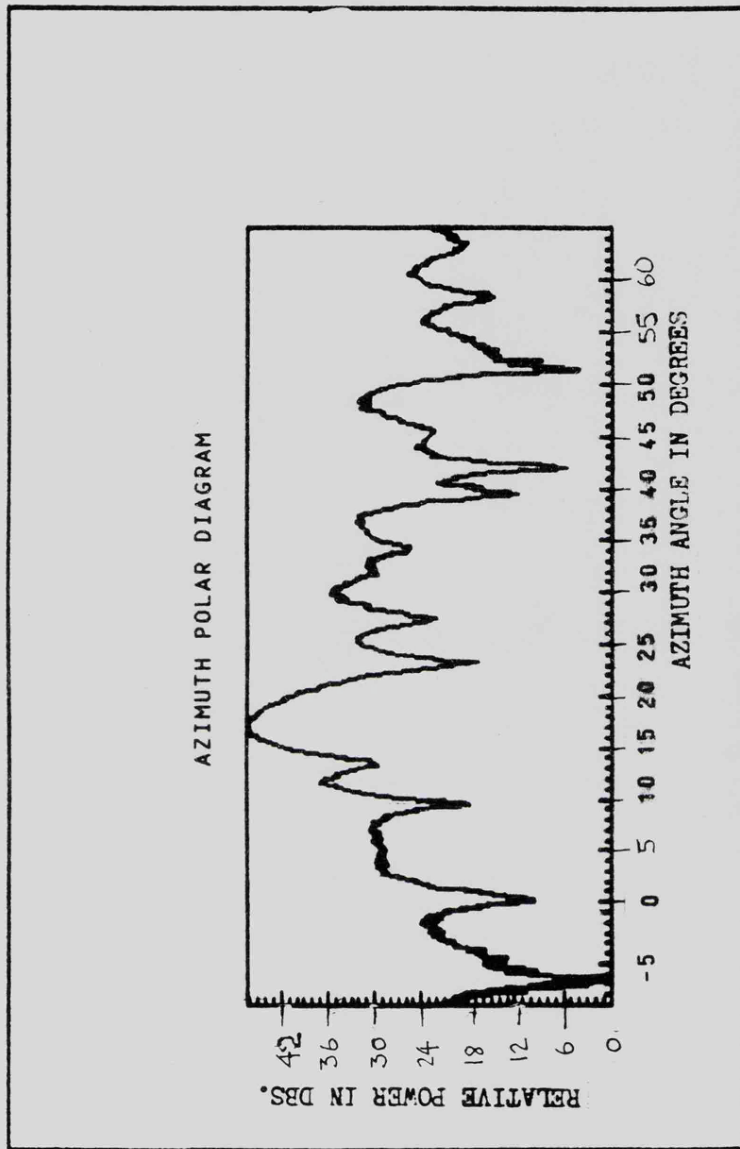
FIGURE 7.5

of between 9.2 and 10.4 Km were recorded, with a mean vector direction of about 273 degrees,westerly.The mean Doppler velocities measured at this angle relative to the radar propogation direction would be from 65 to 18 knots per hour,well below those measured for the short range echoes. Hence, it seemed unlikely that neutral winds were responsible for the generation of these returns. An examination of aircraft echoes was then undertaken as follows;

7.3 Radar echoes from point targets.

The echo characteristics which would normally eliminate point targets such as aircraft,from the list of potential sources were their wide azimuthal extent and their long range-extent.The azimuthal measurements and angular discrimination by the Wick radar are governed by the level of the antenna sidelobes. Now in chapter 4 the Wick sidelobe levels had been suspected of being the cause of the difference in aspect-angle loss figures (derived from Wick and Uppsala data),displayed in fig(4.10).The Uppsala radar had been calibrated,as reported ref (108),1983,by Nielsen et al and found to have very low sidelobe levels,of the order of -30 dbs, and the Wick antenna sidelobes had been expected to be similar. A calibration of these sidelobe levels was arranged during 1984 by means of a helicopter from which a 10 microwatt oscillator and dipole was suspended. This helicopter was being employed at the time by research engineers from other establishments in the Wick area.

Two modes of antenna calibration were employed;

a) A crossing flight path,at constant height and range,so as to monitor the azimuth polar diagram

b) A vertical flight path at constant range in each beam position so as to monitor the elevation polar diagram.

As can be seen from fig(7.5),the Wick antenna sidelobe levels were in fact extremely poor,of the order of only 5 to 9 db below the maximum level.

The variation of the levels in the echo strengths of the short range signals with beam position is plotted in fig(7.6) and it is evident that these signals are of ratio similar to the sidelobe levels. The high residual signal in all beams was,therefore, attributed to the poor sidelobes.

A second method of examining the Wick sidelobe levels was then arranged,by monitoring Cygnus "A" radio star as follows;

The azimuthal crossing rate of this radio star is 11.28 degrees per hour and therefore each antenna beam and its 2 main sidelobes would be traversed in about 1 hour. Hence during the present system integration time of 20 seconds the radio star would have moved in azimuth by 0.06 degrees. Now by increasing the system integration time the resolution of azimuthal position of the star will drop to below 0.1 degree.However the angular discrimination is not of such importance as the comparison of the amplitudes of signal strengths in the sidelobes,in this experiment.An integration period of 60 seconds was selected,corresponding to an azimuthal location accuracy of 0.2 degrees and in order to improve the data averaging,the sampling speed of the SABRE receiver was increased. Because of the limitations of the computer memory, a maximum sampling rate of only 3,000 samples per second was employed.

In order to present the data in a graphical manner from which sidelobes could be studied,a series of graphs similar to fig (7.7) was plotted for each radar beam. A 5-point data smoothing technique was employed in order to reduce the interference levels and the azimuth angle (the horizontal axis) was derived from the equations derived in chapter 4, via computer programme COECYG. The vertical axis of each graph represents the radio star signal level with respect to the peak value,after the receiver background noise has been removed. A comparison of the estimated first sidelobe levels (in db below the peak value) with the results obtained from the helicopter calibration is as follows;

SCHEMATIC ILLUSTRATION OF THE VARIATION OF THE SHORT-RANGE
SIGNAL   REFLECTIVITY WITH BEAM NUMBER.

1983   DAY 242   0912 HOURS TO 0938 HOURS
CURVE A IS FOR A SLANT RANGE OF 202.5 KM
CURVE B IS FOR A SLANT RANGE OF 165 KM.
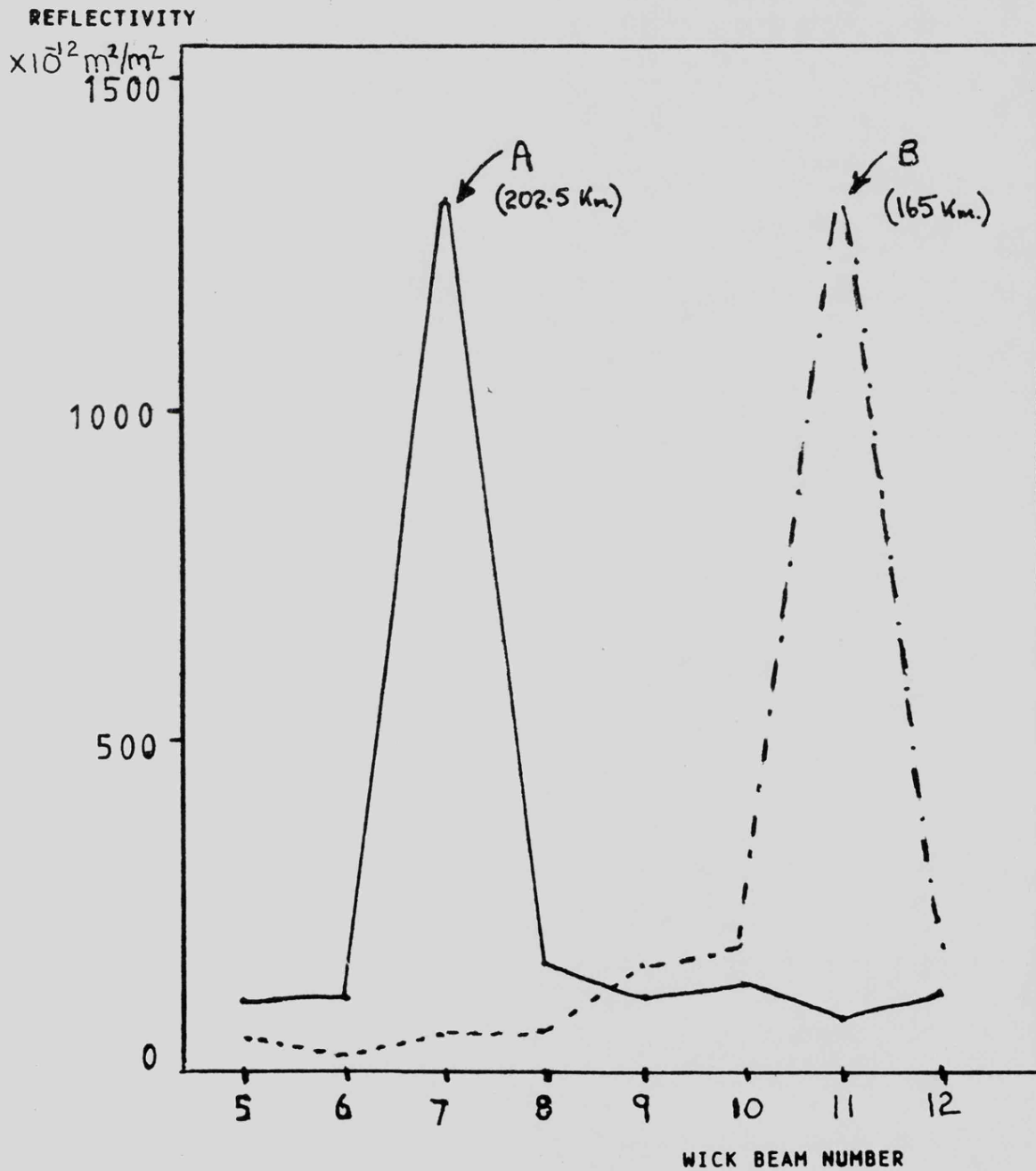
FIGURE 7.6

WICK SABRE DATA FOR BEAM 7

RELATIVE NOISE SIGNAL FROM CYGNUS "A"

AZIMUTH ANGLE IN DEGREES
OF CYGNUS "A"
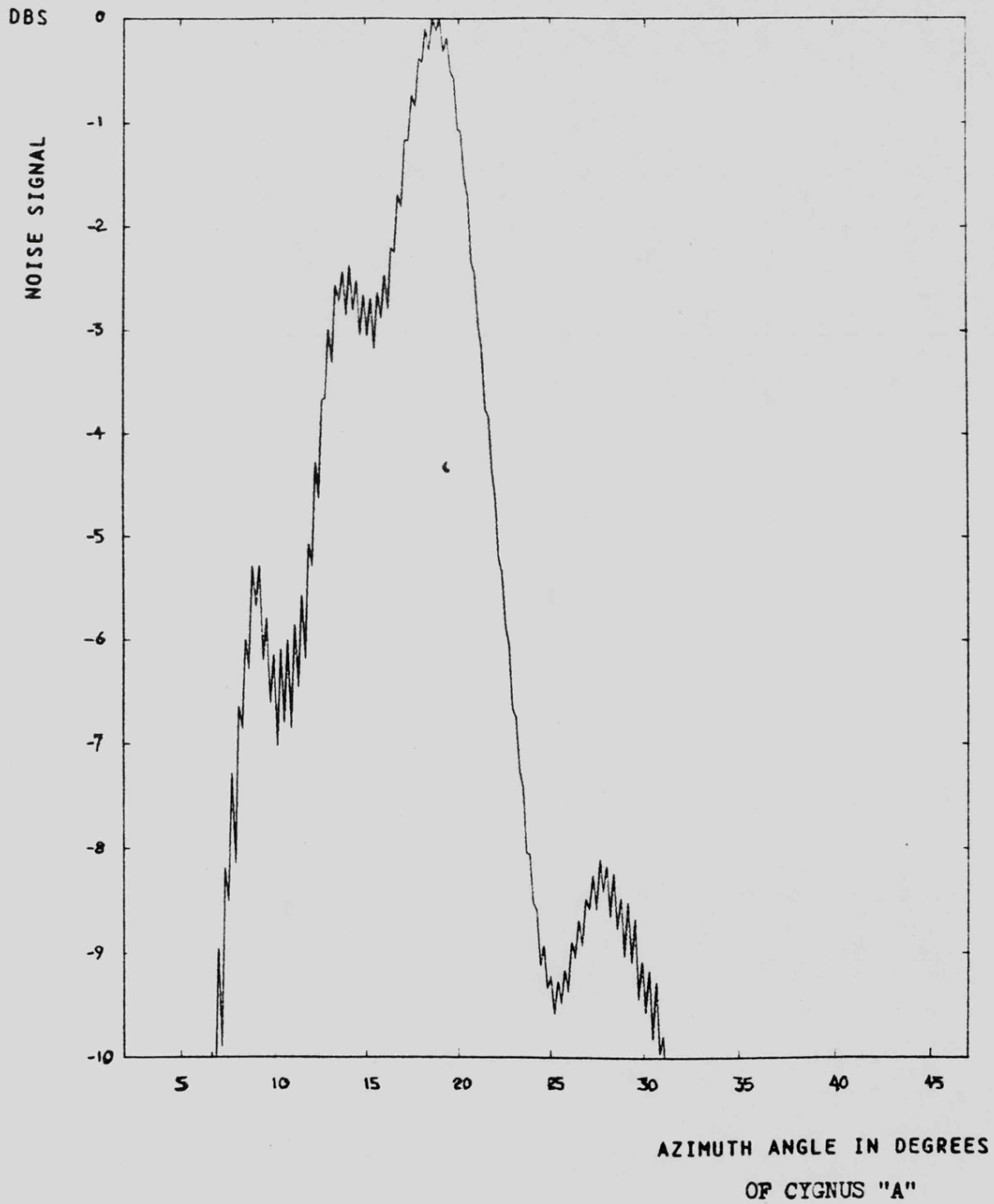
FIGURE 7.7

BEAM NUMBER	5	6	7	8	9	10	11	12
Sidelobe (Cygnus "A")	-7.5	-5.7	-5.5	-4.8	-4.5	-6.0	-4.0	-4.5
Sidelobe (Helicopter)	-13.0	-9.0	-8.0	-9.0	-9.0	-8.0	-5.5	-8.0

This method of estimation cannot be improved until exact allowance for the vertical polar diagram can be made for elevation angles above 12 degrees. At present,(Dec.,1984),this has not been undertaken. However,this method did confirmed that the Wick arrays have relatively poor sidelobe levels.

The next step in the investigation was to examine the range-extent of the echo signals,as follows;

A test pulse was arranged to be fed into the input of a single receiver channel at the Wick site during the hours that a short range echo was being received.The test pulse was of exactly the same frequency as the Wick transmitter,of power level level equal to that of the normal short range echo, but of pulse width selectable,either 100 or 50 microseconds.

The timing of this test pulse was derived from the transmit timing pulse of the NOVA computer and by altering the delay time between the transmit pulse and the time of its injection into the receiver channel,its effective range could be adjusted.The schematic diagram of this test pulse sequence is displayed in fig(7.2)

The results of this experiment at Wick were that the receiver timing and integration system stretched the pulse width to;

    i) for 50 microseconds operation: 2 to 4 range-cells

    ii)for 100   "   " :   2 to 3 range-cells.

At this stage it had become apparent that point targets such as aircraft might be the source of the echoes and a detailed examination of flight corridors was obtained.

7.3.1 Aircraft flight paths.

The Civil Aviation Authority provided details of flight corridors in the Wick viewing area and the radar horizon for each corridor was derived, employing the techniques of chapter 4, from the data displayed in fig (7.8). The 4 main air routes which might provide aircraft echoes, and their radar horizons,are;

a) Aberdeen to Sumbergh. This path is to the right of the Wick radar beams and Sumbergh airfield is approximately 207 Km from Wick.This corridor is normally from 21,000 to 25,000 feet in altitude, and the radar horizons are from 340 to 360 Km.

b) North America to Flesland. This flight path crosses the Wick radar beams at ranges of approximately 370 Km and heights of above 25,000 feet.

c) Aberdeen to Canada. This flight path is to the left of the Wick radar beams and is normally above 21,000 feet. The radar horizon for this flight is approximately 340 Km.

d) Wick to Sumbergh. This flight path is almost directly along the direction of beam 9 of the Wick SABRE radar,of altitude between 3,000 and 18,000 feet.The corresponding radar horizons are approximately 150 to 300 Km. This flight path is generally used for smaller civil aircraft.

The first 3 air corridors are the main civil air routes,but other air-spaces exist to the East of the radar beams which are for military aircraft usage. The military and civil aircraft using routes a) and c) from Aberdeen all appear in the sidelobes only.Route c) will appear as the strongest signal in beam 5 and route a) will be strongest in beam 12. Route b) will appear as a crossing signal at a slant range of about 350 Km.

The radar horizons for these corridors correspond to the maximum ranges of the Short-Range signals, and a further analysis of the echo signals was undertaken as follows;

In order to survey the short range data for the existence of aircraft echoes, a graphical display was developed,as in figs (7.9),(7.10),of the signal strength in each beam against slant range,for periods of 30 to 60

PLOT OF RADAR HORIZON AGAINST TARGET HEIGHT FOR WICK ARRAY HEIGHT OF 4 WAVELENGTHS

DASHED LINE IS FOR ARRAY HEIGHT OF 7.7 WAVELENGTHS
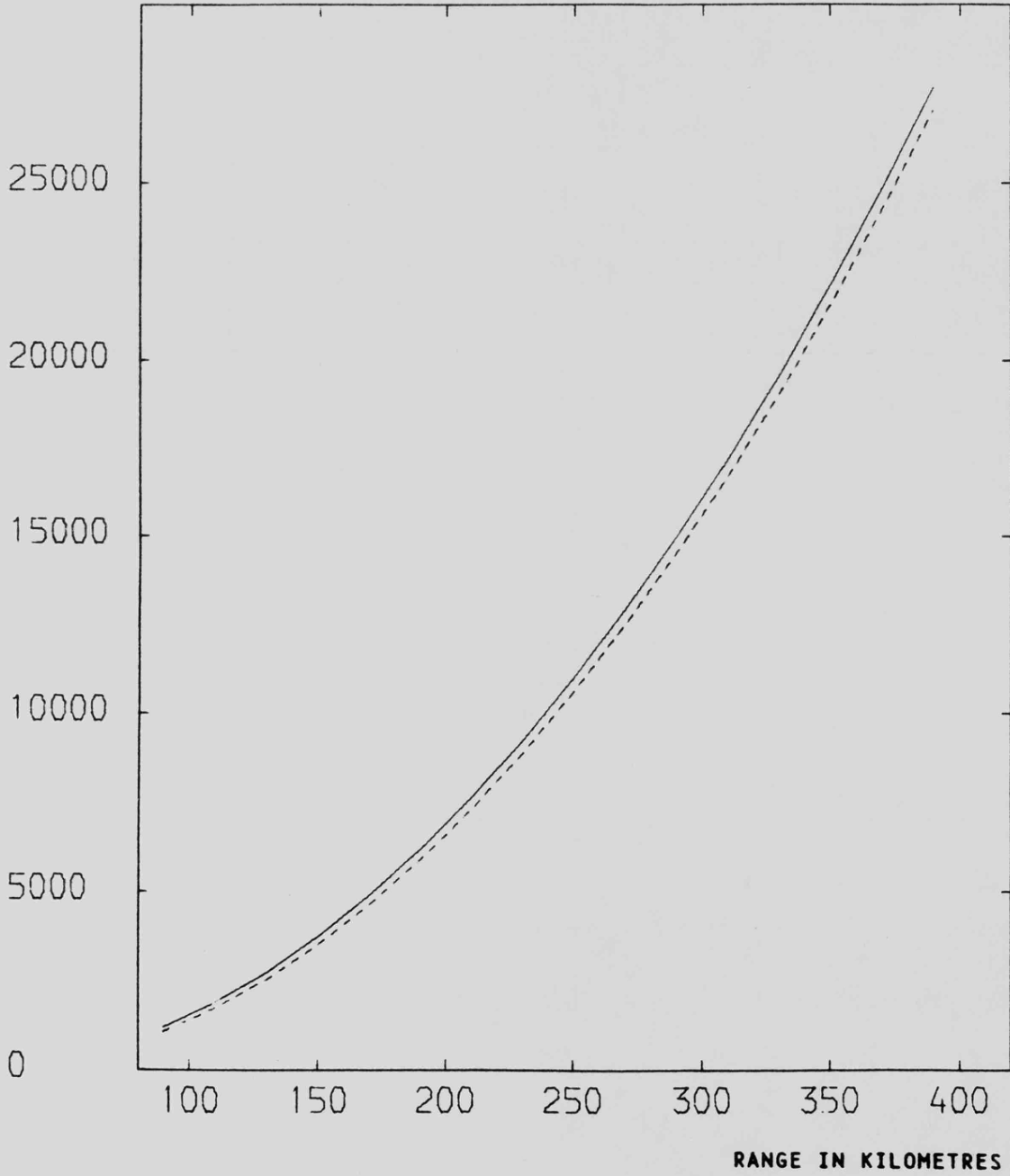
FIGURE 7.8

THE VARIATION OF SHORT-RANGE SIGNAL REFLECTIVITY WITH SLANT

RANGE IN EACH BEAM. THE POSITIONS OF THE AIR CORRIDORS ARE

COMPARED WITH THE POSITIONS OF THE ECHOES.

1983 DAY 242 0911 HOURS TO 0941 HOURS.
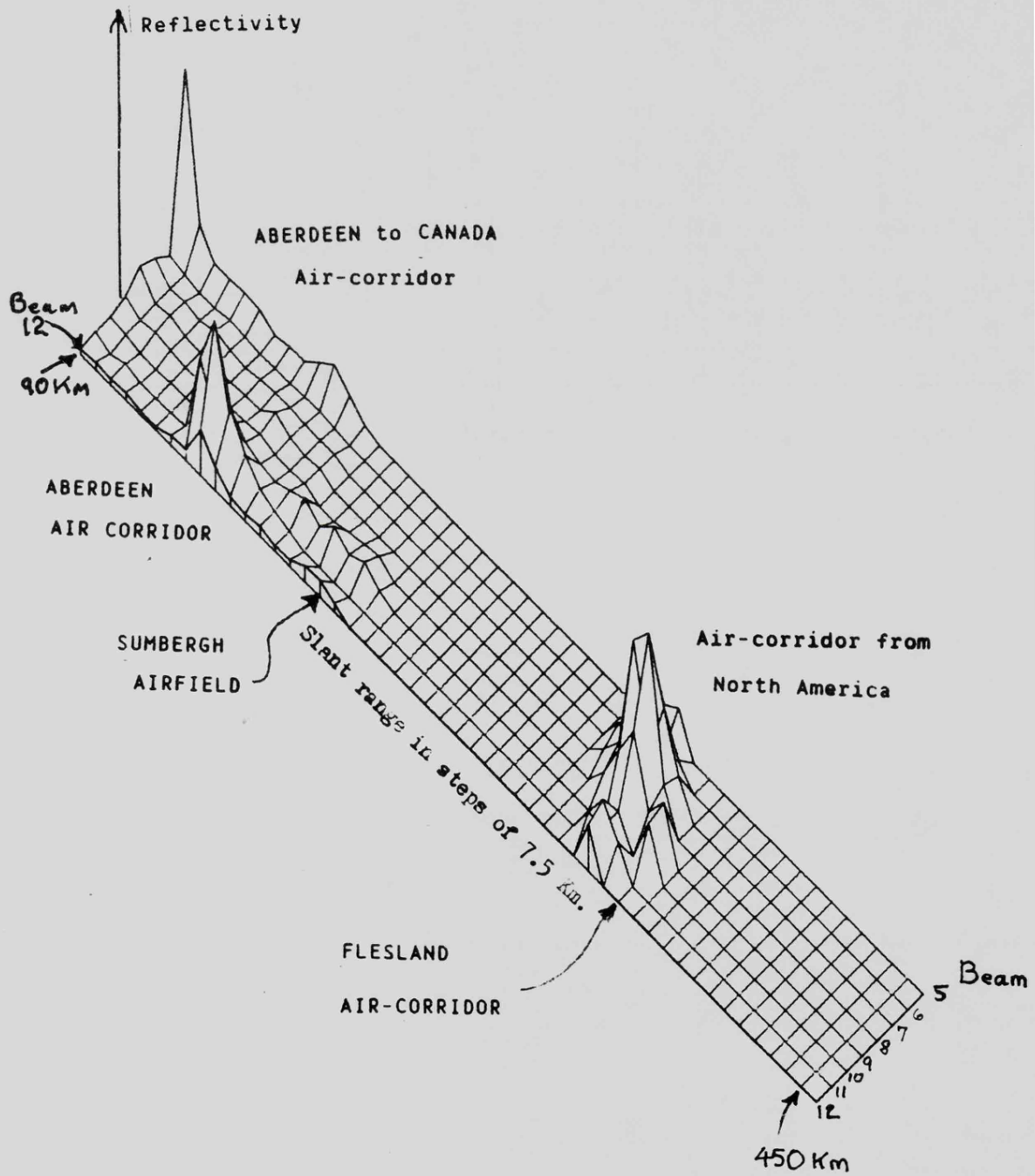
FIGURE 7.9

THE VARIATION OF SHORT-RANGE SIGNAL REFLECTIVITY WITH SLANT

RANGE IN EACH BEAM. THE POSITIONS OF THE AIR CORRIDORS ARE

COMPARED WITH THE POSITIONS OF THE ECHOES.

1983 DAY 242 0941 HOURS TO 1041 HOURS.
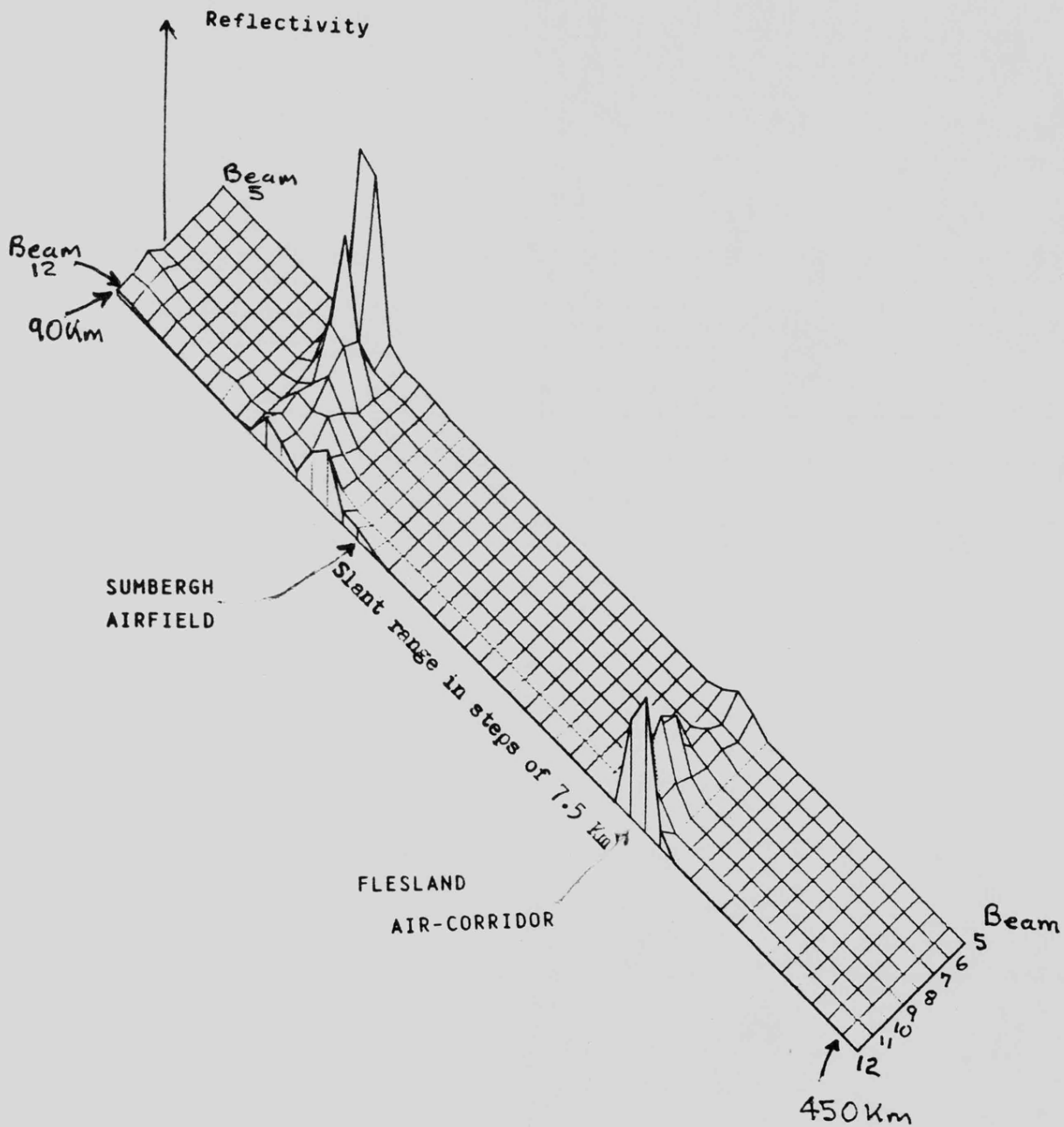
FIGURE 7.10

ILLUSTRATION OF THE VARIATION OF THE SHORT-RANGE SIGNAL REFLECTIVITY WITH SLANT RANGE.

CURVE A IS FOR DAY 319 1982   0745 HOURS.

CURVE B IS FOR DAY 318 1982   1400 HOURS.
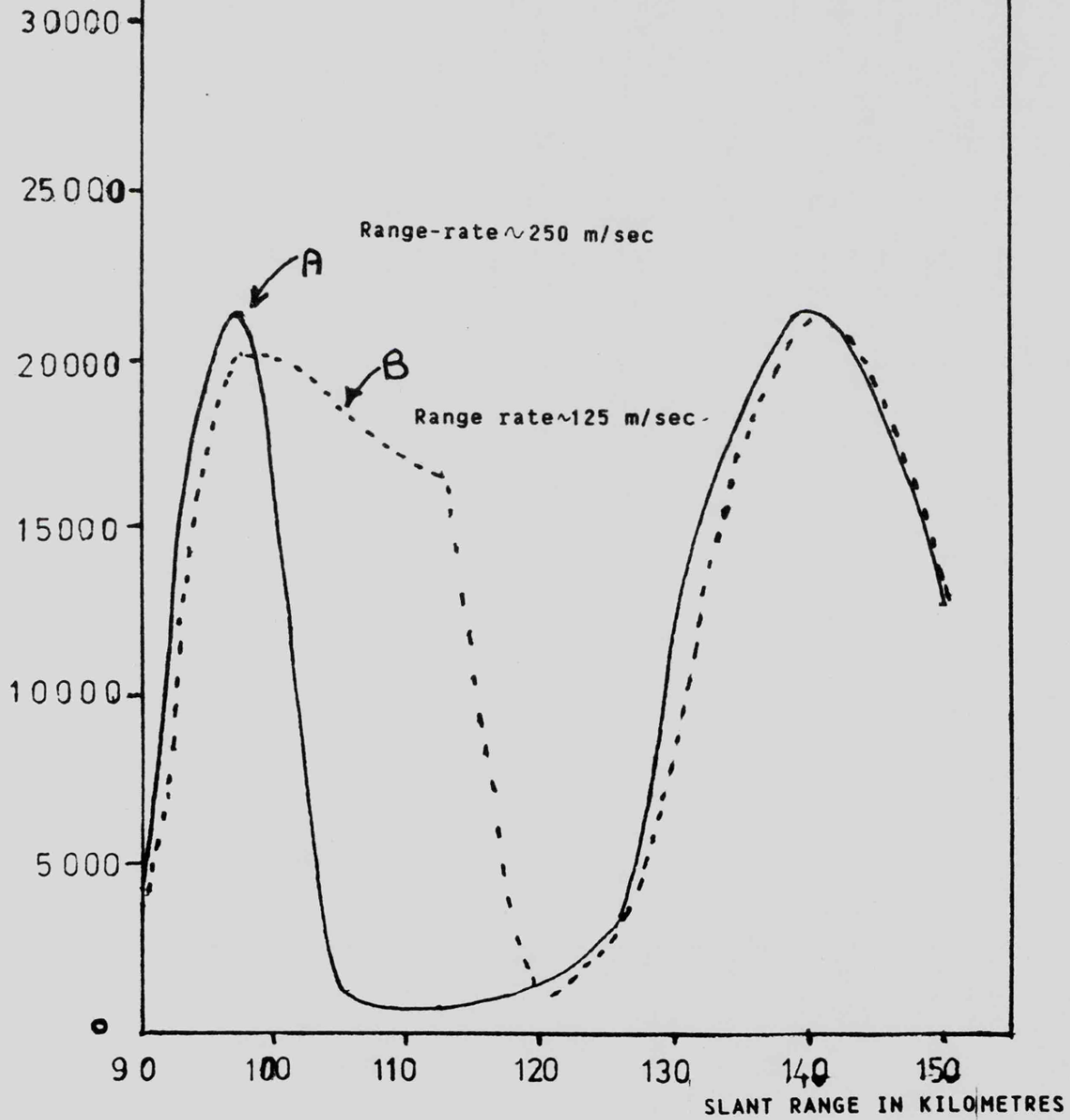
FIGURE7.11

SCHEMATIC ILLUSTRATION OF THE VARIATION OF AIRCRAFT ELEVATION
ANGLE,0E, WITH HEIGHT AND RANGE.
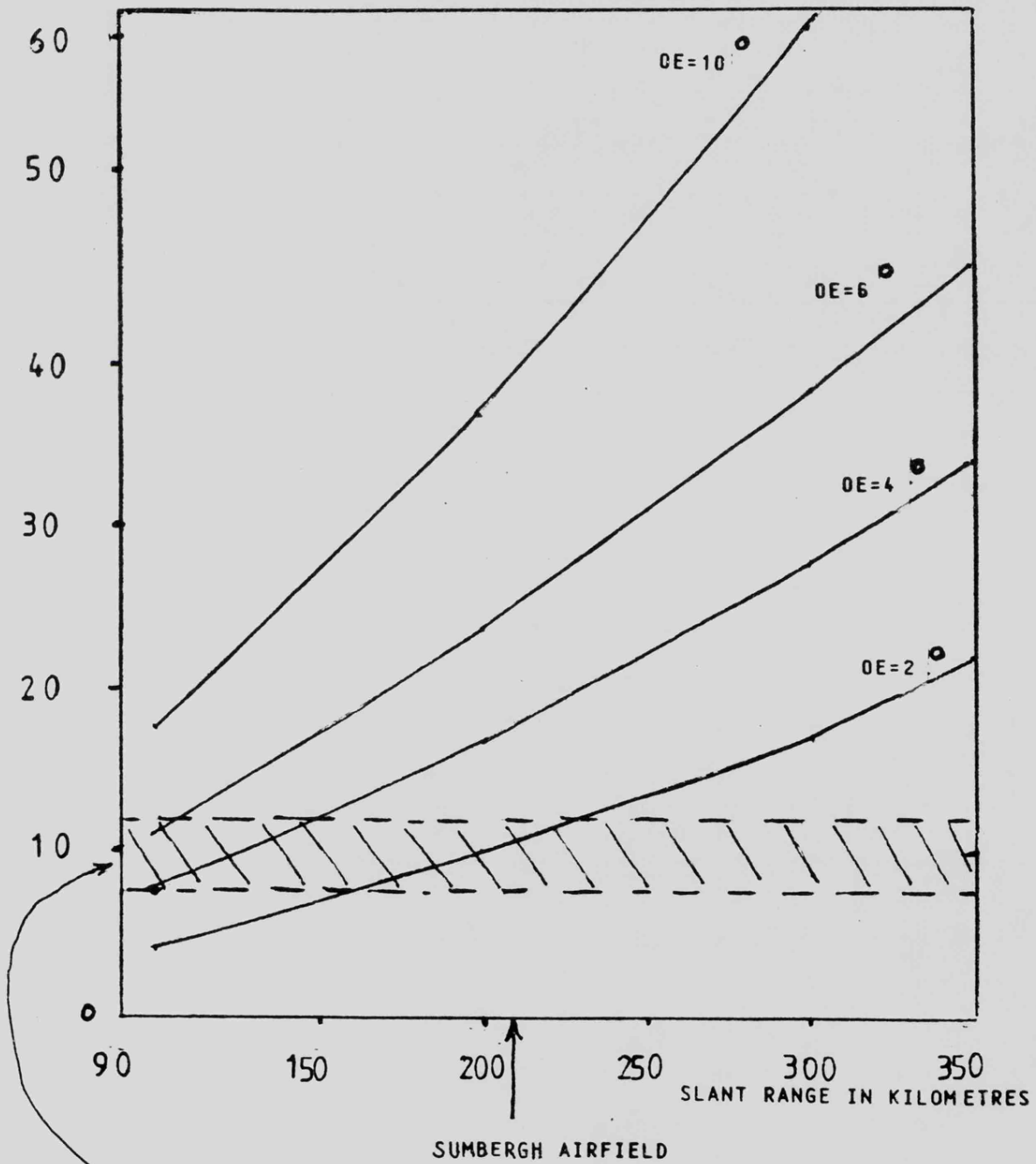
HEIGHT IN KILOMETRES.

FIGURE 7.12

minutes. From a study of such graphs it was apparent that each of the air routes could be detected in the movement of the short range echoes in range and in time. .

For certain days the variation in signal strength with slant range possessed a lobed pattern, as displayed in fig(7.11), for a given beam. From analysis of this lobed pattern a prediction of the height of the target was made, based on the assumption that the lobed pattern reflected the elevation polar diagram of the Wick antennae, as was derived in chapter 4. By comparing the peaks and null in these patterns for different slant ranges and elevation angle, as displayed in fig(7.12), the aircraft heights were as follows;

day 319, 1982, 0745	7 Km to 10 Km	(21,000 to 30,000 feet)
" 318 " 1400	7 " " 9 "	(21,000 " 27,000 ")
" 242 " 0900	8 " " 11 "	(24,000 " 33,000 ")

These estimations of aircraft height are in good agreement with those provided by the Civil Aviation Authority.

7.4 Conclusions drawn from this chapter.

The general conclusion of this analysis is that aircraft are responsible for the short range echo signals, and that the SABRE system required further development in the short range mode, had faulty antenna components which resulted in poor sidelobe levels and should be tested more thoroughly.

The computer programmes developed for this investigation will be described in the next chapter, followed by suggestions for future work programmes which include development of the short range signal mode for SABRE.

CHAPTER EIGHT.

8 . **Description of the computer programmes used in this analysis**

The computer programmes developed for this analysis include:

Coeana	Coespek	Coedot	Coenok	Coenak
Coewaks	Coerang	Coeasta	Coemagf	Coeaspa
Coeref	Coeaxes	Coemer	Coegra	Coerad
Coeplot	Coekomp			

The function of these programmes is as follows:

8 .1 Coeana

Coeana is the main data analysis programme and is used for both SABRE radars and for both normal auroral signals and short range signals. The first section of Coeana converts the SABRE radar data from the Nova computer data format (as used in the SABRE site computers) into the Cyber computer format (as used in the University site computer).

System noise and errors are rejected in the second section which also converts the Doppler frequency data into Doppler velocity, and converts the raw signal data into:

$$(\text{signal power} - \text{noise power}) \div \text{noise power}$$

The SABRE signal and velocity data are extracted from the SABRE data in the sequence as shown in Table (2.1), and are further separated into data corresponding to each of the SABRE beams, and range cell numbers 1 to 50.

Each set of 8 beam positions have the beam position compensation factors added, as described in chapter (4), to allow for the "beam position loss". Also, each set of 8 beam positions is compensated for the small loss due to variation in gain between the receivers. Each range cell is then compensated for the "SEC ϕ_{G}" loss, as described in chapter (4), where ϕ_{G} is the grazing angle of the radar beam at the electrojet.

The values of aspect angle loss for each of the range cells of each beam is then read into the programme from the files Coewow and Coecow. These files are produced from the programme Coemagf which uses refraction theory and the IGRF model, described later.

Coeana can then be programmed to produce a series of graphical outputs representing data which is averaged over periods of time from 15 minutes to 14 hours. This graphical data can either include the effects of compensation of signal power for aspect angle loss, or may include only the effects of compensation for the polar diagram loss.

The bulk of the graphical investigation into the variation of signal power and velocity with slant range has resulted in graphs similar to Figs (7.4) and (3.4). The graphical outputs of Coeana which are available include:

(a) A plot of mean signal power and mean velocity against slant range, with or without compensation for aspect angle loss or polar diagram loss. A plot of the number of occurrences of the signal in each range cell which exceeded 4 dB above noise level is also included. Any one beam out of 8 can be selected.

(b) The same features as (a) but using the peak values of the signal power and signal velocity in each range cell.

(c) A plot of the number of occurrences for each value of Doppler velocity in the spectrum ± 1000 m/sec in 50 m/sec steps. This graph also includes a plot of the mean back-scattered power at each velocity, for the ranges 630 km to 1215 km, in any one beam.

(d) A plot of the mean back-scattered power in each range cell of each of the 8 beams, with or without compensation for aspect angle loss. This plot (as in Fig (7.10)) forms a comparison of the distribution of signals between the beams.

(e) A plot of the aspect angle loss for each range cell of each beam, similar to Fig (7.11), to enable a comparison of the variation of aspect loss between beam positions.

Each graph contains data of the relevant radar parameters and averaging periods. Further system analysis data is printed on the programme itself, including:

(f) Polar diagram null depth
(g) Mean aspect angle loss in dB per degree
(h) Position in time and range of any point targets

(i)   Mean and peak backscattered power and velocity for each range cell of each beam

(j)   The mean velocity for each range cell of one beam on the basis that the backscattered power in any one cell is at least four times the power in the range cell 45 km ahead. This velocity analysis technique is to ensure that the double-pulse velocity measuring system will hence only derive a mean velocity if the unwanted signal from the range cell 45 km ahead is much smaller than the desired signal.

The submit file used for operating this Coeana analysis programme is Coeanas. The system parameters defined in the last line of this file are:

Year, Day, Hour, Minute, Seconds, Type, Skip, Magnetic Index,
Number of 2-hour periods,
where type refers to the data format to be printed, and skip refers to the number of 2-hour periods to be skipped, as follows:

Type = 99   Print short range target signal data and velocity
Type = 0   No print
Skip = 4   Analyse 1 in 5 of the SABRE data records
Skip = 0   Analyse all of the SABRE data records.

8.2 Coespek

One output from Coeana is supplied to this programme, Coespek, whose main graphical output is the scatter-diagram of backscattered power against doppler velocity, as in Fig.3.8, for 2 given ranges. The second graphical output, as in Fig.3.9, is a plot of the mean backscattered power against doppler velocity, for 2 given ranges.

The choice of range-cell or beam number can easily be adjusted within this programme.

8.3 Coedot

Another output from Coeana is supplied to this programme Coedot whose graphical output is as shown in Fig.3.5, a plot of mean doppler velocity and mean backscattered signal power against slant range, in comparison with plots of theoretical curves.

These theoretical curves are derived using typical values of aspect angle loss and polar diagram loss, as was shown in Chapter 4 . These complete graphs enable a comparison to be made between the actual received signal variation with range, and the theoretical model.

8 .4 Coeaxes

This programme also receives the data output from Coeana and presents a graphical display of mean backscattered power or mean doppler velocity for each geographic location of the SABRE beams. Figs.5.1,5.2, are typical outputs of Coeaxes, with power being printed in logarithmic form, after all of the compensation factors in the Sabre Radar equation have been included, as was shown in Chapter 4.

The geographic location of each range-cell of each SABRE radar is read into the programme from the files Coedatw, Coedatu, which are produced by the programme Coemagf, using refraction theory.

The submit-file for using Coeaxes is Coeaxsu which uses the same parameter input format as Coeanas, described above in Section 8 .1.

8 .5 Coemagf

This programme derives the values of aspect angle and geographic location of each range-cell of each SABRE radar, using the equations derived in Chapter 4. Basic refraction theory is used in deriving the range-cell location,
          Each beam position is derived using the radio star calibration technique in Chapter 4 . The aspect angles are derived using the IGRF model,

The submit file for using Coemagf is Coemgfs and the system parameter input format is:

    Latitude, Longitude, Year, Day, Radar, Height
    where Radar = 1.0 refers to Wick radar
          Radar = -1.0 refers to Uppsala radar
          Height refers to the auroral height
          Latitude, Longitude, refer to the SABRE radar position.

8 .6 Coeasta

This programme produces a graphical display of the antenna polar diagrams of each radar, as in Figs 4.20,4.23 using the equations derived in Chapter 4. Coeasta will also produce graphs of the variation of elevation angle from radar to aurora, with and without the effects of refraction,

Coeasta can be used on the Cyber computer by means of the submit file Coeastu.

8 .7 Coegra

This computer programme produces a graphical display of the results of the analysis of Chapters 4 , 5 , namely Figures 4.7, 4.27 .

Coegra contains arrays of values of the data resulting from this analysis and can be used via the submit file Coegras.

8 .8 Coenok, Coenak, Coewak5

These three computer programmes are used to analyse the noise level outputs of either radar and are generally used to study the Cygnus 'A' radio star. Coenok was used to monitor and analyse the noise level output of range-cell 49 of any beam, without any data smoothing or extra integration. Coenak was used to monitor and analyse the noise level output of either range-cell 49, or, the summation of the outputs of all 50 range-cells. A 5-point running mean data smoothing technique was used in order to detect the peak position of the Cygnus 'A' signal. Coewak5 was used to monitor and analyse the noise level outputs of any beam, similar to Coenak, but further integration of the data was used, typically of 60 seconds total. This programme was used in order to study the sidelobe levels of the Wick SABRE receiving array before and after the repairs to the Butler matrix in 1984.

These programmes produce graphical displays of receiver noise against time, as in Fig 7.7, and also produce graphs of mean noise-signal power against Doppler frequency, in order to examine the SABRE receiver frequency response,

The submit files dor these three programmes are Coenoks, Coenaks, Coena5s, using the same system parameter input as for Coeanas.

8 .9 Coemer

This programme uses the combined outputs of Coeana when Coeana has been operated for both SABRE radars over the same period of universal time. In this way the signal power and velocity data from the two radars is combined, so as to produce values of the resultant velocity of the auroral electrojet, as derived in Section   .

The graphical outputs from Coemer, as shown in Fig 5.9 include:

(a) Vector-velocity distribution

(b) Vector flow angle distribution

(c) Wick backscattered signal power distribution

(d) Wick and Uppsala doppler velocity distribution

(e) Wick and Uppsala mean signal power distribution against doppler velocity

(f) A comparison of backscattered signal power, in dBs, against time, for Wick and Uppsala radars.

(g) Normalized mean power against flow angle for each radar

(h) A comparison of resultant electrojet velocity and the R.M.S. backscattered signal power of the 2 radars, against time.

(i) A comparison of the backscattered signal power in each range-cell of any beam for a 1-hour period.

Coemar has been used for specific days of 1982, 1983, 1984 and submit files can be used for the following times:

Time	Wick Data Files		Uppsala Data Files		Submit	Output
1982, 249	Signal	Velocity	Signal	Velocity	Programme	Data File
1430-1530	Coepopw	Coepovw	Coepopu	coepovu	coepers	coeva23
1982, 249 1550-1650	Coeprpw	Coeprvw	Coepru	Coepvu	Coemers	Coecall
1984, 35 1500-1600	Coeropw	Coerovw	Coeropu	Coerovu	Coekers	Coeval4
1982, 250 0110-0200	Coejopw	Coejovw	Coejopu	Coejovu	Coeners	Coeval2

The system parameter input with each submit file is used to denote which geographic location will be used in this analysis, as follows:

$$11 : 64.26°N, 6.00°E$$
$$9 : 66.16°N, 6.66°E$$
$$7 : 66.24°N, 3.56°E$$

8.10 Coekomp

This programme uses the output files of Coemer in order to display graphically the variation of Electrojet mean backscattered power at each value of velocity, in 50m/sec. steps. A typical output of Coekomp is shown in Fig. 5.11

The submit file to be used for this programme is Coekoms.

8.11 Coerad

This computer programme used the equations derived in Section 4 in order to derive the azimuth and elevation angles of the Cygnus 'A' radio star. Typical results of this programme are shown in Figs. 4.16, 4.17 This programme is usually operated at the local computer terminal, without needing a submit file.

8.12 Coeref

This programme uses the refraction-effect equations shown in Section in order to produce tables of elevation angles and slant ranges to the aurora. The effects of refraction upon elevation angle at slant ranges to the aurora of up to 1300 Kilom. are shown in Table 4.1,

The submit file for this programme is Coerefs.

8.13 Coeplot.

This programme utilises the output of Coeana in order to display graphically the variation with time of the backscattered signal in each range cell, of any 1 beam. Alternatively, a series of 8 graphs can be selected, one for each beam, in sequence. Fig 3.2 is a typical output of this programme.

The submit file for Coeplot is Coepltj.

Conclusion of this chapter.

Each of the programmes described in this chapter are available for usage on the University mainframe computer, via the relevant submit programme. Alternatively, the graphical displays and maps can be reproduced, for any days on which SABRE data is available,upon request to the Ionospherics department at Leicester University.

The analysis of the SABRE data is concluded at this point in the Thesis. Suggestions for future work and development of the SABRE radar are detailed in the next chapter.

9. Suggestions for future work.

The bulk of the research in this document has indicated the need for further investigation into 2 main aspects of auroral radar techniques;

a) Determination of the auroral height, and b) spectral analysis.

It was also apparent that the Short-range mode of operation required further development and improvement of the range-gating processor before point targets could be properly analysed.Furthermore it seemed feasible to consider the question of transmitter polarization (and subsequent reception) in the development of a new height-finding facility,since analysis of the irregularity polarization characteristics would provide an insight into the auroral structures.

This section will outline possible developments to the SABRE system and will concentrate on the most immediate requirement,namely determination of auroral height.

9.1 Determination of auroral height using interferometry.

9.1.1 Introduction

In order to resolve the heights of 2 scattering centres in a layer at a given range and azimuth the following system parameters must be considered;

a) For a radar slant range of the order of 500 km,the elevation angle subtended by a 10 km-thick auroral layer is of the order 1 to 1.2 degrees.

b) In order to distinguish between the top and bottom of such a layer,the interferometer must be able to resolve elevation angles to better than 1 degree and slant ranges to better than 1 km.Hence the radar pulse widths

must be of the order of 10 microseconds,(the present SABRE value is 100 microseconds),and the antennae employed in the interferometer must be separated by a distance,d,of at least 60 (λ/d) metres,where λ = operating wavelength.For the SABRE wavelength of 2 metres,the separation must be > 120 metres. If similar angular discrimination is desired in the azimuth plane,the same dimensions will apply to the array width and a "Pencil Beam" will be produced.

c) Interferometer type arrays are most sensitive when viewed broadside or, at most, + 30 degrees off broadside.For elevation angle measurements a calibrated vertical array is preferred to a simple horizontal array,but possible ground effects must be considered,as well as the effects of atmospheric refraction at low elevation angles.

d) A 2-antennae interferometer,of separation >120 m,would produce a polar diagram with many lobes unless very directive antennae are used.The more antennae employed in the interferometer array,the lower the number of lobes encountered.

e) Astronomical interferometers are often employed to study a point target which moves across the field of view,(ie a star or planet),such that the output signal will vary sinusoidally with time.By varying the array spacing each day and subsequently examining the results with Fourier transforms,then the physical extent of the target can be determined in terms of brightness distribution.However,these techniques are not applicable to the SABRE system because of the inconsistency of the Auroral layers.

f) Distributed element arrays,such as the Mills Cross,can utilize computer calculated angular distributions of the overall antenna pattern,by taking the discrete Fourier transform of the aperture distribution. As detailed in Skolnik,ref (96),the far field antenna pattern is directly proportional to the Fourier transform of the aperture distribution. One method of producing a multi-beam interferometer receiver would be to record each antenna signal in amplitude and phase,and then by inserting suitable phase-shifts and

amplitude adjustments,multiple-beam positions can be simulated.This technique would require too much additional SABRE computing effort and at present the Butler matrix performs the same task,in azimuth.

g) The effect of the ground plane upon a vertically stacked array can be to produce a series of interference lobes in elevation,with the first lobe maximum at an elevation angle,Θ_{E1},given by

$$\Theta_{E1} = (\lambda)/(4 \ H_A) \ \text{radians,}$$

where λ is the operating wavelength and H_A is the mean array height.Hence the array vertical radiation pattern will vary with array height,unless the array is tilted back from the vertical in order to keep the beam clear of the ground-plane.If ground-plane effects are avoided,the array angular resolution will be directly proportional to its height difference between top and bottom antennae.

h) If a single 1 degree pencil beam is arranged at a tilt angle of about 10 degrees then the edge of the aurora may be examined at slant-ranges of about 500 km,and conventional pulse-Doppler techniques may be employed in the spectral analysis,without encountering the present SABRE problem of viewing very large areas of aurora in the same beam.

i) Preferably such a narrow pencil beam should be capable of scanning sections of the aurora.Height resolution within a beamwidth could be achieved by phase or amplitude comparison techniques,and auroral height estimation could be accomplished by a knowledge of the beam elevation angle. If a receive-only array were employed with the present SABRE transmission frequencies,then the SABRE transmitter would require suitable adjustment of its pulse-width during the times of height-measurement.

j) The requirements of a narrow elevation angle beamwidth dictate array dimensions in comparison with radar systems including;

RADAR SYSTEM	ANTENNA DIMENSIONS
1.Eiscat VHF array,224 MHz	40 m high by 120 m long.
2.Eiscat UHF dish,933 MHz	32 m diameter.
3.Unwin's "Lloyd's mirror" (covers 0 to 10 degrees in elevation),53.5 MHz	136 m high
4.The VLB array 200 MHz (scans 0.75 to 7.5 degrees in elevation)	80 m high
5. Jicamarca array,49.9 MHz (scans equatorial electrojet with a vertical 1 deg. beam)	290 m x 290 m flat array.

k) By examination of the resultant radiation pattern it may be possible to produce scanning movement of the beam in elevation by either lifting or tilting the array.However,the dimensions of suitable VHF arrays make mechanical movements impractical for day to day auroral monitoring.Phase shifting elements could be inserted between the antennae to permit a limited degree of beam scanning,but these would need to be electronically operated since the Wick SABRE site is unmanned for most of the year,and hence would be expensive to develop and install.Limited beam scanning in elevation may also be possible if,for an array mounted above a ground plane,the operating wavelength were to be slightly changed.For example,the first maxima in the elevation lobe interference pattern is proportional to the operating wavelength,and hence a 10% change in the SABRE transmission frequency would produce a similar change in the elevation angle of the maxima.However,this technique would require modifications to the SABRE transmitter and receivers and would entail investigations of the change in auroral parameters with

changes of frequency.

l) If the top and bottom halves of an array are used to provide angular discrimination within the beamwidth,(either as an amplitude- or phase comparison system),then for a calibrated,fixed beam array the subsequent angular accuracy would probably be 0.1 beamwidth.But,if 2 similar targets were in the same range-cell,then angular separation between the 2 would only be feasible for elevation angle differences of 0.8 beamwidth.For example,if the auroral edges were seen to be in the same range-cell,(about 500 km),but were separated by an elevation angle of 1.1 degrees,then the pencil beamwidth required to separate them would be not greater than 1.38 degrees.Further details of the accuracies of phase- or amplitude comparison techniques can be found in Skolnik,ref(96),1972.

m)The methods of achieving a fixed pencil-beam,(narrow in elevation and azimuth),for the SABRE frequencies include;

i) A tall array,of about 120 m height,120 m width,of such directivity that the ground-plane effects are minimised,and no lobing is present in the radiation pattern.Amplitude tapering across the array in both planes would be necessary to achieve low sidelobe levels.If phase-scanning is employed, the lower angular limit is such that the beam is above the ground-plane. Simultaneous beam positions may be achieved in one plane by means of Butler matrices,with the requirement that the number of antennae linked to the matrix be either 2,4,8,16,32,64,Further details of the Butler matrix systems can be found in ref(123),1962,by Delaney.This type of array is,at present, beyond the capabilities of the SABRE system

ii) An array half-size,60 m by 60 m,which employs the ground-plane at Wick to achieve narrow,fixed-position lobes.An array this size would still present severe mechanical problems,but may prove suitable for limited scanning via frequency sweeping.Again,the cost of developing such a system would be beyond the SABRE system.

iii) The most likely array system to develop for the Wick SABRE radar

height-finding facility would be 2 small arrays,of azimuth dimensions similar to the existing SABRE receiver array,and of heights such that a fixed number of stationary elevation lobes were produced.If the first 2 lobes of each array encompassed the auroral elevation angles,then amplitude or phase comparison interferometer techniques could be employed between these 2 lobes to derive the elevation angle and subsequently the auroral height.This technique could be proven by simple experiments,with 2 basic arrays,one above the other,by monitoring the signal difference pattern between the first 2 lobes.An experimental low-power transmitter could be employed,at a fixed range but of variable height.

n) Interferometer techniques have been employed to study the vertical positions and velocities of the irregularities in the equatorial electrojet employing the large Jicamarca array at 49.9 MHz,as in ref(124),1981,by Farley et al.The peak power transmitted,vertically,was 1 Megawatt,of pulse width 10 microseconds at a PRF of 400 Hz and a 64-point complex FFT spectral analysis was performed upon the received signals.All 4 quarters of the array were used for transmission,but only the East,West,quarters were employed for reception,in a phase-sensitive interferometer,to determine the mean angular position in the East-West plane.The signals were cross-correlated one frequency at a time,since each frequency was assumed to correspond to a particular plasma wave at a different location.

The conclusion reached from this initial survey is that the surest way of developing a height-finding facility at Wick SABRE site is to investigate the effects of the ground-plane upon a simple array,then proceed to 2 arrays,one above the other,and examine the practicallities of phase- and amplitude comparison techniques when ground-plane effects are present. Initially the stacks could be developed at the Leicester site and could be employed to examine the auroral echoes backscattered from the SABRE transmissions,but only after consideration of the differences in ground

reflectivity between the 2 sites.

9.2 Reception of auroral echoes at Leicester.

In the past 2 years it has been shown possible to receive the SABRE system
back-scattered echoes at the Leicester University building,via a simple Yagi
antenna.Analysis of the geometry of the Wick and Leicester sites results in
a table of elevation angles and corresponding slant ranges as follows;

ELEVATION ANGLE (degrees)		SLANT RANGE (kilometers)	
WICK	LEICESTER	WICK	LEICESTER
12.0	4.9	455	1107
10.0	4.4	518	1172
8.0	3.8	597	1254
6.0	3.1	697	1347
4.0	2.2	825	1499
2.0	1.2	987	1645
1.0	0.6	1083	1805

Elevation angle measurements at Leicester should be restricted to values
above 2 degrees unless refraction effects are considered.If accurate ranging
information were available at Leicester as well as at Wick,then auroral
height could be calculated from the known geometry.The slant range of the
echoes received at Leicester could either be measured via a SABRE
transmitter at the University building,(an expensive solution),or by
modifying the Wick transmitter such that its PRF and transmission times were
accurately known at Leicester.For example,the Wick transmitter timing could
be arranged to be governed by a radio transmission common to both Wick and
Leicester,such as one of the 10 kHz transmitters in the Omega chain.The
Eiscat radars actually employ a television synchronising signal,but these
are not common to the SABRE site.
A summary of the elevation stack heights above a ground plane which may be
investigated at the Leicester site,prior to development at Wick are as

follows;

Number of antenna	Estimated beamwidth(-3db)	h	H	Mast height
16	< 1.6 degrees	1.625	8	28.15 m
8	< 3.2 "	1.025	4	13.66 m
6	< 4.8 "	1.875	4	11.99 m
4	< 6.4 "	2.725	4	10.33 m

where h=height of first antenna above the ground plane,in wavelengths,and H = mid-point of the array above the ground plane.The feed to the antennae will be split such that the top half of the stack are fed separately from the bottom half to enable phase-or amplitude-comparison interferometry techniques to be employed.For investigation of polarization effects,each antenna would consist of crossed-dipole elements,each fed with its own harness.If low-loss receiver cable harnesses are fitted,it may not be necessary to have a preamplifier at each antenna,(as with SABRE array),but have one amplifier at each feed,one for the bottom half of the array,one for the top.These 2 amplifiers could each have their own receivers and digital integrators, whose timing was derived from the common radio transmission, (Omega).From analysis of the difference in signal level between these 2 outputs,and the slant range,the elevation angle may be derived from the polar-diagrams of each half of the array.Alternatively,this angle may be derived directly by means of a "monopulse comparator",situated at the centre of the array,into which the signals from each half of the array are fed,as in fig(9.1).The outputs of this VHF comparator are the SUM and DIFFERENCE levels of the 2 inputs.The difference signal has an output of magnitude proportional to the angular distance from the centre of the 2 polar diagrams,and whose sign indicates whether the echo is above or below this centre.This monopulse technique enables angular information to be available for each pulse received,and reduces the computing time required for height assessment.

Details of other forms of monopulse angular measurements,in either

Overlapping radiation pattern corresponding to each half of the vertical stack.

Vertical stack of arrays each containing 16 Yagi antennae. Each half of this stack is fed seperately.

SCHEMATIC ILLUSTRATION OF AMPLITUDE COMPARISON MONOPULSE SYSTEM IN ELEVATION PLANE.

FIGURE 9·1

plane,may be found in ref(96),Skolnik,1972,but basically the amplitude comparison type in fig(9.1) will be applicable to any 2 antennae whose polar diagrams are offset (ie "squinted") from a common boresight,as illustrated in fig(9.1).If the polar diagrams are parallel,then phase-comparison monopulse techniques may be employed,but the site conditions at Wick suggest that it may be difficult to achieve parallel beams in the elevation plane.However, phase comparison monopulse or interferometry techniques could certainly be considered in the azimuth plane,if eventually more precise azimuthal angular measurements are required.If,for example,an array which was broad in the azimuth plane was developed for angular discrimination better than the Butler matrix can provide at present,then by evaluating the change of phase of the signals across the array with time,the azimuthal velocity of a discrete auroral disturbance may be derived.

If a basic amplitude-comparison monopulse system were to be developed at the Leicester site,then the effects of the ground plane upon the polar-diagram difference pattern can be established by the simple experiment in fig(9.1). The 2 array halves could be simulated by 2 antennae,at different heights, feeding into a simple comparator,and receiving the VHF radiation from a low power transmitting antenna of adjustable height.If simple Yagi antennae are utilised,then for a transmit power of 1 watt,and antenna separation of 100 metres,the received power level would be of the order of 0.3 milliwatts.

The effects of changes of polarization upon the difference pattern can also be determined,and a ground mesh of chicken wire may be necessary to fully examine the performance for vertical polarization.

9.3 Developing an elevation stack at Wick

If the height-finding elevation stack is to be fitted into the current SABRE radar at Wick,then the ranging accuracy must be improved,(by reduction of pulse width),and the receiver bandwidths suitably adjusted.It is feasible to suggest that a period of height-measurement be included at regular intervals during the day,during which slant range intervals of about 20 km are

examined with pulse widths of about 10 microseconds,and the amplitudes compared with those from the elevation stack mounted above the receiving array,whose azimuthal beam pattern matched that of SABRE,but whose elevation pattern was offset from SABRE's.

9.4 Polarization techniques.

Investigation of the effect of changes in radar system polarization upon the echo strengths would lead to a deeper understanding of the auroral irregularity structures.The effects of changes of polarization upon the SABRE auroral echoes could be investigated most thoroughly by replacing the existing horizontal antennae with crossed-antennae elements,and with each plane of polarization fed from its own harness.This system would allow for the investigation of plane,elliptical and circular polarization waveforms. Should such a modification prove too costly,then a separate,basic variable polarization radar could be constructed temporarily at the Wick site, employing the 1 Kwatt VHF oscillator as the pulsed transmitter.The transmission frequency could be separated from the SABRE frequency by say 50 MHz so as to reduce interference effects and to provide a comparison of echo strengths at the 2 VHF frequencies.

Auroral polarization effects have been investigated by Sovko and Kavados, ref(61),1971,ref(62),1974,but at the relatively low frequency of 42 MHz.

9.5 Pulse-compression techniques.

The requirement of improved range-resolution in the proposed height-finding system necessitates the reduction of pulse-width and hence degrades the signal to noise ratio of the auroral echoes.This ratio can be improved by the development of pulse compression within the transmitted pulses preferably by means of phase-coding techniques,as described in ref (96),by Skolnik,1972.Such techniques are in operation with the Eiscat radars, refs(6),by Rishbeth,1978,and (9),by Du Castel et al,1974 and the Jicamarca radar,refs(7),by Farley et al,1967, and (8) by Farley,1969.The phase-coding could be achieved by inserting a computer controlled phase shift element in

the low-power section of the transmitter and in each receiver.The phase-shifters could also be employed in a multiple-pulse spectral analysis system,to ensure a difference in phase between each pulse-pair as follows;

9.6 A multipulse spectral analysis without clutter.

SABRE radars employ a double-pulse velocity measuring system in order to determine the mean electrojet velocities.Radars which utilised sequences of pulses in order to derive the velocity spectrum,rather than just the mean, include the Chatanika and Stare radars.One problem with the double-pulse technique is that of "overlapping range returns",or signal clutter,caused by the simultaneous reception of radar echoes from each of the 2 pulses as illustrated in fig (9.2).These 2 echoes will actually originate from different ranges,which are in effect separated by 3 range-cells,corresponding to the inter-pulse spacing.This situation would not,of course,occur for discrete targets,but only for the diffuse auroral type distributed in both range and azimuth,at approximately constant height.One method of reducing the effects of this signal clutter would be to phase-code both transmit pulses individually and selectively filter the received pulses.Ideally a separate amplifier would be required for each of the pulses so filtered,rather than develop a high speed switching unit employing only one amplifier.

A second,simpler,method would be to alter the transmitter phase between each of the 2 pulses.In this way,the signal clutter received from an echo due to the previous transmitter pulse would not correlate so effectively in the integrator.This technique could be extended to the multipulse spectral analysis system,wherebye a phase-shift element inserted in the transmitter, (in the low-power section),could be adjusted by the computer to provide a staggered series of phase shifts between each of the multipulse transmissions.

SCHEMATIC ILLUSTRATION OF THE OVERLAPPING OF ECHO SIGNALS FROM A PAIR OF TRANSMITTED PULSES.

THE 3 TARGETS ARE AT RANGES OF 100,400 AND 700 KM. THE VELOCITY OF THE 400 KM TARGET IS DESIRED, BUT THE OTHER 2 TARGETS OVERLAP.
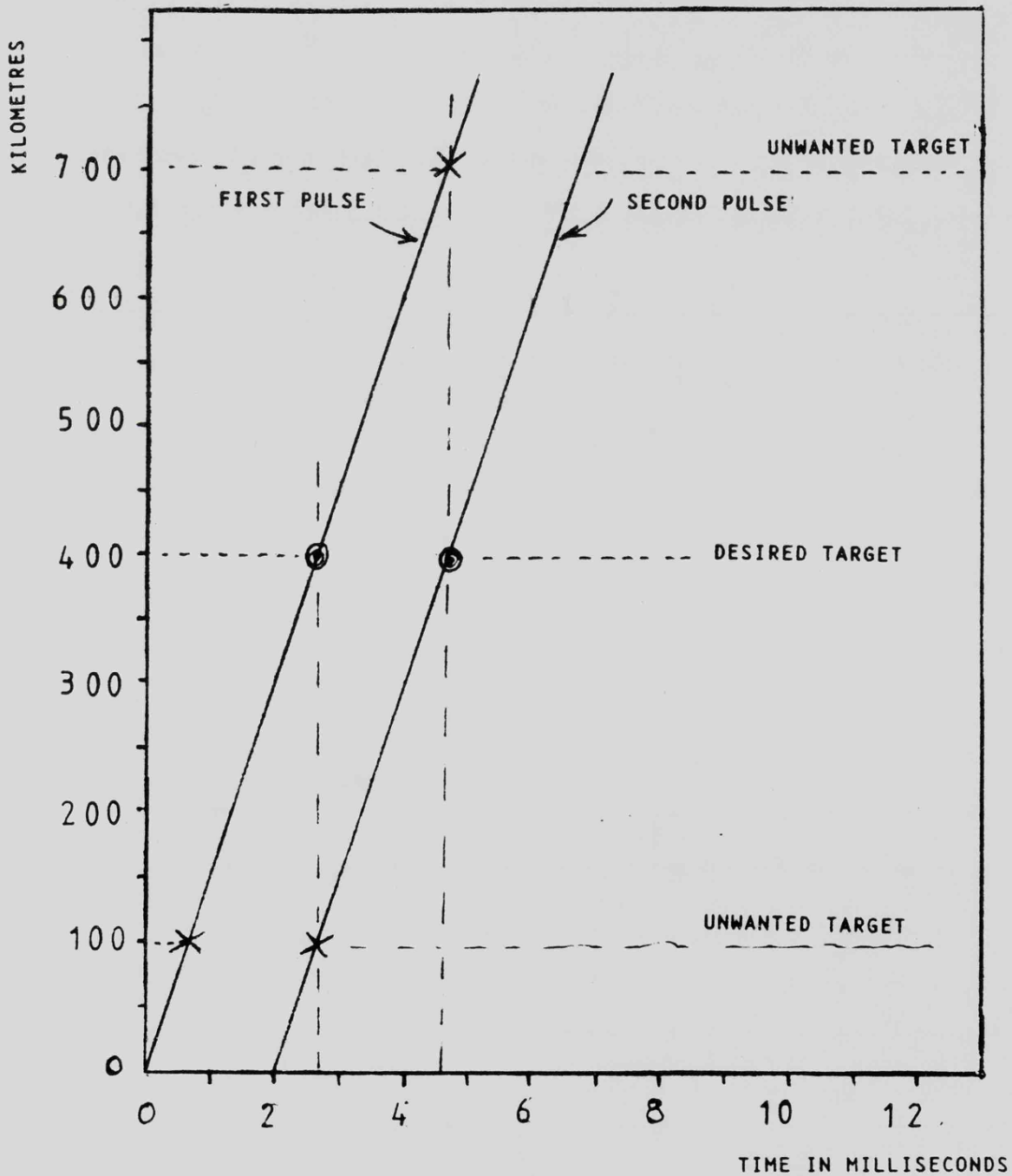
FIGURE 9.2

9.7 Development of the SABRE short-range mode.

A future work programme utilising the short range mode of operation must include a thorough examination of the signal processing programmes and of the antenna components. When this has been completed and SABRE radar is able to distinguish point targets in range and in azimuth, then it is feasible to consider a pulse-Doppler mode of operation for the shorter ranges. This technique, as outlined in chapter 4, will enable the derivation of the Doppler velocity spectrum of a known target (ie a commercial airliner) which can then be compared with the Doppler velocities output from the current SABRE double-pulse velocity measuring system, and a form of calibration achieved. Similarly, a known moving point target may provide an easily measured range-rate which can also be compared with the SABRE velocities.

9.8 Conclusions

If these suggested work programmes are undertaken then the SABRE radar system could become a tool for truly comprehensive analysis of the aurora.

REFERENCES

1. Appleton, E V; Barnett, M A F - "On some direct evidence for downward atmospheric reflection of electric rays"

    Proc Royal Soc (London) vol 109, pp 621-641, 1926

2. Gardner, F F; Pawsey, J L - "Study of the ionospheric D-region using partial reflections"

    J Atmos Terr Phys 1953, 3, 321

3. Eccles, D; King, J W - "Ionospheric probing using vertical incidence techniques"

    J Atmos Terr Phys 32, 517, 1970

    SEE ALSO

    Proc IEEE 1969, 57, 1012

4. Wipperman, D R - "The application of pulse compression techniques to ionospheric sounding"

    Aeronomy Report No 16, March 1967, University of Illinois

5. Beynon, W J G; Williams, P J S - "Incoherent scatter of radio waves from the ionosphere"

    Rep Prog Phys vol 41, 1978, pp 909-956

6. Rishbeth, H - "EISCAT"

    Proc Esrange Symposium ESA SP-135, June 1978

7. Farley, D T; McLure, J P; Sterling, D L; Green, J L

    J Geophys R 1967, 72, 5837-5851

8. Farley, D T - "Faraday rotation measurements using incoherent scatter"

    Radio Science 4, 1969, 143-152

9. Du Castel, F; Testud, J - "Some aspects of the design concept of a European incoherent scatter facility in the auroral zone"

    Radio Science 9, 1974, 113-119

10. Carlson, H C; Gordon, W E; Showers, R L

    J Geophys Research 77, 1972, 1242-50

11. Evans, J V - "High power radar studies of the ionosphere"

    Proc IEEE 1975, 63, Number 12, 1636-1650

12. Farley, D T - "Multiple pulse incoherent scatter correlation function measurements"

    Radio Science 1972, vol 7, 6, 661-666

13. Bauer, P; Waldteufel, P; Vialle, C

    Radio Science 1974, 9, 77-83

14. Taylor, G N; Rishbeth, H; Williams, P J S

    Nature 1973, 242, 109-11

15. Hess, G C; Geller, M A - "The Urbana meteor radar system: Design, development and first observations"

    Aeronomy Report 74, 1976, University of Illinois

16. Barrick, D E; Headrick, J M; Boyle, R W; Crombie, D D

    Proc IEEE 1974, 62, 673-680

17. Shearman, E D R; Sandham, W A; Bramley, E N; Bradley, P A - "Ground wave and sky wave sea state sensing experiments in the UK"

    NATO - AGARD symposium on special topics in HF propagation, May 1979

18. Gibbs, K P; Bowhill, S A - "An investigation of turbulent scatter from the mesosphere as observed by coherent-scatter radar"

    Aeronomy Report 110, April 1983, University of Illinois

19. Planck, V G - "Radar echoes from the atmosphere"

    in Radargrammetry by McGraw - Hill, 1960, pp 222-243

20. Hardy, K R; Atlas, D; Glover, K M - "Multiwavelength back-scatter from the clear atmosphere"

    J Geophys Res 1966, vol 71, 1537-1552

21. Bowles, K L - "Radio wave scattering in the ionosphere"

    Advances in Electronics and Electron Physics 1964, 17, 55-176

22. Woodman, R F; Guillen, A - "Radar observations of winds and turbulence in the stratosphere and mesosphere"

    J Atmos Science 1974, 31, 493-505

23. Goss, L D; Bowhill, S A - "Observations of the upper troposphere and lower stratosphere using the Urbana coherent-scatter radar"

    Aeronomy Report 111, July 1983, University of Illinois

24. Green, J L; Gage, K S; Van Zandt, T E - "Atmospheric measurements by VHF pulsed Doppler radar"
    IEEE Transactions on Geoscience Electronics, October 1979,
    vol GE-17, number 4, 262-280

25. Ecklund, W L; Carter, D A; Balsley, B B - "Continuous measurement of upper atmospheric winds using a VHF Doppler radar"
    JATP 1979, 41, 983-994

26. Balsley, B B; Gage, K S - "The MST radar technique: Potential for middle atmosphere studies"
    Pure Applied Geophysics 118, 452-493, 1980

27. Rottger, J; Schmidt, G - "High resolution VHF radar sounding of the troposphere and stratosphere"
    IEEE Transactions on Geoscience Electronics, October 1979,
    vol GE-17, number 4, 182-189

28. Balsley, B B; Ecklund, W L; Carter, D A; Johnston, P E - "Poker flat MST radar:- First results"
    Geophys Res Letters, 1979

29. Van Zandt, T E; Green, J L; Gage, K S; Clark, W L - "Vertical profiles of refractivity turbulence structure constant: Comparision of observations by the Sunset radar"
    Radio Science 1978, 13, 819-829

30. Carlson, H C; Sundararaman, N - "Real-time jetstream tracking"
    Bull Amer Met Soc 63, 1019-1026, 1982

31. Rottger, J; Rastogi, P K; Woodman, R F - "High resolution VHF radar observations of turbulence structures in the mesosphere"
    Geophys Res Letters, July 1979, vol 6, 7, 617-620

32. Richter, H J - "High resolution radar for remote atmospheric sounding"
    IEEE International Radar Conference 1980, 235-240
    OR
    Radio Science Dec 1969, 4, 12, 1261-1268

33. Lighart, P L - "System considerations of the FM-CW Delft atmospheric research radar DARR"
    IEEE International Radar Conference 1980, 38-43

34. Smith, L P; Hardy, K R; Glover, K M - "Applications of radar to meteorological research"
    Proceedings of the IEEE, 1974, vol 62, 6 , 724-745

35. Battan, L J - "Radar observations of the atmosphere"
    University of Chicago Press, 1973

36. Ratcliffe, J A - "An introduction to the ionosphere and magnetosphere"
    Cambridge University Press, 1972

37. Jones, A V J - "Aurora"
    Reidel Publishing Company, 1974

38. Harang, L; Stoffregen, W - "Scattered reflections of radio waves from a height of more than 100 km"
    Nature, 1938, 142, 832

39. Anonymous - "Auroral reflections"
    QST, 1939, vol 23, p 78

40. Bowles, K L - "Some recent experiments with VHF radio echoes from aurora"
    Res Report EE248, Tech Rep 22, 1955, Cornell University, New York

41. McNamara, A G - "Double-Doppler radar investigations of aurora"
    J G Res, 60, 257, 1955

42. Booker, H G - "Theory of radar scattering from aurora"
    JATP 1956, 8, 204

43. Nichols, B - "Drift motions of auroral ionisation"
    JATP 1957, 11, 292

44. Leadabrand, R L; Yabroff, I - "Geometry of auroral communications"
    IRE Transactions of Antennae and Propagation, Jan 1958, 80-87

45. Presnell, R I; Leadabrand, R L; Peterson, A M; Dyce, R B; Schlobohm, J C; Berg, M R - "VHF and MHF radar observaions of the aurora at College, Alaska"
    JGR 64, 1179, 1959

46. Blevis, B C; Day, J W B; Roscoe, O S - "The occurrence and characteristics of radar auroral echoes at 488 and 944 MHz"
    Can J Phys 41, 1359, 1963

47. Bates, H F; Sharp, R D; Belon, A E; Boyd, J S - "Spatial relationships
     between HF radar aurora, optical aurora and electron precipitation"
          Planetary Space Science 17, 83, 1969

48. Hofstee, J; Forsyth, P A - "Ion-acoustic waves in the auroral plasma"
          Can J Phys 47, 2797, 1969
     SEE ALSO
          J Atmos Terr Physics 34, 893, 1972

49. Forsyth, P A - "The rate of occurrence of VHF radio aurora over an
     11-year period"
          J Atmos Terrest Physics 31, 313, 1969

50. Camnitz, H G; Tsunoda, R T; Barczys, D A - "Auroral echoes and the
     2 stream instability"
          Tech Rpt RG-2460-P-1, 1969, Cornell Aeronaut Labs, New York

51. Abel, W G; Newell, R E - "Measurements of the afternoon radio aurora
     at 1295 MHz"
          J G R 74, 231, 1969

52. Leadabrand, R L - "A comparision of radar auroral reflection data with
     acoustic wave theory"
          Radio Science 69D, 959, 1965

53. Hodges, J; Leadabrand, R L - "Auroral radar echo wavelength dependence"
          J G R 71, 19, 4545-4549, 1965

54. McDiarmid, I B - "Ion-acoustic waves and radio aurora"
          Can J Phys 48, 1863, 1970

55. Hagfors, T - "Some properties of radar auroral echoes as observed at a
     frequency of 1295 MHz"
          Agard Technical Meeting Report, session 2, paper 9, NATO, Brussels, 1971

56. Hagfors, T; Johnson, R G; Power, R A - "Simultaneous observation of
     proton precipitation and auroral radar echoes"
          J G R 76, 6093, 1971

57. Unwin, R S; Knox, F B - "Radio aurora and electric fields"
          Radio Science 6, 1061, 1971

58. Hofstee, J; Forsyth, P A - "Ion acoustic waves and aspect sensitivity
    in radio aurora"
         J A T P 34, 893, 1972

59. Balsley, B B; Ecklund, W L - "VHF power spectra of the radar aurora"
         J G R 77, 4746, 1972

60. Knox, F B - "A theory of discrete radio aurora"
         J A T P 34, 747, 1972

61. Sofko, G J; Kavadas, A - "Polarisation characteristics of 42 MHz auroral
    back-scatter"
         J G R 76, 1778, 1971

62. Sofko, G J - "Aurora"
         page 219, published by D Reidel, Holland, 1974

63. McDiarmid, D R - "On the aspect sensitivity of radio aurora"
         Can J Phys 50, 2557, 1972

64. Leadabrand, R L; Larson, A G; Hodges, J C - "Preliminary results on the
    wavelength dependence and aspect sensitivity of radar auroral echoes
    between 50 MHz and 3000 MHz"
         J G R 72, 3877, 1967

65. Ecklund, W L; Balsley, B B; Greenwald, R A - "Crossed beam measurements
    of the diffuse radar aurora"
         J G R 80, 13, 1975

66. Unwin, R S; Baggaley, W T - "The radio aurora"
         Ann Geophys 28, 111, 1972

67. Czechowsky, P; Lange-Hesse, G - "Optical and radio observations of aurora"
         The Radiating Atmosphere, p 314, 1971, by D Reidel Publishers, Holland

68. Greenwald, R A; Ecklund, W L; Balsley, B B - "Auroral currents,
    irregularities and luminosity"
         J G R 78, 8193, 1973

69. Ecklund, W L; Balsley, B B; Greenwald, R A - "Doppler spectra of
    diffuse aurora"
         J G R 78, 4797, 1973

70. Baron, M J - "Electron densities within aurorae and other auroral
    E-region characteristics"
        in Symposium on Magnetospheric Substorms IAGA, Kyoto
        See also: Radio Science, 9, 341, 1974

71. Banks, P M; Doupnik, J R
        J Atmos Terr Physics 37, 951-72, 1975

72. Tsunoda, R T; Presnell, R I; Leadabrand, R L - "Radar auroreal
    echo characteristics as seen by the 398MHz phased array radar
    operated at Homer"
        J G R 79(31), 4709-4724, 1974

73. Ecklund, W L; Balsley, B B; Greenwald, R A - "Crossed beam
    measurements of the diffuse radar aurora"
        J G R, 80, 13, 1805-1809, 1975

74. Greenwald, R A; Ecklund, W L - "A new look at radar auroral motions"
        J G R, 80, 25, 3642-3648, 1975

75. Tsunoda, R T - "Doppler velocity maps of the diffuse radar aurora"
        J G R, 81(4), 425-435, 1976

76. Kamide, Y R; Brekke, A - "Altitude of the eastward and westward
    electrojets"
        J G R, 82(19), 2851-2853, 1977

77. Greenwald, R A; Weiss, W; Nielsen, E; Thomson, N R - "STARE: a
    new radar auroral backscatter experiment in Northern Scandinavia"
        Radio Science, 13, 6, 1021-1039, 1978

78. Moorcroft, D R; Tsunoda, R T - "Rapid scan doppler velocity maps of
    the UHF diffuse aurora"
        J G R, 83, A4, 1482-1491, 1978

79. Cahill, L J; Greenwald, R A; Nielsen, E - "Auroral radar and rocket
    double probe observations of the electric field across the HARANG
    DISCONTINUITY"
        Geophys Res Lett, 5, 687, 1978

80. Greenwald, R A - "An alternative explanation of the doppler spectra
    of current-driven instabilities"
        J G R, 84, 433, 1979

81. Baumjohann, W; Untiedt, J; Greenwald, R A - "Three-dimensional
    current flows associated with a sub-storm-intensified eastward electrojet"
        J G R, 85, 1963, 1980

82. Zanetti, Jr, L J; Arnoldy, R L; Cahill, L J; Behm, D A;
    Greenwald, R A - "Comparative rocket observations of ionospheric
    electric fields in the aurora"
        Space Sci Instr, 5,183, 1980

83. Schlegel, K; Nielsen, E - "Derivation of drifts and electric fields
    from the STARE auroral radar measurements using the kinetic theory of
    the 2-stream instability"
        Rep. MPAE-W-04-81-12   Max Planck Inst., Germany, 1981

84. Unwin, R S; Johnston, P V - "Height dependence in the power spectrum
    of diffuse radar aurora"
        J G R, 86, A7, 5733-5745, 1981

85. Andre, D - "The dependence of the relative backscatter cross-section
    of 1 metre density fluctuations in the auroral electrojet on the
    angle between electron drift and radar wave vector"
        J G R, 1983 88, A10

86. Haldoupis, C; Nielsen, E - "Results on relative scattering cross-
    section of 140MHz auroral backscatter"
        J G R, 1984, 89, A4

87. Nielsen, E; Schlegel, K - "A comparison of STARE and EISCAT electron
    drift velocity measurements"
        J G R, 88, 5745, 1983

88. Whitehead, J D; Ierkic, H M; Nielsen, E - "Splitting and divergence
    of STARE auroral radar velocities"
        J G R, 88, A3, 2147-2154, 1983

89. Nielsen, E; Haldoupis, C I; Fejer, B G; Ierkic, H M - "Dependence of
    auroral power spectra variations upon electron drift velocity in the
    eastward electrojet"
        J G R, 1984, 89, A1

90. Balsley, B B - "Some characteristics of non-2-stream irregularities
    in the equatorial electrojet"
        J G R, 74, 2333-2347, 1969

91. Farley, D T; Balsley, B B - "Instabilities in the equatorial electrojet"
      J G R, 78, 227-239, 1973

92. Fejer, B G; Farley, D T; Balsley, B B; Woodman, R F - "Oblique
    VHF radar spectral studies of the equatorial electrojet"
      J G R, 80, 10, 1307-1312, 1975

93. Prakash, S; Gupta, S P; Subbaraya, B H - "Electrostatic plasma
    instabilities in the equatorial electrojet"
      Nature, 233, 56-58, 1971

94. Richmond, A D - "Equatorial electrojet - 2 - Use of a model to
    study the equatorial ionosphere"
      J Atmos Terr Phys, 35, 1105-1118, 1973

95. Moorcroft, D R; Tsunoda, R T - "Rapid scan doppler velocity maps
    of the UHF diffuse radar aurora"
      J G R, 83, A4, 1482-1492, 1978

96. Skolnik, M I - "Radar handbook"

    published by McGraw-Hill, 1972

97. Blake, L V - "Radio ray (radar) range-height-angle charts"
      Naval Res Lab Rpt 6650, Jan 1968
    also Microwave Journal, Vol 4, Oct 1968

98. Millman, G H - "Atmospheric effects on VHF and UHF propagation"
      Proc. IRE, Vol 46, 1492-1501, 1958

99. McNally, D - "Positional Astronomy"
      published by Muller Educational, 1874

100. Brown, J T; Manson, C W M - "The elements of analytical geometry"
      published by Macmillan, 1968

101. Jordan, E C - "Electromagnetic waves and radiating systems"
      published by Constable, 1962

102. Walker, A D M; Greenwald, R A -
      Planetary Space Science, 29, 293-305, 1981

103. Nielsen, E; Sofko, G; Axford, E I
      Nature, 299, 238-240, 1982

104. Akasofu, S   "polar and magnetospheric substorms"

     published by D.Reidel,Holland 1968

105. Inhester, B; Baumjohann,E;Greenwald RA; Nielsen,E

     JGR, 49, 155-162, 1981

106. Greenwald,RA "Electric fields in the Ionosphere and magnetosphere"

     Space Science Review   34, 1983

107. Ierkic,M; Fejer BG; Farley DT;

         "Angular dependence of the scattering cross section

         of equatorial electrojet irregularities".

         EOS Trans   AGU   58, 449, 1977

108. Nielsen E; Guttler W; "A new radar auroral backscatter experiment"

     Nature   304, 5928, 712, 1983

109. Moorcroft DR   "Dependence of radio aurora at 398 MHz on electron

         density and electric field".

         Can.J Physics   57, 687, 1979

110.Sudan RN; Akinrimsi J;Farley DT; "Generation of small scale

         irregularities in the equatorial electrojet"

         JGR 78, 240, 1973

111. Fejer BG; Kelley MC; "Ionospheric irregularities"

         Rev.Geophys.and Space Phys. 18, 401, 1980

112. Timofeev E; Miroshnikov Y; "Altitude characteristics of Radar

         Aurora as seen by a 90 MHz double-altitude radar

         system"   JG'   51, 44, 1982

113. Meade E.L.,Jr "A 2 Kwatt PEP amplifier for 144 MHz"

         QST DEC 1973 page 34; QST JAN 1974 page 26.

114.   The American Ephemeris and Nautical Almanac.

     Published by the U.S. Government Printing Office,1982

115.Cochran WT; Cooley WJ; et al "What is the fast fourier transform "

Proc.IEEE   55,   10,   1967

116. Blackman and Tukey;   "The measurement of power spectra"

Published by Dover,New York,1958

117. Farley DT Jr; "A plasma instability of field-aligned irregularities

in the ionosphere" JGR   68,   22,   1963

118.Fejer BG;farley DT; et al "Vertical structure of the backscattering

region in the equatorial electrojet and the

gradient drift instability" JGR 80, 10, 1975

119.Keskinen MJ; et al "Temporal and spatial power spectrum studies of

numerical simulations of type 2 gradient drift irregularities

in the equatorial electrojet" JGR   84, A4, 1979

120. Smith PG;   "Measurement of the complete far-field pattern of

large antennae using a radio star"

IEEE Trans Ant Propag   AP-14, 6-16, 1966

121. Czechowsky P; "Phasengestenate Flackenantenne im VHF bereich"

Antennen 1982

122. McClintock WJ;   Marconi Review   1981,   pages 224-269

123. Delaney WP; "An RF multiple beam-forming technique"

IRE Transactions on Military Science, 1962

124. Farley DT; Ierkic M; Fejer BG; "Radar interferometry"

JGR 86,   A3,   1981

125. Heelis RA;   "The polar ionosphere"

Reviews of Geophysics and Space Physics 20, 3, 1982

126. Davies K.;   "Ionospheric Radio Propagation"

Dover publications,New York. 1966

127. Hargreaves   "The upper atmosphere and solar-terrestrial relations"

by Van Nostrand Rheinhold company, 1979

128. Ferch , Sudan ; "Numerical simulations of type 2 gradient drift

irregularities in the equatorial electrojet"

JGR 82, 2283--2288 1977

129. Unwin RS;   JATP   28   1183-1194 1966

130. Belrose JS; Burke MJ; "Study of the lower ionosphere using partial

reflection".

JGR vol 69, 13, 1964

131. Bauer JR; Mason ; Wilson; "Radio refraction in a cool exponential

atmosphere".

MIT Lincoln Lab report, 186.

ASTIA number 202331, 1958.

132. Farley DT; "Radio wave scattering from the ionosphere"

Methods of Experimental Physics, Vol 9B, p139

Academic, N.York   1971

133. Haldoupis C; Nielsen E; Goertz C.K.; "Experimental evidence of the

dependence of 140 MHz radio auroral backscatter

characteristics on Ionospheric conductivity".

JGR 87, A9, 1982

134. Malin SRC; Barraclough DR; "An algorithm for synthesizing the

geomagnetic field".

Institute of Geological Sciences, Edinburgh. 1981

135. Taylor RE; "136/400 MHz radio sky maps"

Proc.I.E.E.E.   April, 1973, p469.

RADAR STUDIES OF THE AURORA.

G.COE

ABSTRACT

The investigation of the high-latitude aurora by means of the V.H.F. auroral radar SABRE,(Swedish And British auroral Radar Experiment),developed by the Leicester University Ionospheric Physics group, is described. The first two chapters review previous studies of the atmosphere by radar techniques and includes a description of the SABRE radar. The basic radar equation and velocity relationships are derived and the various loss factors examined.From analysis of the echo signal data for the diffuse aurora,and examination of signal data from a radio star,the SABRE radar parameters are established. An investigation is then undertaken of the variation of the electrojet parameters, (derived from application of the radar equation to the SABRE data), with height,electric field strength and geomagnetic conditions. Evidence is found of backscattering from irregularities generated by both two-stream and gradient drift processes.

An examination is also made of the echo signals detected at relatively short ranges,of below 370 km, and several causal mechanisms are investigated including scattering processes in the neutral atmosphere. It is evident that aircraft are predominantly the cause of these short-range echoes.

This investigation also reveals a number of software and hardware faults in the initial radar configuration.

This Thesis is concluded with suggestions for future development of the radar system, which include the implementation of a height-finding facility and improved spectral resolution.